

# Cytoskeletal proteins and early neurodegenerative mechanisms in Alzheimer's disease

**Ineka T. Whiteman B.Sc (Hons)**

in fulfillment of the requirements for

**Brain & Mind Research Institute  
Discipline of Anatomy & Histology  
Sydney Medical School**

**The University of Sydney**

**March 2011**



Thesis submitted to the University of Sydney  
in fulfillment of the requirements for  
the Degree of Doctor of Philosophy.



## Statement of Originality

This thesis describes original research work undertaken by the candidate between July 2007 and February 2011, the majority of which was conducted in the Alzheimer's Disease Cell Biology laboratory of the Brain & Mind Research Institute at the University of Sydney, under the supervision of Dr Claire Gokisbuey. Some of this research work was also conducted in the Department of Biochemistry and Molecular Biology at Colorado State University under the supervision of Professor James Samborg between the months October to December 2009 and February to August 2010.

# PART I

These results are solely the author's, except where otherwise acknowledged. This thesis contains original material which has not been previously submitted and will not be submitted for the award of any other degree or qualification.

The use of animals has been approved by the University of Sydney Animal Ethics Committee or the Institutional Review Board, Colorado State University. Ethics approval for the use of human brain tissue was obtained from the University of Sydney Human Ethics Committee or the Institutional Review Board, Colorado State University.

To the author's best knowledge, this thesis contains no material previously published or written by any other person, except where appropriate reference is made.



Ineka T. Whitamen

SID: 305183834

## Statement of Originality

This thesis describes original research work undertaken by the candidate between July 2007 and February 2011, the majority of which was conducted in the Alzheimer's Disease Cell Biology laboratory of the Brain & Mind Research Institute at the University of Sydney, under the supervision of Dr Claire Goldsbury. Some of this research work was also conducted in the Department of Biochemistry and Molecular Biology at Colorado State University under the supervision of Professor James Bamberg between the months October to December 2009 and February to August 2010.

These results are solely the work of the author, except where otherwise acknowledged. This thesis contains original material which has not been previously submitted and will not be submitted for the award of any other degree or qualification.

The use of animals has been approved by the University of Sydney Animal Ethics Committee or the Institutional Review Board, Colorado State University. Ethics approval for the use of human brain tissue was obtained from the University of Sydney Human Ethics Committee or the Institutional Review Board, Colorado State University.

To the author's best knowledge, this thesis contains no material previously published or written by any other person, except where appropriate reference is made.

[Redaction]

Ineka T. Whiteman

[Redaction]



## Acknowledgements

My deepest and sincerest gratitude goes to my supervisor, Claire Goldsbury, who has given me constant support, guidance and encouragement over the past 5 years. As both an I would like to thank Claire Goldsbury, who has not only been my supervisor for the past 3½ years, but also a great colleague to work alongside, a bro and a wealth of knowledge. It's been a really valuable journey and I am grateful for all your time, effort and support. Thank you to the members of the Goldsbury Lab who have all given me support and friendship over the years - Erica Jeong, Erikar Eco, De Lian Goh, Marie Therese Weil, Gloria Castellano Gonzales, Natasha Deters and Denise Nergenu.

To Jim Bamburg and Laurie Minamide who make the perfect team in every possible way; you guys go above and beyond the role of 'supervisors' and 'collaborators' and I will be forever grateful for the opportunity and experience you have given me in Colorado. Laurie – thank you for all your wisdom and exceptional technical guidance and advice, and above all, for your love, support...and lemon bars! Jim – thank you for your incredible wisdom, your fatherly care, encouragement and your frank and honest guidance. Through the 'speed-bumps' and challenges of this project, you have gently pushed and encouraged me and helped me become a better scientist every day. To my fellow JRBils, what a pleasure and privilege it has been to work in such a caring, kind and brilliant team. O'Neil Wiggan, Alisa Shaw, Chi Pak, Ian Marsden, Barbara Bernstein, Lubna Tahtamouni, Elizabeth Akin and Imarhia Enogieru, thank you all for your help, friendship and some of the fondest memories that I will cherish always. In particular, thanks to O'Neil for the many incredibly valuable scientific and cerebral discussions in the lab, over sushi or in the corridors at all hours of the night. Your wisdom, insight and thought-provoking questions have helped me more than you know.

My deepest and sincere gratitude to Frank Lovicu who has given me constant support, guidance and encouragement over the past 6 years. As both an academic advisor and a friend, you are an inspiration and a breath of fresh air.

To my amazing family: Mumma, Pops, Brett, Angie, Jackson and Ella. Your love, faith and unwavering support means more to me than words could ever say. Thank you for giving me the wings to fly and endless opportunities to grow, learn and appreciate life to the fullest. I could not have done any of this without you guys there, and so this PhD is yours as much as it is mine.

To my dear friends, Zorba and Cassie who have become like family to me over the past 8 years. Thank you for all the wonderful ways you have loved and supported me throughout the years. I am truly blessed to have you in my life.

And to my darling Branden. My best friend, my rock and strength. Thank you for everything you are and everything you do. What a wonderful journey we've shared so far...

Table of Contents

PART I

Statement of Originality.....iv  
Acknowledgements.....v  
Table of Contents.....viii  
Publications Arising from this PhD.....xiii  
Published Abstracts Arising from this PhD.....xiv  
Przekaz.....xv  
Conference Attendance.....xv  
Oral Presentations.....xvi  
Poster Presentations.....xvi  
Scholarships and Grants.....xvii  
Abbreviations.....xviii  
List of Figures and Tables.....xx  
Author Contributions.....xxii

This thesis is dedicated to Branden.

SUMMARY.....xxiv

By your side, all things are possible. I love you.

PART II

xxxx

CHAPTER 1: General Introduction.....2  
1.1 A Global "Epidemic".....3  
1.2 Neuropathology of AD.....3  
1.3 Familial and Sporadic AD.....5  
1.4 The microtubule associated protein (MAP) tau.....8  
1.4.1 Tau structure.....8  
1.4.2 Functions of tau.....9  
1.4.3 Phosphorylation regulates tau function.....12  
1.4.4 Abnormal tau pathology in AD.....14  
1.4.5 A role on other structural MAPs.....16  
1.5 Actin and Actin Depolymerizing Factor (ADF)/Cofilin.....18  
1.5.1 Actin and ADF/cofilin (AC) structure.....19  
1.5.2 A role on transcription.....19  
1.5.3 Functions of Actin and AC.....21  
1.5.4 Actin and AC Abnormalities in AD.....22



## Table of Contents

### PART I

Statement of Originality.....	iv
Acknowledgements.....	v
Table of Contents.....	viii
Publications Arising from this PhD.....	xiii
Published Abstracts Arising from this PhD.....	xiv
Prizes.....	xv
Conference Attendance.....	xv
Oral Presentations.....	xvi
Poster Presentations.....	xvii
Scholarships and Grants.....	xvii
Abbreviations.....	xviii
List of Figures and Tables.....	xx
Author Contributions.....	xxiii
<b>SUMMARY.....</b>	<b>xxiv</b>

### PART II

<b>CHAPTER 1: General Introduction.....</b>	<b>2</b>
1.1 A Global 'Epidemic'.....	3
1.2 Neuropathology of AD.....	3
1.3 Familial and Sporadic AD.....	5
1.4 The microtubule associated protein (MAP) tau.....	8
1.4.1 Tau structure.....	8
1.4.2 Functions of tau.....	9
1.4.3 Phosphorylation regulates tau function.....	12
1.4.4 Abnormal tau pathology in AD.....	14
1.4.5 A note on other structural MAPs.....	16
1.5 Actin and Actin Depolymerizing Factor (ADF)/Cofilin.....	18
1.5.1 Actin and ADF/cofilin (AC) structure.....	18
1.5.2 A note on nomenclature.....	19
1.5.3 Functions of Actin and AC.....	21
1.5.4 Actin and AC Abnormalities in AD.....	22

1.6 Amyloid-beta (A $\beta$ ) in AD.....	24
1.6.1 The Amyloid Cascade Hypothesis.....	24
1.6.2 A $\beta$ and tau.....	27
1.6.3 A $\beta$ and AC-actin.....	29
1.6.4 Soluble versus insoluble A $\beta$ in AD.....	30
1.7 The 'Mitochondrial Hypothesis' of AD.....	31
1.7.1 Mitochondria and the ageing brain.....	31
1.7.2 Mitochondria and A $\beta$ , tau and AC-actin pathologies.....	33
<b>1.8 Research Hypothesis and Aims.....</b>	<b>36</b>
<b>1.8.1 Main Hypothesis.....</b>	<b>36</b>
<b>1.8.2 Specific Aims.....</b>	<b>37</b>
<b>CHAPTER 2: General Materials and Methods.....</b>	<b>39</b>
2.1 Antibodies.....	40
2.2 Primary neuron culture generation & maintenance.....	41
2.2.1 Chick tectal neurons.....	41
2.2.2 Primary human neurons.....	42
2.2.3 Primary rat hippocampal neurons.....	43
2.3 Cell treatments.....	44
2.4 Immunofluorescence.....	45
2.4.1 Primary dissociated neuron culture.....	45
2.4.2 Human brain tissue.....	46
2.5 Microscopy and Analysis.....	47
2.6 Western blotting.....	48
2.7 Statistics.....	50
2.8 Plasmid constructs and transfection.....	51
2.8.1 E. coli transformation with vector constructs.....	51
2.8.2 Midi-prep extraction of DNA from E. coli.....	51
2.8.3 Transfection of primary neurons.....	52
2.9 Organotypic brain slice culture.....	53
2.10 Ethics Statement.....	55



**PART III**

**CHAPTER 3: Activation of ADF/cofilin sequesters phosphorylated MAP/tau into AD-like neuritic inclusions.....57**

Preface.....58

3.1 Introduction.....58

3.2 Specific Materials and Methods.....60

    3.2.1. ATP luminescent measurements.....60

    3.2.2. Plasmids and transfection.....61

    3.2.3. FRET analysis.....62

    3.2.4. Human tissue and rat hippocampal slices.....62

    3.2.5. A $\beta$  peptide treatments.....63

    3.2.6. Analysis and statistics.....64

3.3 Results.....64

    3.3.1 Neuritic pMAP accumulation in striated rods, resembling structures in postmortem Alzheimer brain, is induced in primary neurons by energy depletion.....64

    3.3.2 pMAP-containing striations induced by ATP-depletion co-localize with ADF/cofilin-actin rods.....69

    3.3.3 Activated cofilin sequesters and is closely associated with pMAP in rods.....78

    3.3.4 Silencing ADF prevents pMAP accumulation in rods.....83

    3.3.5 Latrunculin B enhances and Jasplakinolide represses pMAP-staining in rods.....87

    3.3.6 A $\beta$  peptides enhance pMAP-accumulation at ADF/cofilin rods.....90

3.4 Discussion.....93

**CHAPTER 4: Rapid changes in phospho-MAP/tau epitopes during neuronal stress: cofilin-actin rods primarily recruit MAP/tau phosphorylated in the microtubule binding domain.....99**

Preface.....100

4.1 Introduction.....100

4.2 Specific Materials and Methods.....104

    4.2.1 Nuclear accumulation analysis.....104

    4.2.2 Human tissue preparation.....105

    4.2.3 Transmission Electron Microscopy.....105

4.3 Results.....	106
4.3.1 Mitochondrial inhibition induces cellular redistribution and epitope-specific persistent phosphorylation or dephosphorylation of MAP/tau.....	106
4.3.2 12E8 but not other MAP/tau epitopes redistributes to AC rods during mitochondrial inhibition.....	118
4.3.3 Actin depolymerization mimics effects of mitochondrial inhibition on MAP/ tau phosphorylation and redistribution.....	120

4.4 Discussion.....	123
---------------------	-----

## **CHAPTER 5: Elucidating pathogenic mechanisms of AD in tau transgenic mice: a role for ADF/cofilin in mediating $\beta$ -amyloid and tau?.....131**

5.1 Introduction.....	132
-----------------------	-----

5.2 Specific Materials and Methods.....	138
---	-----

5.2.1 Transgenic MAPT mice.....	138
5.2.2 Transgene determination by Polymerase Chain Reaction (PCR).....	139
5.2.3 Mouse brain preparation for Western blot.....	140
5.2.4 Immunostaining of mouse brain slices.....	141
5.2.5 Human amyloid- $\beta$ dimer/trimer (HA $\beta$ d/t) purification.....	142
5.2.6 Testing HA $\beta$ d/t in rodent dissociated cell culture.....	144
5.2.7 Treating organotypic brain slices with HA $\beta$ d/t.....	146
5.2.8 Confocal Microscopy.....	147
5.2.9 Rod analysis.....	149

5.3 Results.....	151
------------------	-----

5.3.1 Preliminary work.....	151
<i>Tau is expressed in htau mice but not tau KO mice.....</i>	151
<i>Hippocampal brain slices retain organotypic organization for up to 48 days ex vivo.....</i>	152
<i>Endogenous mouse cofilin aggregates into rods during ATP depletion.....</i>	154
<i>Optimizing fixation and permeabilization protocols for cofilin and MAP/tau rods in organotypic brain slices.....</i>	155
5.3.2 Human amyloid- $\beta$ peptides induce cofilin and MAP/tau rods in the dentate gyrus.....	159
5.3.3 The formation of cofilin rods is not dependent on the presence of tau but may be enhanced by human tau expression.....	160
5.3.4 Initiation of cofilin rods coincides with the generation of MAP/tau inclusions in transgenic tau mouse brain slices.....	162
5.3.5 Formation of KXGS-positive rods is markedly reduced in tau KO slices.....	163

5.4 Discussion.....	168
---------------------	-----



## PART IV

Publications arising from this PhD

### CHAPTER 6: General Discussion & Future Directions.....176

#### 6.1 General Discussion and Future Directions.....177

- 6.1.1 How do AC-actin and MAP/tau inclusions interact?.....183
- 6.1.2 Does the presence of MAP/tau confer any special property to AC rods? .....184
- 6.1.3 What is the role of these inclusions in neurites?.....186

#### 6.2 Potential therapeutic avenues.....191

- 6.2.1 Antioxidants and pro-mitochondrial compounds.....191
- 6.2.2 The importance of diet and exercise in AD prevention.....193
- 6.2.3 Preventing development of cytoskeletal pathologies.....195

## PART V

### REFERENCES.....198

### APPENDIX.....227

- Publications.....228



Publications arising from this PhD

**Whiteman IT**, Minamide LS, Guillemin GJ, Goh DL, Bamburg JR and Goldsbury C (2011) Rapid Changes in Phospho-MAP/tau Epitopes During Neuronal Stress: Cofilin-Actin Rods Primarily Recruit Microtubule Binding Domain Epitopes. *PLoS One* 6(6):e20878

Bamburg JR, Bernstein BW, Davis RC, Goldsbury C, Maloney MT, Marsden IT, Bamburg JR, Bernstein BW, Davis RC, Flynn KC, Goldsbury C, Jensen JR, Maloney MT, Marsden IT, Minamide LS, Pak CW, Shaw AE, **Whiteman I**, Wiggan O. (2010) ADF/cofilin-actin rods in neurodegenerative disease. *Current Alzheimer Research* 7(3):241-50.

Goldsbury C, Bamburg JR, Cullen KM, Guillemin G, Minamide LS, **Whiteman IT**, Gervasio OL, Cullen KM, Guillemin GJ, Jeong EV, Witting PK, Antao ST, Minamide LS, Bamburg JR and Goldsbury C (2009) Activated Actin-Depolymerizing Factor/Cofilin Sequesters Phosphorylated Microtubule-Associated Protein during the Assembly of Alzheimer-Like Neuronal Cytoskeletal Striations. *Journal of Neuroscience* 29(41):12994-13005.

Goldsbury C, **Whiteman IT**, Jeong E and Lim YA (2008), Oxidative stress increases levels of endogenous amyloid- $\beta$  peptides secreted from primary chick brain neurons; *Aging Cell* 7:771-775.

## Published Abstracts arising from this PhD

2010 John Irvine Hunter Research Prize – University of Sydney for **Whiteman IT**, Minamide LS, Bamburg JR and Goldsbury C (2010) Redistribution of phosphorylated tau is induced by modulation of the actin cytoskeleton. *Alzheimer's and Dementia* 6(4) (Suppl) 1:S156

Sydney Medical School, University of Sydney, for **Whiteman et al.** (2009) Bamburg JR, Bernstein BW, Davis RC, Goldsbury C, Maloney MT, Marsden IT, Minamide LS, Pak CW, Perry G, Podlisny MB, Selkoe DJ, Shaw AE, Siedlak SL, **Whiteman IT** (2010) ADF/cofilin-actin rods and synaptic loss in Alzheimer's disease. *Alzheimer's and Dementia* 6(4) (Suppl) 1:S378

Goldsbury C, Bamburg JR, Cullen KM, Guillemin G, Minamide LS, **Whiteman IT** (2009) Accumulation of microtubule-associated protein in striated neurites is induced by mitochondrial dysfunction. *Alzheimer's and Dementia* 5(4) (Suppl) 1:P313

**Whiteman IT**, Cullen KM, Antao ST, Witting PK, Bamburg JR, Goldsbury C. (2008) Mitochondrial dysfunction induces the accumulation of microtubule-associated protein in Alzheimer-like striated neurites. *Molecular Biology of the Cell* 19 (Suppl): Abstract 1069.

- Society for Neuroscience (USA) Annual Meeting: 2009 (Washington DC, USA)
- Joint Meeting of the Societies for Free Radical Research Australasia & Japan: 2009 (Sydney)
- Bosch Young Investigators Annual Symposium: 2010, 2009, 2008 (Sydney)
- International Brain Research Organization: 2007 (Melbourne – joint IANS)

## Oral Prizes

- 2010 John Irvine Hunter Research Prize – University of Sydney, for *Whiteman et al. (2009) J Neuroscience*.
- 2010 Dean's Research Student Publication Prize – Highly Commended, Sydney Medical School, University of Sydney, for *Whiteman et al. (2009) J Neuroscience*.
- 2009 Sapphire Biosciences Best Postgraduate Presentation – University of Sydney, Bosch Institute Young Investigators Symposium

## Conference Attendance

- Australian Neuroscience Society Annual Meeting: 2011 (Auckland), 2010 (Sydney), 2009 (Canberra), 2008 (Hobart), 2007 (Melbourne)
- International Conference on Alzheimer's Disease: 2010 (Honolulu, USA)
- Society for Neuroscience (USA) Annual Meeting: 2009 (Washington DC, USA)
- Joint Meeting of the Societies for Free Radical Research Australasia & Japan: 2009 (Sydney)
- Bosch Young Investigators Annual Symposium: 2010, 2009, 2008 (Sydney)
- International Brain Research Organization: 2007 (Melbourne – joint ANS)



## Oral Presentations

- 2011 **Whiteman IT**, Minamide LS, Goh DL, Bamburg JR, Goldsbury C. Mitochondrial inhibition induces Alzheimer-like redistribution of phosphorylated tau epitopes. Australian Neuroscience Society 31<sup>st</sup> Annual Meeting. Auckland, New Zealand.
- 2010 **Whiteman IT**, Minamide LS, Bamburg JR, Goldsbury C. Redistribution of phosphorylated tau is induced by modulation of the actin cytoskeleton. International Conference on Alzheimer's Disease. Honolulu, USA
- 2009 **Whiteman IT**. Mitochondrial dysfunction, cytoskeletal proteins and the pathogenesis of Alzheimer's Disease. Bosch Young Investigators Annual Symposium. University of Sydney, Australia.
- 2009 **Whiteman IT**, Cullen KM, Antao ST, Witting PK, Bamburg JR and Goldsbury C. Mitochondrial dysfunction triggers neuronal Alzheimer-like cytoskeletal striations containing phosphorylated microtubule-associated protein tau and actin. Australian Neuroscience Society 29<sup>th</sup> Annual Meeting. Canberra, Australia.
- 2008 **Whiteman, IT**, Cullen KM and Goldsbury C. Striated neurites containing phosphorylated tau and actin are induced by energy depletion: a potential mechanism in Alzheimer's disease. Society for Neuroscience 38<sup>th</sup> Annual Meeting. Washington DC, USA.
- 2008 **Whiteman IT**, Cullen KM, Antao ST, Witting PK, Bamburg JR and Goldsbury C. Mitochondrial dysfunction triggers Alzheimer-like neuritic striations containing phosphorylated tau and actin. Bosch Young Investigators Annual Symposium. University of Sydney, Australia.

## Poster Presentations

- 2010 **Whiteman IT**, Minamide LS, Bamburg JR and Goldsbury C. Microtubule-associated protein tau phosphorylated at specific residues is recruited to actin-ADF/cofilin neuritic aggregates: pathogenic mechanisms in early Alzheimer's. Australian Neuroscience Society 30<sup>th</sup> Annual Meeting. Sydney, Australia.
- 2010 **Whiteman IT**, Minamide LS, Bamburg JR, Goldsbury C. Mitochondrial dysfunction induces Alzheimer-like redistribution of phosphorylated tau. Bosch Young Investigators Annual Symposium. University of Sydney, Australia.
- 2009 **Whiteman IT**, Minamide LS, Witting P, Antao S, Goh DL, Nergenu D, Cullen K, Guillemin GJ, Bamburg JR and Goldsbury C. Neuronal energy crisis in Alzheimer's Disease: Mitochondrial dysfunction and the initiation of neurodegeneration. The 5<sup>th</sup> Joint Meeting of the Societies For Free Radical Research Australasia and Japan. Sydney, Australia.

## Scholarships and Grants

- 2010 International Conference on Alzheimer Disease (ICAD) Travel Fellowship (Full Fellowship)
- 2010 Sydney Medical School Travel Fellowship
- 2010 Brain and Mind Research Institute Education Grant
- 2010 Dick Smith Individual Philanthropic Grant
- 2008 Sydney University Medical School Top Up Scholarship
- 2008 Novartis Pharmaceuticals Education Grant
- 2007 Australian Postgraduate Award (APA)



## Abbreviations

3R Three microtubule-binding domain repeat tau; 4R, Four repeat microtubule-binding domain repeat tau

### A

A $\beta$ , Amyloid  $\beta$ ; A $\beta$ syn, Synthetic amyloid  $\beta$ ; AD, Alzheimer's disease; ADDLs, A $\beta$ -derived diffusible ligands; ADF, Actin depolymerizing factor; AC, ADF/cofilin; AM, Antimycin; APP, Amyloid precursor protein; ATP, Adenosine triphosphate

### B

Bp, Base pair; BSA, Bovine serum albumin

### C

CA1, Cornu Ammonis area 1; CA3, Cornu Ammonis area 3; CCCP, carbonyl cyanide 3-chlorophenylhydrazone; CHO, Chinese hamster ovary; CM, conditioned media; CN, CHO non-conditioned media; CNS, Central nervous system; Complex III, Cytochrome b-c1 complex

### D

DAPI, 4',6-diamidino-2-phenylindole; ddH<sub>2</sub>O, double distilled water; DG, Dentate gyrus; DIV, days *in vivo*; DMEM, Dulbecco's modified eagle's medium; DMSO, Dimethyl sulphoxide; dNTPs, Deoxyribonucleotide triphosphates; DPBS, Dulbecco's phosphate buffered saline; d/t, dimer/trimer

### E

E7, embryonic day 7; *E. coli*, *Escherichia coli*; EDTA, Ethylene diamine tetraacetic acid; EGFP, enhanced green fluorescence protein; EGTA, Ethylene glycol tetraacetic acid; EM, Electron microscopy; EtOH, Ethanol

### F

FAD, Familial Alzheimer's disease; FAT, Fast axonal transport; FBS, Fetal bovine serum; FCS, Fetal calf serum; FOV, Field of view; FTD Frontotemporal dementia; FTDP-17 Frontotemporal dementia with Parkinsonism linked to chromosome 17

### G

GAPDH, Glyceraldehyde 3-phosphate dehydrogenase; GBSS, Gey's Balanced Salt Solution; GDP, Guanosine diphosphate; GFP, green fluorescence protein; GSK3 Glycogen synthase kinase 3; GTP, Guanosine triphosphate

### H

HA $\beta$ , Human A $\beta$ ; HA $\beta$ m, Human A $\beta$  (monomeric); H<sub>2</sub>O<sub>2</sub>, Hydrogen peroxide; HBSS, Hanks Balanced Salt Solution; HRP, Horseradish peroxidase; HS Horse serum;

### I

IF, immunofluorescence

**J**

Jasp, Jasplakinolide

**K**

kDa, kilo Dalton

**L**

Lat B, Latrunculin B; LTP, Long term potentiation

**M**

MAP Microtubule-associated protein; MAPT Microtubule-associated protein tau (gene); MeOH, Methanol; MT, Microtubule; MTBD, Microtubule binding domain of tau; MW, Molecular weight

**N**

NaOH, Sodium hydroxide; NFT Neurofibrillary tangles; NMDA, N-methyl-D-aspartic acid; NMDA-R, NMDA receptor; NT, Neuropil threads

**P**

P7, Postnatal day 7; PAGE, Polyacrylamide gel electrophoresis; PBS Phosphate buffered sodium; PCR Polymerase chain reaction; Pen-Strep, Penicillin-Streptomycin; PFA Paraformaldehyde; PHFs Paired helical filaments; PiD Pick's disease; PKA Protein kinase A; PP1 Protein phosphatase 1; PP2A Protein phosphatase 2A; PP2B Protein phosphatase 2B; PP2C Protein phosphatase 2C; Pro, Proline; PS-1 Presenilin-1; PS-2 Presenilin-2

**R**

RIPA, Radioimmunoprecipitation assay; ROS Reactive oxygen species; RT, Room temperature

**S**

SAD Sporadic Alzheimer's disease; SAP/JNK Stress-activated kinase c-Jun N-terminal kinase; SDS Sodium dodecyl sulphate; SEC, Size exclusion chromatography; SEM, Standard error of the mean; Ser, Serine

**T**

TBE, Tris-borate-EDTA; TBS, Tris-buffered saline; TBS-T, Tris-buffered saline/0.1% Tween; TDP-43 TAR-DNA-binding protein 43; TE, Tris-EDTA; TEMED, N,N,N',N'-Tetramethylethylenediamine; Thr, Threonine; Tyr, Tyrosine; TIF, Tagged Image Files; TX, Triton X-100

**W**

WB, Western blot



## List of Figures and Tables

<b>Figure 1.1</b> Reduction in temporoparietal glucose metabolism in subjects with Alzheimer disease (AD).....	4
<b>Figure 1.2</b> Neuropathological hallmarks of AD.....	7
<b>Figure 1.3</b> Schematic representation of the human tau gene and the six central nervous system (CNS) tau isoforms.....	9
<b>Figure 1.4</b> Model showing relationship between tau, microtubules, axonal transport and AD.....	11
<b>Figure 1.5</b> Sequence homology of MAP2c and tau.....	17
<b>Figure 1.6</b> Actin filament turnover and the role of ADF/cofilin (AC).....	20
<b>Figure 1.7</b> Pathological features of human AD as seen by electron microscopy.....	24
<b>Figure 1.8</b> Amyloidogenic and non-amyloidogenic processing of APP.....	26
<b>Figure 3.1</b> Neuritic striations in human AD.....	66
<b>Figure 3.2</b> Neuropathological hallmarks of human AD can be recapitulated in ATP-deprived human and chick primary neurons.....	67
<b>Figure 3.3</b> Chicken tau is highly homologous to human and rodent tau.....	68
<b>Figure 3.4</b> Cell body F-actin labeling increases following ATP depletion.....	70
<b>Figure 3.5</b> Co-localization of actin, cofilin and ADF occurs in pMAP inclusions following ATP-depletion.....	72
<b>Figure 3.6</b> Co-localization of cofilin and pMAP occurs in ATP-depleted rat organotypic hippocampal slices.....	73
<b>Figure 3.7</b> pMAP and ADF/cofilin rods form after mitochondrial inhibition but tubulin remains uniformly distributed.....	74
<b>Figure 3.8</b> Optimizing fixing and permeabilization protocols for MAP and ADF/cofilin.....	75
<b>Figure 3.9</b> Mitochondrial inhibition induces activation of ADF/cofilin and is correlated to pMAP-positive rod formation.....	77

<b>Figure 3.10</b> Cofilin-GFP forms rods that sequester pMAP during ATP depletion.....	80
<b>Figure 3.11</b> pMAP is selectively sequestered into cofilin-GFP rods following ATP-depletion.....	82
<b>Figure 3.12</b> Reduction of the cellular ADF/cofilin pool inhibits the formation of rods and sequestration of pMAP.....	85
<b>Figure 3.13</b> Dynamic F-actin enhances pMAP and actin rod formation.....	89
<b>Figure 3.14</b> Amyloid peptides enhance pMAP sequestration to rods in primary chick neurons.....	92
<b>Figure 4.1</b> ATP reduction causes persistent phosphorylation of 12E8 epitope and dephosphorylation at other sites.....	110
<b>Figure 4.2</b> Specific phosphorylated forms of MAP/tau redistribute in neurons during ATP reduction.....	112
<b>Figure 4.3</b> AT100 labels a non-tau component in the nucleus during mitochondrial inhibition, actin depolymerization and in postmortem AD brain.....	114
<b>Figure 4.4</b> Distinct rod-shaped aggregates are specific to 12E8-MAP/tau and are best preserved with Triton-X permeabilization.....	117
<b>Figure 4.5</b> Recruitment of MAP/tau to AC rods during ATP reduction is specific for 'KXGS' phosphorylated species.....	119
<b>Figure 4.6</b> Rod-like accumulations in neurites of primary neurons contain densely packed filaments.....	121
<b>Figure 4.7</b> 12E8 MAP/tau but not other epitopes aggregates and co-localizes with AC rods during actin depolymerization.....	122
<b>Figure 5.1</b> The rodent hippocampus.....	137
<b>Figure 5.2</b> Western blot showing fractions of human A $\beta$ monomers (HA $\beta$ m) and dimer/trimers (HA $\beta$ d/t) purified from 10x concentrated culture medium of 7PA2 cells.....	144
<b>Figure 5.3</b> A $\beta$ d/t fraction from 7PA2 cells, but not monomer, induces rods in dissociated hippocampal neurons.....	148
<b>Figure 5.4</b> Dentate gyrus fields of view (FOV) for imaging and analysis.....	150



**Figure 5.5** Confirming expression of tau in human tau (htau) transgenic mice but not tau knockout (KO) mice.....152

**Figure 5.6** Organotypic rodent hippocampal brain slices.....154

**Figure 5.7** ATP-depletion induces cofilin rods in mouse organotypic hippocampal slices.....157

**Figure 5.8** Human A $\beta$  dimer/trimer (d/t) induces MAP/tau and cofilin rods in organotypic hippocampal slices of tau transgenic mice.....165-67

**Figure 6.1** Proposed mechanism of how AC rods might facilitate formation of AD tau pathologies.....182

**Table 5.1** Optimization studies for simultaneous preservation and visualization of MAP/tau and cofilin rod inclusions.....158

I would like to take this opportunity to formally thank and acknowledge my

provided me with reagents and cells to allow me to undertake this work:  
 Claire Goldsbury, Jim Bamburg, Laura Minamide, Othon Goryaino, De Lian  
 Goh, Ian Marsden, Karen Cullen, Gilles Guillemin, Eric Jeong, Paul Witting  
 and Shane Arora.

Individual contributions have been acknowledged in Figure Legends and/or  
 Materials & Methods sections.



## SUMMARY

Alzheimer's Disease (AD) is a devastating neurodegenerative disorder that is histopathologically characterized by several hallmark lesions, including extracellular plaques comprised of amyloid beta (A $\beta$ ) peptides, neurofibrils and intra-neuronal neurofibrillary tangles (NFTs) which are comprised of hyperphosphorylated microtubule-associated protein tau. Neurofibrils are one of the earliest lesions observed in AD brain and the extent of

### Author Contributions

I would like to take this opportunity to formally thank and acknowledge my colleagues and collaborators who have contributed to the work of this thesis or provided me with reagents and cells to allow me to undertake this work:

Claire Goldsbury, Jim Bamburg, Laurie Minamide, Othon Gervasio, De Lian Goh, Ian Marsden, Karen Cullen, Gilles Guillemin, Erica Jeong, Paul Witting and Shane Antao.

Individual contributions have been acknowledged in Figure Legends and/or Materials & Methods sections.

oxidative stress are common in AD and a growing body of evidence suggests these mitochondrial changes may play a central role in the pathogenesis of sporadic AD. The key question therefore is can mitochondrial dysfunction induce histopathological features of AD and if so, by what mechanisms? Answers to these important questions may be pivotal in the development of more effective AD therapeutics.

## SUMMARY

Alzheimer's Disease (AD) is a devastating neurodegenerative disorder that is histopathologically characterized by several hallmark lesions, including extracellular plaques comprised of amyloid beta ( $A\beta$ ) peptides, neuropil threads and intra-neuronal neurofibrillary tangles, both of which are comprised of hyperphosphorylated microtubule-associated (MAP) protein tau. Neuropil threads are one of the earliest lesions observed in AD brain and the extent of their presence correlates with cognitive decline and disease progression. In addition, rod-like aggregates of actin and actin depolymerizing factor (ADF)/cofilin ('AC' or 'cofilin' rods) have also been described throughout the neuropil of AD brains.

Sporadic AD accounts for over 90% of all AD cases and although aging has been identified as the most significant risk factor for developing this form of the disease, the pathogenic mechanisms involved in initiation of sporadic AD remain poorly understood. Decreased mitochondrial function and increased oxidative stress are common features of the aging brain and a growing body of evidence suggests these mitochondrial changes may play a central role in the pathogenesis of sporadic AD. The key question therefore is can mitochondrial dysfunction induce histopathological features of AD and if so, by what mechanisms? Answers to these important questions may be pivotal in the development of more effective AD therapeutics.



This thesis investigated the effects of mitochondrial dysfunction on the interrelationships between two AD-related cytoskeletal systems, MAP/tau and AC-actin. Employing primary neuron culture models, organotypic brain slice cultures and a range of immuno-labeling and microscopy techniques, we show that mitochondrial dysfunction rapidly induces rod-like aggregations of activated AC throughout neurites that subsequently recruit AD-relevant epitopes of phosphorylated MAP/tau. The resulting cytoskeletal complexes closely resemble neuropil threads observed in human AD brain. Mechanistically, the relationship between these inclusions was explored through use of actin-modifying drugs, knockdown of ADF/cofilin in primary neuron culture and knockout of tau in transgenic mouse brain slices. Overall, the results suggest that during neuronal stress, AC rods form rapidly and serve as a nucleation seed for subsequent recruitment of phosphorylated MAP/tau. Moreover, this initial recruitment is specific to MAP/tau phosphorylated in the functional microtubule-binding domain which is of significance, since this is one of the first phospho-sites identified during the early pathogenesis of AD tau pathology. Furthermore, treatments with synthetic or naturally-secreted preparations of A $\beta$  peptides induced the same effects in primary neuron and brain slice cultures, thus suggesting that the major histopathologies of AD may all be reconciled in one common pathway.

The studies reported here provide evidence suggesting that mitochondrial dysfunction is central to the pathogenesis of two AD-related cytoskeletal pathologies: MAP/tau neuropil threads and AC rods. Moreover, the results



presented here show for the first time that these two neuritic inclusions are closely interrelated and together implicate a disrupted cytoskeletal network that may account for the widespread axonal transport deficits and axonal degeneration characteristic of this disease. To that extent, we propose that association of MAP/tau and AC-actin proteins constitutes one of the earliest events in the pathogenesis of sporadic AD.

## PART II

1

**PART II**

## 1.1 A Global 'Epidemic'

Dementia is a progressive neurodegenerative disorder predominantly affecting older people, over 65 years. Alzheimer's disease (AD) is the most common type of dementia, accounting for over 60% of all reported cases and like other dementias, is characterized by progressive loss of memory, cognition and the ability to perform everyday activities. Currently, there are an estimated 35.6 million people with dementia worldwide, a figure which is conservatively projected to exponentially increase to over 115 million by 2050, largely owing to an ageing global population (Brookmeyer et al., 2007) (Alzheimer Disease International, World Alzheimer Report 2010 (International AD, 2010)). The total estimated worldwide economic burden of dementia in 2010 was \$184 billion, suggesting

# General Introduction

that this disorder should not only be considered a health and social issue in society, but one with serious economic impacts.

## 1.2 Neuropathology of AD

Macroscopically, the AD brain is characterized by progressive cerebral atrophy, particularly of the medial temporal lobes, including the hippocampus, entorhinal, perirhinal and parahippocampal cortices (Braak and Braak, 1991), structures that play a central role in memory function (Squire et al., 1993). In addition, reduced vascular perfusion and glucose metabolism in these regions are also features of the AD brain (Fig. 1.1) (Hock et al., 1996; Farkas and Luján, 2001;



## 1.1 A Global 'Epidemic'

Dementia is a progressive neurodegenerative disorder predominantly affecting older people, over 65 years. Alzheimer's disease (AD) is the most common type of dementia, accounting for over 60% of all reported cases and like other dementias, is characterized by progressive loss of memory, cognition and the ability to perform everyday activities. Currently, there are an estimated 35.6 million people with dementia worldwide, a figure which is conservatively projected to exponentially increase to over 115 million by 2050, largely owing to an ageing global population (Brookmeyer et al., 2007) (Alzheimer Disease International, World Alzheimer Report 2010 (International AD, 2010)). The total estimated worldwide cost of dementia in 2010 was US\$604 billion, suggesting that this disorder should not only be considered a health and social issue in society, but one with serious economic impacts.

## 1.2 Neuropathology of AD

Macroscopically, the AD brain is characterized by progressive cerebral atrophy, particularly of the medial temporal lobes, including the hippocampus, entorhinal perirhinal and parahippocampal cortices (Braak and Braak, 1991), structures that play a central role in memory function (Squire et al., 1993). In addition, reduced vascular perfusion and glucose metabolism in these regions are also features of the AD brain (Fig. 1.1) (Hock et al., 1996; Farkas and Luiten, 2001;

Mosconi, 2005), although whether these events are a direct cause or only a correlate of neuron loss and disease pathogenesis is contentious and the subject of ongoing research.

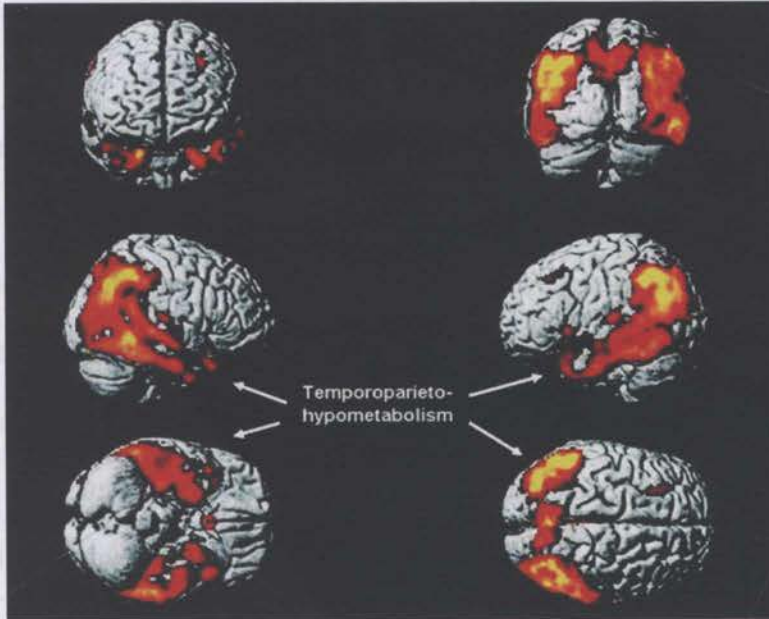


**Figure 1.1 Reduction in temporoparietal glucose metabolism in subjects with Alzheimer disease (AD).** Statistical parametric mapping (SPM) of fluoro-2-deoxy-D-glucose positron emission tomography (FDG-PET) images reveal relative reduction of glucose uptake in temporal, parietal and posterior cingulated cortices in AD subjects compared with healthy controls. Regions are illustrated in red and yellow, with yellow representing areas with the most significant reductions in glucose uptake. Source: (Edison et al., 2007).

Microscopically, AD is characterized by several hallmark lesions, namely neurofibrillary tangles (NFTs) and neuropil threads (NTs) comprised of hyperphosphorylated microtubule-associated protein (MAP) tau, neuritic plaques comprised of aggregated amyloid- $\beta$  ( $A\beta$ ) protein and Hirano bodies, paracrystalline intracellular inclusions containing actin and actin binding



proteins. Additionally, other changes in the actin cytoskeleton have been described in AD brain, which can be grouped and referred to as cofilin pathologies, because of changes in activity or organization of the actin binding protein cofilin (Bamburg and Bloom, 2009) (Fig. 1.2). These cytoskeletal pathologies are each discussed in further detail below. Decreased synaptic density is another histopathological feature of AD and constitutes one of the strongest anatomical correlates of cognitive impairment in this disease (Hsia et al., 1999; Mucke et al., 2000). An increasing body of evidence links cytopathologies with axonal transport defects (Praprotnik et al., 1996; Hiruma et al., 2003; Mandelkow et al., 2004; Baas and Qiang, 2005; Maloney et al., 2005; Zhang et al., 2005; Wirths et al., 2007; Vessel et al., 2010) (reviewed in (Bamburg and Bloom, 2009)) and is a likely mechanism contributing to synaptic decay and neuronal death in AD.

### 1.3 Familial and Sporadic AD

From a genetic standpoint, AD is a heterogeneous disorder with both familial and sporadic forms although by the disease end-stages, they are neuropathologically indistinguishable. Familial AD (FAD) is a very rare autosomal dominant disorder with an onset before age 65 years. A handful of mutations causing FAD have been identified in the amyloid precursor protein (*APP*) and the highly homologous presenilin 1 (*PSEN1*) and presenilin 2 (*PSEN2*) protein genes, all of which are involved in A $\beta$  metabolism. However,

combined, these mutations account for less than 1% of all AD cases (reviewed in (Harvey et al., 2003) and (Blennow et al., 2006)). Interestingly, although tau protein is a major constituent of hallmark lesions in AD, no FAD cases have been genetically linked to the tau protein locus, although other tau-related dementias such as frontotemporal dementia with Parkinsonism (FTDP) have (for reviews see (Buee et al., 2000; Lee et al., 2001)).

By contrast, sporadic AD (SAD) accounts for the vast majority of AD cases and while causes of this form remain more elusive, it is widely accepted that ageing is the most significant risk factor (Blennow et al., 2006). Apolipoprotein E (ApoE), a plasma protein involved in cholesterol transport, has also been identified as a risk factor for SAD, with a significantly amplified risk of developing the disease in heterozygous and homozygous carriers of the ApoE  $\epsilon 4$  allele (Corder et al., 1993). This allele, which is present in 15-27% of the general population occurs in 45-77% of AD patients, however since ApoE  $\epsilon 4$  is present in people who do not get the disease, this allele is considered a risk factor and not a determinant of AD (Lucotte et al., 1994). The majority of SAD cases are therefore most likely due to a complex relationship between ageing, genetic and environmental influences and associated pathological processes, including reduced cellular metabolism, increased oxidative stress, inflammation, altered gene expression and dysfunction of proteins. Some of these aspects are discussed in further detail below.



## 1.4 The microtubule associated protein (MAP) tau

## 1.4.1 Tau

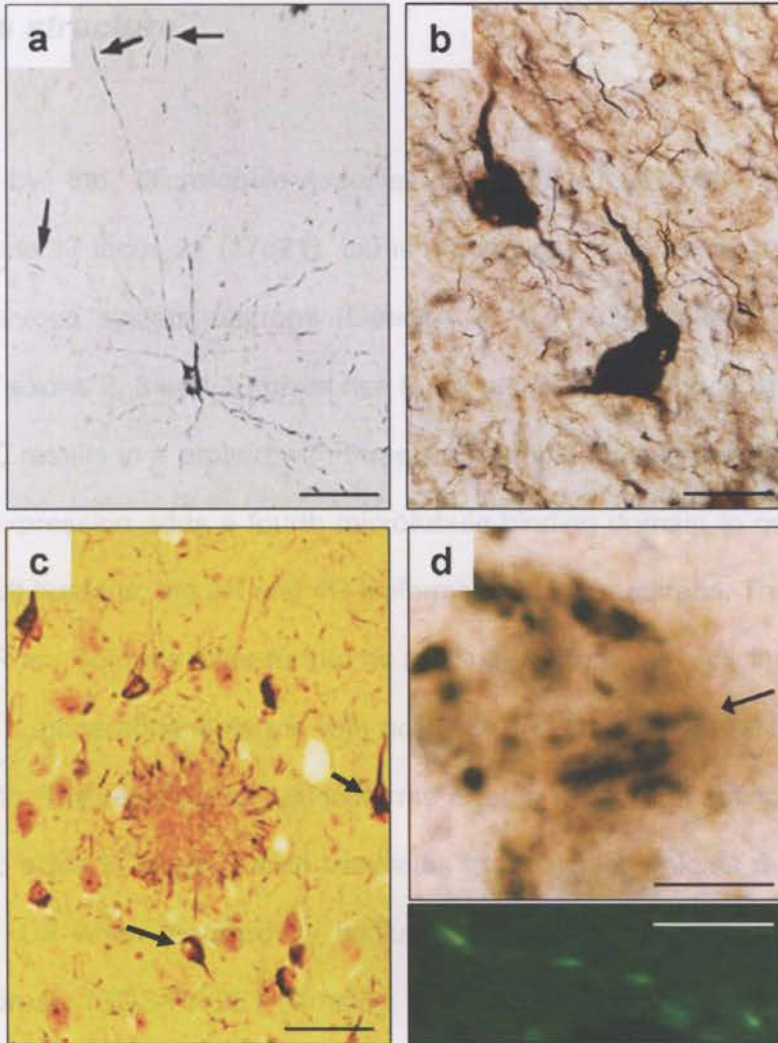


**Figure 1.2 Neuropathological hallmarks of AD.** Neuropil threads (**a**) are comprised of hyperphosphorylated tau that forms striated inclusions throughout neurites (**a**, arrows). Intracellular neurofibrillary tangles (NFTs; **b**) also contain hyperphosphorylated tau and take on a classic flame-shape appearance. Amyloid- $\beta$  plaques (**c**, centre) are extracellular aggregates that often appear in the vicinity of NFTs (**c**, arrows). Lesions in (**a-c**) visualized with silver staining. Aggregates of cofilin (**d**) often occur in linear arrays throughout neurites (arrow, upper panel), shown here amid an amyloid plaque (immunocytochemical label). Immunofluorescence (**d**, lower panel) revealing a tandem array of neuritic cofilin inclusions. Sources: (**a**, (Braak et al., 1994); **b**, author's own image; **c**, (Selkoe, 1998); **d**, (Minamide et al., 2000). Scale bars: (**a**, **c**) 100  $\mu$ M; (**b**) 20  $\mu$ M; (**d**) 10  $\mu$ M.

## 1.4 The microtubule associated protein (MAP) tau

### 1.4.1 Tau structure

Encoded by the *Microtubule-Associated Protein Tau (MAPT)* gene on chromosome 17 locus 21 (17q21), tau is predominantly expressed in axons of central nervous system neurons (Goedert et al., 1989). Alternative mRNA splicing of exons 2, 3 and 10 gives rise to six tau isoforms (Fig. 1.3). Exclusion of exon 10 results in a protein with three microtubule-binding repeats (3R tau), while its expression adds a fourth microtubule-binding domain to generate 4R tau. In adult humans, the 3R and 4R isoforms exist in equal ratio. The triplets of 3R and 4R tau isoforms differ further as a result of alternative splicing of exon 2 and exon 3, generating isoforms with no (0N), one (1N) or two (2N) 29-amino acid inserts. The resulting six tau isoforms exist in range 353 amino acids and 441 amino acids in length, which translates to molecular weights ranging from 45 to 65 kDa when resolved by sodium dodecyl sulfate polyacrylamide gel electrophoresis (SDS-PAGE) (Goedert et al., 1989). Tau has two functional domains - the carboxy-terminal microtubule-binding domain (MTBD) and an amino-terminal projection domain.

The two main regions in the so-called microtubule binding domain (MTBD) induces polymerization and stabilization of MT, while unfolding enables depolymerization and thus extensive rearrangements of MT within the cell (Nicolson and Mieschner, 1984; Lee et al., 1989; Drachet et al., 1992) (Fig. 1.4). Tau thus plays an essential role in axonal development, elongation and organization (Brandt and Lee, 1993).



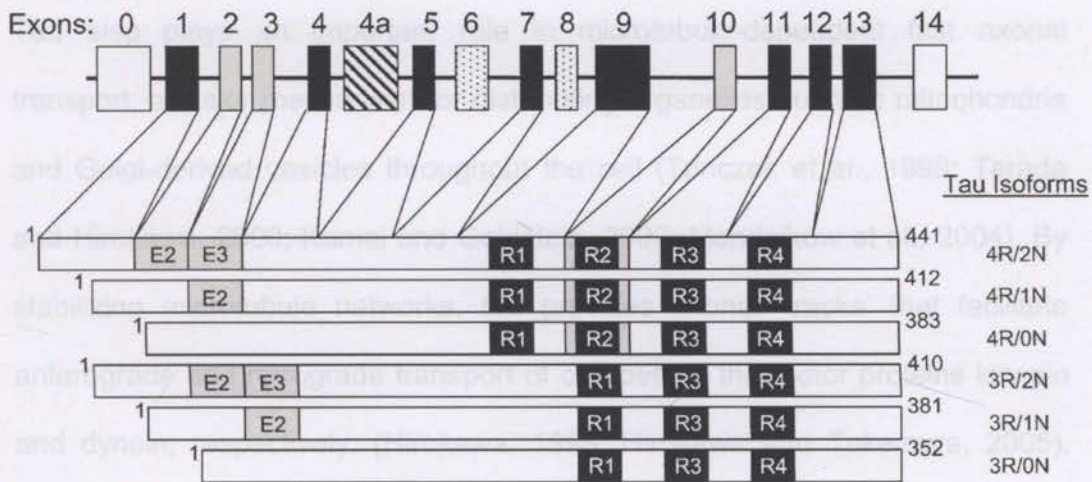


**Figure 1.3 Schematic representation of the human tau gene and the six central nervous system (CNS) tau isoforms.** Alternative mRNA splicing of exons 2, 3 and 10 generates isoforms containing zero (0N), one (1N) or two (2N) amino terminal inserts and either three (3R) or four (4R) microtubule-binding domains comprised of 18-amino acid repeats (black bars). Source: (Lee et al., 2001)

### 1.4.2 Functions of tau

Tau is a cytoskeletal 'structural MAP' protein predominantly expressed in axons of CNS neurons. The best characterized function of tau is its role in facilitating microtubule (MT) dynamics by enabling polymerization and depolymerization of  $\alpha$ - and  $\beta$ -tubulin polypeptide chains (Weingarten et al., 1975; Cleveland et al., 1977). Binding of tau via repeat regions in the so-called microtubule binding domain (MTBD) induces polymerization and stabilization of MT, while unbinding enables depolymerization and thus extensive rearrangements of MT within the cell (Mitchison and Kirschner, 1984; Lee et al., 1989; Drechsel et al., 1992) (Fig. 1.4). Tau thus plays an essential role in axonal development, elongation and organization (Brandt and Lee, 1993).



Tau also plays an important role in microtubule-dependent fast axonal transport, a major mechanism for distributing organelles such as mitochondria and Golgi-derived vesicles throughout the cell (Trinczek et al., 1999; Terada and Hirokawa, 2000; Kamal and Goldstein, 2002; Mandelkow et al., 2004). By stabilizing microtubule networks, tau provides axonal 'tracks' that facilitate anterograde and retrograde transport of cargoes by the motor proteins kinesin and dynein, respectively. (Hirokawa, 1998; Hirokawa and Takemura, 2005). Moreover, tau has been shown to influence cellular cargo trafficking more directly by influencing the activity of kinesin and to a lesser extent, dynein. Studies show that tau over-expression primarily inhibits kinesin motor activity, leading to a gradual accumulation of mitochondria, APP vesicles and other organelles near the cell body (Ebner et al., 1998; Seitz et al., 2002; Stamer et al., 2002; Baas and Qiang, 2005). Mechanistically, tau is proposed to induce these effects either by aggregating and creating physical 'obstacles' to kinesin molecules as they 'walk' along MTs (Dixit et al., 2008), by MTBD interactions with the kinesin complex constituent c-Jun N-terminal kinase-interacting protein 1 (JIP1) (Ittner et al., 2009), or a combination of both.

Figure 1.4 Model showing relationship between tau, microtubules, axonal transport and AD. In the dephosphorylated state, tau binds and stabilizes microtubules (MTs), red and blue. A large body of work supports a role for tau in binding and cross-linking actin filaments (Griffith and Pollard, 1978, 1982; Selden and Pollard, 1983; Selden and Pollard, 1986; Correas et al., 1990; Yamauchi and Purich, 1993; Farias et al., 2002; Dehmelt and Halpain, 2004b; Fulga et al., 2006), a function which is predominantly attributed to the MTBD (Correas et al., 1990; Moraga et al.,

1993), although more recent studies also indicate a role for the proline (Pro)-rich region of the N-terminus in binding actin (He et al., 2009). Through these interactions, tau proteins may indeed facilitate complex interactions between microtubules and actin polymers in the organization of the neuronal cytoskeletal network.

Independent monoclonal antibodies against tau, mass spectrometry and sequencing, over thirty phosphorylation sites have been described, all of which are localized outside the MTBD with the exception of a few, most notably Ser262 in the first repeat region and Ser356 in the fourth

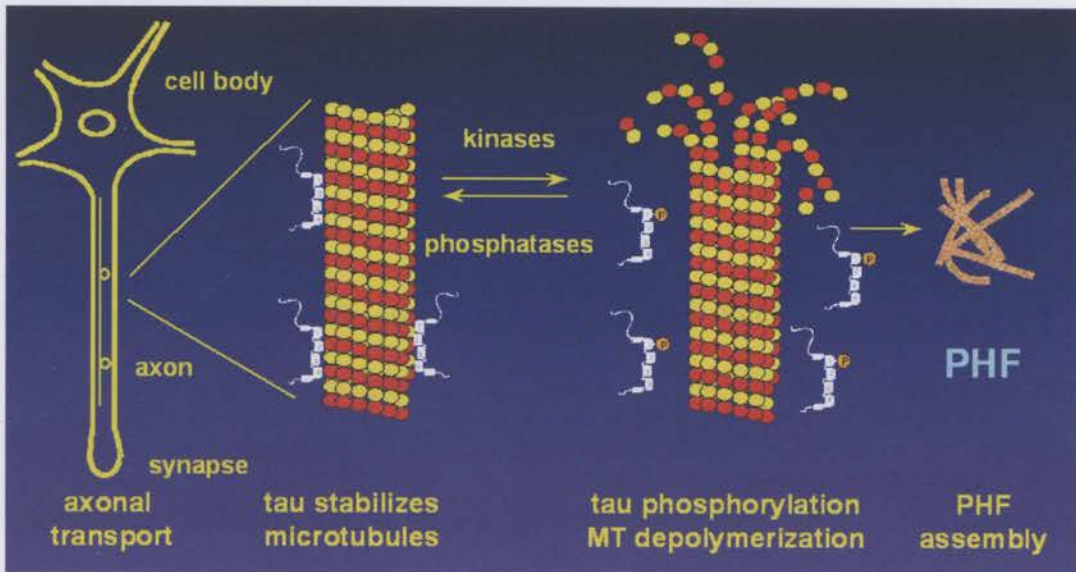


**Figure 1.4 Model showing relationship between tau, microtubules, axonal transport and AD.** In the dephosphorylated state, tau binds and stabilizes microtubules (MTs; red and yellow subunits) via the microtubule binding domain (MTBD; depicted by white boxes). Phosphorylation of crucial MTBD sites by kinases detaches tau from MTs, inducing MT disassembly. In AD, hyperphosphorylation of these sites induces MT breakdown, impaired axonal transport and accumulation of tau aggregated into paired helical filaments (PHFs). Source: Max-Planck-Unit for Structural Molecular Biology, Hamburg Germany. [http://www.mpasmb-hamburg.mpg.de/webpage\\_tau/hypothese](http://www.mpasmb-hamburg.mpg.de/webpage_tau/hypothese).



### 1.4.3 Phosphorylation regulates tau function

There are seventy nine putative Serine (Ser) or Threonine (Thr) phosphorylation sites on the longest brain tau isoform (441 amino-acids). Using phosphorylation-dependent monoclonal antibodies against tau, mass spectrometry and sequencing, over thirty phosphorylation sites have been described, all of which are localized outside the MTBD with the exception of a few, most notably Ser262 in the first repeat region and Ser356 in the fourth repeat. Most of these phosphorylation sites are on Ser-Pro and Thr-Pro motives (Goedert et al., 1994) (reviewed in (Mandelkow et al., 1995; Buee et al., 2000)).

In its dephosphorylated state, tau is able to bind and promote MT polymerization, while phosphorylation decreases its MT binding affinity and facilitates depolymerization (Lindwall and Cole, 1984; Drechsel et al., 1992). Specifically, phosphorylation in the MTBD, particularly at Ser262, strongly reduces the binding affinity of tau to MT, induces rapid MT disassembly and concomitant self-assembly of MTBD-phosphorylated tau (Biernat et al., 1993; Seubert et al., 1995; Drewes et al., 1997; Alonso et al., 2001; Zhou et al., 2006; Fischer et al., 2009). Under normal physiological conditions, tau is heterogeneously phosphorylated such that some but not all sites are phosphorylated at any given time. It is estimated that generally only 20-50% of intracellular tau is attached to MTs with the remaining unbound tau existing in a



relatively unfolded conformation in the cytosol (Cleveland et al., 1977; Ferreira et al., 1989; Mukrasch et al., 2009).

The different states of tau phosphorylation result from the activity of specific kinases and phosphatases towards these sites. Most of the kinases involved are part of the proline-directed protein kinase family which target Ser/Thr-Pro sites and include mitogen activated protein kinase (MAPK), glycogen synthase kinase 3 (GSK3) and cyclin dependent kinases 2 and 5 (cdk2 and cdk5) (Drewes et al., 1992; Baumann et al., 1993; Planel et al., 2002). Additionally, stress-activated protein kinases (SAPK) also phosphorylate tau (Buee-Scherrer and Goedert, 2002; Yoshida and Goedert, 2006) and together, these kinases generate most Alzheimer-related epitopes. The family of kinases that phosphorylate Ser residues of the MTBD 'KXGS' motifs, thereby inducing dissociation of tau from MTs is the so-named MAP/microtubule affinity regulating kinase (MARK) (Drewes et al., 1997; Biernat et al., 2002; Mandelkow et al., 2004). All of these sites can be cleared by protein phosphatase 2A (PP2A) and calcineurin (Drewes et al., 1993; Goedert et al., 1995; Sontag et al., 1996; Gong et al., 2000) and to this extent, it is the fine balance between kinase and phosphatase activity that regulates the physiological functions of tau and a dynamic MT cytoskeleton.

#### 1.4.4 Abnormal tau pathology in AD

In AD, tau becomes hyperphosphorylated at both physiological and abnormal 'non-physiological' sites and aggregates into the non-soluble hallmark lesions neuropil threads and NFTs, as mentioned above (for reviews see (Goedert, 1993; Goedert et al., 1994; Buee et al., 2000; Lee et al., 2001)) (Fig. 1.2a, b) . The sequence of tau cytoskeletal changes during the progression of AD is well-documented and is closely correlated to cognitive decline, according to six *Braak Stages* (Braak and Braak, 1991; Braak et al., 1993; Braak and Braak, 1995; Braak and Braak, 1997; Braak et al., 2006). In the earliest stages of AD, abnormal dystrophic neurites or 'neuropil threads' (NTs) are common and widespread throughout ventromedial temporal lobe and association cortices, appearing before 'pre-tangle' and NFT inclusions (Arnold et al., 1991; Braak and Braak, 1991; Schmidt et al., 1993; Velasco et al., 1998; Mitchell et al., 2000). By end-stage AD, these lesions comprise over 85% cortical tau pathology (Giannakopoulos et al., 2007). Ultrastructurally, the dominant components of NTs are initially straight and twisted filaments which most likely progress into the paired helical filaments (PHFs) observed in NTs of later-stage AD (Perry et al., 1991). PHFs are composed of two strands of tau filament twisted around one another with a periodicity of 80 nm and a width varying from 8 to 20 nm (Fig. 1.7b), whereas straight filaments lack this helical periodicity (Crowther, 1991; Crowther and Goedert, 2000).



Subsequent to appearance of NT, small somal granular inclusions of hyperphosphorylated tau become apparent, developing into loosely packed fibrils in the somatodendritic compartment and later, into densely-packed PHFs that displace the nucleus and cytoplasm and give rise to the classic flame-shaped NFTs (Braak et al., 1994; Braak et al., 2006). By late-stage AD, NFTs extrude into the extracellular space and are referred to as “ghost tangles”.

Whether hyperphosphorylation is a cause or consequence of tau aggregation is still unclear, but mounting evidence suggests that abnormal hyperphosphorylation precedes tau deposition in AD brain (Braak et al., 1994; Augustinack et al., 2002) (also reviewed in (Lee et al., 2001; Avila et al., 2004)). It is hypothesized that hyperphosphorylation specifically in the MTBD detaches tau from MTs which in turn increases the unbound pool of tau and its propensity to self-aggregate, ultimately forming PHFs and straight filaments (Biernat et al., 1993; Alonso et al., 2001; Fischer et al., 2009) (Fig 1.4). As such, this MTBD-hyperphosphorylation is purported to constitute one of the first pathological changes in the initiation of AD cytopathology. This hypothesis is supported by studies showing that S262 in the MTBD is one of the most prominent sites of tau phosphorylation in neuropil threads and ‘pre-tangles’ in brains of early-AD cases (Augustinack et al., 2002).



### 1.4.5 A note on other structural MAPs

In addition to tau, several other types of MAPs are found in eukaryotes, including MT plus-end-binding proteins, centrosome-associated proteins, enzymatically active MAPs and structural MAPs (reviewed in (Tucker, 1990; Dehmelt and Halpain, 2004a)). Closely related to tau is the structural MAP2 family which in vertebrates includes MAP4 and four isoforms of MAP2 proteins (MAP2a-d). Like tau, this family is best known for their MT-stabilizing activity and for their role in regulating MT networks in axons and dendrites of neurons (Dehmelt and Halpain, 2004a). Whereas MAP2 and tau are found in neurons, MAP4 is present in many other tissues but is generally absent from neurons. MAP2 has four alternative spliced forms all of which share a conserved carboxy-terminal domain with tau that contain three or four 18-residue MT-binding repeats with 'KXGS' motifs, separated by 13-14 residue inter-repeats (IRs) (Lewis et al., 1988; Kindler and Garner, 1994; Al-Bassam et al., 2002) (Fig. 1.5). Amino terminal projections in tau and MAP2 isoforms vary in size. The main MAP2 isoforms are MAP2c which is relatively short, composed of several bands around 70 kDa in SDS-PAGE and predominantly expressed during embryonic brain development, and MAP2a/b, which are substantially larger (~280 kDa) and expressed in both the developing and adult brain (Riederer and Matus, 1985; Kindler and Garner, 1994). Interestingly, MAP2 like tau, has been shown to interact with and bundle F-actin *in vitro* (Griffith and Pollard, 1982; Correias et al., 1990; Yamauchi and Purich, 1993), a property

which was attributed specifically to MAP2c via its MTBD (Ozer and Halpain, 2000; Roger et al., 2004). Although no MAP2 pathology has been described in AD or other tau-related dementias (Dehmelt and Halpain, 2004a), we cannot conclusively rule out a role for this protein family in cytopathological pathways and as such, these MAPs are one consideration of the current study.

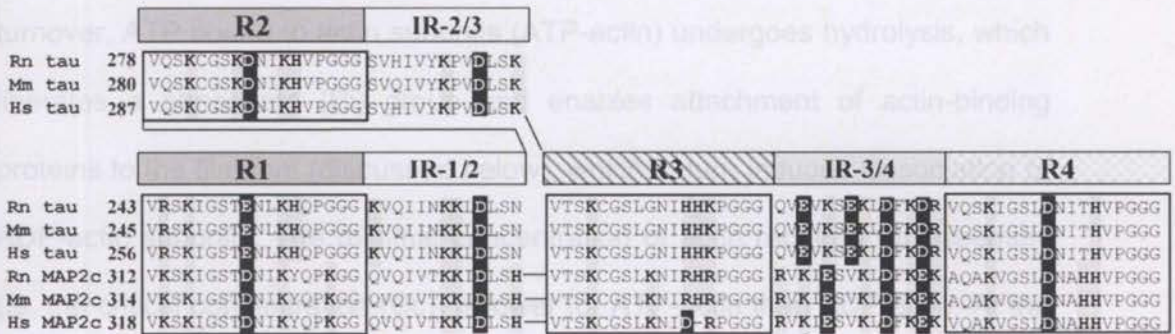


**Figure 1.5 Sequence homology of MAP2c and tau.** Microtubule binding domain (MTBD) repeats and inter-repeat regions (IRs) of MAP2/tau have higher homology across species than with neighbouring MTBD repeats and IRs. MAP2c/tau sequence alignments are shown for human (Hs), mouse (Mm), and rat (Rn) sequences of three-repeat MAP2c and four-repeat tau genes. Schematic diagram of MTBD repeats (labelled R1–R4) and IRs are shown above aligned sequences (the IR between repeats 3 and 4 is designated "IR-3/4", etc). The comparison suggests that R2, IR-2/3 modules have higher homology to R1, IR-1/2 modules than to R3, IR-3/4 modules, respectively. Source: (Al-Bassam et al., 2002).



## 1.5 Actin and Actin Depolymerizing Factor (ADF)/Cofilin

### 1.5.1 Actin and ADF/cofilin (AC) structure

Actin is a major constituent of the cytoskeleton in almost all eukaryotic cells. Existing either in monomeric globular form (G-actin) or filamentous form (F-actin), actin is highly dynamic and undergoes constant cycles of polymerization and depolymerization, a process known as filament turnover. During filament turnover, ATP bound to actin subunits (ATP-actin) undergoes hydrolysis, which liberates a phosphate ( $P_i$ ) group and enables attachment of actin-binding proteins to the filament (discussed below), which in turn induces dissociation of ADP-actin subunits. The minimal concentration of actin required for assembly (ie. the critical concentration ( $C_c$ )) is lower for ATP-actin than ADP-actin. At the  $C_c$  of the filament end, the rate of subunit addition to the end of the filament equals the rate of subunit dissociation from the same end. Net F-actin polymerization occurs when the G-actin concentration is higher than  $C_c$  and net depolymerization occurs when the G-actin concentration is lower than  $C_c$  (Wegner, 1982) (Fig. 1.6). Filaments have a pointed 'minus' end where addition of G-actin subunits is relatively slow, and a barbed 'plus' end that is fast-growing. At steady state, G-actin concentration is such that a net assembly of subunits equals net disassembly at the minus end, a process called treadmilling, whereby F-actin length remains relatively constant (Carlier and Pantaloni, 1997; Carlier et al., 1999; Chen et al., 2000).

ADF/cofilin (AC), members of the actin binding protein family, enhance filament turnover by binding and severing F-actin, liberating G-actin and generating more filament ends for assembly or disassembly (Fig. 1.6). ADF was first isolated from embryonic chick brain in 1980 and named for its ability to depolymerize low concentrations of F-actin into G-actin (Bamburg et al., 1980). Cofilin-1 was isolated 4 years later from porcine brain and named for its ability to co-sediment with F-actin (co-filamentous with actin) (Maekawa et al., 1984). Further characterization showed that both ADF and cofilin-1 could enhance F-actin turnover. Although encoded for by different genes, ADF and cofilin isoforms from the same species have about 70% amino acid sequence identity. Isoforms are differentially expressed between species where, for example, mammalian neurons contain around 5 to 10-fold more cofilin than ADF (Minamide et al., 2000; Garvalov et al., 2007), while chick neurons contain 3-fold more ADF than cofilin (Devineni et al., 1999). One of the most highly conserved regions of AC between species is the known actin-binding domains, including the single regulatory Ser3 phosphorylation site, discussed below (Bamburg, 1999; Bamburg and Bernstein, 2008).

### **1.5.2 A note on nomenclature**

Generally, references to ADF/cofilin here will be abbreviated to 'AC'. When specifically referring to human or rodent neurons however, the term 'cofilin' will be used interchangeably with 'AC' in this thesis, since mammalian neurons



contain around 5-10 fold more cofilin than ADF. Conversely, when referring to chicken neurons, which contain 3-fold more ADF than cofilin, the term 'ADF' will be used interchangeably with 'AC'.

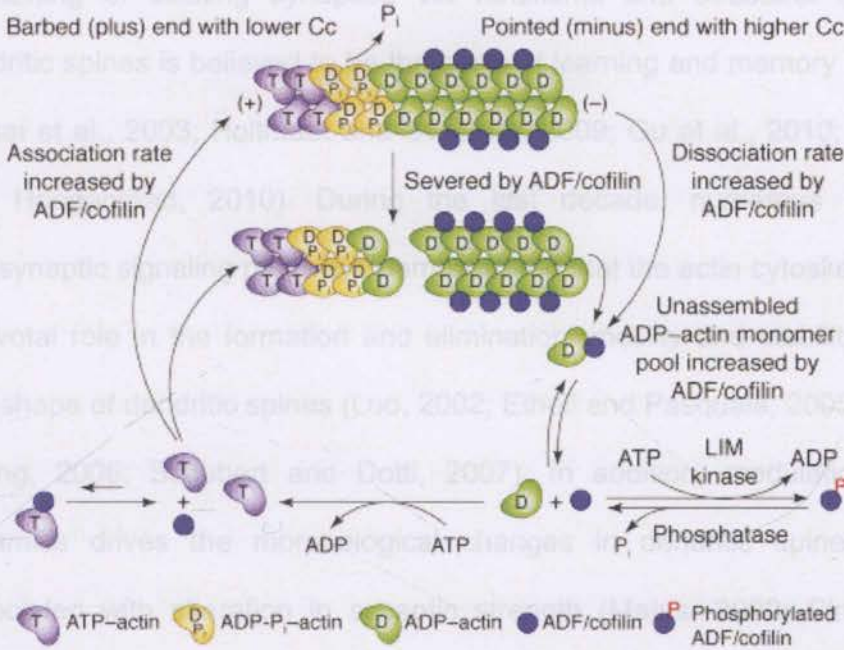


**Figure 1.6 Actin filament turnover and the role of ADF/cofilin (AC).** AC binding increases the dissociation rate at the pointed (minus) end and can enhance the association rate at the barbed (plus) end. The dissociation of phosphate (Pi) from ADP-Pi-actin filaments promotes AC binding to the filament. Filament severing by AC creates short filaments with additional free pointed and barbed ends that can contribute to enhanced turnover. Phosphorylation of AC prevents its association with ADP-actin, while dephosphorylation reactivates it to bind and depolymerize actin filaments. Cc, critical concentration. Source: (Chen et al., 2000).

### 1.5.3 Functions of Actin and AC

In neurons, F-actin turnover in response to extracellular signals underlies a wide variety of basic cellular processes including morphogenesis and modulation of dendritic spine architecture. The capacity of neurons to function within neuronal circuits is mediated via synapses, such that strengthening or weakening of existing synapses via functional and structural changes of dendritic spines is believed to be the basis of learning and memory in the brain (Kasai et al., 2003; Holtmaat and Svoboda, 2009; Gu et al., 2010; Hotulainen and Hoogenraad, 2010). During the last decade, numerous studies on postsynaptic signaling pathways demonstrated that the actin cytoskeleton plays a pivotal role in the formation and elimination, motility and stability, and size and shape of dendritic spines (Luo, 2002; Ethell and Pasquale, 2005; Tada and Sheng, 2006; Schubert and Dotti, 2007). In addition, modulation of actin dynamics drives the morphological changes in dendritic spines that are associated with alteration in synaptic strength (Matus, 2000; Cingolani and Goda, 2008). At synapses, the actin cytoskeleton does not only contribute to overall structure of synapses but also plays important roles in synaptic activities that range from organizing the postsynaptic density (Sheng and Hoogenraad, 2007) and anchoring postsynaptic receptors (Renner et al., 2008) to facilitating the trafficking of synaptic cargos (Schlager and Hoogenraad, 2009).

The actin-modulating activity of AC is negatively regulated by phosphorylation of the highly conserved Ser3 by LIM (Lin-11, Isl-1 and Mec-3) kinase which



prevents AC from binding (Carrier et al., 1997; Bamburg, 1999; Bamburg and Bernstein, 2008). Dephosphorylation by slingshot or chronophin phosphatases (Bamburg and Bernstein, 2008; Huang et al., 2008) enables AC to bind a slightly twisted form of F-actin, thus stabilizing the twisted state, enhancing severing and disassembly (McGough et al., 1997) (Fig 1.6).

#### **1.5.4 Actin and AC Abnormalities in AD**

Cofilin-actin enriched inclusions are a common feature observed in AD brain, often taking on the form of rod-shaped bundles of filaments throughout neurites (Bamburg and Wiggan, 2002; Maloney and Bamburg, 2007). Tandem arrays of cofilin-immunostaining occur in neurites of the hippocampus and frontal cortex of human AD but not human control brain (Minamide et al., 2000) (see also Fig. 1.2d). EM analysis of AC rods in rat hippocampal brain slices (Davis et al., 2009) and 'likely' cofilin rods observed in human AD brain tissue (Fig 1.7a) implicate a disrupted actin cytoskeletal network. Since synaptic dysfunction is one of the most established correlates of cognitive decline in AD (Terry et al., 1991) and since AC rods induced in primary neuron culture have been shown to block axonal transport (Maloney et al., 2005), formation of neuritic cofilin rods in AD neurons and the resulting defects in transport of vital cellular cargoes to the synapse is one proposed mechanism by which cofilin rods may effect synaptic decay in the disease (Bamburg and Bloom, 2009;

Bamburg et al., 2010). This is supported by recent studies in *Aplysia kurodai* neurons whereby microinjection of cofilin led to cofilin rod formation, synapse loss and distal to the rod, impairment of synaptic plasticity and LTP, as measured by electrophysiological methods (Jang et al., 2005). In addition, abnormalities in cofilin regulatory mechanisms have also been reported in AD brain. Marked downregulation of the upstream cofilin phosphorylation modulator p21-activated kinase (PAK) has been reported in AD brains, which could lead to enhanced cofilin activity and rod formation (Zhao et al., 2006). Similarly, a decrease in cofilin-related microRNAs (miRNAs), short non-coding RNAs that bind and repress mRNA translation, were recently described in postmortem AD brain (Wang et al., 2008a; Nelson and Wang, 2010; Yao et al., 2011). Specifically, reduced levels of miRNA miR-107 which is tantamount to increased cofilin protein expression (Yao et al., 2011), were identified in temporal cortical samples from human AD cases (Wang et al., 2008a; Nelson and Wang, 2010). Decreased levels of miR-107 and miR-103 were subsequently reported in a transgenic mouse model of AD, which was associated with an increase in cofilin activation and formation of cofilin rods (Yao et al., 2011). Given the vital role of cofilin-actin in the organization and function of dendritic spines as discussed above, it follows that abnormalities in cofilin expression, activity and distribution in AD brain may indeed play a central role in memory deficits characteristic of this disease.



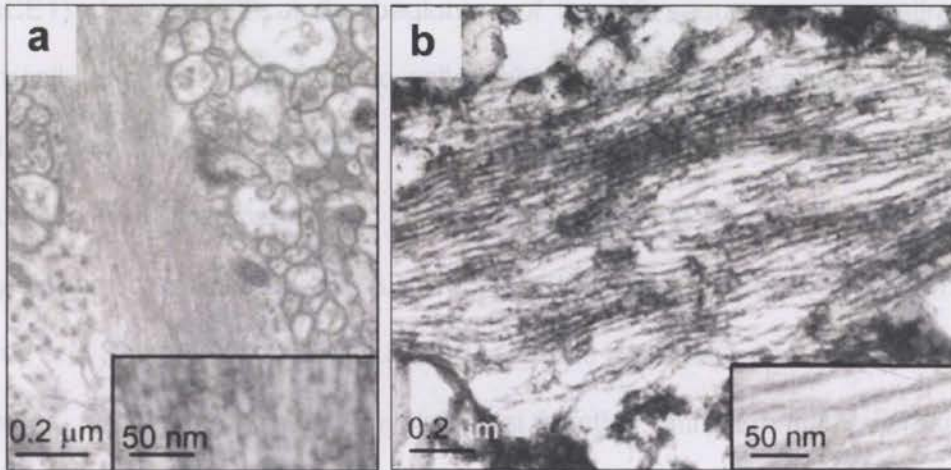


**Figure 1.7 Pathological features of human AD as seen by electron microscopy.** (a) A likely cofilin-actin rod with a morphology identical to those induced in organotypic rat brain slices (Davis et al., 2009). Inset at higher magnification shows filaments are thinner (8-9 nm) than tau-containing paired helical filaments (b), which are comprised of 20 nm-wide twisted ribbon-like structures (better seen in magnified inset). Source (adapted here): (Bamburg and Bloom, 2009).

## 1.6 Amyloid-beta ( $A\beta$ ) in AD

### 1.6.1 The Amyloid Cascade Hypothesis

$A\beta$ , the major constituent of extracellular plaques in both familial and sporadic AD (Fig. 1.2c), is derived from the amyloid- $\beta$  precursor protein (APP). APP is an integral membrane protein with a single membrane-spanning domain, a large extracellular N-terminus and shorter cytoplasmic C-terminus. The amyloidogenic processing of APP involves two sequential cleavages by the  $\beta$ - and  $\gamma$ -secretases at the N- and C-termini of APP respectively. The  $\beta$ -secretase

(BACE1) cleaves APP at the beginning of the A $\beta$  sequence, generating an extracellular soluble fragment, so-called s $\beta$ APP, and an intracellular C-terminal end, termed C99. C99 is further cleaved within the membrane, by  $\gamma$ -secretase, producing A $\beta$  fragments of different length, the most common and amyloidogenic species being A $\beta_{40}$  and A $\beta_{42}$  (Haass et al., 1992; Selkoe, 1998; Hardy and Selkoe, 2002) (Fig. 1.8). Indeed A $\beta$  is a normally secreted product in neurons, suggesting it has a physiological function, although little is presently known about these possible roles. Early onset FAD is linked with high penetrance to mutations that lead to increased production of A $\beta_{1-42}$ , greater propensity of A $\beta$  to form fibrils or decreased capacity for A $\beta$  clearance/degradation (reviewed in (Hardy and Selkoe, 2002; Goedert and Spillantini, 2006)). Around 20 mutations have been identified in the *APP* gene, but by far the most common cause of FAD are mutations in the *presenilin-1* gene, with over 160 mutations identified to date (reviewed in (Goedert and Spillantini, 2006)). Presenilin proteins are central components of the complexes responsible for  $\gamma$ -secretase cleavage of APP.

The 'amyloid cascade hypothesis' (or 'A $\beta$  cascade hypothesis') holds that cerebral A $\beta$  induces other AD-related pathological changes such as tau hyperphosphorylation/aggregation, mitochondrial dysfunction or physical disruption/dystrophy of neurites, and that cumulative effects over years to decades exacerbates cognitive decline, neurodegeneration and further plaque deposition (Hardy and Selkoe, 2002; Vickers et al., 2009). In this respect, familial forms of AD are more easily accounted for with regards to role of A $\beta$



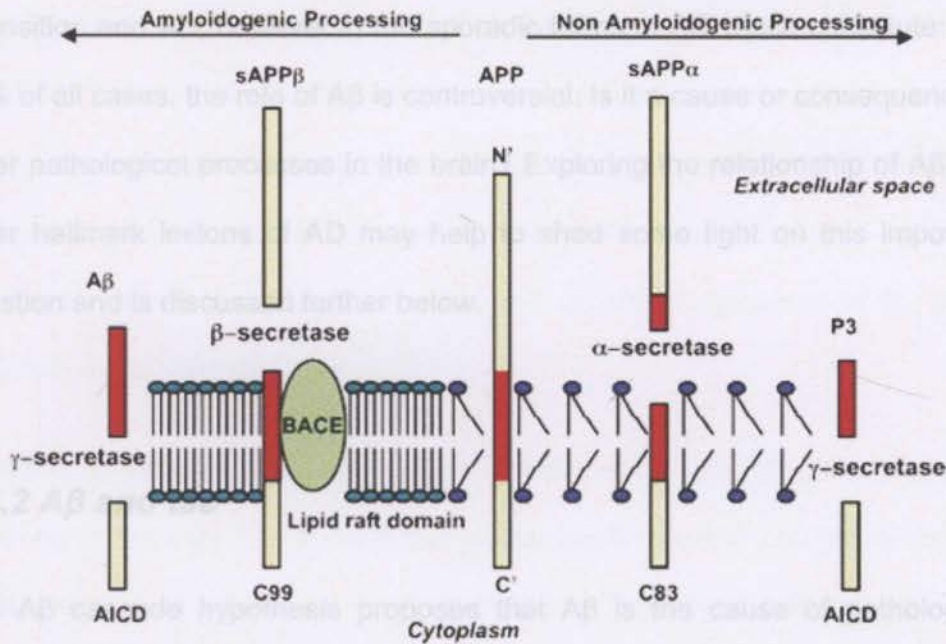


**Figure 1.8 Amyloidogenic and non-amyloidogenic processing of APP.** The transmembrane protein APP is cleaved by α-secretases in cholesterol- and sphingolipid-poor domains and by β-secretase (BACE) in lipid rafts domains generating the correspondent C-terminal fragments (CTFs) C83 and C99 and the large ectodomains sAPPα and sAPPβ respectively. α-cleavage of APP precludes the formation of Aβ. γ-secretase cleavage of C83 results in the release of P3. Aβ is the result of γ-secretase activity of sAPPβ. In both pathways γ-secretase releases APP intracellular domain (AICD), which may be involved in nuclear signaling. Source: (Posse de Chaves, 2006).

The 'amyloid cascade hypothesis' (or 'Aβ cascade hypothesis') holds that cerebral Aβ induces other AD-related pathological changes such as tau hyperphosphorylation/aggregation, mitochondrial dysfunction or physical disruption/dystrophy of neurites, and that cumulative effects over years to decades exacerbates cognitive decline, neurodegeneration and further plaque deposition (Hardy and Selkoe, 2002; Vickers et al., 2009). In this respect, familial forms of AD are more easily accounted for with regards to role of Aβ

deposition and AD, however in the sporadic forms of AD which constitute over 90% of all cases, the role of A $\beta$  is controversial. Is it a cause or consequence of other pathological processes in the brain? Exploring the relationship of A $\beta$  and other hallmark lesions of AD may help to shed some light on this important question and is discussed further below.

and cognition (Roberson et al., 2007; Roberson et al., 2011).

Emerging evidence suggests that instead, it is an integral synergistic relationship between tau and A $\beta$  that is responsible for the detrimental effects

### **1.6.2 A $\beta$ and tau**

The A $\beta$  cascade hypothesis proposes that A $\beta$  is the cause of pathological changes in tau. This theory is best supported by studies showing that presence of A $\beta$  either by direct intracerebral A $\beta$  injections or expression of mutant APP exacerbates hyperphosphorylation of tau and neurofibrillary tangle (NFT) formation in tau transgenic mice (Goetz et al., 2001; Lewis et al., 2001). Similarly, a triple transgenic mouse model showed that deposition of fibrillar A $\beta$  occurred before the appearance of tau pathology and memory deficits (Oddo et al., 2006). In AD human brain, familial 'amyloidogenic' PS1 mutations have been shown to induce significantly greater numbers of tau-positive NFTs and dystrophic neurites when compared to sporadic 'idiopathic' AD cases (Woodhouse et al., 2009).

for (NMDA-R)-mediated postsynaptic excitotoxicity (Ittner et al., 2010), synaptic transmission and plasticity defects (Roberson et al., 2011) and learning and memory deficits (Roberson et al., 2011; Roberson et al., 2011). This apparently synergistic relationship between tau and A $\beta$  that proven to be poor correlates of cognitive impairment (McLean et al., 1999) and leads to synaptic decay might be mediated by Fyn tyrosine kinase, a substrate that rather the presence of tau pathology, both NFTs and NTs, is a far more



reliable correlate, as discussed in Section 1.4 (Braak and Braak, 1995; Velasco et al., 1998; Braak et al., 2006). Furthermore, evidence for the principal role of tau in neurodegeneration lies in studies that have shown that reducing endogenous tau levels in AD mouse models ameliorates A $\beta$ -induced deficits at the level of synapses, neural networks and cognition (Roberson et al., 2007; Roberson et al., 2011).

Burgeoning evidence suggests that instead, it is an integral synergistic relationship between tau and A $\beta$  that is responsible for the detrimental effects in AD neurons. A substantial number of studies suggest an integral role of tau in mediating the neurotoxic effects of A $\beta$  (Goetz et al., 2001; Lewis et al., 2001; Rapoport et al., 2002; Oddo et al., 2003; King et al., 2006; Oddo et al., 2006; Roberson et al., 2007; Amadoro et al., 2009; Ittner et al., 2010; Vossel et al., 2010; Roberson et al., 2011; Shipton et al., 2011). A $\beta$  oligomers have been shown to induce tau hyperphosphorylation (De Felice et al., 2008; Amadoro et al., 2009; Tomiyama et al., 2010; Shipton et al., 2011), tau missorting into the somatodendritic compartment and microtubule breakdown (Zempel et al., 2010). Furthermore, reduction of tau in human APP (hAPP) transgenic mice over-expressing A $\beta$  ameliorates axonal transport defects (Vossel et al., 2010), *N*-methyl-d-aspartate receptor (NMDA-R)-mediated postsynaptic excitotoxicity (Ittner et al., 2010), synaptic transmission and plasticity defects (Roberson et al., 2011) and learning and memory deficits (Roberson et al., 2007; Roberson et al., 2011). This apparently synergistic relationship between tau and A $\beta$  that leads to synaptic decay might be mediated by Fyn tyrosine kinase, a substrate

of which is the NMDA-R (Ittner et al., 2010; Roberson et al., 2011), or by glycogen synthase kinase 3 (GSK3) which phosphorylates tau and has been shown to mediate A $\beta$ -induced LTP impairment (Shipton et al., 2011).

#### 1.6.4 Soluble versus insoluble A $\beta$ in AD

#### 1.6.3 A $\beta$ and AC-actin

A $\beta$  exists in several different physical states, including as monomers,

Over the past decade, mounting evidence has also suggested a role for ADF/cofilin in mediating the neurotoxic effects of AD amyloid pathology. Treatment of rat primary hippocampal neurons or organotypic hippocampal slice culture with synthetic or naturally secreted A $\beta$  has been shown to induce aggregation of actin (Hiruma et al., 2003) and activation and accumulation of AC into rod-shaped structures (Maloney et al., 2005; Davis et al., 2009; Davis et al., 2011) which are reminiscent of aberrant actin-cofilin accumulations in AD brain (Minamide et al., 2000). This rod formation, together with A $\beta$ -induced F-actin reorganization has been shown to inhibit axonal transport of vesicles and organelles, including mitochondria and APP vesicles (Jang et al., 2005; Maloney et al., 2005; Maloney et al., 2008; Henriques et al., 2010), which probably contributes to synaptic pruning of affected neurites by preventing transport of essential cargoes out to pre-synaptic terminals. In addition, A $\beta$  treatment has also been shown to induce a net decrease in pre-synaptic dendritic spines, effects of which are also attributed to AC (Shankar et al., 2007). Indeed AC inclusions, in addition to tau, may therefore represent

the anti-A $\beta$  antibody 8E10 with A $\beta$  oligomers neutralizes the oligomer-induced



another mediating factor causally linking A $\beta$  with neuronal deficits and degeneration in AD.

#### **1.6.4 Soluble versus insoluble A $\beta$ in AD**

A $\beta$  exists in several different physical states, including as monomers, oligomers, or fibrils. Evidence from *in vitro* studies demonstrates that synthetic A $\beta$  monomers aggregate in a time-dependent fashion to form oligomers which in turn, frequently form fibrils (Walsh et al., 1997; Walsh et al., 2000). Several lines of evidence have converged recently to demonstrate that soluble oligomers of A $\beta$ , but not monomers or insoluble fibrils, are indeed responsible for neurotoxicity and synaptic dysfunction in human AD brains and in AD animal models. Soluble A $\beta$  oligomers, also referred to as A $\beta$ -derived diffusible ligands (ADDLs) (Lambert et al., 1998), are very potent toxic species, as even nanomolar concentrations have been shown to induce synaptic dysfunction, reduced long term potentiation (LTP) and neuron death in hippocampal slices of rats (Lambert et al., 1998; Wang et al., 2002; Shankar et al., 2007) and mice (Townsend et al., 2006). Microinjection into living rats of culture medium containing picomolar concentrations of naturally secreted human A $\beta$  revealed that A $\beta$  oligomers (in the absence of monomers and fibrils) can inhibit hippocampal LTP *in vivo* (Walsh et al., 2002), which specifically disrupts cognitive function (Cleary et al., 2005). Importantly, the concomitant injection of the anti-A $\beta$  antibody 6E10 with A $\beta$  oligomers neutralizes the oligomer-induced

LTP dysfunction (Klyubin et al., 2005). These data strongly support the idea that soluble oligomers are the fundamental species responsible for mediating A $\beta$  toxicity in AD, although the precise molecular mechanisms involved remain poorly understood and are the subject of extensive ongoing research.

## 1.7 The 'Mitochondrial Hypothesis' of AD

### 1.7.1 Mitochondria and the ageing brain

By far, the greatest risk factor for sporadic AD is aging, and mitochondria have been thought to contribute to aging through the accumulation of mitochondrial DNA (mtDNA) mutations, abnormal mitochondrial dynamics and net production of reactive oxygen species (ROS) (Navarro and Boveris, 2007; Boveris and Navarro, 2008) (also reviewed in (Lin and Beal, 2006)). A rapidly growing body of evidence suggests mitochondrial dysfunction indeed plays a direct and causal role in the major histopathological and pathophysiological features of SAD, such that the aging brain and SAD are thought to be converging events (reviewed in (Swerdlow and Khan, 2004; Lin and Beal, 2006; Swerdlow and Khan, 2009; Wang et al., 2009a; Su et al., 2010)).

The majority of the cellular energy molecule adenosine triphosphate (ATP) is produced by mitochondrial oxidative phosphorylation, a process that encompasses electron transfer between the complexes of the respiratory chain, proton (H<sup>+</sup>) release into the inter-membrane space, and H<sup>+</sup> re-entry to the



matrix through  $F_0$  with ATP synthesis by  $F_1$ -ATP-synthase (Boveris and Navarro, 2008). Mitochondria are highly dynamic organelles, undergoing continual fusion and fission (Chen and Chan, 2005). Common features of mitochondria in aging cells are reductions of complex I and complex IV activity, reduced membrane potential, decreased electron transfer through the electron transport chain, increased mitochondrial size and increased fragility (reviewed in (Swerdlow and Khan, 2004, 2009)). The result of these changes are the continuous decrease of the capacity to produce ATP by oxidative phosphorylation and concomitant increase in ROS production (Navarro and Boveris, 2007; Boveris and Navarro, 2008). In healthy mitochondria, ROS generation is balanced by a large and complex antioxidant defense capacity involving coenzyme Q10, glutathione and enzymes manganese superoxide dismutase (MnSOD) and glutathione peroxidase, to name a few (reviewed in (Lin and Beal, 2006)). Damaged mitochondria have a decreased capacity for antioxidant defense, triggering a vicious feed-forward cycle whereby excess ROS can further damage mitochondria, causing more ROS production and loss of antioxidant capacity (Lin and Beal, 2006).

Of all cell types, neurons are one of the most critically dependent on mitochondria, owing to their large energy requirement for generating action potentials, facilitating synaptic transmission and maintaining ion gradients across the plasma membrane, and because of their comparatively limited capacity for producing ATP by glycolysis (Chen and Chan, 2006; Moreira et al., 2010). Although the brain only represents 2% of body weight, it receives 15%

of cardiac output and 20% of total body oxygen consumption. It thus follows that any decrease in mitochondrial function may be detrimental to the normal function of the human brain and a contributor to neuropathological processes. Indeed, several lines of evidence demonstrate that mitochondrial dysfunction has a causal role in formation of several AD pathologies and that furthermore, these pathologies may bring about further mitochondrial dysfunction in a feedforward manner.

Mitochondrial dysfunction has also been linked to AD-related tau pathology.

Oxidative stress has been shown to induce tau hyperphosphorylation of AD-

### **1.7.2 Mitochondria and A $\beta$ , tau and AC-actin pathologies**

Mitochondrial oxidative damage is believed to be the earliest event in the pathogenesis of AD, preceding the appearance of significant A $\beta$  plaque pathology (Nunomura et al., 2001). In APP transgenic mouse models, oxidative damage precedes A $\beta$  deposition (Praticò et al., 2001; Fukui et al., 2007) and is associated with early upregulation of genes relating to mitochondrial metabolism and apoptosis in affected neurons (Reddy et al., 2004). In primary neuron culture, it has been shown that hydrogen peroxide-induced oxidative stress leads to increased secretion of A $\beta$  peptides (Goldsbury et al., 2008). Other studies have showed that A $\beta$  detrimentally affects mitochondrial function and metabolism by stimulating excessive ROS production through a mechanism requiring NMDA-R activation (De Felice et al., 2007; Decker et al., 2010), disrupting mitochondrial fission and fusion dynamics (Wang et al., 2008b), modulating Cyclophilin D-dependant mitochondria permeability



transition pores (Du et al., 2008), uncoupling the respiratory chain via complex IV modulation (Tillement et al., 2011), decreasing neuronal ATP by triggering hexokinase 1 release (Saraiva et al., 2011) and interfering with mitochondrial distribution and trafficking in axons (Wang et al., 2009b; Du et al., 2010). The latter studies identified synaptic mitochondria as the most vulnerable to A $\beta$ -induced damage and are therefore proposed as a mediating factor in A $\beta$ -related synaptic decay in AD.

Mitochondrial dysfunction has also been linked to AD-related tau pathology. Oxidative stress has been shown to induce tau hyperphosphorylation of AD-relevant sites in superoxide dismutase 2 (*sod2*)-null mice, an effect that was ameliorated by antioxidant treatment (Melov et al., 2007). In primary neurons, treatment with the naturally occurring complex I inhibitor Annonacin induced redistribution of tau from axons to the somatodendritic compartment and inhibited MT-dependent axonal transport (Escobar-Khondiker et al., 2007). On the other hand, several studies have demonstrated a role for tau in inhibiting mitochondrial function. Tau overexpression has been implicated with mitochondrial transport defects in primary neuron culture (Ebner et al., 1998) and with decreased activity of respiratory chain components, decreased antioxidant enzymes and increased ROS production in tau transgenic mouse models (David et al., 2005). Moreover, studies in triple transgenic mouse models have revealed that when over-expressed together, tau and A $\beta$  synergistically and potently induce neuronal oxidative stress and mitochondrial dysfunction (Rhein et al., 2009).

Finally, the third major AD lesion, cofilin pathology, is also associated with mitochondrial dysfunction. Although no studies have yet investigated the relationship between mitochondrial dysfunction and cofilin pathologies in human AD brain, *in vitro* studies in rat and mouse primary neuron culture have demonstrated that cofilin rods form rapidly in response to neuronal stressors (Minamide et al., 2000; Davis et al., 2009), which bear striking resemblance to cofilin rods observed in postmortem AD brain. Treatment with peroxide, glutamate or ATP-depleting medium induces cofilin rods which often form in tandem arrays along neurite processes where cofilin and actin concentrations are high (Minamide et al., 2000; Davis et al., 2009).

Indeed mitochondrial dysfunction appears to reconcile the major histopathological features of sporadic AD. However, many important questions remain. How do mitochondria mechanistically induce these changes? Which pathologies form first in response to mitochondrial dysfunction? And how are these pathologies inter-related? Answers to these questions are major considerations of this project.



## **1.8 Research Hypothesis and Aims**

### **1.8.1 Main Hypothesis**

Etiological mechanisms of sporadic AD remain elusive. By far, the most significant risk factor for SAD is aging and one of the most common features of aging neurons is decreased mitochondrial function. It thus follows, that mitochondrial dysfunction may play a central and causal role in the initiation of major histopathology and neurodegenerative pathways in the AD brain. Since the ubiquitous cytoskeletal proteins MAP/tau and actin-ADF/cofilin are implicated in several major histopathologies of AD, namingly NFTs, NTs and cofilin pathologies, we wanted to investigate and characterize changes to these respective endogenous proteins following induced mitochondrial dysfunction to ascertain whether decreased cell metabolism is sufficient to recapitulate these major cytoskeletal pathologies and in doing so, attribute the pathogenesis of these lesions, at least in part, to mitochondrial dysfunction. To that extent, this study was non-hypothesis-driven in nature at the outset.

In carrying out these investigations, the overall objectives of this project were three-fold. Firstly, we wanted to know whether mitochondrial dysfunction was sufficient to induce AD-like changes in endogenous MAP/tau and actin-AC proteins in simple primary neuron cell culture models. Secondly, we asked whether there was a relationship (direct or indirect) between these two cytoskeletal proteins during mitochondrial dysfunction. Thirdly, we asked

whether introduction of the third major constituent of AD pathology, A $\beta$ , which is also implicated in mitochondrial dysfunction, played any role in the initiation of these cytopathologies. In doing so, this project sought to shed light on the very earliest pathogenic mechanisms involved in triggering sporadic AD.

### **1.8.2 Specific Aims**

**AIM 1: Can mitochondrial dysfunction induce AD-like hyperphosphorylation and cellular redistribution of endogenous tau?**

Tau hyperphosphorylation, particularly in the MTBD, is reportedly one of the first major pathological changes in the early stages of AD. Concomitant with this is the redistribution and aggregation of hyperphosphorylated tau into neuropil thread inclusions (see Section 1.4.4). With particular emphasis on the AD-relevant epitopes, we asked whether these changes could be instigated by mitochondrial dysfunction in primary neuron and organotypic brain slice culture models.

**AIM 2: Do tau inclusions induced by mitochondrial dysfunction bear any relationship to AC-actin inclusions generated under the same conditions?**

Cofilin-actin rich inclusions are frequently observed in AD brain and AC-actin inclusions highly reminiscent of these pathologies can be induced in primary neuron and organotypic brain slice cultures by neuronal stressors such as mitochondrial dysfunction (see Section 1.8.2). Given that MAP/tau and actin



have been known to associate under physiological conditions and these interactions have been proposed to play a role in initiating AD cytopathology (see Section 1.4.2), we asked therefore if any apparent relationship existed between MAP/tau inclusions (if any; AIM 1) and AC inclusions generated by mitochondrial dysfunction. This would indeed suggest generation of these two respective lesions converge on the same pathogenic pathway.

### **AIM 3: Can A $\beta$ disrupt AD-relevant cytoskeletal proteins?**

A $\beta$ , the other major histopathological constituent of AD, has been shown to disrupt several aspects of mitochondrial function and metabolism (see Section 1.8.2). Moreover, A $\beta$  is known to interact with both tau and AC-actin (see Sections 1.7.2-3). By employing A $\beta$  treatments, we aimed to investigate the effects of A $\beta$  on both AC and MAP/tau proteins to see whether A $\beta$  might mediate formation of AC and MAP/tau cytopathologies. In doing so, we aimed to further delineate the complex relationship between these apparently convergent constituents, namingly mitochondrial dysfunction, tau, AC and A $\beta$ .

**AIM 4: Can these cytopathologies be recapitulated *ex vivo*?** By employing rat and mouse organotypic hippocampal brain slice cultures, our aim was to see whether we could recapitulate the cytoskeletal changes and inter-relationships in these more complex 'organ-like' environments and in doing so, we sought to take a step closer to understanding these pathogenic mechanisms in the human *in vivo* brain.

## 2.1 Antibodies

Antibodies were used for immunofluorescence (IF) or Western blotting (WB). Mouse monoclonal antibodies against phosphorylated tau epitopes: AT8 (1:100 IF, 1:250 WB), AT100 (1:100 IF, 1:50 WB), AT180 (1:100 IF, 1:250 WB), AT270 (1:250 IF, 1:500 WB) (all Sigma-Aldrich), 12E8 (1:500 IF, 1:1000 WB) (Eli Lilly USA) (Seubert et al., 1995). Other mouse monoclonal antibodies included GAPDH (1:1000 WB) (Sigma-Aldrich), actin (1:100 IF) (1A4; Dako),  $\beta$ -actin (1:5000 WB) (Abcam),  $\alpha$ -tubulin (1:1000 WB) (Sigma-Aldrich) and  $\beta$ (III) tubulin (1:1000 IF) (Abcam). Rabbit polyclonal antibodies against phosphorylated tau epitopes: S212 (1:100 IF, 1:1000 WB) (Bioss), S405 (1:250 IF, 1:1000 WB) (Biossource), S494 (1:250 IF, 1:1000 WB) (Biossource), S422 (1:250 IF, 1:1000 WB) (Sigma-Aldrich) and total tau (1:1000 IF, 1:15,000 WB) (Dako, USA). Other rabbit polyclonal antibodies were 1439 (which recognizes chick ADF, and both ADF and cofilin in humans and rodents) (1  $\mu$ g/ml IF, 0.5  $\mu$ g/ml WB) (Shaw et al., 2004), ADF (1:1500 IF) (D6815; Sigma-Aldrich), Ser3-phosphorylated ADF/actin (1  $\mu$ g/ml IF, 0.5  $\mu$ g/ml WB) (Shaw et al., 2004), cofilin (1:250 IF, 1:5000 WB) (C8736; Sigma-Aldrich) and actin (1:250 IF) (A2066; Sigma-Aldrich). Alexa Fluor 488-conjugated phalloidin (1:20, Invitrogen) was used to visualize F-actin. Secondary antibodies for IF were Alexa Fluor-conjugated goat anti-mouse and goat anti-rabbit 488, 568, 594 and 647 (1:200, Invitrogen) and for chemiluminescence detection for WB horseradish peroxidase-conjugated anti-mouse or anti-rabbit (1:2000, Amersham).

## General Materials and Methods

# 2



## 2.1 Antibodies

Antibodies were used for immunofluorescence (IF) or Western blotting (WB). Mouse monoclonal antibodies against phosphorylated tau epitopes: AT8 (1:50 IF, 1:250 WB), AT100 (1:100 IF, 1:50 WB), AT180 (1:100 IF, 1:250 WB), AT270 (1:250 IF, 1:500 WB) (all Sigma-Aldrich), 12E8 (1:500 IF, 1:4000 WB) (Elan USA)(Seubert et al., 1995). Other mouse monoclonal antibodies included GAPDH (1:1000 WB) (Sigma-Aldrich), actin (1:100 IF) (1A4; Dako),  $\beta$ -actin (1:5000 WB) (Abcam),  $\alpha$ -tubulin (1:1000 WB) (Sigma-Aldrich) and  $\beta$ (III)-tubulin (1:1000 IF) (Abcam). Rabbit polyclonal antibodies against phosphorylated tau epitopes: S214 (1:100 IF, 1:200 WB) (GenScript, USA), S396 (1:500 IF, 1:1000 WB) (Biosource), S404 (1:250 IF, 1:1000 WB) (Biosource), S422 (1:250 IF, 1:1000 WB) (Sigma-Aldrich) and total tau (1:1000 IF, 1:15,000 WB) (Dako, USA). Other rabbit polyclonal antibodies were 1439 (which recognizes chick ADF, and both ADF and cofilin in humans and rodents) (1  $\mu$ g/ml IF, 0.5  $\mu$ g/ml WB)(Shaw et al., 2004), ADF (1:1500 IF) (D8815; Sigma-Aldrich), Ser3-phosphorylated ADF/cofilin (1  $\mu$ g/ml IF, 0.5  $\mu$ g/ml WB)(Shaw et al., 2004), cofilin (1:250 IF, 1:5000 WB) (C8736; Sigma-Aldrich) and actin (1:250 IF) (A2066; Sigma-Aldrich). Alexa Fluor 488-conjugated phalloidin (1:20, Invitrogen) was used to visualize F-actin. Secondary antibodies for IF were Alexa Fluor-conjugated goat anti-mouse and goat anti-rabbit 488, 555, 594 and 647 (1:200, Invitrogen) and for chemiluminescence detection for WB: horseradish peroxidase-conjugated anti-mouse or anti-rabbit (1:2000, Amersham).

The use of antibodies against phosphorylated tau epitopes underpins a central component of this thesis. It must be noted however, that although many of these antibodies have been well-characterized and widely employed, one of the limitations of this method of analysis is the possibility of cross-reactivity and non-specific labeling. For example, 12E8 antibody is widely used as a label for tau, but since the binding 'KXGS' motif is also present in other MAP proteins (Lewis et al., 1988; Dehmelt and Halpain, 2004a), we cannot discount that positive labeling is not, at least in part, due to cross-reactivity of these proteins (discussed further in Chapters 4 and 5). In the present studies, we must therefore exercise some caution in interpretation of data and not exclude the possibility of at least some protein cross-reactivity and non-specific labeling.

## **2.2 Primary neuron culture generation & maintenance**

All reagents used for primary neuron culture were obtained from Gibco, Invitrogen unless stated otherwise.

### **2.2.1 Chick tectal neurons**

Cultures of dispersed primary neurons were freshly prepared from telencephalon (cerebral hemispheres) of 7-days-in-ovo chicken embryos (E7), using protocols adapted from previously described methods (Sensenbrenner et al., 1978; Pettmann et al., 1979; Goldsbury et al., 2008). Glass coverslips (12 mm; sterilized by submersion in absolute ethanol followed by flaming) or



plastic tissue cultures dishes (30 – 100 mm) were coated overnight at 37 °C in freshly prepared 0.1 mg/ml poly-D-lysine hydrobromide (MW 70,000-150,000; Sigma-Aldrich) diluted in Dulbecco's PBS (DPBS, 14200). Before plating of neurons, coverslips and dishes were washed with three changes of DPBS and air-dried. Telencephalons of E7 embryos were dissected out in ice cold Hanks Balanced Salt Solution (HBSS, 14185), dissociated in 0.1% trypsin-EDTA (15400), centrifuged at 1450 g for 3 min and re-suspended in warm plating media comprised of Dulbecco's Modified Eagle's Medium (DMEM, High Glucose, 11960044) with 10% Fetal Bovine Serum (FBS) (HyClone, USA), 1% Glutamax (35050) and 1% Penicillin-Streptomycin (15140-122). Cell density was estimated using a haemocytometer and neurons were plated in plating media at densities of  $0.3 \times 10^6 / \text{cm}^2$  in dishes or  $0.1 \times 10^6 / \text{cm}^2$  on coverslips. 3 h after plating, cell media was changed and cultures maintained in Neurobasal medium (21103049) containing 2% B27 supplement (17504-044), 1% GlutaMAX (35050) and 1% Penicillin-Streptomycin (15140-122). Neurons were cultured at 37°C with 5% CO<sub>2</sub> in a humidified atmosphere for 6 days before use in experiments.

Primary rat hippocampal neurons were prepared from 18-day old embryos (E18), as previously described (Maniatis et al., 2000). Following decapitation of freshly removed embryos, hippocampi were dissected out in ice cold HBSS.

### **2.2.2 Primary human neurons**

Cells were dissociated in 0.1% trypsin-EDTA for 10 min, trypsin removed and

Human fetal brains were obtained from 14- to 18-week-old fetuses collected after therapeutic termination following informed consent (see Section 2.10 for Ethics Statements). Primary neuron cultures were prepared using a protocol

adapted from previously described methods (Kerr et al., 1998; Guillemain et al., 2007). Cerebral portions of fetal brains were washed thoroughly with PBS to remove visible meningeal tissue and blood vessels, and then forced through a 100  $\mu\text{m}$  nylon mesh with the plunger of a plastic syringe. The suspension was centrifuged at 500  $g$  for 5 min and the cell pellet re-suspended in Neurobasal medium (as described in 2.2.1) containing 0.5% glucose. Cells were plated at a density of  $0.1 \times 10^6 / \text{cm}^2$  on 12 mm glass coverslips coated with Matrigel (Becton Dickinson, USA) diluted 1:20 in Neurobasal medium. Medium was changed every 3–4 days. Neurons were cultured for 2-3 weeks before use in experiments. Human primary neuron cultures were kindly prepared and maintained at UNSW by Dr. Gilles J. Guillemain, Neuroinflammation Laboratory, Department of Pharmacology. All human primary neuron experiments were carried out in the Neuroinflammation Laboratory.

## 2.3 Cell treatments

### 2.2.3 Primary rat hippocampal neurons

For ATP depletion studies, cells were treated with fresh dilutions of 1–2  $\mu\text{M}$  Primary rat hippocampal neurons were prepared from 18-day old embryos (E18), as previously described (Minamide et al., 2000). Following decapitation of freshly removed embryos, hippocampi were dissected out in ice cold HBSS. Cells were dissociated in 0.1% trypsin-EDTA for 10 min, trypsin removed and cells washed twice and gently re-suspended with Neurobasal medium containing 10% FBS. Cells density was calculated and cells either plated immediately or stored in 10% (v/v) Dimethyl Sulfoxide (DMSO, Sigma-Aldrich)



in Neurobasal/FBS at a density of  $10^6$  cells/ml at  $-80$  °C overnight before transferal to liquid nitrogen. For freshly plated cells, 12 mm coverslips were coated with poly-D-lysine and cells plated at a density of  $0.1 \times 10^6$  /cm<sup>2</sup> in plating media, followed by a change to Neurobasal media as described in 2.2.1 above. For plating cells from frozen stocks, vials were thawed quickly at  $37$  °C, diluted into warmed Neurobasal medium containing 10% FCS and plated according to protocols described above. Neurons were cultured for 5 days before use in experiments. Rat hippocampal neurons were kindly prepared and in some cases maintained and processed by Laurie S. Minamide of the Bamburg Laboratory, Biochemistry and Molecular Biology Department, Colorado State University. All rat primary neuron experiments were carried out in the Bamburg Laboratory.

### 2.3 Cell treatments

For ATP depletion studies, cells were treated with fresh dilutions of  $1-2$   $\mu$ M antimycin (AM; a mitochondrial complex III inhibitor),  $3$   $\mu$ M carbonyl cyanide 3-chlorophenylhydrazone (CCCP: a mitochondrial uncoupling agent), or  $100$   $\mu$ M hydrogen peroxide (all Sigma-Aldrich) in PBS pre-warmed to  $37$  °C. Actin-manipulating drugs were Jasplakinolide (Jasp, an actin stabilizer; Calbiochem 420127, CA) or Latrunculin B (Lat B, an actin depolymerizer; Calbiochem 428020, CA) both used at  $1$   $\mu$ g/ml in warmed PBS. Cells left without a medium change or treated with PBS or DMSO acted as controls. After treatments, cells

were immediately fixed (cells on coverslips) or prepared for Western blot analysis (plated cells). Stock solutions of the reagents were prepared at 1mM (AM and CCCP) or 1 mg/ml (Lat B and Jasp) in DMSO and stored at  $-20^{\circ}\text{C}$ .

## 2.4 Immunofluorescence

### 2.4.1 Primary dissociated neuron culture

Following aspiration of treatment solutions, cells were washed once with PBS pre-warmed to  $37^{\circ}\text{C}$  and fixed with 4% paraformaldehyde (PFA, Electron Microscopy (EM)-grade; Electron Microscopy Sciences, USA (16% solution) or Sigma-Aldrich (36% solution)) in fresh PBS at  $37^{\circ}\text{C}$  for 35 minutes. For optimal preservation of ADF/cofilin rods (when staining for actin-associated proteins alone), 0.1% glutaraldehyde was added to the fix solution (EM-grade; Electron Microscopy Sciences, USA). Cells were washed three times with PBS and permeabilized for 90 sec with either 0.05% Triton X-100 (Sigma-Aldrich) or 80% ice cold methanol/PBS (Sigma-Aldrich). The permeabilization method utilized depended on the protein of interest in each experiment, since optimal immunostaining for rod localization of phospho-MAP/tau epitope 12E8 requires Triton X-100 permeabilization (avoiding methanol) and optimal immunostaining for rod localization of ADF/cofilin using the 1439 antibody requires methanol (avoiding Triton), as shown in previous studies (Davis et al., 2009) and discussed further in Chapter 3. Cells were blocked for 45 min in 5% heat-



inactivated goat serum (60 °C for 30 min; Invitrogen) in PBS and incubated with primary antibody for 1 h at room temperature (RT), diluted in 5% goat serum. For co-labeling studies, primary antibodies were applied sequentially with several gentle PBS washes in between. Secondary antibodies were diluted in 5% goat serum and applied for 45 min at RT. Following three PBS washes, cells were incubated in the DNA stain 4',6-diamidino-2-phenylindole (DAPI, Sigma-Aldrich) for 10 min (1:1000 in PBS) staining, washed three times and coverslips mounted with ProLong Gold Antifade (Invitrogen) on glass slides (Menzel-Gläser).

#### **2.4.2 Human brain tissue**

45 µm free-floating sections and 7 µm paraffin-embedded sections were used in this study, as stipulated in subsequent chapters. Prior to blocking, paraffin-embedded sections were first deparaffinized for 20 min in Hemo-De (Fisher Scientific), rehydrated to distilled water through decreasing concentrations of ethanol and microwaved in water for 8 min. Free floating sections were incubated in three changes of 50 % ethanol (15 min each) then 50 % ethanol/3 % hydrogen peroxide for 20 min. All sections were blocked with either 1 % bovine serum albumin (BSA, Sigma-Aldrich) or 5% goat serum in Tris-buffered saline (TBS, pH 7.4) for 1 h at RT. Primary antibodies were diluted in the appropriate blocking buffer and incubated overnight at 4 °C. For co-labeling studies, primary antibodies were incubated simultaneously. Following three

TBS washes (15 min), secondary antibodies (plus DAPI) were diluted in blocking buffer and incubated for 1 h at RT. Sections were washed three times in TBS (15 min) and mounted with ProLong Gold Antifade (Invitrogen) on glass slides (Menzel-Gläser).

## 2.6 Western blotting

Following aspiration of treatment solutions, cells in 20 mm dishes were washed

## 2.5 Microscopy and Analysis

Epifluorescence images were obtained on a Zeiss Axioplan 2 microscope, captured with a charge-coupled device (CCD) camera driven by AxioVision software (Bosch Advanced Microscope Facility, University of Sydney), or with a Nikon Diaphot inverted microscope captured with a CCD camera driven by Metamorph software (Microscopy Facility, Biochemistry and Molecular Biology Department, Colorado State University). Scanning confocal images were obtained on a Zeiss LSM 510 Meta driven by LSM 510 software (Bosch Advanced Microscope Facility, University of Sydney). Spinning disk confocal images were obtained with a CSU22 confocal head (Yokogawa Instruments, Japan) captured with a Cascade II EMCCD camera driven by SlideBook software (Microscopy Facility, Biochemistry and Molecular Biology Department, Colorado State University). Single labeled cells were used to check for bleed-through in all double-label immunofluorescence studies and secondary antibody-only labeled cells used to subtract background. All captured images were converted to Tagged Image Files (TIF) for subsequent analysis and presentation. For determination of relative fluorescence intensities, general



measurements and image adjustments, Image J freeware (v1.38x, National Institutes of Health freeware; <http://rsb.info.nih.gov/ij>) was used.

## 2.6 Western blotting

Following aspiration of treatment solutions, cells in 30 mm dishes were washed once with warmed PBS and lysed with 150  $\mu$ l ice cold radioimmunoprecipitation assay (RIPA) buffer (50 mM Tris pH 8.0, 150 mM NaCl, 1% NP40, 5 mM EDTA, 0.5% sodium deoxycholate and 0.1% sodium dodecyl sulfate (SDS); all Sigma-Aldrich) in the presence of Complete Protease and Phosphatase Inhibitor Cocktails (both Roche, Switzerland). Cells were harvested with rubber cell scrapers and kept on ice for 30 min. Samples were centrifuged at 12,000 rpm for 20 min at 4 °C and supernatant aliquotted (for protein assays and Western blotting) and stored at -80 °C.

Protein concentration was determined with a commercial Lowry Assay (Bio-Rad), a colorimetric detergent compatible (DC) protein assay based on the Lowry method (Lowry et al., 1951). BSA was used as a protein standard. Protein samples (5  $\mu$ l) were first mixed with reagent S (25  $\mu$ l) and A (1  $\mu$ l) in a 96-well tissue culture plate, followed by reagent B (200  $\mu$ l). Samples were incubated for 15 min at RT and absorbance was recorded with a Chameleon V Microplate reader set to wavelength 750 nm.

For sodium dodecyl sulfate – polyacrylamide gel electrophoresis (SDS-PAGE), 10-12% gels with 10- or 15-well combs (thickness 1.5mm) were prepared. Gels consisted of a bottom resolving gel: 10-12% acrylamide/Bis solution (Bio-Rad), 375 mM Tris (pH 8.0), 0.1% SDS, 0.1% ammonium persulphate and 0.04-0.06% N,N,N',N'-Tetramethylethylenediamine (TEMED; Sigma-Aldrich), and an upper stacking gel: 5% acrylamide/Bis solution, 125 mM Tris (pH 6.8), 0.1% SDS, 0.1% ammonium persulphate and 0.1% TEMED. Protein samples were denatured in 4X Laemmli buffer (25% v/v 1 M Tris-HCl, 20% v/v  $\beta$ -mercaptoethanol, 40% v/v glycerol, 9.2% w/v SDS, 0.2% w/v bromophenolblue in ddH<sub>2</sub>O) by heating samples for 3 min at 60 °C. Equal amounts of protein samples (2-10  $\mu$ g) were loaded into the SDS-PAGE gels and separated at 80-110V for 2-3 h in an electrophoresis chamber (Bio-Rad) submerged in running buffer (25 mM Trizma base, 0.2 M Glycine, 0.1% SDS). A molecular weight (MW) marker ladder was used to identify target protein bands (SeeBlue Pre-Stained Standard, 4-250 kDa, Invitrogen). Proteins were electrophoretically transferred to a nitrocellulose membrane (Hybond ECL Amersham, Australia) equilibrated in blotting buffer (10% running buffer, 20% methanol, 70% ddH<sub>2</sub>O), using a Trans-Blot SD Semi-Dry Transfer Cell (Bio-Rad) at 20 V for 40-60 min.

## 2.7 Statistics

To block unspecific binding sites, nitrocellulose membranes were incubated in 5% non-fat milk powder dissolved in TBS containing 0.1% Tween 20 (Sigma-Aldrich) (TBS-T) at RT for 1 h on a shaking platform. Membranes were incubated with primary antibodies in TBS-T overnight at 4°C on a shaking



platform, followed by three 10 min washes in TBS-T and incubated with alkaline phosphatase-coupled secondary antibodies for 45 min at RT on a shaking platform. Membranes were washed three times for 10 min in TBS-T, incubated for 5 min incubation with Immobilon Chemiluminescent AP substrate (Millipore, Australia). Protein bands were detected in a ChemiDoc XRS detection system (BioRad) driven by Quantity One software. For re-use, membranes were stripped by washing in ddH<sub>2</sub>O for 5 min, 10 min in 0.2 M NaOH and a further 5 min in ddH<sub>2</sub>O at RT. Membranes were blocked again before antibody re-probing.

For analysis of target protein bands, images were converted to TIF and band densities of the appropriate MW size were measured using Image J (v1.38x, National Institutes of Health freeware; <http://rsb.info.nih.gov/ij>). Background intensity was subtracted and bands normalized to individual  $\beta$ -actin, GAPDH or  $\alpha$ -tubulin loading controls. Averages and Standard Errors of the Mean (S.E.M) for each treatment condition were determined and results presented as a percentage of control band intensities.

## 2.7 Statistics

Data are represented as means  $\pm$  S.E.M, unless otherwise stated. For statistical comparison, the Student's *t* test was used. Only *p* values of <0.05 were considered statistically significant.

## 2.8 Plasmid constructs and transfection

All plasmids used in this study were kindly provided by James R. Bamberg, Biochemistry and Molecular Biology Department, Colorado State University.

### 2.8.1 *E. coli* transformation with vector constructs

To generate large quantities of each vector construct used in this project (human cofilin-pEGFP-N1, chick ADF siRNA-pAdtrack, human Pak2 siRNA-pAdtrack, pEGFP-N1 vector only or pAdtrack vector only), competent *E. coli* cells were first transformed with the DNA constructs. 10-20 pg of DNA construct was added to a vial containing 25  $\mu$ l of competent *E. coli* cells (OneShot TOP10 Cells, Invitrogen) and incubated on ice for 30 min. *E. coli* were then heat-shocked for 30 sec at 42 °C and 125  $\mu$ l of warm SOC Medium (a modified lysogeny broth (LB), Invitrogen) added. Vials were incubated for 1 h at 37 °C in a shaker set to 225 rpm. LB agar plates (1.5%) containing 100  $\mu$ g/ml kanamycin (Invitrogen) were inoculated with 200  $\mu$ l of transformed cells and incubated (inverted) overnight at 37 °C. Since the vectors used in this project contain a kanamycin-resistant gene, only those *E. coli* cells that have taken up the DNA construct will grow.

### 2.8.2 Midi-prep extraction of DNA from *E. coli*

Single *E. coli* colonies grown on LB agar plates were selected and inoculated in 250 ml flasks containing 50 ml LB medium and 50 mg/ml kanamycin. *E. coli* were allowed to grow overnight at 37°C at 300 rpm. *E. coli* suspension was



transferred to a 50 ml tube and centrifuged for 15 min at 4°C at 6000 g. The JETstar 2.0 Plasmid Purification Midi kit (Genomed, Germany; 210050) was used to extract DNA from cells. The supernatant was discarded and the pellet re-suspended in Buffer P1. Buffer P2 was added, gently mixed and incubated for 5 min at RT. Buffer P3 was added, gently mixed and incubated on ice for 15 min. The lysate was then filtered with a midi filter-cartridge. The supernatant was transferred to a JETstar tip pre-equilibrated with buffer and the supernatant drained by gravity. The tip was washed twice with buffer and the flow through discarded. Filtered DNA was eluted, precipitated by addition of isopropanol and centrifuged at 5000 g for 60 min at 4 °. The supernatant was discarded and the DNA pellet washed with 70% ethanol and centrifuged at 5000 g for a further 60 min at 4 °C. The supernatant was discarded and the pellet air-dried for 30 min. DNA was resolved in 400 µl freshly prepared 1x Tris-EDTA (TE; 10 mM, Tris-HCl pH 8, 1 mM EDTA) buffer and stored at -20°C.

### **2.8.3 Transfection of primary neurons**

Transfections were carried out on primary chick neurons cultured on glass coverslips in 24-well tissue culture plates as described above in 2.2.1.

For each individual well, 2 µg of plasmid DNA was added to 100 µl Opti-MEM medium (Gibco, Invitrogen) (Mixture A) and in a separate vial 2 µl of Lipofectamine LTX (Invitrogen, 15338500) was added to 100 µl Opti-MEM

(Mixture B). Mixtures A and B were left at RT for 5 min, then combined and incubated at RT for 20 min to allow DNA and Lipofectamine to form a complex. Primary cells were meanwhile washed once with warmed Opti-MEM and returned to incubator with 300  $\mu$ l fresh Opti-MEM. 200  $\mu$ l of Mixture (A+B) was added to cells and incubated for 2-3 h at 37 °C, after which Opti-MEM mixture was aspirated and replaced with fresh Neurobasal maintenance media (see 2.2.1 above). Cells were incubated another 48 h to ensure plasmid expression before treatment and fixing, as per 2.3-2.4 above.

## 2.9 Organotypic brain slice culture

Protocols were adapted from previously described methods (Zimmer and Gähwiler, 1984; Stoppini et al., 1991). All reagents used for brain slice culture were obtained from Gibco, Invitrogen unless stated otherwise.

Glass coverslips (12 x 22 mm) were sterilized by dipping sequentially in absolute ethanol, dH<sub>2</sub>O, absolute ethanol and then passed through a flame. Coverslips were then submersed in 2% 3-aminopropyltriethoxysilane in acetone (Sigma-Aldrich) for 10 sec, rinsed in dH<sub>2</sub>O and thoroughly air dried. Both sides of each coverslip were UV sterilized for 20 min.

Rat or mouse pups at postnatal day 7 (P7) were anaesthetized by inhalation of halothane and decapitated with scissors. Whole brains were removed in ice cold Gey's Balanced Salt Solution (GBSS; Sigma-Aldrich G9779) containing



0.5% glucose and 1% Pen-Strep. Hippocampi were carefully dissected out whole (where possible) with a portion of fimbria retained ventrally (this increases brain slice survival in culture) and sliced at 320  $\mu\text{m}$  thickness on a McIlwain Mechanical Tissue Chopper (UK) fitted with 0.1 mm platinum chrome razor blades. Hippocampal sections submersed in ice cold GBSS/glucose were carefully separated with forceps under a dissection microscope.

Brain slices were mounted onto 4  $\mu\text{l}$  of chicken plasma (Cocalico Biologicals, Inc., PA, USA) on coverslips. 4  $\mu\text{l}$  of thrombin (150 NIH units/ml; MP Biomedicals Inc., USA) was added to the plasma and mixed gently by pipetting up and down, with care taken to completely submerge the brain slice in plasma/thrombin mix. Slices were left to sit for 3-4 min to allow plasma to clot. Coverslips were then inserted hippocampal side up on flat bottom tissue culture tubes (Nunclon Delta Tubes, Nalge Nunc, NY, USA) and 600  $\mu\text{l}$  of warmed Neurobasal A medium containing 10% horse serum (heat inactivated at 56  $^{\circ}\text{C}$  for 30 min; Sigma-Aldrich, H1270), 2% B27 Supplement, 0.8% Glutamax, 0.5% Pen-Strep and 0.1% glucose was added. Tubes were placed at a 5  $^{\circ}$  angle in holding racks and placed in a roller apparatus set at 35  $^{\circ}\text{C}$  with a rotation 10 revolutions per hour. The following day, medium was replaced with serum-free Neurobasal A (containing 2% B27 Supplement, 0.8% Glutamax, 0.5% Pen-Strep and 0.1% glucose). Serum-free media was changed every third day and slices were cultured for up to 48 days before use in experiments. Slice cultures were prepared and maintained at the Bamberg Laboratory, Colorado State University with the technical assistance of Laurie S. Minamide.

## 2.10 Ethics Statement

Experiments involving the use of animals were approved by the University of Sydney Animal Ethics Committee, Australia (chicken embryos; Chief Investigator (CI), Dr Claire Goldsbury) or the Institutional Review Board, Colorado State University, USA (rodents; CI, Prof. James R. Bamberg). Use of human fetal tissue was approved by the University of New South Wales Human Ethics Committee (CI, Dr. Gilles J Guillemin). Donated adult human brain tissue was obtained from the New South Wales Brain Bank, Australia (CI, Dr Karen Cullen) or the Alzheimer Disease Research Center, University of California San Diego, USA (CI, Prof. James R. Bamberg) and approved for use by the University of Sydney Human Ethics Committee or the Institutional Review Board, Colorado State University, respectively.



# 3

## PART III

Activation of MAP/tau by cyclin sequesters phosphorylated MAP/tau into AD-like neuritic inclusions

## Preface

The majority of work in this chapter is based on recently published work (Whiteman et al., 2009) and therefore appears here in published format albeit with some additional supplementary material of relevance to the study.

# 3

## 3.1 Introduction

Alzheimer disease (AD) is a progressive, degenerative dementia histopathologically characterized by neurofibrillary tangles of tau protein and amyloid plaques. Neurofibrillary tangles are composed of hyperphosphorylated microtubule-associated protein (MAP) tau forms striated thread-like structures in neurites, so-called neurofibrils (Augustinack et al., 2002; Velasco et al., 1998), that correlate with cognitive decline and comprise >95% of end-stage cortical tau pathology (Velasco et al., 1998; Braak et al., 2000; Giannakopoulos et al., 2007).

Tau, like other MAPs, stabilizes neuronal microtubules (MT) and facilitates MT dynamics through its phosphorylation and dephosphorylation (Tanzi et al., 2003; reviewed in Garcia and Cleveland, 2001). While normal adult neurons exhibit low levels of tau phosphorylation, neurons of AD brain and other tau-related neurodegenerative diseases show high levels of tau phosphorylation at both physiological and pathological disease-specific residues. This tau hyperphosphorylation prevents binding and stabilization of MT and causes abnormal translocation of tau from axonal MT tracks to



## Preface

The majority of work in this chapter is based on recently published work (Whiteman et al., 2009) and therefore appears here in published format, albeit with some additional supplementary material of relevance to this study.

## 3.1 Introduction

Alzheimer disease (AD) is a progressive, degenerative dementia histopathologically characterized by neurofibrillary tangles of tau protein and amyloid- $\beta$  ( $A\beta$ ) plaques. In early stages of AD, hyperphosphorylated microtubule associated protein (pMAP) tau forms striated thread-like structures in neurites, so-called 'neuropil threads' (Augustinack et al., 2002; Velasco et al., 1998), that correlate with cognitive decline and comprise >85% of end-stage cortical tau pathology (Velasco et al., 1998; Braak et al., 2006; Giannakopoulos et al., 2007).

Tau, like other MAPs, stabilizes neuronal microtubules (MT) and facilitates MT dynamics through its phosphorylation and dephosphorylation (Timm et al, 2003; reviewed in Garcia and Cleveland, 2001). While normal adult neurons exhibit low levels of tau phosphorylation, neurons of AD brain and other tau-related neurodegenerative diseases show high levels of tau phosphorylation at both physiological and pathological disease-specific residues. This tau hyperphosphorylation prevents binding and stabilization of MT and causes abnormal translocation of tau from axonal MT tracks to

neuropil thread inclusions, dendritic processes and cell bodies where it accumulates and aggregates (Terry, 1998; Garcia and Cleveland, 2001). The phosphorylation of tau at Serine 262 (S262) in the microtubule-binding domain is one of the earliest markers of AD neuropathology, readily detected in 'pre-tangle' neuropil threads (Augustinack et al., 2002).

Another prominent feature widespread in the AD brain is abnormal aggregates of the actin associated protein cofilin that forms punctuate and rod-like linear arrays through the neuropil (Minamide et al., 2000). Neuronal cofilin plays important roles in learning and memory pathways by modulating actin-rich dendritic spine architecture (Hotulainen et al., 2009; reviewed in Bamberg and Bloom, 2009). The activity of cofilin and related protein actin depolymerizing factor (ADF) is negatively regulated by phosphorylation of the conserved Ser3 by LIM and other kinases and reactivated upon its dephosphorylation by slingshot or chronophin phosphatases (Huang et al., 2008; reviewed in Bamberg and Bloom, 2009) allowing it to actively bind and sever filamentous actin (F-actin), thus regulating actin turnover (Bamberg and Bloom, 2009, Carlier et al., 1997).

ADF/cofilin-actin rods comparable to those observed in the AD brain are inducible in neuronal cell culture through inhibition of mitochondrial ATP generation and other neurodegenerative stimuli such as oxidative stress or exposure to A $\beta$  peptides (Minamide et al., 2000; Maloney et al., 2005; Davis et al., 2009). Since actin dynamics in neurons are purported to use ~50% of total cellular ATP (Bernstein and Bamberg, 2003), ADF/cofilin-actin rods have been proposed to represent an early neuroprotective mechanism during times of transient stress since virtually all ADF/cofilin is sequestered



into non-dynamic polymers of ADF/cofilin-actin, inhibiting actin turnover and thereby preserving ATP (Bernstein et al., 2006). While mitochondrial dysfunction has been linked to AD (Smith et al., 2005; Wang et al., 2009), the relationship between mitochondrial dysfunction, the generation of tau inclusions and their relationship to cofilin aggregates remains elusive.

In this study, we aimed to determine the effects of mitochondrial dysfunction on cellular pMAP/tau distribution compared to ADF/cofilin-actin rod distribution (Minamide et al., 2000; Huang et al., 2008). Using primary neuronal cell culture models, we demonstrate that cytoskeletal rods containing ADF/cofilin sequester and bind pMAP. The resulting striated pMAP-positive rods bare striking resemblance to neuropil threads observed in postmortem AD brain labeled with the same pMAP antibody. This process may well represent an early pathogenic event in AD leading to synaptic loss and neurodegeneration.

## 3.2 Specific Materials and Methods

### 3.2.1. ATP luminescent measurements

Following treatments (in triplicate), primary chick neurons were harvested and assessed for total ATP (ATPLite, Perkin Elmer) using a Victor III Multi-label plate reader. Protein measurements were determined using the identical samples and the Bicinchoninic acid assay (Sigma-Aldrich). Total ATP was normalized against total protein to account for any difference in

cell density. Statistical analysis used Prism software (v3.0, GraphPad Software Inc).

neuronal cultures at 3 days were transfected using Lipofectamine 2000 (Invitrogen). Four days following transfection, neurons were treated with AM

### **3.2.2. Plasmids and transfection**

Plasmid-mediated expression of wild-type human cofilin has been previously described (Davis et al., 2009). Human cofilin cDNA in a pET vector (a gift from Alan Weeds, MRC Laboratory of Molecular Biology, Cambridge, UK) was modified by PCR with a 5' PCR primer containing an EcoRI site and a 3' primer that removed the stop codon and introduced an XmaI site at the 3' end. EcoRI and XmaI were then used to cut the PCR product and the cDNA was ligated into pEGFP-N1 (Clontech) in frame with the green fluorescent protein to give pCofilin-GFP. A plasmid vector for expressing small interfering RNAs for chick ADF was made by inserting DNA oligonucleotides (Macromolecular Resources, Fort Collins, CO) into a plasmid expression vector (pSuper; (Brummelkamp et al., 2002) containing the H1 polymerase III promoter. The oligonucleotide product from the pol III promoter is a double-stranded hairpin RNA (antisense-linker-sense) that is processed into a functional siRNA in the cell. The modified inserts including the H1 pol III promoter from the pSuper vector were excised and ligated into the pAdTrack vector (He et al., 1998). The siRNA sequence contained within the hairpin used for chick ADF is 5'-GTGGAAGAAGGCAAAGAGATT-3'. A plasmid made identically but which makes a hairpin RNA to silence human Pak2 (5'-GTCTCTGGGTATCATGGCTAT-3') was used as a transfection control in the chick cells. The ability of the shRNA-expressing plasmid to



effectively knockdown ADF in chick cells was tested in cultures of chick skin fibroblasts (Marsick et al., submitted). For plasmid-mediated expression, neuronal cultures at 3 days were transfected using Lipofectamine 2000 (Invitrogen). Four days following transfection, neurons were treated with AM (1  $\mu$ M or 2  $\mu$ M for 10 or 20 min).

### **3.2.3. FRET analysis**

Cells were plated on glass bottomed Mattek dishes and imaged in PBS using a Zeiss LSM 510 and C-Apochromat 40x water immersion objective and the Argon (488 nm) (for GFP donor) and HeNe1 (543) (for Alexa fluor 555 acceptor) laser lines. For photobleaching of acceptor, regions of interest in the transfected cells were bleached using the 543 nm laser line at 100% power. FRET efficiency was calculated from the increase in the fluorescence intensity of the donor after the acceptor was selectively photobleached (Gervásio et al., 2008). The donor fluorescence was measured from at least five bleached and five unbleached rods per cell.

### **3.2.4. Human tissue and rat hippocampal slices**

Free-floating sections (45  $\mu$ m) of formalin fixed superior frontal cortex and basal forebrain from normal adult and confirmed Alzheimer's disease patients obtained from the New South Wales Brain Bank were immunostained as previously described (Cullen et al., 2005). Sections were incubated overnight at 4°C in primary antibody. Bound antibody was

visualized using Alexa Fluor-conjugated secondary antibody (Invitrogen) or using ABC-peroxidase (Vector) and DAB (Sigma).

For quantification of cells containing rod structures, cells with rods were counted for each treatment condition from randomly selected fields on each

Organotypic rat hippocampal slices were grown for 14 days on membrane as described (Davis et al., 2009). Slices were treated with 2  $\mu$ M AM in PBS for 1 h, fixed in 4% formaldehyde for 1 h, permeabilized 90 sec in 0.05% Triton X-100 in PBS and immunostained overnight with 1439 (cofilin) (2  $\mu$ g/ml) and mouse 12E8 (4  $\mu$ g/ml) antibodies. Secondary antibody incubations were 2 h (see Chapter 2 for further detail)

DAPI staining, were excluded from the data. Following adjustment to background, mean and standard error of the mean (s.e.m.) intensities were

3.2.5. *A $\beta$  peptide treatments* significance was measured using the student

Stock solutions of lyophilized A $\beta$  peptides (Bachem) were solubilized to 2 mM in DMSO, aliquoted and stored at -20°C. Immediately before application to cells, the stock solutions were diluted to 100  $\mu$ M in PBS and agitated at 1200 rpm on a laboratory shaker for 30 minutes at 37°C to generate mixtures of polymorphic oligomeric and fibrillar aggregates as previously described (Goldsbury et al., 2000). The peptide assemblages were then applied to cells in 24 well plates at final concentrations of 1 or 2  $\mu$ M. Control wells were treated with the same volume of DMSO in PBS.

We used the monoclonal phosphorylation-dependent 12E8 antibody raised against the pMAP tau, an established early marker for neurofibrillary tangles in AD (Augustineck et al., 2002), to determine whether pMAP accumulates in primary neuronal models derived from human, rat or chick following



### 3.2.6. Analysis and statistics

For quantification of cells containing rod structures, cells with rods were counted for each treatment condition from randomly selected fields on each coverslip and cells containing rods structures were then expressed as a percentage of the total cell population or mean number of rods per cell. Treatments and measurements were repeated in triplicate using independently prepared cell cultures. For determination of relative fluorescence intensities for phalloidin or ADF, immunofluorescent intensity was measured using Image J. Cells with abnormal nuclei, as indicated by DAPI staining, were excluded from the data. Following adjustment to background, mean and standard error of the mean (s.e.m.) intensities were calculated for each condition. Significance was measured using the student *t*-test.

## 3.3 Results

### 3.3.1 Neuritic pMAP accumulation in striated rods, resembling structures in postmortem Alzheimer brain, is induced in primary neurons by energy depletion

We used the monoclonal phosphorylation-dependent 12E8 antibody raised against the pMAP tau, an established early marker for neuropil threads in AD (Augustinack et al., 2002), to determine whether pMAP accumulates in primary neuronal models derived from human, rat or chick following

mitochondrial inhibition. Probing AD brain sections with the AT8 (Fig. 3.1a, b) or 12E8 antibodies (Fig. 3.2a, b) showed numerous striated rod-like inclusions within neuropil threads and cytoplasmic accumulations of pMAP, indistinguishable from previous observations in human AD (Augustinack et al., 2002). Additionally, linear striations of rod accumulations labeled with cofilin antibodies were also observed in AD brains (Fig 3.1c).

Treatment of primary human CNS neurons cultured for 7 days *in vitro*, with the mitochondrial complex III inhibitor antimycin (AM) elicited a rapid accumulation of 12E8-labeled protein into rod inclusions (Fig. 3.2e, arrows) comparable to those seen in the AD neurons (Fig. 3.2a, b, arrows). The rods sequestered the fraction of MAP serine-phosphorylated in the microtubule-binding-domain KXGS motifs specific for the 12E8 antibody, rather than total MAP/tau because a polyclonal antibody against total tau yielded a more uniform labeling along neurites of both human and chick neurons (Fig. 3.2c, d). During AM-treatment, primary chick CNS neurons derived from embryonic tectum also generated pMAP-positive rod-like structures (Fig. 3.2d, e) morphologically identical to those from human neurons. Thus, the readily accessible chick neurons are a useful model system for studying the mechanism by which pMAP accumulates into rods. The conserved 12E8 epitopes in the pMAP sequence reside within the microtubule binding domain in human tau (S262/S356 residues) and chicken tau (S253/S378) (Fig 3.3a, b) (Yoshida and Goedert, 2002). Primary chick tectal neurons express five isoforms of tau that are highly homologous to human tau isoforms and exhibit conservation of



phosphorylation-specific epitopes recognized by antibodies against human tau (Fig 3.3c) (Yoshida and Goedert, 2002).

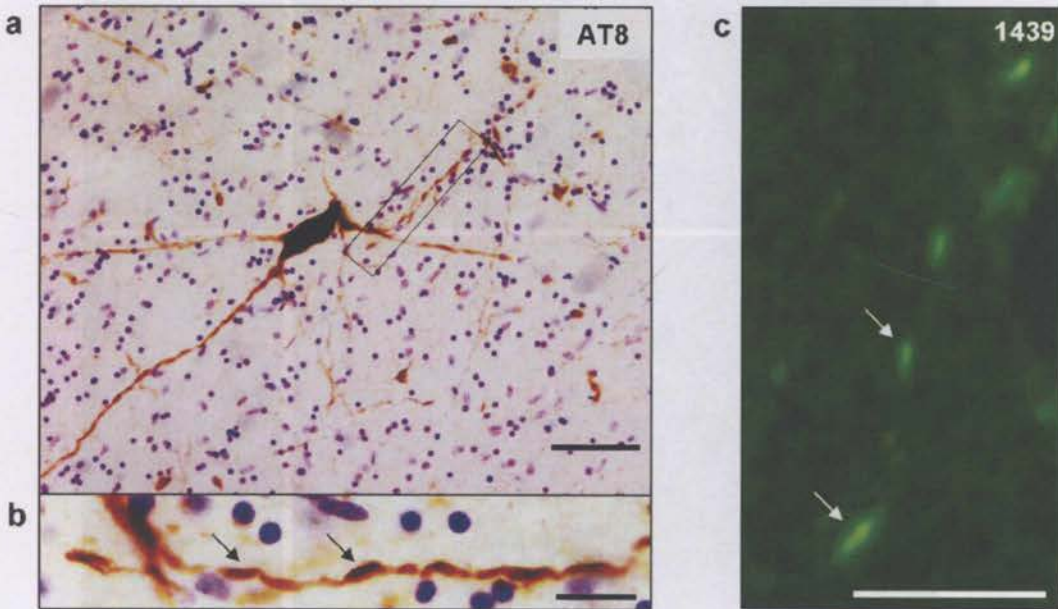


**Figure 3.1 Neuritic striations in human AD.** (a) An AD forebrain neuron, still containing a nucleus, shows accumulations of tau phosphorylated at Ser202/Thr205 (as indicated by AT8 immunoreactivity) throughout the cell body and neurites. Inset (magnified in (b)) shows striation of the neurites with linear arrays of AT8-positive inclusions (arrows). This AD case was classified with early stage (Braak Stage II) accumulation of tau pathologies. (c) Paraffin section (6–7  $\mu\text{m}$ ) of frontal cortex from a confirmed AD brain immunolabelled with 1439 (cofilin). Linear striations of rod accumulations are evident (arrows). Scale bars = 10  $\mu\text{m}$  (a, c); 3  $\mu\text{m}$  (b). The author gratefully acknowledges Karen M. Cullen for images (a) and (b) and Laurie S Minamide for image (c).

Figure 3.2 Neuropathological hallmarks of human AD can be recapitulated in ATP-depleted human and chick primary neurons. (a, b) Immunofluorescent staining of sections of frontal cortex from human AD brain show strong 12E8 reactivity in neurofibrillary tangles (NFT) in individual neurons (a) and abundant linear arrays of 12E8-labeled inclusions in neurites (a, b, arrows). (c) Human primary neuronal cell cultures (labeled with the 12E8 antibody (red) and total tau antibody (green), following 30 min ATP treatment (plus DAPI in blue in merged image). Tapered pMAP-positive rods were observed throughout the neurites (arrows). (d, e) Primary chick neurons (7 DIV) treated with AM for 15 min also rapidly accumulate rod-like 12E8-positive inclusions (rod) that frequently form linear striations within single neurites (a, arrowheads). Rods were not enriched with total tau (d, green), indicating that inclusions contain MAP/tau specifically phosphorylated within the microtubule-binding KXCS motifs, as immunostained with 12E8 (red). (f) Control chick neurons show evenly distributed 12E8 staining along neurites with only the occasional rod-like accumulation (arrow). Scale bars = 10  $\mu\text{m}$  (a, b), 20  $\mu\text{m}$  (c–f).

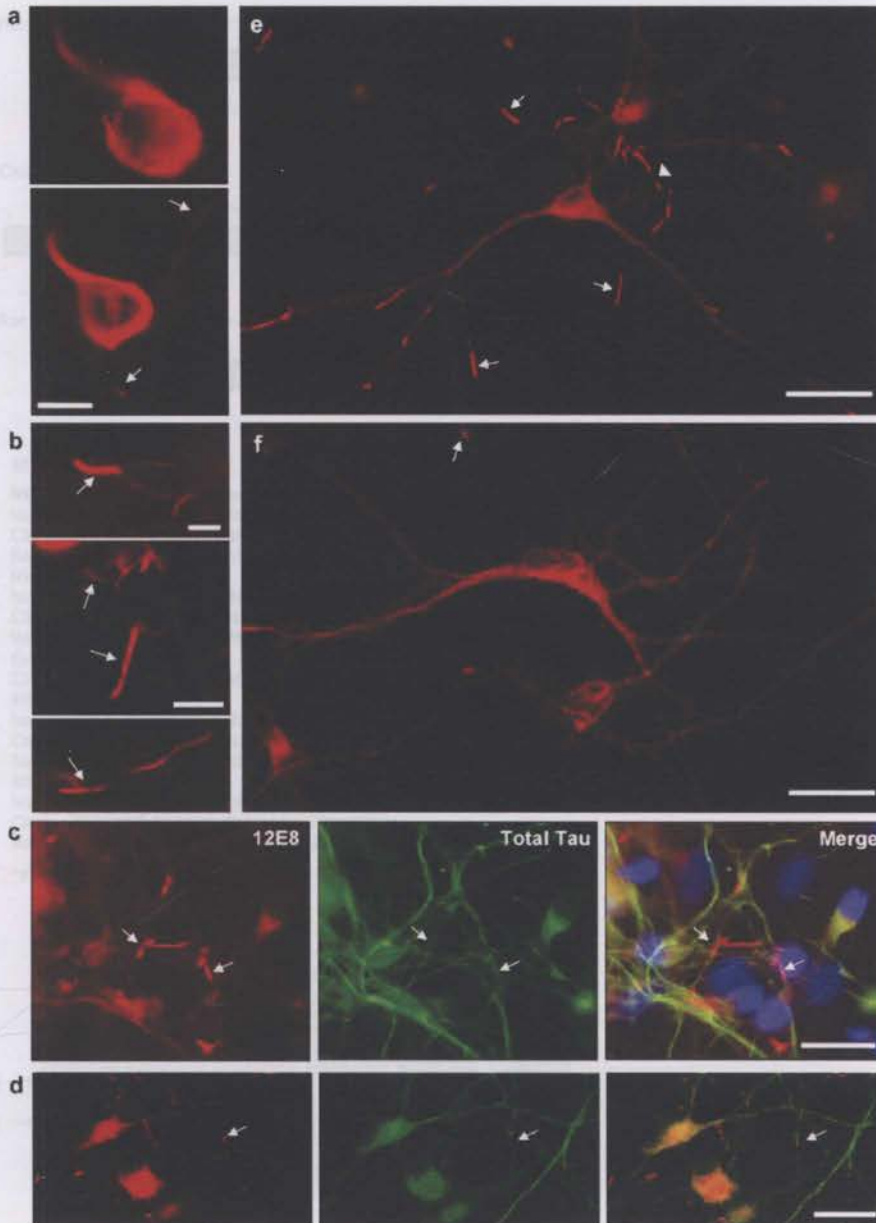


**Figure 3.2 Neuropathological hallmarks of human AD can be recapitulated in ATP-deprived human and chick primary neurons.** (a, b) Immunofluorescent staining of sections of frontal cortex from human AD brain show strong 12E8 reactivity in neurofibrillary tangles (NFT) in individual neurons (a) and abundant linear arrays of 12E8-labeled inclusions in neurites (a, b, arrows). (c) Human primary neuronal cell cultures labeled with the 12E8 antibody (red) and total tau antibody (green), following 30 min AM treatment (plus DAPI in blue in merged image). Tapered pMAP-positive rods were observed throughout the neurites (arrows). (d,e) Primary chick neurons (7 d.i.v) treated with AM for 15 min also rapidly accumulate rod-like 12E8-positive inclusions (red) that frequently form linear striations within single neurites (e, arrowhead). Rods were not enriched with total tau (c,d, green), indicating that inclusions contain MAP/tau specifically phosphorylated within the microtubule-binding KXGS motifs, as immuno-stained with 12E8 (red). (f) Control chick neurons show evenly-distributed 12E8 staining along neurites with only the occasional rod-like accumulation (arrow). Scale bars = 10  $\mu\text{m}$  (a, b); 20  $\mu\text{m}$  (c-f).





**Figure 3.3 Chicken tau is highly homologous to human and rodent tau.** (a) Epitope map of phosphorylated sites recognized by tau antibodies in human, chicken (Yoshida and Goedert, 2002) and rat brain. Schematic representations of the longest tau isoforms are shown (441 amino acid residues in human tau, 463 in chicken and 432 in rat). The phosphorylation-dependent anti-tau antibodies (AT270, AT8, AT180, 12E8 and pS396) are shown with their corresponding target residues. Positions of the various alternatively spliced inserts are shown in blue. Green boxes denote tandem amino acid sequence repeats, which constitute the microtubule-binding domain (MTBD). (b) Amino acid sequence alignment of MTBD regions of human, chicken and rat tau demonstrate strong homology in this region. (c) Western blots of primary chicken neuronal cultures were probed with anti-tau antibodies. Six tau bands ranging from 50-64 kDa are identified with a phosphorylation-independent antibody (total tau). Probing with phosphorylation-dependent antibodies (12E8, AT8, AT180, AT270 and pS396) reveals preferential phosphorylation of specific epitopes on different isoforms. Marker positions (kDa) indicated by arrows.

### **3.3.2 pMAP-containing striations induced by ATP-depletion co-localize with ADF/cofilin-actin rods**

Actin dynamics are highly dependent on ATP availability (Bernstein and Bamburg, 2003) and ATP depletion is associated with an increase in cellular F-actin and an increase in ADF/cofilin activity (Minamide et al., 2000). It follows that acute inhibition of mitochondrial function used here to generate pMAP-immunostained rods, may result in changes to the actin cytoskeleton. Consistent with this, AM-treated chick neurons exhibited a 1.9-fold increase in overall phalloidin staining in cell bodies indicative of increased F-actin content (Fig. 3.4a-c). The pMAP-positive rods however, did not overlap with phalloidin-labeling (Fig. 3.4b).

In ATP-depleted rat hippocampal neurons, the rapid dephosphorylation of cofilin leads to the development of cofilin-actin rods in neurites (Minamide et al., 2000). These rods contain actin, as evidenced by both antibody immunostaining and ultrastructure, but do not stain with phalloidin, indicating they are probably saturated with ADF/cofilin which stabilizes the "twisted" form of the filament and eliminates the phalloidin binding site (McGough et al., 1997). We therefore asked whether rods induced by ATP-depletion contain both pMAP and ADF/cofilin. Double labeling revealed that ADF/cofilin-actin rods in part co-localize with pMAP in chick (Fig. 3.5a-c, asterisks), human (Fig. 3.5d, asterisk) and rat hippocampal neurons (Fig. 3.5e, asterisk). Co-localization of cofilin and pMAP in rod structures in ATP-depleted organotypic rat hippocampal slice cultures was also revealed (Fig. 3.6). Moreover, staining for  $\beta$ (III)-tubulin did not accumulate at rods, further



suggesting the specificity of pMAP and ADF/cofilin in formation of neuritic rods (Fig. 3.7). However, ADF/cofilin-stained rods that do not stain for pMAP (arrowheads in Fig. 3.5c, e) and pMAP-stained rods that do not stain for ADF (arrow in Fig. 3.5b) were both observed.

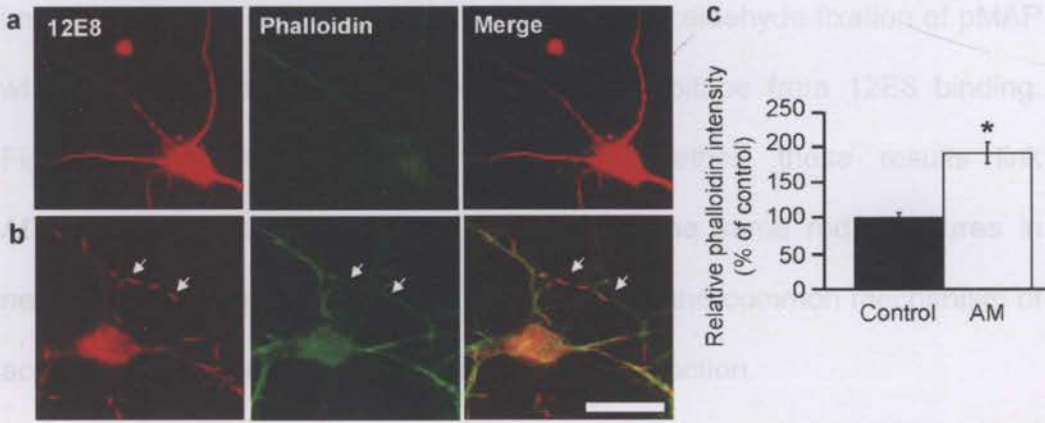


**Figure 3.4 Cell body F-actin labeling increases following ATP depletion.** (a, b) Chick neurons (7 d.i.v) were co-stained with phalloidin (green) and 12E8 (red) before treatment (a) and after treatment (b) with AM for 15 min. Merged images from double-labeling are shown on the right. Rods forming in the neurite shaft did not stain with phalloidin (b, arrows). (c) Intensity of phalloidin staining in AM-treated cells increased significantly compared to controls ( $*p < 0.001$ ,  $n = 25$  cells for each treatment condition. Error bars represent s.e.m.). Scale bar = 20  $\mu\text{m}$ .

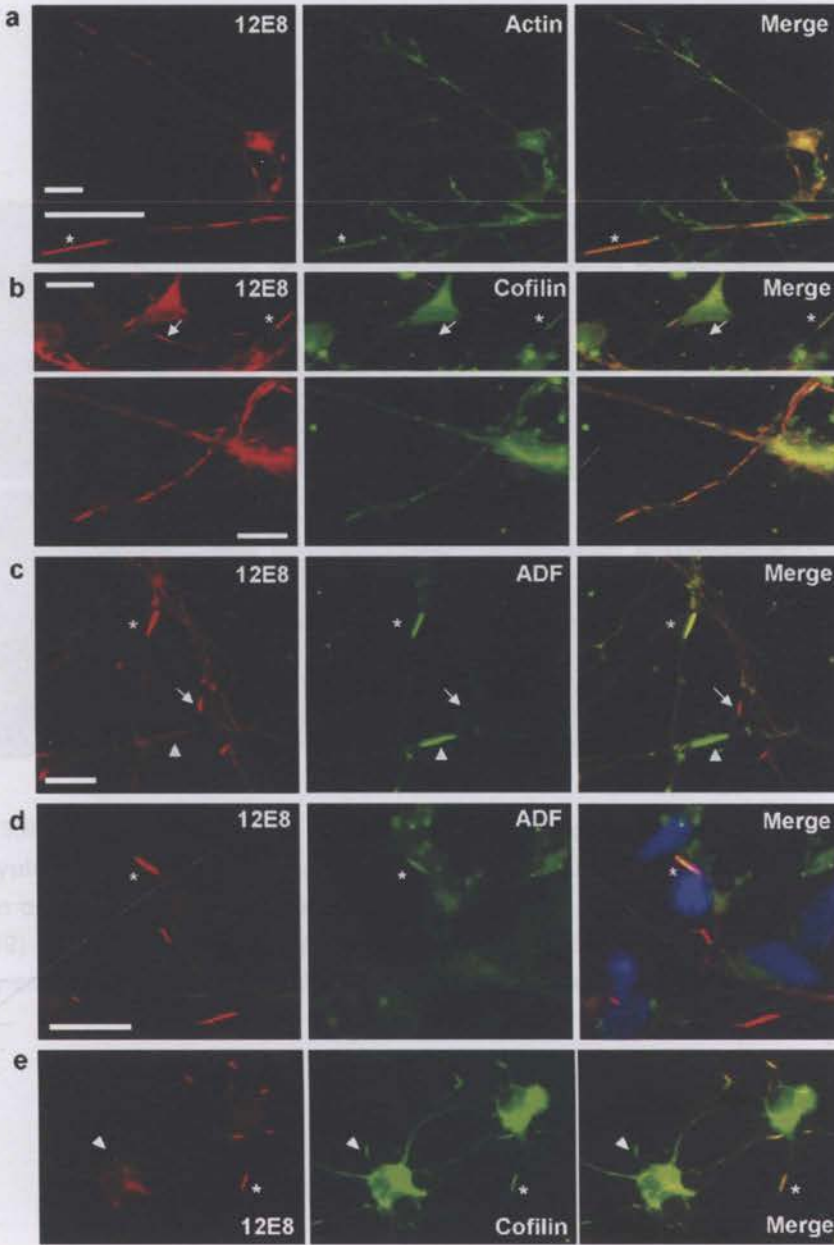
Since optimal immunostaining for pMAP requires Triton X-100 permeabilization (avoiding methanol) and optimal immunostaining for ADF/cofilin requires methanol (avoiding Triton) structures that stain for one and not the other may be sub-optimally permeabilized or immunostained. However, we cannot exclude that the detected inclusions may represent a heterogeneous population of rod structures. Surprisingly, in hippocampal neurons derived from rat there was no change in the diffuse and uniform

distribution of pMAP staining following ATP-depletion, fixation in 4% paraformaldehyde and 0.1% glutaraldehyde, and brief (90 s) 0.05% Triton X100 permeabilization, which looked identical to the staining of pMAP in untreated human, rat and chick neurons (Fig. 3.1f). However, rat neurons subjected to AM-induced ATP-depletion, followed by fixation in 4% formaldehyde and permeabilization as above did exhibit rod-like 12E8 immunostaining (Fig. 3.5e), suggesting that glutaraldehyde fixation of pMAP when it is in a rod-like structure, masks its epitope from 12E8 binding. Figure 3.8 summarizes these findings. Together, these results link ADF/cofilin-actin and pMAP inclusions within the same rod structures in neurites, which can be induced in cell culture by the common mechanism of acute ATP depletion through mitochondrial dysfunction.

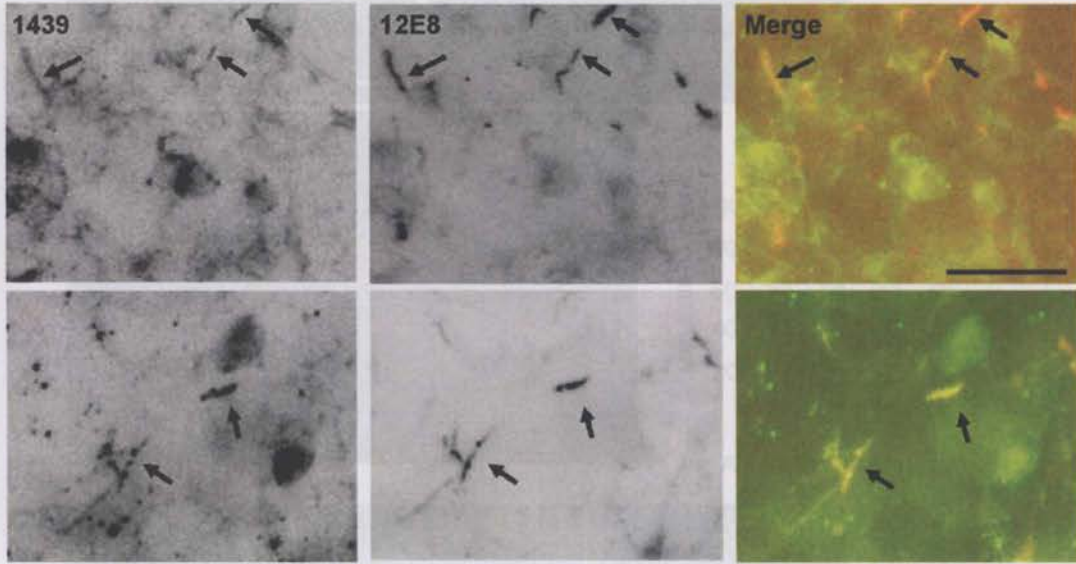


Figure 3.5 Co-localization of actin, cofilin and ADF occurs in pMAP inclusions following ATP-depletion. Chick neurons treated with AM were double-labeled with 12E8 (red) and (a) actin, (b) cofilin (C67D6; Sigma) or (c) ADF (D8815; Sigma) antibodies as indicated (green). Merged images are shown on the right. Rods containing pMAP also stained positively for actin (asterisk in a), cofilin (asterisk in upper panel b) and ADF (asterisk in c). Double-labeled strings of rods were often observed within single neurites (lower panel b). pMAP inclusions in (a) primary human and (a) rat hippocampal (S d l v) neurons also co-labeled with ADF (D8815) (d) and cofilin (C67D6) (e). Some rods contained pMAP but were weakly labeled or negative for cofilin or ADF (arrows, b and c) while others stained strongly for ADF or cofilin but only weakly or negative for pMAP (arrowheads, c, e). This is suggestive of a heterogeneous population of rod-like structures under sub-optimal immunolabeling-conditions for the respective structures (see text). Scale bars = 10  $\mu$ m. The author gratefully acknowledges Claire Gobbarty for images (a-d) and Laurie S. Minamide for image (e).





**Figure 3.5 Co-localization of actin, cofilin and ADF occurs in pMAP inclusions following ATP-depletion.** Chick neurons treated with AM were double-labeled with 12E8 (red) and (a) actin, (b) cofilin (C8736; Sigma) or (c) ADF (D8815; Sigma) antibodies as indicated (green). Merged images are shown on the right. Rods containing pMAP also stained positively for actin (asterisk in a), cofilin (asterisk in upper panel b) and ADF (asterisk in c). Double-labeled strings of rods were often observed within single neurites (lower panel b). pMAP inclusions in (d) primary human and (e) rat hippocampal (5 d.i.v) neurons also co-labeled with ADF (D8815) (d) and cofilin (1439) (e). Some rods contained pMAP but were weakly labeled or negative for cofilin or ADF (arrows, b and c) while others stained strongly for ADF or cofilin but only weakly or negative for pMAP (arrowheads, c, e). This is suggestive of a heterogeneous population of rod-like structures and/or sub-optimal immunostaining conditions for the respective structures (see text). Scale bars = 10  $\mu$ m. The author gratefully acknowledges Claire Goldsbury for images (a-d) and Laurie S. Minamide for image (e).



**Figure 3.6 Co-localization of cofilin and pMAP occurs in ATP-depleted rat organotypic hippocampal slices.** Following ATP-depletion, rod-like accumulations are evident in organotypic rat (P8) hippocampal slices and are positive for both cofilin (labeled with 1439) and pMAP (labeled with 12E8) (arrows). Scale bar = 10  $\mu$ m. The author gratefully acknowledges Laurie S. Minamide for these images.

Figure 3.7 pMAP and ADF/cofilin rods form after mitochondrial inhibition but tubulin remains uniformly distributed. (a) Single stainings of chick neurons with primary antibodies against pMAP (12E8), cofilin (C8736, Sigma), and ADF (1439) (as indicated) were conducted on cells following 10 min treatment with AM. Formation of rod-like structures was apparent in each staining condition. (b) Whereas ADF (DB919, Sigma) (green) accumulates in rod-like structures in cells treated with AM for 15 min,  $\beta$ -tubulin (red) staining remained evenly distributed throughout neurites (arrows). (c) In non-treated cells, both  $\beta$ -tubulin and ADF staining was evenly distributed except for a characteristic ADF increase and lack of tubulin in growth cones (asterisk). (d) To determine cell viability, cells were stained with Trypan blue following 0, 10, 30 or 60 min AM treatment.  $94.6 \pm 0.1\%$  cells were viable after 10 min AM treatment (normalized to control),  $17.2 \pm 0.1\%$  after 30 min AM and  $71.5 \pm 0.14\%$  after 60 min (mean  $\pm$  standard deviation expressed as % control,  $n=10$  fields per treatment condition). Scale bars = 10  $\mu$ m (a); 20  $\mu$ m (b, c).



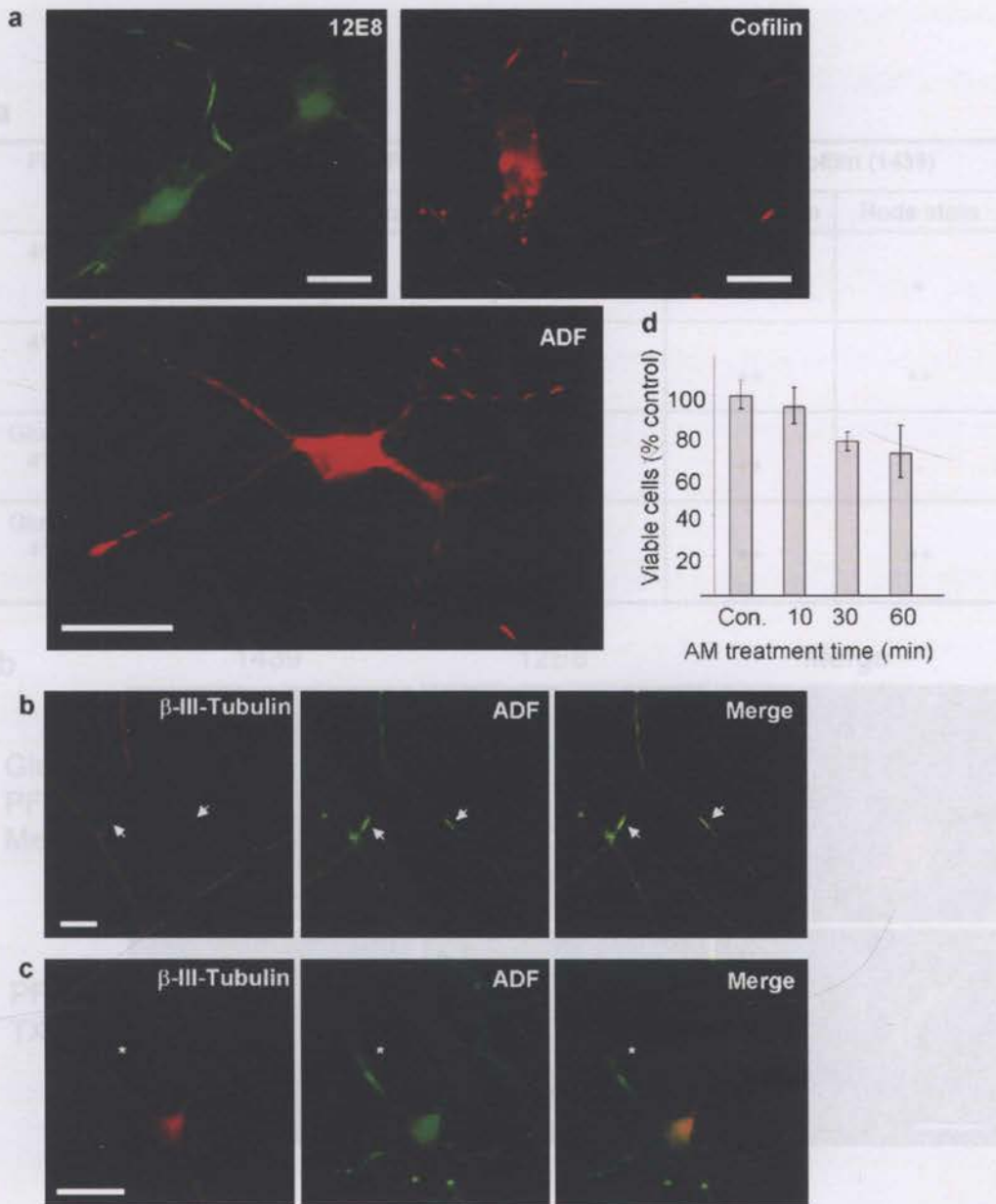


**Figure 3.7 pMAP and ADF/cofilin rods form after mitochondrial inhibition but tubulin remains uniformly distributed.** (a) Single stainings of chick neurons with primary antibodies against pMAP (12E8), cofilin (C8736; Sigma), and ADF (1439) (as indicated) were conducted on cells following 10 min treatment with AM. Formation of rod-like structures was apparent in each staining condition. (b) Whereas ADF (D8815; Sigma) (green) accumulates in rod-like structures in cells treated with AM for 15 min,  $\beta$ (III)-tubulin (red) staining remained evenly distributed throughout neurites (arrows). (c) In non-treated cells, both  $\beta$ (III)-tubulin and ADF staining was evenly distributed except for a characteristic ADF increase and lack of tubulin in growth cones (asterisk). (d) To determine cell viability, cells were stained with Trypan blue following 0, 10, 30 or 60 min AM treatment.  $94.6 \pm 0.1\%$  cells were viable after 10 min AM treatment (normalized to controls),  $77.2 \pm 0.1\%$  after 30 min AM and  $71.5 \pm 0.14\%$  after 60 mins (mean  $\pm$  standard deviation expressed as % control,  $n > 10$  fields per treatment condition). Scale bars = 10  $\mu$ m (a); 20  $\mu$ m (b, c).

To establish the activation state of ADF/cofilin during pMAP accumulation, we used an antibody specific for phosphorylated (inactive) ADF/cofilin

**a**

Fixative	Permeabilize Method	Phospho-tau (12E8)		ADF/Cofilin (1439)	
		Overall stain	Rods stain	Overall stain	Rods stain
4% PFA	TritonX-100 (0.05%)	++	++	+	+
4% PFA	Methanol (100%)	+	-	++	++
Glut (0.1%)/ 4% PFA	TritonX-100 (0.05%)	++	-	++	-
Glut (0.1%)/ 4% PFA	Methanol (100%)	+	-	++	++

**b**

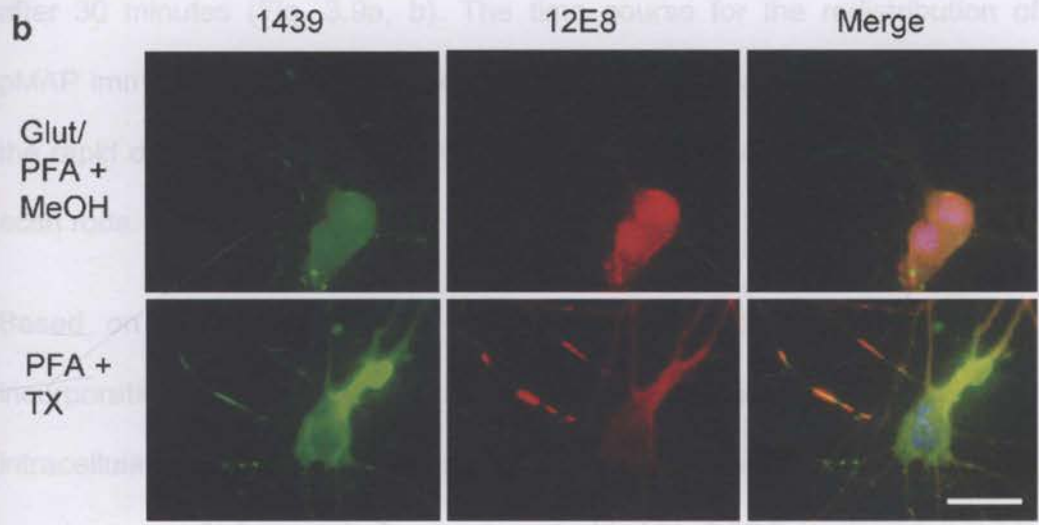


**Figure 3.8 Optimizing fixing and permeabilization protocols for MAP and ADF/cofilin.** Rat hippocampal and chick tectal primary neurons were treated with AM and fixed and permeabilized as indicated in (a). Whereas AC rods were well preserved with either paraformaldehyde (PFA) or PFA/Glutaraldehyde (Glut) permeabilization, presence of Glut resulted in smooth and evenly distributed 12E8 labeling, with no apparent rods (b). Methanol (MeOH) permeabilization preserved AC rods, but not 12E8-positive inclusions, whereas TritonX-100 (TX) permeabilization combined with PFA fixation resulted in excellent preservation of 12E8-positive inclusions and good preservation of AC rods (b) (+, good; ++, excellent; -, negative). Scale bar = 20 μm.



To establish the activation state of ADF/cofilin during pMAP accumulation, we used an antibody specific for phosphorylated (inactive) ADF/cofilin (Minamide et al., 2000; Maloney et al., 2005). ADF/cofilin actin-binding activity is negatively regulated by phosphorylation of the N-terminal Ser3 (Huang et al., 2008; Kim et al., 2009). Upon ATP depletion with AM, ADF/cofilin was rapidly dephosphorylated (activated) in chick tectal neurons, as early as 2 min after treatment (Fig 3.9a, b), consistent with studies in primary rat hippocampal neurons (Minamide et al., 2000). Peroxide ( $H_2O_2$ )-treated tectal neurons also showed nearly complete ADF/cofilin activation after 30 minutes (Fig. 3.9a, b). The time course for the redistribution of pMAP immunostaining into the rod-like inclusions (Fig. 3.9c) correlated with the rapid dephosphorylation of ADF/cofilin and the formation of ADF/cofilin-actin rods.

Based on the above results, we expected that the extent of pMAP incorporation into rods would be inversely proportional to the level of intracellular ATP. To explore this relationship, we measured ATP levels in tectal neurons before and after treatment with AM, CCCP (carbonyl cyanide 3-chlorophenylhydrazone, a mitochondrial uncoupling agent) or  $H_2O_2$  (Fig. 3.9d). Consistent with the notion that activation of ADF/cofilin induced by intracellular ATP depletion correlates with pMAP accumulation, there was an inverse relationship between the % of cells in the culture that contained pMAP-stained rods (Fig 3.9c) and the level of ATP detected in the cell treatment groups (Fig. 3.9d). Cell viability tests revealed 95% cell survival in 10 min AM-treated chick neuronal cultures (compared to control cultures) and 77% survival in 30 min treated cultures (Fig. 3.7d). Likewise, abundant

pMAP-positive rod formation was recapitulated in primary human neurons treated with AM for 30 min ( $24 \pm 2$  rods per field for AM treated compared with  $8 \pm 1$  rods per field in controls, mean  $\pm$  SD;  $p < 0.001$ ). Together, these results suggest ATP-depletion is an important correlate for redistribution of pMAP into rods.

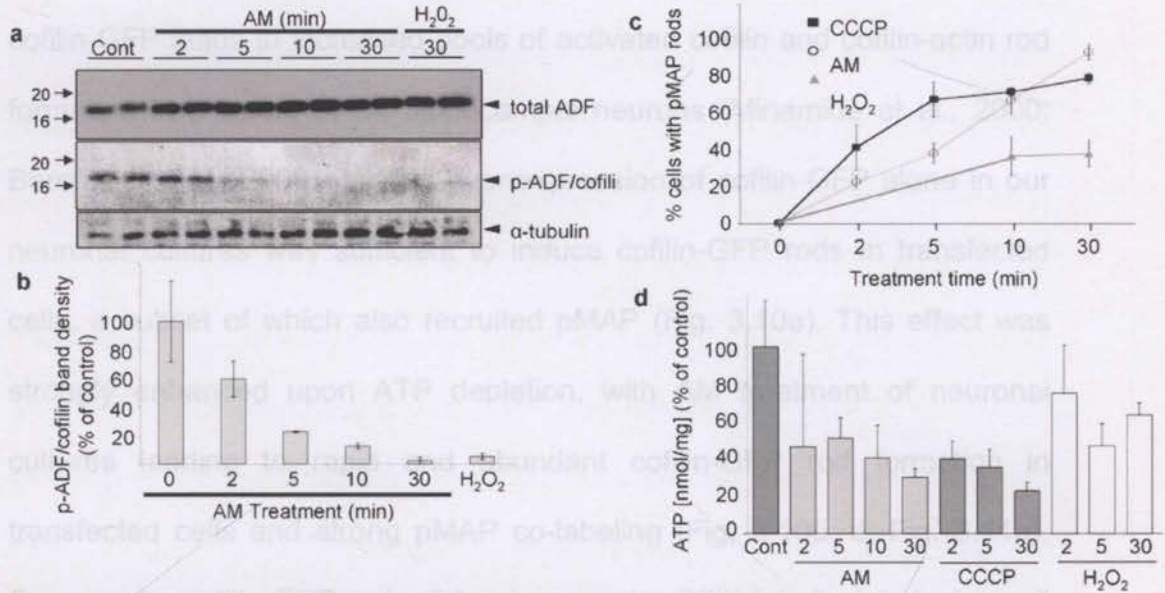


**Figure 3.9 Mitochondrial inhibition induces activation of ADF/cofilin and is correlated to pMAP-positive rod formation.** Dephosphorylation at the N-terminal (Ser3) leads to ADF/cofilin activation. (a) Chick neurons were treated with AM or  $H_2O_2$  for the indicated times, lysed and immunoblotted. Whereas total ADF levels (probed with 1439) remained the same (or slightly increased) compared to control cells, ATP depletion resulted in rapid dephosphorylation of ADF/cofilin as early as 2 mins following AM treatment (p-ADF/cofilin antibody is Ser3-specific). Similarly,  $H_2O_2$  treatment induced almost complete dephosphorylation. (b) Graph shows time course of ADF/cofilin dephosphorylation. Band intensities from duplicate samples were normalized to  $\alpha$ -tubulin loading controls and calculated as a percentage of control band intensities. (c) Coverslips were treated with AM, CCCP or  $H_2O_2$  and immunostained in parallel for quantification of the extent of rod generation. AM-treated cells ultimately contained the greatest abundance of pMAP-positive rods, although CCCP-treated cells initially developed rods more rapidly.  $\sim 40\%$  of  $H_2O_2$ -treated cells developed rods over 30 mins. Data points and error bars represent mean and s.e.m. values from three independent experiments. (d) Luminescence measurements were carried out to ascertain ATP levels following AM, CCCP or  $H_2O_2$  treatment. Compared to control samples, cells treated with AM and CCCP showed a rapid decline in ATP levels, while those treated with  $H_2O_2$  showed a more modest decline. Error bars represent s.e.m. of triplicate samples. Together, these data suggest an inverse correlation between number of pMAP rods formed and level of ATP. The author gratefully acknowledges Shane T Antao for data analysis and bar graph in (d).



### **3.3.3 Activated cofilin sequesters and is closely associated with pMAP in rods**

after bleaching the Alexa-555 fluorophore (Fig. 3.10c, right, arrows), with a measured FRET efficiency of  $41 \pm 3\%$  ( $n = 52$ ). Since ADF/cofilin-actin rods co-stained for pMAP and rod formation depends on activation of ADF/cofilin, we asked whether transfected cofilin-GFP rods sequestered pMAP. Previous work has shown that expression of cofilin-GFP leads to increased pools of activated cofilin and cofilin-actin rod formation in neurites of rat hippocampal neurons (Minamide et al., 2000; Bernstein et al., 2006). Indeed over-expression of cofilin-GFP alone in our neuronal cultures was sufficient to induce cofilin-GFP rods in transfected cells, a subset of which also recruited pMAP (Fig. 3.10a). This effect was strongly enhanced upon ATP depletion, with AM treatment of neuronal cultures leading to rapid and abundant cofilin-GFP rod formation in transfected cells and strong pMAP co-labeling (Fig. 3.10b, c; Fig. 3.11a). Conversely, cofilin-GFP rods did not sequester  $\beta$ (III)-tubulin label when all other conditions were identical (Fig. 3.10d). When non-neuronal cells in culture formed cofilin-GFP rods, these were negative for both pMAP and  $\beta$ (III) tubulin (Fig. 3.10e), neither of which is expressed in non-neuronal cells. Taken together, these results suggest that activated cofilin first accumulates into rods and subsequently sequesters pMAP into these cytoskeletal inclusions.

To further evaluate the interaction between cofilin and pMAP in rods, we exploited fluorescence resonance energy transfer (FRET) between the GFP (donor) and Alexa-555 (acceptor) fluorophores. FRET between co-localized cofilin-GFP and pMAP/Alexa-555 was measured using acceptor

photobleaching (Fig. 3.10c). The cofilin-GFP fluorescence signal in rods increased significantly after bleaching the Alexa-555 fluorophor (Fig. 3.10c, right, arrows), with a measured FRET efficiency of  $41 \pm 3 \%$  ( $n = 52$ ). By contrast, cofilin-GFP fluorescence did not significantly increase in adjacent rods in the same cells where the Alexa-555 fluorophor was not bleached (Fig. 3.10c, right, asterisks). Furthermore, a much reduced FRET signal was detected in neurons between cofilin-GFP and Alexa-555 immunostained pMAP in adjacent non-rod forming regions of neurites and cell bodies (Fig. 3.11b). Control experiments demonstrated no FRET between cofilin-GFP and control antibody labeled epitopes –  $\beta$ (III) tubulin/Alexa-555 or Src/Alexa-555 - even in regions where the fluorescence appeared co-localized (Fig. 3.11c, d). Cells expressing free GFP and treated with AM to generate pMAP-positive rods labeled with 12E8/Alexa-555 also never produced FRET (Fig. 3.11d). These results demonstrate that cofilin-GFP and the secondary antibody labeling pMAP are co-localized  $<10$  nm apart within the cytoskeletal rod complex indicating a close proximity of pMAP and cofilin in these inclusions.



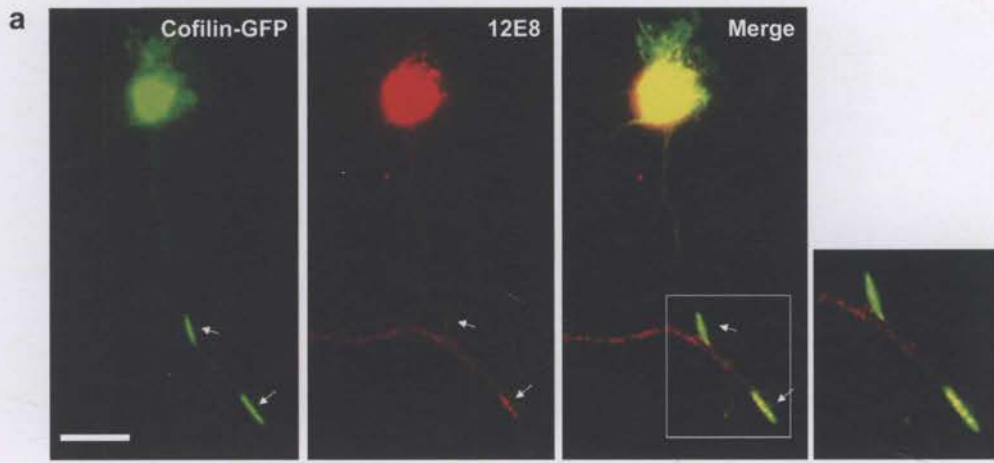
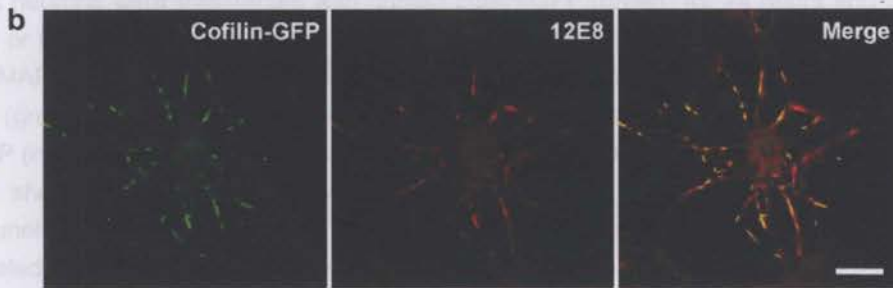
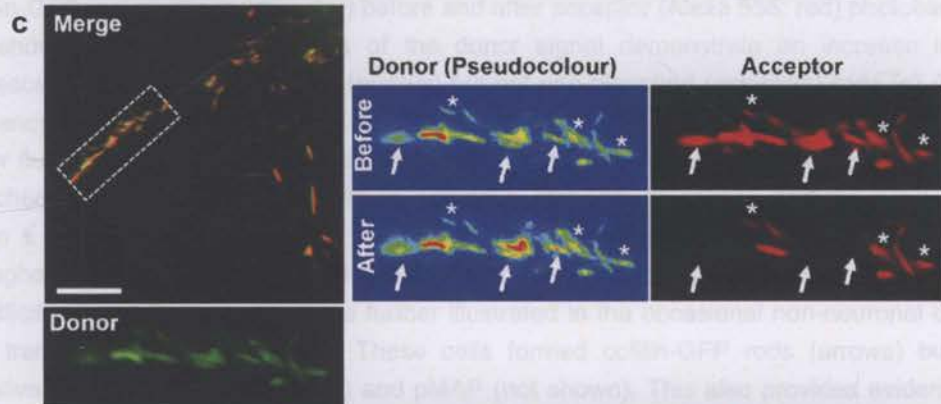


Figure 3.10 Cofilin-GFP forms rods that sequester pMAP during ATP depletion. Primary

check immediately fixed to calculate the percentage of cells with pMAP rods (n=100). After ATP depletion, pMAP rods were observed in 100% of cells. Immunofluorescence revealed that pMAP rods were associated with Cofilin-GFP rods (n=100). These results indicate that pMAP rods are formed in neurons after ATP depletion and that Cofilin-GFP rods sequester pMAP.



Before and after ATP depletion, pMAP rods were observed in neurons. These rods were associated with Cofilin-GFP rods. The percentage of cells with pMAP rods was 100% before and 100% after ATP depletion. The percentage of cells with Cofilin-GFP rods was 100% before and 100% after ATP depletion. The percentage of cells with pMAP rods associated with Cofilin-GFP rods was 100% before and 100% after ATP depletion. These results indicate that pMAP rods are formed in neurons after ATP depletion and that Cofilin-GFP rods sequester pMAP.



These cells formed Cofilin-GFP rods (arrows) but were not associated with pMAP (not shown). This also provided evidence that Cofilin-GFP rods sequester pMAP.

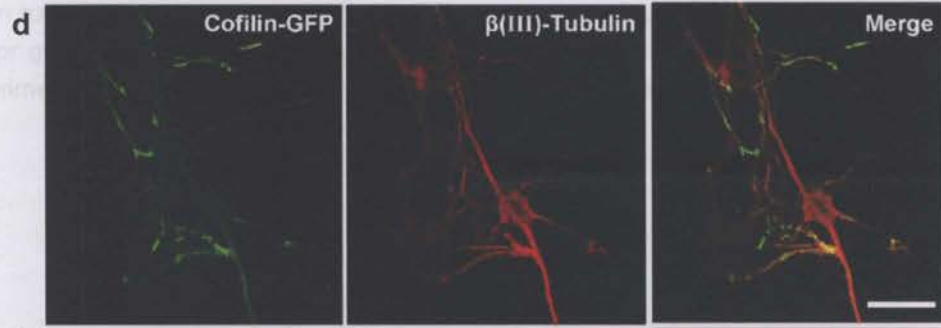




**Figure 3.10 Cofilin-GFP forms rods that sequester pMAP during ATP depletion.** Primary chick neurons were transfected with human cofilin-GFP (green) for 24 hours and immediately fixed or treated with AM to enhance rod assembly prior to fixation. Cells were immunolabeled for pMAP using 12E8 and Alexa 555 secondary anti-mouse (red). (a) Spontaneous cofilin-GFP rods (green, arrows) were observed in non-treated transfected cells and often co-labeled for pMAP (red, arrows), better visualized at higher magnification (inset on far right). (b) AM-treated cells showed greater number of cofilin-GFP rods that frequently co-localized with 12E8 immunolabel (red). See merged images in right panel (yellow). (c) FRET measurements revealed a close proximity between pMAP immunolabel and cofilin-GFP rods. Images of donor (cofilin-GFP: green or pseudo color) before and after acceptor (Alexa 555: red) photobleaching are shown. Pseudo color images of the donor signal demonstrate an increase in GFP fluorescence in acceptor-bleached (arrows) but not non-bleached (asterisks) rods (c) A FRET efficiency of  $41 \pm 3\%$  (mean  $\pm$  s.e.m.;  $n=52$ ) was quantified by measuring the % increase in donor fluorescence after acceptor bleaching (B). No significant FRET signal was seen in non-bleached (N.B) rods in the same cells (c, asterisks) (donor fluorescence increase =  $2.2 \pm 1.1\%$ , mean  $\pm$  s.e.m.;  $n=52$ ) (\*  $p<0.0001$ ). (d)  $\beta$ (III)-tubulin remains smooth and evenly distributed throughout cofilin-GFP transfected cells and is not enriched at cofilin-GFP rods. (e) The specificity of pMAP sequestration is further illustrated in the occasional non-neuronal cell that was transfected with cofilin-GFP. These cells formed cofilin-GFP rods (arrows) but were negative for both  $\beta$ (III)-tubulin (red) and pMAP (not shown). This also provides evidence that cofilin rods form in the absence of pMAP. Scale bars =  $20 \mu\text{m}$  (a, b, d, e);  $10 \mu\text{m}$  (c). The author gratefully acknowledges the work of Othon Gervasio and Claire Goldsbury for FRET experiments (c), images in (d) and (e) and assistance with images in (b).

Figure 3.11 pMAP is selectively sequestered into cofilin-GFP rods following ATP depletion. (a) Co-localization of cofilin-GFP and pMAP (indicated by yellow in merged images) occurs following AM treatment. Transfected cells appear to accumulate more pMAP rods compared to surrounding non-transfected cells (arrows). (b) In contrast to rods, significant FRET between cofilin-GFP and Alexa 555 was not observed in non-rod containing regions of cell bodies (left arrow) or neurites (right arrow). (c) FRET was not observed between cofilin-GFP and  $\beta$ (III)-tubulin/Alexa 555. (d) Summary of quantification of FRET efficiency (% change in donor fluorescence) in acceptor and control. Only acceptor-bleached pMAP positive cofilin-GFP rods gave rise to a significant FRET signal. Scale bars =  $20 \mu\text{m}$  (a);  $5 \mu\text{m}$  (b, c). The author gratefully acknowledges the work of Othon Gervasio and Claire Goldsbury for FRET experiments.



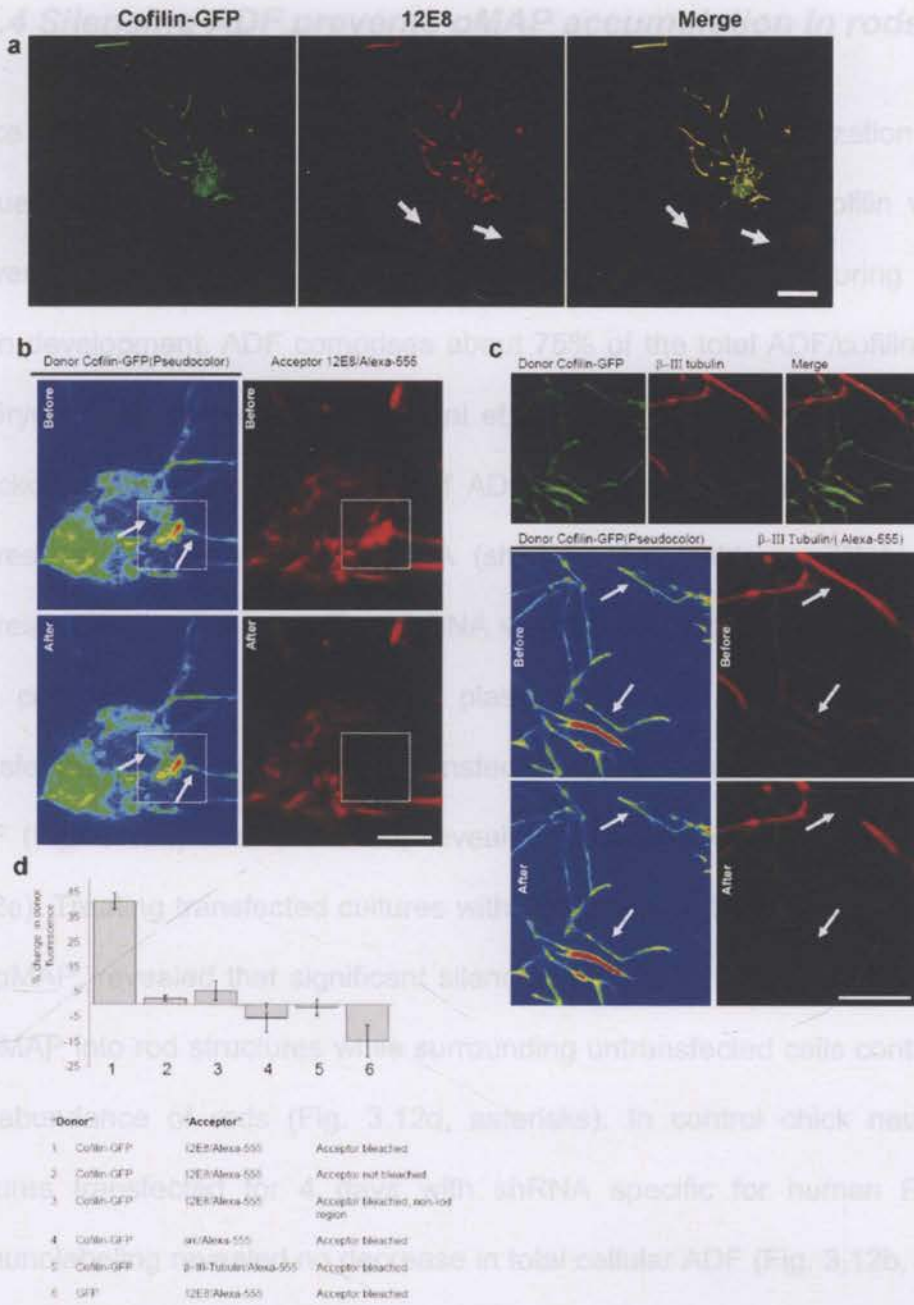


**Figure 3.11 pMAP is selectively sequestered into cofilin-GFP rods following ATP-depletion.** (a) Co-localization of cofilin-GFP and pMAP (indicated by yellow in merged images) occurs following AM treatment. Transfected cells appear to accumulate more pMAP rods compared to surrounding non-transfected cells (arrows). (b) In contrast to rods, significant FRET between cofilin-GFP and Alexa 555 was not observed in non-rod containing regions of cell bodies (left arrow) or neurites (right arrow). (c) FRET was not observed between cofilin-GFP and  $\beta$ (III)-tubulin/Alexa-555. (d) Summary of quantification of FRET efficiency (% change in donor fluorescence) in experiment and controls. Only acceptor-bleached pMAP-positive cofilin-GFP rods gave rise to a significant FRET signal. Scale bars = 20  $\mu$ m (a); 5  $\mu$ m (b, c). The author gratefully acknowledges the work of Othon Gervasio and Claire Goldsbury for FRET experiments.

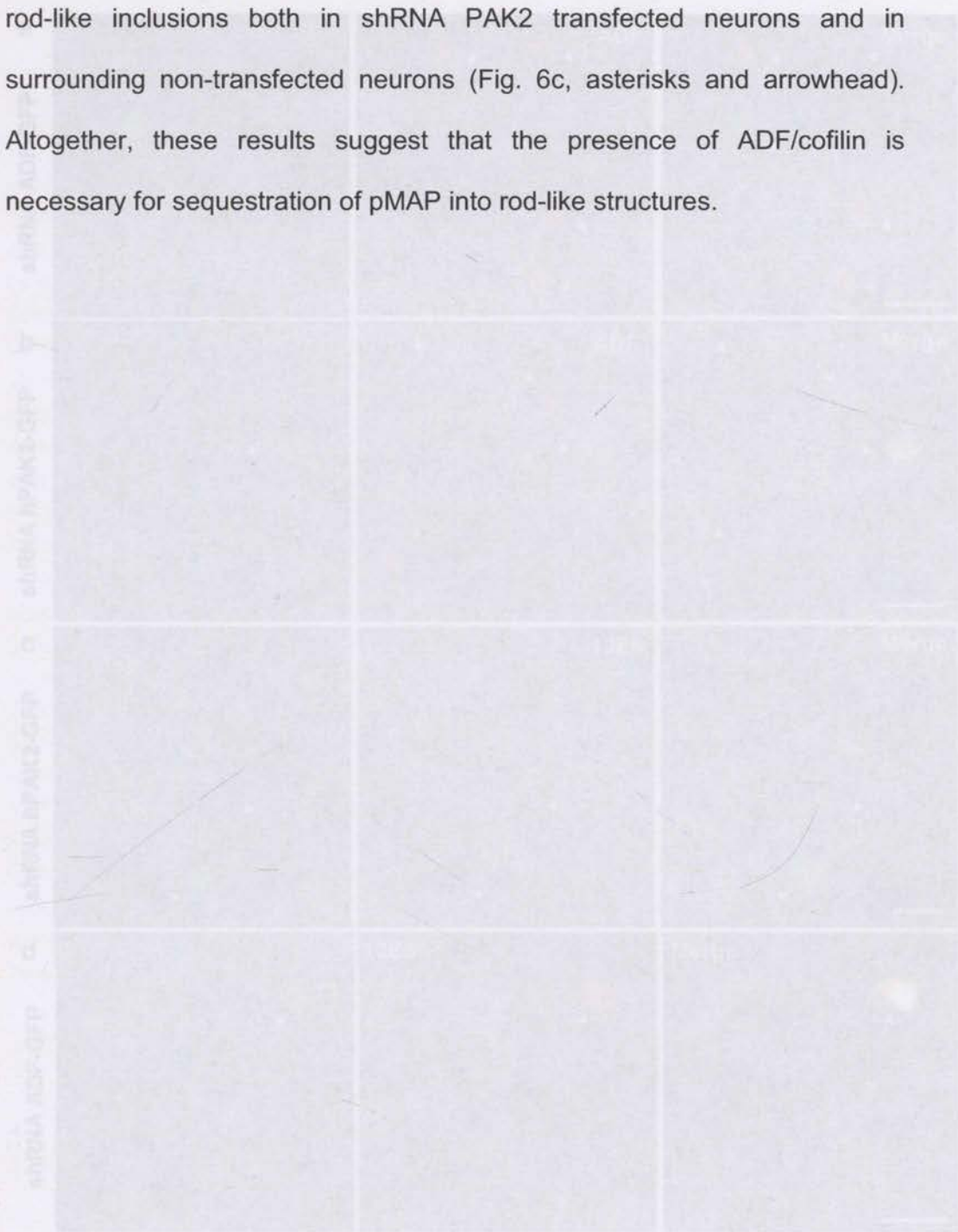
### 3.3.4 Silencing ADF prevents pMAP accumulation in rods

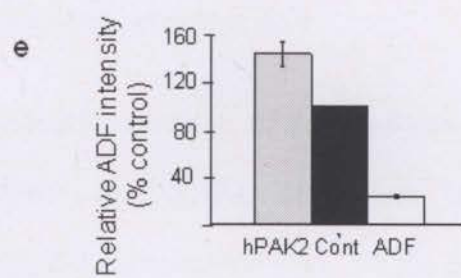
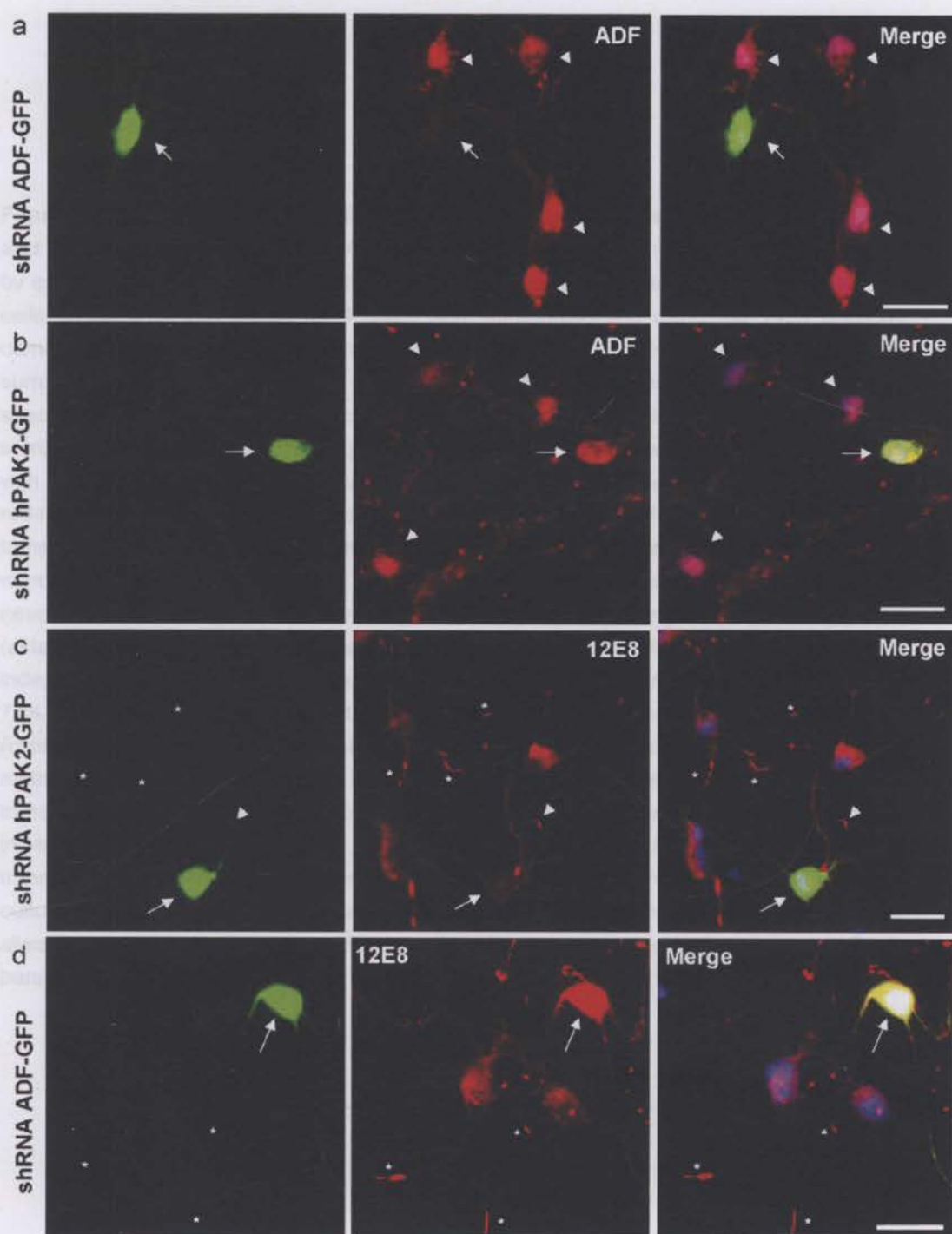
Since induction of ADF/cofilin rods leads to the reorganization and sequestering of pMAP, we asked whether silencing ADF or cofilin would prevent sequestering of pMAP under the same conditions. During chick brain development, ADF comprises about 75% of the total ADF/cofilin from embryonic day 14 onwards (Devineni et al., 1999). We therefore chose to knockdown the total cellular pool of ADF specifically, using a plasmid for expression of a small hairpin RNA (shRNA) that yields a siRNA when expressed and processed. The shRNA was transfected into chick neurons and co-expressed from the same plasmid as GFP for visualization of transfected cells. Four days post-transfection, cells were immunolabeled for ADF (Fig. 3.12a) and quantified, revealing 75% knockdown of ADF (Fig. 3.12e). Treating transfected cultures with AM (1 $\mu$ M for 10 min) and staining for pMAP, revealed that significant silencing of ADF inhibited accumulation of pMAP into rod structures while surrounding untransfected cells contained an abundance of rods (Fig. 3.12d, asterisks). In control chick neuronal cultures transfected for 4 days with shRNA specific for human PAK2, immunolabeling revealed no decrease in total cellular ADF (Fig. 3.12b, e). In fact, transfecting with this construct induced an unexpected and significant increase in ADF ( $p < 0.002$ ). An explanation for this is beyond the scope of this particular study since tests would be required to ascertain whether (though unlikely) this human PAK2 shRNA construct may assert activity in the chick system. Nonetheless, results yielded from this control construct are still valid given that we are concerned with effects of ADF *reduction* on pMAP rod formation and furthermore, pMAP was still seen to accumulate in



rod-like inclusions both in shRNA PAK2 transfected neurons and in surrounding non-transfected neurons (Fig. 6c, asterisks and arrowhead).

Altogether, these results suggest that the presence of ADF/cofilin is necessary for sequestration of pMAP into rod-like structures.







### 3.3.5 Latruncullin B enhances and Jasplakinolide represses pMAP-staining in rods

Since activation of ADF/cofilin coincided with pMAP recruitment into

**Figure 3.12 Reduction of the cellular ADF/cofilin pool inhibits the formation of rods and sequestration of pMAP.** (a) ADF was knocked down in primary chick tectal neurons by expression of shRNA from a plasmid also encoding GFP for visualization of transfected cells. In cultures transfected for 4 days, ADF immunolabeling using the 1439 antibody demonstrated significant ADF knockdown in transfected cells (arrow) compared to surrounding non-transfected cells (arrowheads). (b) Cells transfected with an shRNA specific for human PAK2 as a control (arrow), showed no reduction of ADF compared to surrounding non-transfected cells (arrowheads) (c, d) Transfected cultures were treated with 1  $\mu$ M AM and immunolabeled with 12E8 to determine whether pMAP accumulates into rod-like structures following significant reduction of ADF. Whereas hPAK2 shRNA-transfected cells (c, arrow) formed pMAP-positive rods (arrowhead) comparable to surrounding non-transfected cells (asterisks), ADF shRNA-transfected cells (d, arrow) never accumulated pMAP-positive rods, although surrounding cells frequently did (asterisks). Images represent single examples from >50 ADF shRNA transfected cells in 3 independent experiments. (e) Quantification of ADF (1439) staining intensity revealed a 75% knockdown in ADF shRNA-transfected cells compared to nearby non-transfected (control) cells (transfected cell staining intensity =  $24.1 \pm 1.5$ , expressed as % of control cells, mean  $\pm$  s.e.m.;  $n=25$ ;  $p<0.001$ ). By contrast, ADF staining intensity of hPAK2 shRNA-transfected cells compared to surrounding non-transfected cells was not reduced (intensity increase compared to controls =  $144.2\% \pm 10.8\%$ ;  $n=25$ ;  $p<0.002$ ). A minimum of 20 transfected cells were analyzed per experiment (carried out in three independent neuronal cultures). All transfected cells included in this data had discernible neurites (although not always apparent in images above due to optimal image contrasting for presentation). Scale bars 20  $\mu$ m.

is a net decrease in the G-actin pool (Bubb et al., 1994). Since Jasp competes for the phalloidin-binding site on F-actin, stabilized F-actin cannot be visualized with fluorescent phalloidin in the presence of Jasp (Fig. 3.13a). However, ADF/cofilin cannot bind to phalloidin-stabilized F-actin (Mizumoto et al., 2000) and thus also would not likely bind to the Jasp-stabilized actin filaments.

Antibody labeling of Lat B-treated neurons revealed formation of both pMAP- and ADF-positive rods which frequently co-localized in double-labeling experiments (Fig. 3.13b). By contrast, neurons treated with Jasp (or

### **3.3.5 Latrunculin B enhances and Jasplakinolide represses pMAP-staining in rods**

Since activation of ADF/cofilin coincided with pMAP recruitment into ADF/cofilin-actin rods, we asked whether other manipulations of F-actin assembly could influence pMAP sequestration to rods. To address this, we used pharmacological manipulation (enhancing or suppressing) of F-actin pools and stained for pMAP. Latrunculins sequester monomeric G-actin to form a non-polymerizable 1:1 complex, thereby inhibiting F-actin reassembly and thus promoting overall F-actin depolymerization (Coue et al., 1987). Latrunculins however, compete weakly with ADF/cofilin for actin binding (Bernstein et al., 2006) and can actually induce ADF/cofilin-actin rod formation (Pendleton et al., 2003). The decline in the phalloidin-stainable F-actin pool after latrunculin B (Lat B) treatment is indeed evident (Fig. 3.13a) although it should be noted that phalloidin cannot stain ADF/cofilin saturated F-actin. By contrast, jasplakinolide (Jasp) binds and stabilizes F-actin resulting in a net decrease in the G-actin pool (Bubb et al., 1994). Since Jasp competes for the phalloidin-binding site on F-actin, stabilized F-actin cannot be visualized with fluorescent phalloidin in the presence of Jasp (Fig. 3.13a). However, ADF/cofilin cannot bind to phalloidin-stabilized F-actin (Minamide et al., 2000) and thus also would not likely bind to the Jasp-stabilized actin filaments.

Antibody labeling of Lat B-treated neurons revealed formation of both pMAP- and ADF-positive rods which frequently co-localized in double-labeling experiments (Fig. 3.13b). By contrast, neurons treated with Jasp (or



co-treated with Jasp and AM or Jasp and Lat B) exhibited a total absence of pMAP and ADF rods (Fig. 3.13a and data not shown). We then compared the rate and abundance of pMAP-stained rods following Lat B compared to AM treatments and found the chronology of their formation indistinguishable between conditions (Fig 3.13c). That Lat B treatment only moderately reduced ATP in neurons (Fig. 3.13d) yet still induced ADF/cofilin-actin and pMAP rod formation comparable to mitochondrial inhibitors suggests that ATP depletion is not a direct cause of rod formation, but an upstream event. These data collectively suggest that subunit release from F-actin is required for the generation of pMAP-positive rods and that in neurons this can be induced by ADF/cofilin activation. It also appears that ADF/cofilin binding to F-actin is essential for the formation of cytoskeletal rods. Dissociated actin subunits saturated with activated ADF/cofilin thereby form cytoskeletal rod inclusions that appear to sequester and accumulate pMAP.

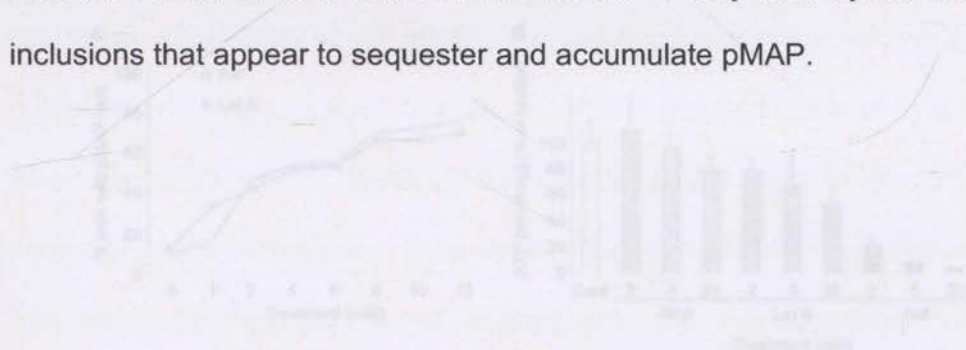


**Figure 3.13** Dynamic F-actin enhances pMAP and with rod formation (a) Following treatment with Latrunculin B (Lat B) but not jasplakinolide (Jasp) the assembly of pMAP into rod-like structures occurred. The chick neurons were stained for pMAP (12E8) and F-actin (phalloidin-488). Co-staining with phalloidin showed only very weak labeling of F-actin in both Lat B- and Jasp-treated cells. (b) Treating cells with Lat B induced formation of pMAP (red; 12E8) and ADF (green; 1439) rods, as seen in single stainings. Co-labeling revealed frequent co-localization of both proteins (arrows). (c) To compare the rate and abundance of rod formation under either mitochondrial inhibition or F-actin overaccumulation, rods were counted in cells treated with AM or Lat B for increasing times, as indicated. The pattern of rod-formation in both conditions was comparable. (d) To ascertain the relationship between rod formation and ATP levels under these conditions, luminescence assays were conducted. Whereas Jasp-treated cells had levels of ATP comparable to controls and AM-treated cells had a dramatic decrease, only moderate decline in ATP levels in Lat B-treated cells was evident. Error bars represent the S.E.M. from triplicate samples. Scale bars = 20  $\mu$ m. The author gratefully acknowledges Shanshan T. Antao for data analysis and bar graph W (d).

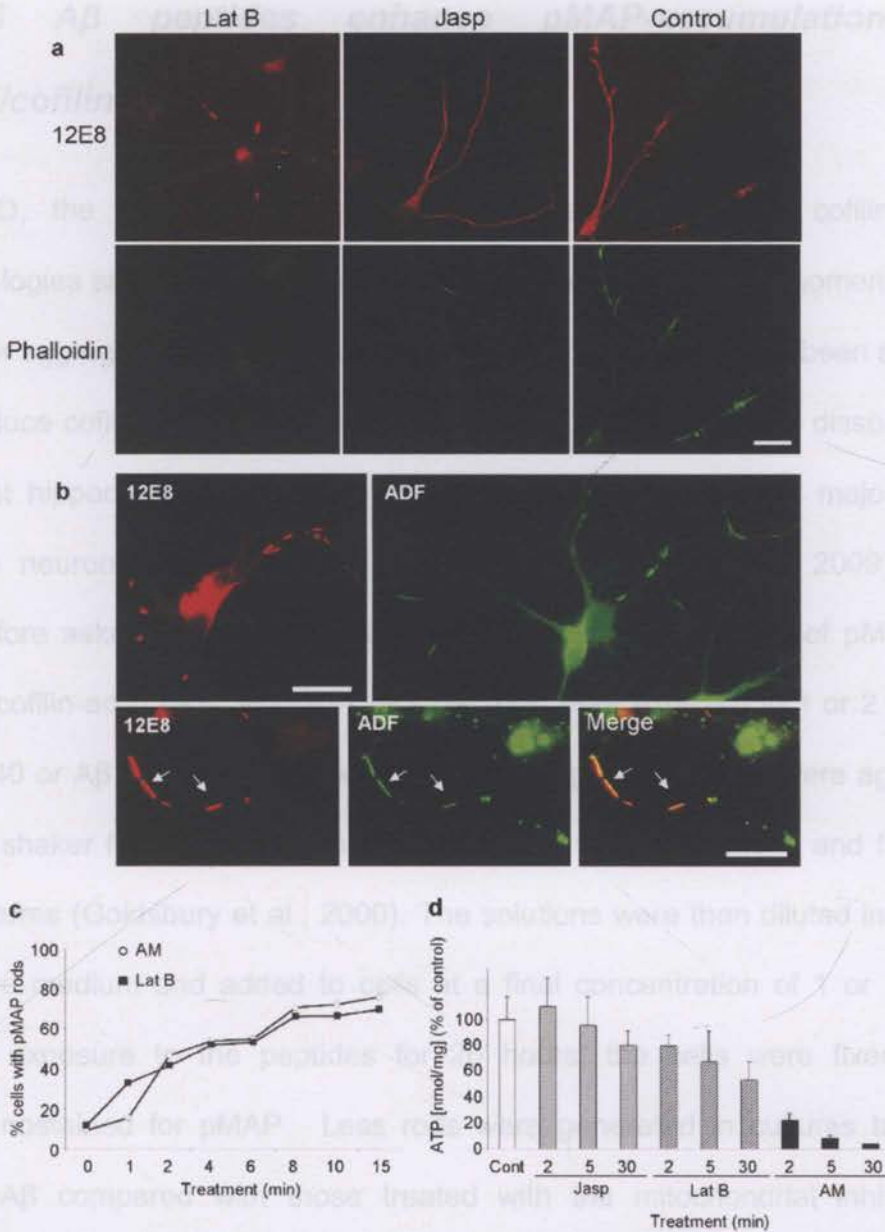


**Figure 3.13 Dynamic F-actin enhances pMAP and actin rod formation** (a) Following treatment with Latrunculin B (Lat B) but not Jasplakinolide (Jasp) the assembly of pMAP into rod-like structures occurred. The chick neurons were stained for pMAP (12E8) and F-actin (phalloidin-488). Co-staining with phalloidin showed only very weak labeling of F-actin in both Lat B- and Jasp-treated cells. (b) Treating cells with Lat B induced formation of pMAP (red; 12E8) and ADF (green; 1439) rods, as seen in single stainings. Co-labeling revealed frequent co-localization of both proteins (arrows). (c) To compare the rate and abundance of rod formation under either mitochondrial inhibition or F-actin manipulation, rods were counted in cells treated with AM or Lat B for increasing times, as indicated. The pattern of rod-formation in each condition was comparable. (d) To ascertain the relationship between rod formation and ATP levels under these conditions, luminescence assays were conducted. Whereas Jasp-treated cells had levels of ATP comparable to controls and AM-treated cells had a dramatic decrease, only moderate decline in ATP levels in Lat B-treated cells was evident. Error bars represent the S.E.M. from triplicate samples. Scale bars = 20  $\mu$ m. The author gratefully acknowledges Shane T Antao for data analysis and bar graph in (d).



### 3.3.6 $A\beta$ peptides enhance pMAP-accumulation at ADF/cofilin rods

In AD, the relationships between pMAP/tau pathologies, cofilin-actin pathologies and amyloid pathologies arising from  $A\beta$  peptide oligomerization and/or aggregation are poorly understood. Synthetic  $A\beta_{1-42}$  has been shown to induce cofilin-actin rod pathology in up to 20% of neurons in dissociated rodent hippocampal cultures (Maloney et al., 2005), with the majority of these neurons located in the dentate gyrus (Davis et al., 2009). We therefore asked whether  $A\beta$  could influence the sequestering of pMAP to ADF/cofilin-actin rods. Primary chick neurons were exposed to 1 or 2  $\mu\text{M}$  of  $A\beta_{1-40}$  or  $A\beta_{1-42}$ . Before applying to cells, peptide solutions were agitated on a shaker for 30 minutes to generate mixtures of oligomeric and fibrillar structures (Goldsbury et al., 2000). The solutions were then diluted into cell culture medium and added to cells at a final concentration of 1 or 2  $\mu\text{M}$ . After exposure to the peptides for 20 hours, the cells were fixed and immunostained for pMAP. Less rods were generated in cultures treated with  $A\beta$  compared with those treated with the mitochondrial inhibitors, consistent with previous studies of ADF/cofilin-actin rod generation in hippocampal neurons treated with  $A\beta$  peptides (Maloney et al., 2005). However, when mean numbers of pMAP-positive rods per cell were quantified on vehicle control and  $A\beta$ -treated coverslips, a significant increase in the number of rods was revealed in  $A\beta$ -treated cells (Fig. 3.14a). No difference was observed between cells treated with 1 and 2  $\mu\text{M}$  peptide or between cells treated with  $A\beta_{1-40}$  and  $A\beta_{1-42}$ . The presence of F-actin rich active growth cones in  $A\beta$ -treated neurons containing pMAP rods in the

neurite shafts indicates the continuing viability of the neurons, despite the formation of pMAP-positive rods (Fig 3.14b, white arrows). We confirmed that rods in Aβ-treated neurons contained both pMAP and ADF (Fig. 3.14c, arrows). In conclusion, these results show that synthetic Aβ aggregates can induce the recruitment of pMAP to ADF/cofilin-actin rods in a subset of neurons in these primary cultures.

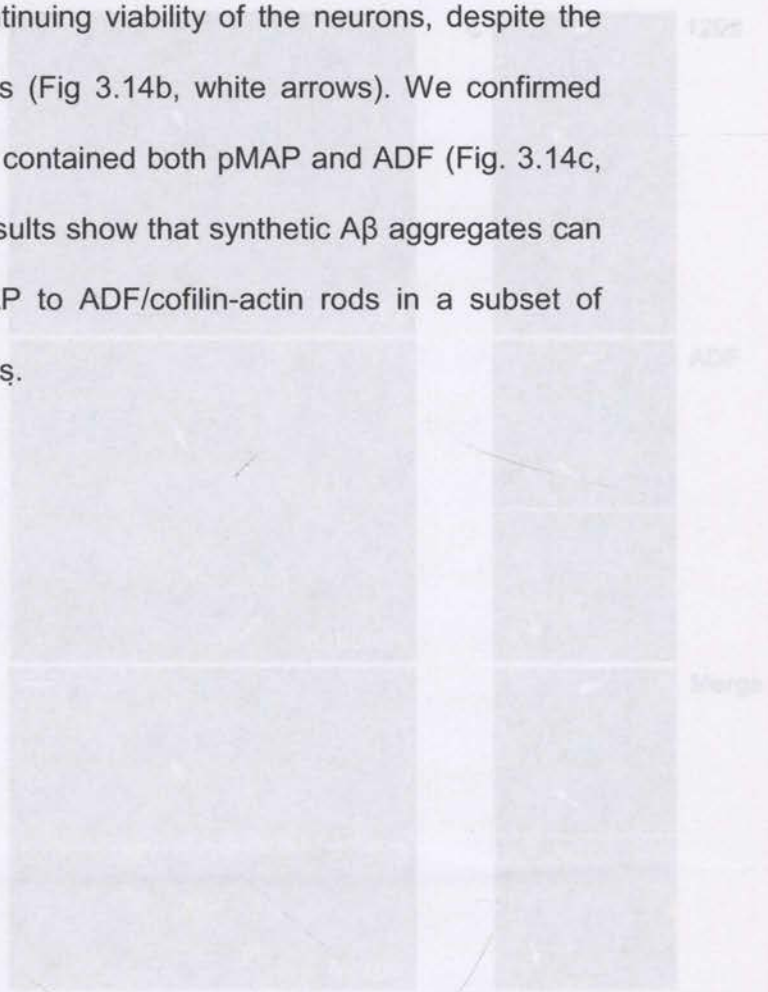
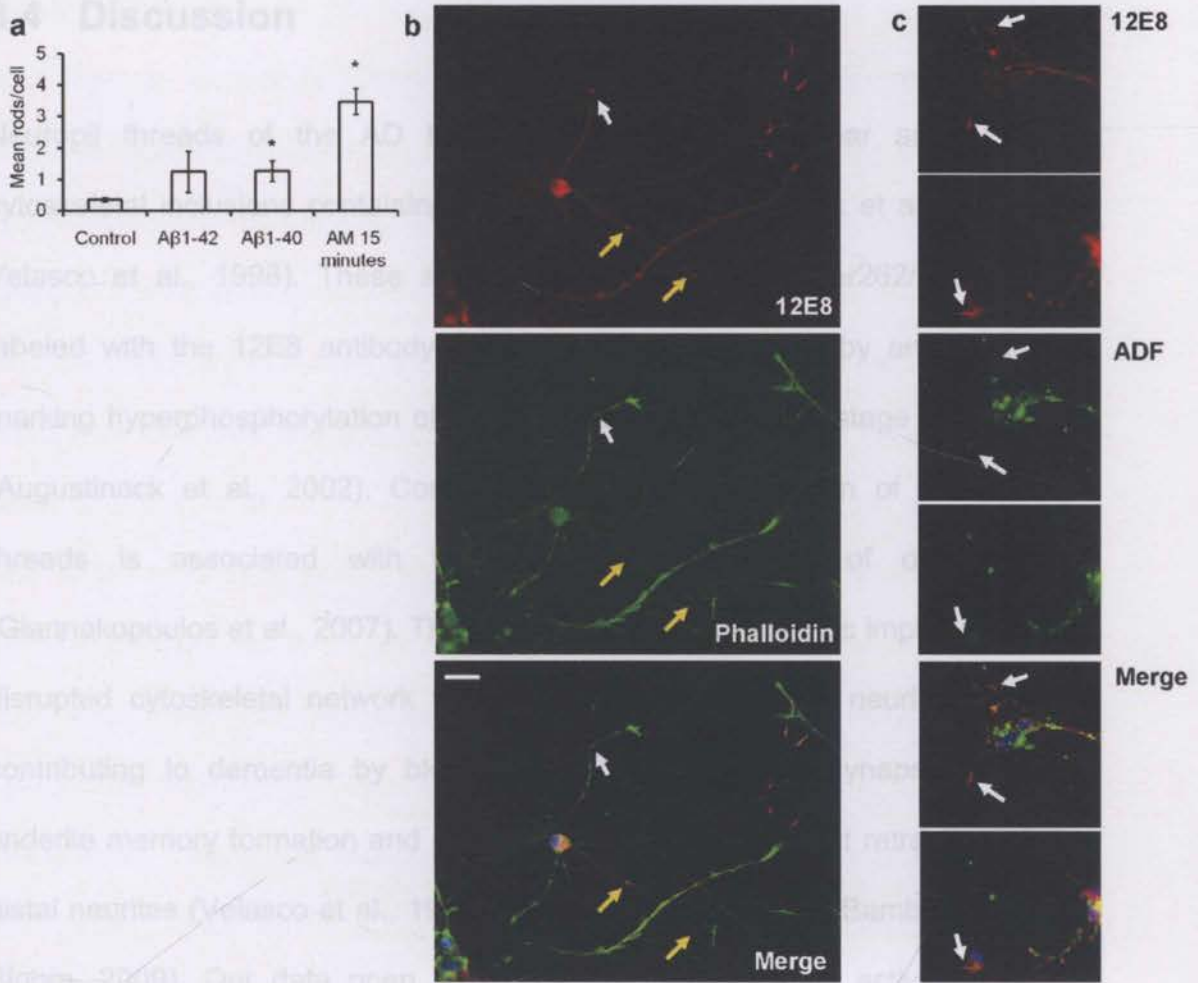


Figure 3.14 Amyloid peptides enhance pMAP sequestration to rods in primary chick neurons. Primary neurons were treated for 20 hours with solutions of Aβ peptides (1 or 2 μM) and double-labeled with the 12E8 antibody (red) and either phalloidin-488 or ADF (both green) as indicated. (a) The mean number of pMAP-positive rods per cell was quantified in >10 fields on control coverslips and coverslips treated with Aβ peptides for 20 hours or AM for 15 min. pMAP-positive rods per cell increased significantly after incubation with AM or Aβ solutions compared to vehicle (DMSO) control (1.3 ± 0.3 rods/cell for both 5 μM Aβ<sub>1-42</sub> and Aβ<sub>1-40</sub> and 3.5 ± 0.4 rods/cell for AM-treated compared with 0.4 ± 0.1 rods/cell for control cells, mean ± s.e.m., \*p<0.02, n=20. Results are from duplicate experiments). Since no difference was seen between 1 μM versus 2 μM peptide treatments, results have been pooled. (b) pMAP-positive rods in Aβ-treated neurons (shown rods for Aβ<sub>1-42</sub>) often formed at distal regions near the base of phalloidin-positive (F-actin-rich) active growth cones (white arrows). They also formed in neurite shafts associated with collapsed growth cones (b, yellow arrows). (c) Rods assembling in Aβ-treated neurons (shown here for Aβ<sub>1-42</sub>) accumulated both pMAP (red) and ADF (green) (arrows). Merged image (plus DAPI in blue) shown in bottom panels. Scale bar = 20 μm. The author gratefully acknowledges Claire Goldsbury and Erica Jeong for experiments and images.





**Figure 3.14 Amyloid peptides enhance pMAP sequestration to rods in primary chick neurons.** Primary neurons were treated for 20 hours with solutions of A $\beta$  peptides (1 or 2  $\mu$ M) and double-labeled with the 12E8 antibody (red) and either phalloidin-488 or ADF (both green) as indicated. (a) The mean number of pMAP-positive rods per cell was quantified in >10 fields on control coverslips and coverslips treated with A $\beta$  peptides for 20 hours or AM for 15 min. pMAP-positive rods per cell increased significantly after incubation with AM or A $\beta$  solutions compared to vehicle (DMSO) control ( $1.3 \pm 0.3$  rods/nuclei for both aged A $\beta_{1-40}$  and A $\beta_{1-42}$  and  $3.5 \pm 0.4$  rods/nuclei for AM-treated compared with  $0.4 \pm 0.1$  rods/nuclei for control cells; mean  $\pm$  s.e.m.; \* $p < 0.02$ ,  $n > 20$ . Results are from duplicate experiments). Since no difference was seen between 1  $\mu$ M versus 2  $\mu$ M peptide treatments, results have been pooled. (b) pMAP-positive rods in A $\beta$  treated neurons (shown here for A $\beta_{1-40}$ ) often formed at distal regions near the base of phalloidin-positive (F-actin-rich) active growth cones (white arrows). They also formed in neurite shafts associated with collapsed growth cones (b, yellow arrows). (c) Rods assembling in A $\beta$ -treated neurons (shown here for A $\beta_{1-40}$ ), accumulated both pMAP (red) and ADF (green) (arrows). Merged images (plus DAPI in blue) shown in bottom panels. Scale bar = 20  $\mu$ m. The author gratefully acknowledges Claire Goldsbury and Erica Jeong for experiments and images.

### 3.4 Discussion

Neuropil threads of the AD brain are comprised of linear arrays of cytoskeletal inclusions containing the pMAP tau (Augustinack et al., 2002; Velasco et al., 1998). These structures are positive for Ser262/356 tau labeled with the 12E8 antibody prior to extensive staining by antibodies marking hyperphosphorylation of tau that is observed in late-stage disease (Augustinack et al., 2002). Corresponding to this, formation of neuropil threads is associated with the early clinical stages of dementia (Giannakopoulos et al., 2007). The structure of neuropil threads implicates a disrupted cytoskeletal network that spans the width of the neurite likely contributing to dementia by blocking cargo trafficking to synapses that underlie memory formation and cognition, causing subsequent retraction of distal neurites (Velasco et al., 1998; reviewed in Terry, 1998; Bamburg and Bloom, 2009). Our data open the possibility that abnormal activation of cofilin, an actin-binding protein, in the AD brain and generation of cofilin-actin cytoskeletal rods is a triggering factor for the sequestration and accumulation of Ser262/356 phosphorylated tau in some neuropil threads. This process may well represent an early pathogenic event in AD neurodegeneration.

Neurodegenerative stimuli including oxidative stress, mitochondrial dysfunction, excitotoxic glutamate, ischemia, and soluble forms of A $\beta$  lead to activation of cofilin and the related protein ADF and the generation of ADF/cofilin-actin rods in primary neuronal cell culture (reviewed in Bamburg and Bloom, 2009). These rods resemble the cofilin aggregates that are



widely distributed in the AD brain (Minamide et al., 2000). At a low ratio to actin and in an active (dephosphorylated) state, ADF/cofilin maximally enhance subunit turnover of F-actin, dynamically remodeling the actin cytoskeleton and thus playing an integral role in regulating actin-dependent synaptic stabilization (reviewed in Bamburg and Bloom, 2009). ADF/cofilin bind cooperatively to F-actin and, at higher ratios to actin, they can saturate regions of filaments and stabilize the pieces of filaments that remain after severing (Chan et al., 2009, Andrianantoandro and Pollard, 2006). Because ADF/cofilin bind to a minor, slightly twisted conformation of F-actin, they stabilize this "twisted" form, which prevents binding of the commonly used F-actin stain, phalloidin (McGough et al., 1997). In the brain, mitochondrial dysfunction and energy depletion associated with AD (Smith et al., 2005; Wang et al., 2009) could feasibly serve as a pathway for F-actin remodeling in neurons, since up to 50% of neuronal energy is dedicated to actin dynamics (Bernstein and Bamburg, 2003). We propose mitochondrial dysfunction is one potential pathway upstream of the assembly of cytoskeletal rods because direct electron transport chain inhibitors elicit cofilin activation, concomitant with rod assembly in primary neurons and organotypic rat hippocampal brain slices. This pathway results in a precipitous drop in ATP, and the release of the cofilin phosphatase chronophin from an inhibitory complex with Hsp90, resulting in cofilin-actin rod formation (Huang et al., 2008). However, cofilin-actin rods can also be induced while maintaining higher levels of cellular ATP, such as with peroxide (Fig. 3.9), which activates the cofilin phosphatase slingshot by oxidizing and removing inhibition by 14-3-3 and leads to almost complete

cofilin dephosphorylation and cofilin-actin rod formation (Kim et al., 2009). The common thread is an increased pool of active ADF/cofilin with respect to the amount of F-actin such that ADF/cofilin-saturated pieces of F-actin are available and coalesce into rods.

Supporting the concept that pMAP $\tau$  accumulation and toxicity is linked to

What is the role of pMAP at the cofilin-actin rods? Rods isolated from neurons and non-neuronal cell lines contain ADF/cofilin:actin in a 1:1 complex and indeed can be formed *in vitro* from these purified proteins (Minamide et al., 2010). Thus, as is also shown here, pMAP is not essential for cofilin-actin rod formation. Nevertheless, pMAP association with most cofilin-actin rods occurs very early in the rod formation process. Rods isolated from cortical neurons and those formed from endogenous proteins from a non-neuronal cell line both have similar stabilities to alterations in pH, ionic strength, reducing agents, Ca<sub>2</sub><sup>+</sup>/EGTA, ATP and detergents (Minamide et al., 2010). Therefore the presence of pMAP on the neuronal rods does not appear to confer in them any special property related to their stability. The question then arises – do the rods confer any special property on the associated pMAP? The tandem arrays of the rapidly formed cofilin-actin rods are similar in size and distribution to the neuritic striations of the neuropil threads in AD. The ultrastructure of most striated neuropil threads from AD brain clearly shows these to consist of the ~20 nm diameter paired helical filaments (PHFs; Velasco et al., 1998), not of the cofilin-actin bundles containing approximately 10 nm diameter filaments that we observe in organotypic hippocampal slices treated with A $\beta$ <sub>1-42</sub> peptide oligomers (Davis et al., 2009). Thus, we suggest that the cofilin-actin rods serve as a template for recruitment and binding of pMAP, and that this association facilitates



further phosphorylation of pMAP and its self-assembly leading to the eventual replacement of the cofilin-actin rods with PHF bundles. Further long-term studies are needed to test this hypothesis.

Supporting the concept that pMAP/tau accumulation and toxicity is linked to interactions with the actin cytoskeleton is work in *Drosophila* models that showed that toxicity of over-expressed hyperphosphorylated tau could be modified by genetic ablation or co-expression of actin associated proteins (Fulga et al., 2006). Interestingly, tau phosphorylation at the 12E8 antibody epitope was shown to be essential for the initiation of tau toxicity and its downstream hyperphosphorylation in *Drosophila* (Nishimura et al., 2004). Mutated tau non-phosphorylatable at the 12E8 epitope did not confer toxicity in *Drosophila* and exhibited reduced downstream phosphorylation at other AD-relevant phospho-tau epitopes (Nishimura et al., 2004). These findings are consistent with the premise that the sequestration of 12E8-specific pMAP to cofilin-actin rods demonstrated here could represent an essential early event in a neurodegenerative pathway. The recent finding that tau reduction can ameliorate toxicity induced by amyloid precursor protein (APP) overexpression or exposure of cells to A $\beta$  oligomers is also consistent with the key involvement of pMAP/tau in response to toxic events (King et al., 2006; Roberson et al., 2007). Potential deleterious effects of cytoskeletal rods on neurons are multifold. Firstly, rods that assemble in axons and dendrites of cultured neurons form transport blockades inhibiting the free movement of vesicles and organelles leading to synaptic dysfunction (Maloney et al., 2005, 2008; Jang et al., 2005). Secondly, the accumulation of actin and cofilin in rod structures could directly impinge on the availability

of cofilin for its function in modulating actin dynamics at the synapse (Hotulainen et al., 2009). Likewise the sequestration of pMAP/tau to the rod matrix could adversely affect the role of tau in stabilizing and regulating the axonal MT network of tracks for fast axonal transport.

The generation of cytoskeletal rods in response to stressors may be an initial compensatory response to slow down energy-consuming actin dynamics and thereby protect neurons under conditions where ATP supply is compromised (Bernstein et al., 2006). However repeated or prolonged stress would likely be detrimental. Increasing evidence suggests declining mitochondrial function and reduced energy metabolism to be early events in the AD brain, preceding severe pathological changes (Smith et al., 2005; Wang et al., 2009). Ageing is the major risk factor for sporadic AD and on the one hand, electron transport chain activity declines with age while on the other, oxidative stress increases, potentially impacting on the availability of ATP in cells (Lin and Beal, 2006). Moreover, the reduction of glucose uptake in AD brain cells and concomitant decline in glycolysis would also negatively impact ATP levels. Precedents of local mitochondrial dysfunction could be multifold and varied in the ageing brain, for example low brain perfusion due to vascular insufficiency, stroke and A $\beta$  peptide-mediated perturbation of mitochondria (Cullen et al., 2005; Du et al., 2008; Cho et al., 2009). Mechanisms linking this metabolic dysfunction with the formation of neuropathological lesions in the AD brain need to be established. Interestingly, it was demonstrated that environmental toxin inhibitors of mitochondrial respiratory chain complexes induce somatic inclusions of



phosphorylated tau in neuronal cell culture and neurodegeneration in tau-related disease (Escobar-Khondiker et al., 2007).

Advanced neuropathology involving pMAP and cofilin accumulation and aggregation may be a result of increased vulnerability to normal environmental stress in brains expressing mutant tau (i.e. in hereditary Frontotemporal Dementias), or from elevated oxidative/mitochondrial stress in brains expressing wild-type endogenous tau (in sporadic AD). In a healthy brain, a fine balance between these stressors and compensatory defense mechanisms must normally occur, given that development of tau pathology and AD are not an inevitable part of ageing. Recent evidence showing that neuronal cell bodies attached to dystrophic neurites in AD-related transgenic mice are still be viable and otherwise healthy (Adalbert et al., 2009) holds promise for future work to develop methods to disrupt the formation of the cofilin-actin rods and/or the interaction between cofilin and pMAP for establishing new therapeutic strategies to combat this disease early in its development.

## Preface

The content of this chapter is based on a recently published work (Whiteman et al., 2011) and therefore appears here in the standard manuscript format.

# 4

## 4.1 Introduction

Neuronal-histopathological hallmarks of Alzheimer's disease (AD) include neurofibrillary tangles (NFT) and neuropil threads comprised of aggregated hyperphosphorylated microtubule-associated protein (MAP) tau. These of end-stage cortical neurofibrillary tangles with cognitive decline, including the hippocampus, are associated with neurofibrillary tangles and neuropil threads of the cerebral cortex (Schmidt et al., 1983; Velasco et al., 1998; Mitchell et al., 2000; Augenbach et al., 2002; Break et al., 2006; Giannakopoulos et al., 2007). The major known function of tau, like other MAPs, is its stabilization and regulation of microtubule (MT) dynamics necessary for neurite outgrowth, morphogenesis and since tau is predominantly an axonal protein, it plays an important role in facilitating MT-dependent axonal transport (for reviews see (Garcia and Cleveland, 2001; Denmeit and Halpain, 2004a)). The activity of tau is negatively regulated by phosphorylation/dephosphorylation cycles, such that phosphorylation at specific sites detaches tau from MTs and allows MT depolymerization, while

### **Rapid changes in phospho-MAP/tau epitopes during neuronal stress: cofilin-actin rods primarily recruit MAP/tau phosphorylated in the microtubule binding domain**



## Preface

The content of this chapter is based on a recently published work (see Whiteman et al., 2011) and therefore appears here in the submitted manuscript format.

## 4.1 Introduction

Neuronal histopathological hallmarks of Alzheimer's disease (AD) include neurofibrillary tangles (NFT) and neuropil threads comprised of aggregated hyperphosphorylated microtubule-associated protein (MAP) tau. These aggregates develop in cell bodies and neurites respectively. Comprising >85% of end-stage cortical tau pathology, neuropil threads correlate with cognitive decline, probably owing in part to their prominence in select subfields and layers of the ventromedial temporal lobe and association cortices (Schmidt et al., 1993; Velasco et al., 1998; Mitchell et al., 2000; Augustinack et al., 2002; Braak et al., 2006; Giannakopoulos et al., 2007). The major known function of tau, like other MAPs, is its stabilization and regulation of microtubule (MT) dynamics necessary for neurite outgrowth, morphogenesis and since tau is predominantly an axonal protein, it plays an important role in facilitating MT-dependent axonal transport (for reviews see (Garcia and Cleveland, 2001; Dehmelt and Halpain, 2004a)). The activity of tau is negatively regulated by phosphorylation/dephosphorylation cycles, such that phosphorylation at specific sites detaches tau from MTs and allows MT depolymerization, while

tau dephosphorylation enables it to bind and stabilize MT via its MT binding domain (MTBD) (Lindwall and Cole, 1984; Mandelkow et al., 1995). In AD, tau becomes hyperphosphorylated at both physiological and disease-specific sites, leading to destabilization of the MT network and concomitant tau self-aggregation. Over 39 phosphorylation sites have been characterized for tau although only two of these are located in the MTBD at the 'KXGS' amino acid motifs corresponding to residues S262 and S356 (Biernat et al., 1993; Mandelkow et al., 1995; Zhou et al., 2006). Phosphorylation of these KXGS motifs, particularly at S262, is one of the earliest markers of AD pathology (Augustinack et al., 2002), readily detectable in 'pretangle' neuropil threads with the monoclonal antibody 12E8 (Seubert et al., 1995). Phosphorylation of the MTBD sites has been shown to induce rapid MT disassembly whereby the new unbound pool of tau is susceptible to self-aggregation into paired helical filaments (PHF) (Biernat et al., 1993; Drewes et al., 1997; Alonso et al., 2001; Fischer et al., 2009). *In rod-like inclusions (AC rods) are also independently induced in cell culture by the inhibition of ATP generation via blocking*

Neuropil threads generally precede the appearance of extensive NFTs, suggesting tau first accumulates in neurites during the development of AD pathology before the proliferation of cell body aggregates (Goedert, 1993; Braak and Braak, 1995; Velasco et al., 1998; Augustinack et al., 2002; Haass and Selkoe, 2007). An *in vitro* cell model for neuropil thread assembly may therefore help mimic early cellular events relevant to the disease mechanism. To this end, we recently demonstrated in primary neuronal culture and



organotypic slice culture that mitochondrial dysfunction initiates formation of 12E8-positive neuritic inclusions that bear morphological resemblance to neuropil threads observed in AD brain (Whiteman et al., 2009). The relevance of this model lies in an increasing body of evidence that implicates mitochondrial dysfunction in AD (for reviews see (Blass, 2000; Lin and Beal, 2006; Wang et al., 2009; Su et al., 2010)). Reduced mitochondrial function and increased oxidative stress are reported to precede cognitive decline, brain atrophy or classic pathologies (Blass, 2000), suggesting that mitochondrial dysfunction plays an integral role in initiating pathological cascades that result in the varied cytopathology of AD. We found that the 12E8-positive neuritic inclusions co-localized with the actin-associated proteins (actin depolymerizing factor) ADF/cofilin. This highlights another prominent feature of AD: aggregates of cofilin and actin that form punctate and rod-like linear arrays through the neuropil of AD brain (Minamide et al., 2000) (reviewed in (Bamburg et al., 2010)). ADF/cofilin-actin rod-like inclusions (AC rods) are also independently induced in cell culture by the inhibition of ATP generation via blocking mitochondrial membrane complexes, thus potentially linking the formation and co-localization of AC rods and MAP/tau inclusions to mitochondrial dysfunction (Whiteman et al., 2009). Moreover, interaction of tau and actin in the organization of the cytoskeletal network is well-documented (Griffith and Pollard, 1978, 1982; Selden and Pollard, 1983; Correas et al., 1990; Moraga et al., 1993; Yamauchi and Purich, 1993; Dehmelt and Halpain, 2004b; He et al., 2009) and emerging evidence suggests that these interactions may be central

to the processes involved in the initiation and development of early AD pathology (Fulga et al., 2006; Gallo, 2007; Whiteman et al., 2009; Bamburg et al., 2010).

#### 4.2 Specific Materials and Methods

Since AD neuropathology involves hyperphosphorylation of numerous epitopes of tau and not just those in the MTBD, the aim of this study was to investigate the phosphorylation pattern and re-distribution of several other key MAP/tau epitopes in addition to 12E8 in the primary neuronal culture model. In asking this question, we focused on both physiological as well as AD-specific sites. We utilized the chick primary neuron model since chick neurons express five forms of tau that are highly homologous to human tau isoforms and exhibit highly conserved phosphorylation-specific epitopes recognized by antibodies against human MAP/tau (Yoshida and Goedert, 2002). Using a series of commercially available and well characterized phospho-MAP/tau antibodies, we measured time-dependent effects of mitochondrial dysfunction on the phosphorylation and distribution patterns of these epitopes. We found that cellular ATP reduction gave rise to rapid overall dephosphorylation at most epitopes with the exception of the 12E8 site that exhibited rapid and persistent phosphorylation over the 120 min treatment time. Likewise, while most other phospho-MAP/tau epitopes showed initial redistribution to spheroid-like aggregates as opposed to AC rods in ATP-depleted neurites, 12E8 was the only epitope specifically recruited to AC rods generated under these conditions within the time frame investigated. These results further highlight the MTBD of



MAP/tau as a potential early player in the initiation of tau aggregation in neurons of the AD brain.

## 4.2 Specific Materials and Methods

### 4.2.1 Nuclear accumulation analysis

For quantification of cells containing nuclear accumulation of AT100 label in control, AM- and Lat B-treated conditions, a number of randomly selected fields on each coverslip were selected and cells containing nuclear AT100 were counted and expressed as a percentage of the total number of counted cells. For the most part, nuclear AT100 accumulation was highly distinct in a subset of cells. Inclusion criteria for nuclear accumulation were (i) general neuron morphology appeared normal (including intact nucleus) (ii) neuron exhibited obvious co-localization of AT100 label with DAPI nuclear label and (iii) nucleus exhibited AT100 fluorescence intensity  $>1.5x$  the intensity of nuclei of surrounding, apparently unaffected cells, as measured using Image J. Over 200 cells were counted for each condition in duplicate experiments using independently prepared cell cultures.

### **4.2.2 Human tissue preparation**

Frontal cortex and hippocampal sections from normal adult and confirmed Alzheimer's disease patients were obtained from the Alzheimer Disease Research Center, University of California, San Diego and approved for use by Colorado State University. Post-mortem time to fixation in formalin was 3 h. For immunofluorescence, paraffin sections (6-7  $\mu\text{m}$ ) were deparaffinized for 20 min in Hemo-De (Fisher Scientific), rehydrated to distilled water through decreasing concentrations of ethanol, microwaved in water for 8 min, blocked with 5% goat serum for one hour and immunostained (see Chapter 2 for more detail).

### **4.2.3 Transmission Electron Microscopy**

Primary chick neurons were grown on glass coverslips, treated, washed with warm PBS and fixed for 30 min with 2.5% glutaraldehyde (Electron Microscopy Sciences, USA) in 0.1 M sodium cacodylate buffer (Sigma-Aldrich). Cells were rinsed with buffer and post-fixed for 30 min in cold 1% osmium tetroxide (Sigma-Aldrich). Cells were rinsed again and stained for 2 h with 1% uranyl acetate (Sigma-Aldrich), filtered through 0.22 $\mu\text{m}$  Biofil Syringe filter in 0.05 M sodium acetate (Sigma-Aldrich). To prepare TEM grids, cells were dehydrated through increasing concentrations of ethanol (v/v) (50%, 70%, 95% and ultra-dry 100%), then infiltrated with Spurr's resin in increasing ratios to 100% ethanol (1:1, 2:1 and 3:1). Cells on coverslips were embedded in 100% Spurr's



resin and cured at 60 °C overnight. To remove coverslips, resin blocks were placed in liquid nitrogen for ~15 sec, transferred to warm water and carefully removed. Resin blocks were section using a diamond knife (70 nm) and placed on 200-mesh copper TEM grids that were subsequently post-stained for 10 min with uranyl acetate and lead citrate. Images were acquired with a Phillips CM 120 Biofilter TEM at 120 kV.

## 4.3 Results

### ***4.3.1 Mitochondrial inhibition induces cellular redistribution and epitope-specific persistent phosphorylation or dephosphorylation of MAP/tau***

In AD neurons, tau is hyperphosphorylated and abnormally aggregates both in neurites and the somatodendritic compartment, although the mechanisms by which these processes occur are not understood. The aim of this study was to test the hypothesis that inhibiting mitochondrial function influences the phosphorylation state and localization of tau protein in neurons. Primary chick neuron cultures were treated for 10, 30, 60 or 120 min with the mitochondrial Complex III inhibitor AM which has previously been shown to reduce the level of ATP in these neurons by 60% within 10 min while cells remain >90% viable (Whiteman et al., 2009). Cells were then lysed or fixed for immunostaining and probed with a battery of phospho-MAP/tau antibodies including AT270, AT8, AT100, S214, AT180, 12E8, S396, S404 or S422 that have been raised against

different AD-relevant phosphorylated epitopes on human MAP/tau and have analogous corresponding epitopes in chicken MAP/tau (Fig. 4.1A). Western blot analysis of lysates revealed that compared to untreated (control) cells, ATP reduction leads to dephosphorylation of epitopes S396, AT8, AT270, AT180, S404 and S422 over the 120 min treatment time when normalized for loading to GAPDH (Fig. 4.1B, C). Total tau was observed to decrease transiently before returning to control levels at 120 min. By contrast, the blots revealed a strong and sustained phosphorylation of the MAP/tau KXGS motifs recognized by the 12E8 antibody (Fig. 4.1D, E). Consistent with this, the ratio of 12E8 phosphorylation to total tau band intensities increased >2-fold by 60 min whereas the AT8:total tau ratio declined over the same time frame to near zero (Fig. 4.1D). This trend of 12E8 persistent phosphorylation was reproducible in a second independent experiment and combined (n=4), these data reveal a peak increase to  $232 \pm 69\%$  at 60 min and sustained phosphorylation even at 120 min ( $155 \pm 4\%$ ,  $p < 0.05$ ) (mean  $\pm$  SEM) (Fig. 4.1E).

*In AM-treated cells, in addition to labeling neuritic tau inclusions, AT100*  
Next, we conducted immunofluorescent labeling for the same MAP/tau epitopes in AM-treated neurons to investigate distribution patterns of these epitopes throughout neurons following mitochondrial inhibition. Interestingly, while some epitope labeling remained smooth and relatively evenly distributed throughout neurites of AM-treated cells, other epitope labels aggregated into spheroid inclusions resulting in beading along affected processes (Fig. 4.2A-J). Staining intensity, indicative of phosphorylation state, of epitopes AT8, S214



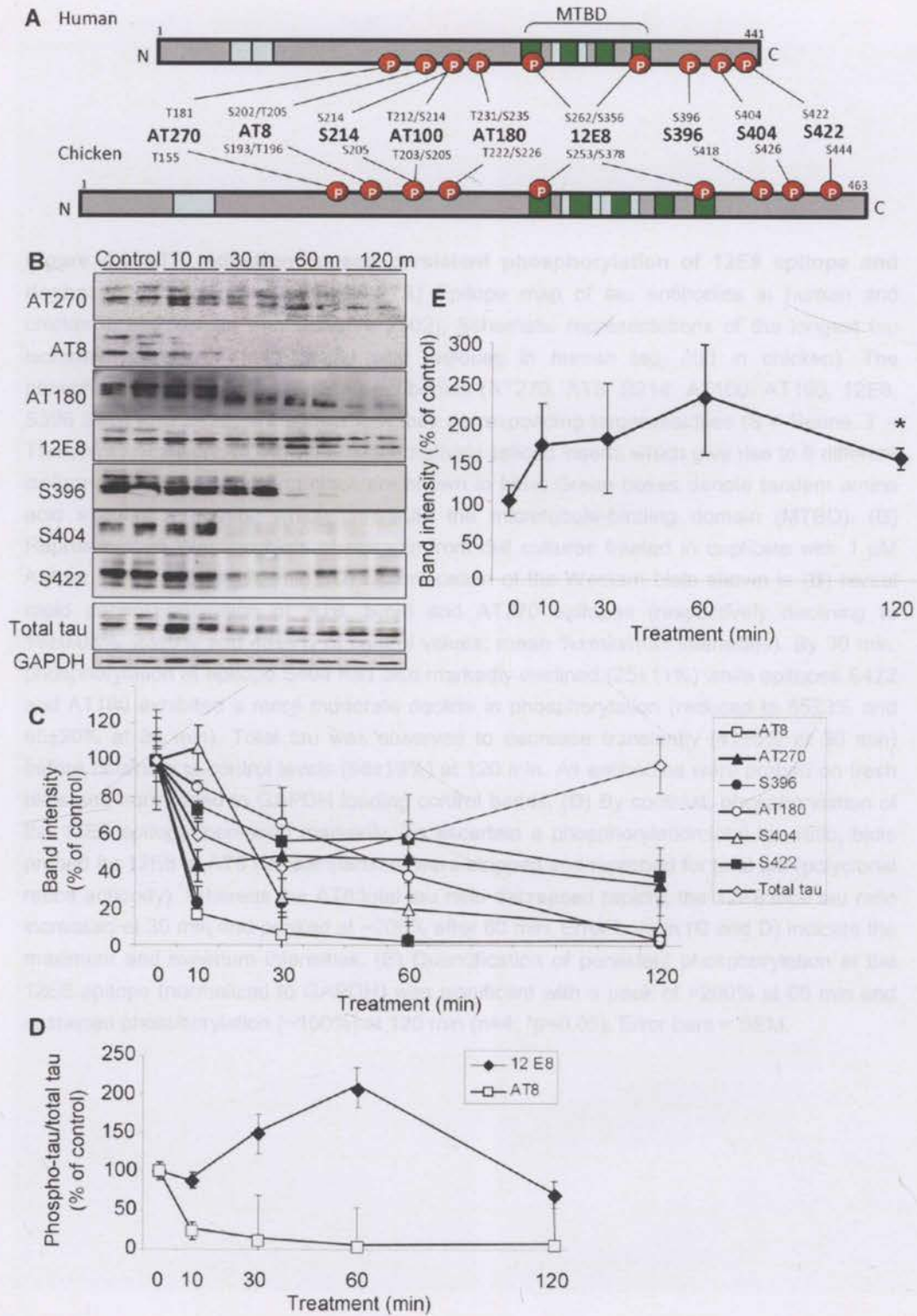
and AT180 was somewhat reduced (AT8 = ~30% intensity of control cells after 15 min AM treatment), but otherwise comparable to control cells with regards to its even distribution. By contrast, AT270, AT100, S396, S404, S422 and total tau labeling aggregated into spheroids that were rarely seen in untreated control cells. Overall cell body staining intensity for some of these epitopes was also found to be reduced (AT270 ~40% intensity compared to control cells). Although the 12E8-antibody occasionally labeled some spheroids, it predominantly labeled rod-shaped aggregates throughout neurites (Fig. 4.2F) which are shown below to be AC rods. The insets in Fig. 4.2 illustrate the appearance of spheroids and rods respectively. Rod-shaped structures were observed less often with the S404, S422 and AT270 immunolabels (Fig. 4.2A and G, insets). As shown for AT270 below, these structures only rarely colocalized with AC which was in contrast to 12E8 which largely colocalized with AC rods.

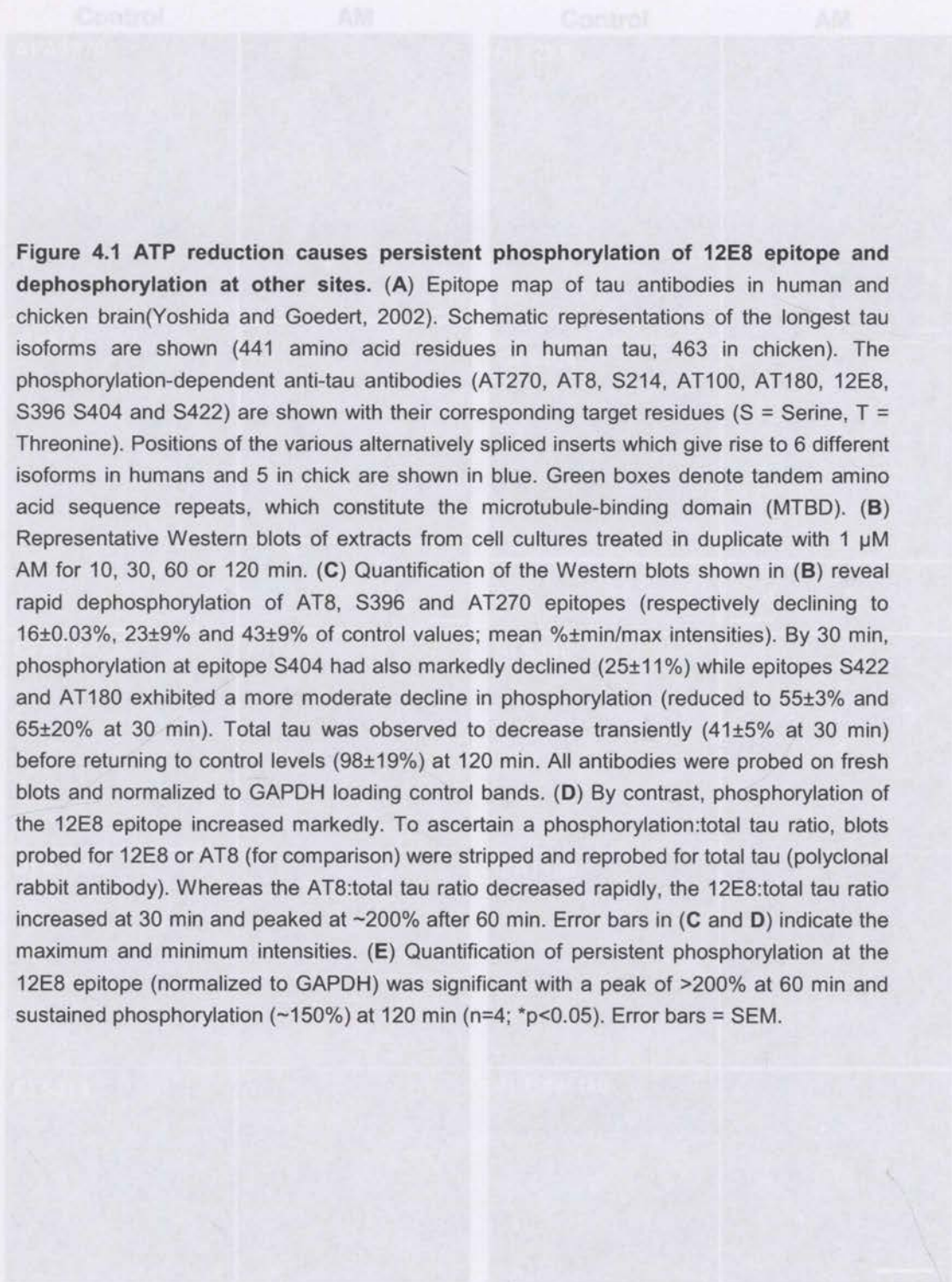
In AM-treated cells, in addition to labeling neuritic tau inclusions, AT100 revealed a redistribution into cell nuclei in a subset of neurons (~36%), as indicated by colocalization with the nuclear stain DAPI (Fig. 4.2D, asterisks), which was never observed for any other MAP/tau epitope (Fig. 4.3). However, further analysis demonstrated that this nuclear epitope does not represent tau protein as AT100 also labeled nuclei of mouse tau knockout neurons (LS Minamide, IT Whiteman and JR Bamberg unpublished observations). Moreover, S214 (which shares the serine-214 recognition site of AT100) and

total tau labels were never seen to accumulate in nuclei of AM-treated cells further suggesting this AT100 accumulation to be non tau-related. Interestingly however, the same nuclear localization of the AT100 label was seen in post mortem AD tissue (Fig. 4.3F).

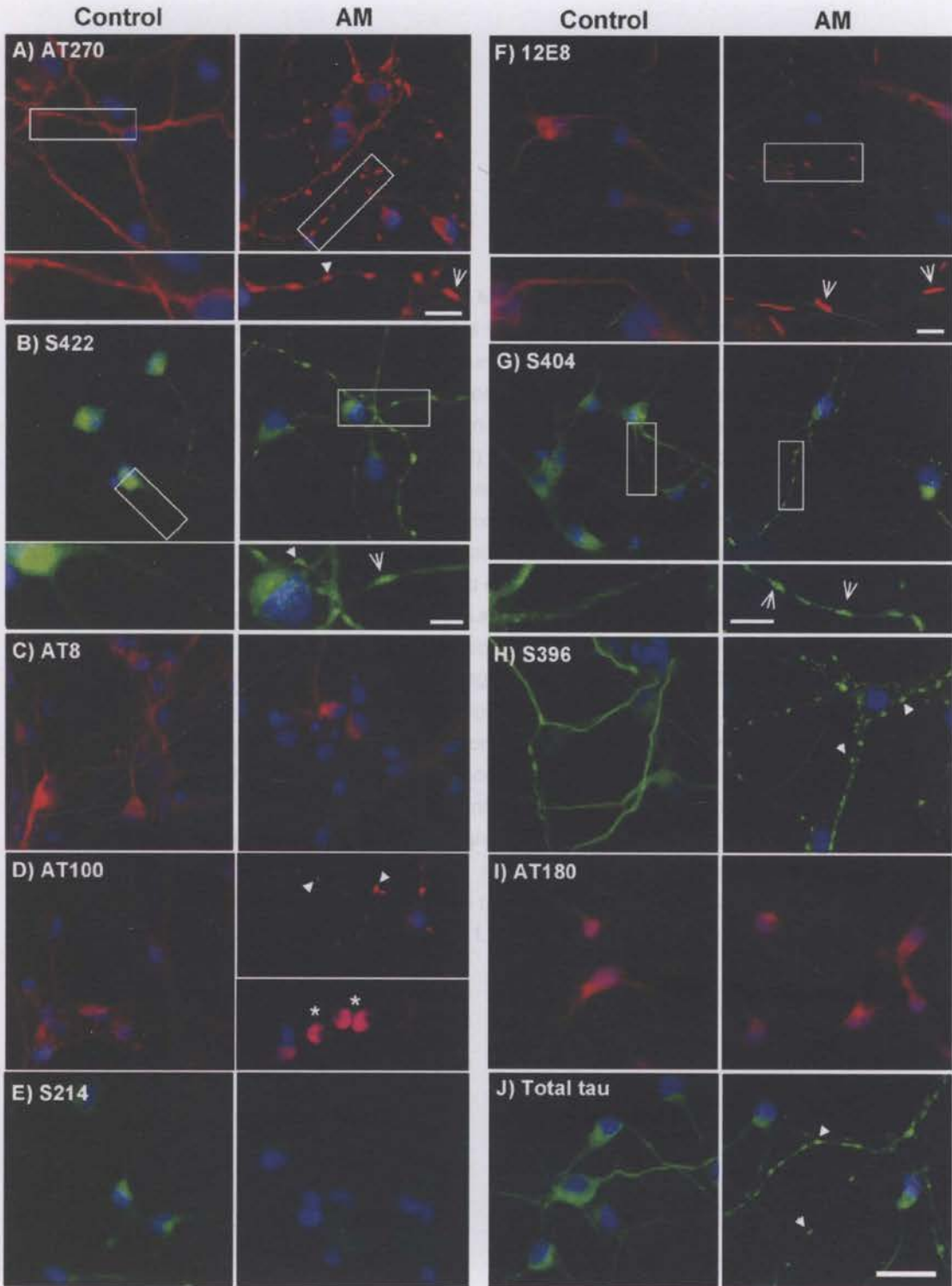












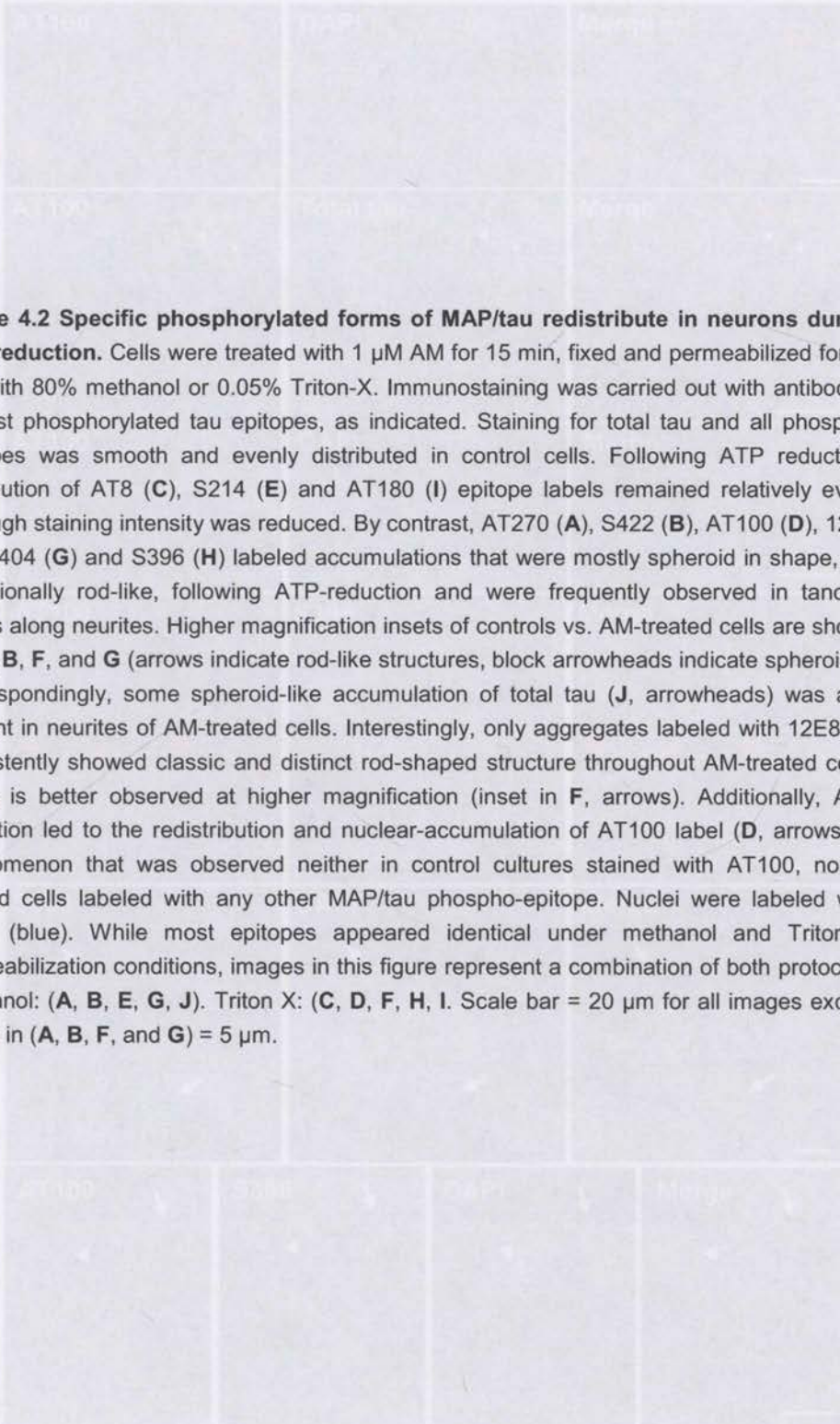
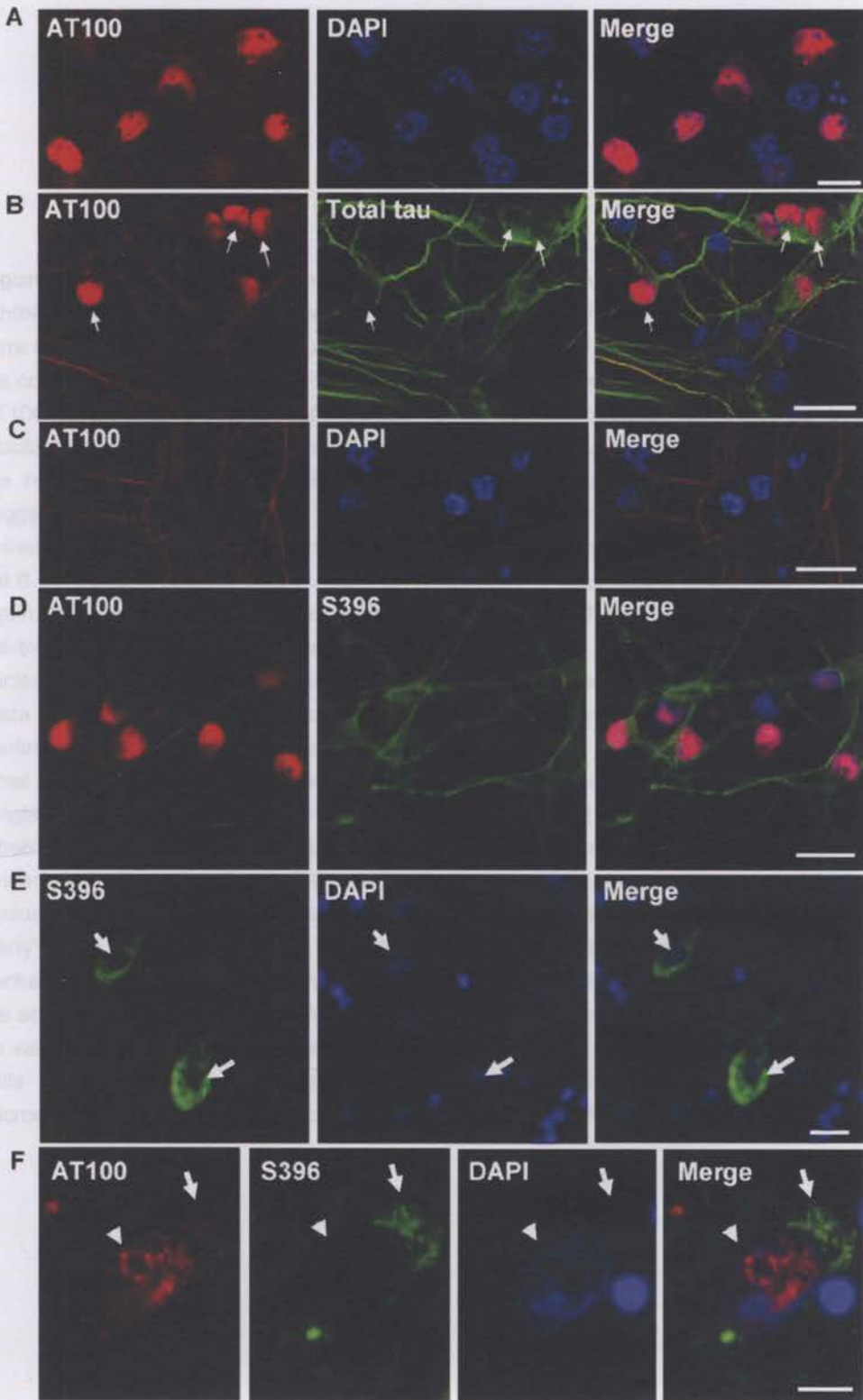


**Figure 4.2 Specific phosphorylated forms of MAP/tau redistribute in neurons during ATP reduction.** Cells were treated with 1  $\mu$ M AM for 15 min, fixed and permeabilized for 90 sec with 80% methanol or 0.05% Triton-X. Immunostaining was carried out with antibodies against phosphorylated tau epitopes, as indicated. Staining for total tau and all phospho-epitopes was smooth and evenly distributed in control cells. Following ATP reduction, distribution of AT8 (C), S214 (E) and AT180 (I) epitope labels remained relatively even, although staining intensity was reduced. By contrast, AT270 (A), S422 (B), AT100 (D), 12E8 (F), S404 (G) and S396 (H) labeled accumulations that were mostly spheroid in shape, but occasionally rod-like, following ATP-reduction and were frequently observed in tandem arrays along neurites. Higher magnification insets of controls vs. AM-treated cells are shown for A, B, F, and G (arrows indicate rod-like structures, block arrowheads indicate spheroids). Correspondingly, some spheroid-like accumulation of total tau (J, arrowheads) was also evident in neurites of AM-treated cells. Interestingly, only aggregates labeled with 12E8 (F) consistently showed classic and distinct rod-shaped structure throughout AM-treated cells, which is better observed at higher magnification (inset in F, arrows). Additionally, ATP reduction led to the redistribution and nuclear-accumulation of AT100 label (D, arrows), a phenomenon that was observed neither in control cultures stained with AT100, nor in treated cells labeled with any other MAP/tau phospho-epitope. Nuclei were labeled with DAPI (blue). While most epitopes appeared identical under methanol and Triton X permeabilization conditions, images in this figure represent a combination of both protocols. Methanol: (A, B, E, G, J). Triton X: (C, D, F, H, I). Scale bar = 20  $\mu$ m for all images except insets in (A, B, F, and G) = 5  $\mu$ m.





Co-labeling studies of spheroids in AM-treated cells revealed strong co-localization of AT100 (Fig. 4.4A) and AT270 (Fig. 4.4B) respectively with total tau and co-localization of S396 with AT100 (Fig. 4.4C) and 12E8 (Fig. 4.4D), suggesting that these observed neurotic aggregates in ATP-depleted cells are composed of tau phosphorylated at serine sites.

**Figure 4.3 AT100 labels a non-tau component in the nucleus during mitochondrial**

**inhibition, actin depolymerization and in postmortem AD brain.**

Primary chick neurons were treated with 1  $\mu$ M AM or 1  $\mu$ g/ml Lat B for 15 min, fixed, immunostained and analyzed

via confocal laser scanning. ATP reduction with AM induced nuclear accumulation of the

AT100 label in a proportion of neurons ( $36 \pm 2$  %; mean  $\pm$  SEM), as indicated by co-

localization with DAPI (A, B). Co-stainings revealed no obvious translocation of total tau into

the nuclear compartment in cells exhibiting AT100 nuclear accumulation (B, arrows),

suggesting the AT100 antibody is labeling a protein other than tau. AT100 labeling in

untreated cells (C) remained contained in the neurites. Similarly, actin depolymerization with

Lat B gave rise to nuclear accumulation of AT100 label in  $22 \pm 2$  % cells (mean  $\pm$  SEM) (D) and

again, lack of total tau and other epitopes such as S396 (D) in the nucleus. Interestingly,

pre-treating cultures for 2 min with the F-actin stabilizing drug jasplakinolide prevented

nuclear accumulation of AT100 in cultures subsequently treated with either AM or Lat-B

(data not shown). Formalin-fixed 7  $\mu$ m brain sections from the hippocampal region of

confirmed AD cases were immunostained for phospho-tau epitopes. S396 label (E) and

other tau epitopes (data not shown) often accumulated in classic flame-shaped 'early' ghost

tangles, though remained largely absent from the nucleus (E, arrows). By contrast, double-

labeling studies showed AT100 label frequently appearing in the nuclear compartment as

evidenced by its co-localization with DAPI (F, arrowhead). In the same neurons, S396 was

exclusively contained within the somal compartment (F, arrow). This may well represent an

'early' ghost tangle, since S396 phospho-tau in the soma appears granular and loosely-

packed. Although characterization and identification of this AT100-positive protein is beyond

the scope of the present study, further investigation of this stress-induced response would

be valuable as the appearance of the epitope in the nucleus specifically occurs in stressed

cells (ATP depleted) or AD brain and not control cells. Images in (A-D): confocal

microscope; (E, F): optical microscope. Scale bars = 10  $\mu$ m (A, F); 20  $\mu$ m (B-E).



Co-labeling studies of spheroids in AM-treated cells revealed strong co-localization of AT100 (Fig. 4.4A) and AT270 (Fig. 4.4B) respectively with total tau and co-localization of S396 with AT100 (Fig. 4.4C) and 12E8 (Fig. 4.4D), suggesting that these observed neuritic aggregates in ATP-depleted cells are comprised of MAP/tau phosphorylated at many sites. By contrast, rod-like structures immunolabeled for the 12E8 epitope did not co-label with other phospho-MAP/tau epitopes (Fig. 4.4E). We had previously demonstrated 12E8-MAP/tau to be recruited to AC rods (Whiteman et al., 2009) (see also Chapter 3), which we confirm here in both Triton X and methanol permeabilized cells (Fig. 4A and data not shown). It should be noted however, that 12E8 labeled both spheroids and AC rods; the labeling of AC rods was best preserved under Triton X permeabilization (Fig. 4.4E) whereas methanol permeabilization resulted mostly in spheroid labeling (Fig. 4.4D). Further, 12E8-labeled AC rods do not co-localize with S396 label (Fig. 4.4E) which by contrast only localizes to spheroid structures in the same cells (arrows Fig 4.4E). This further documents the distinct and separate nature of AC rods versus spheroids.

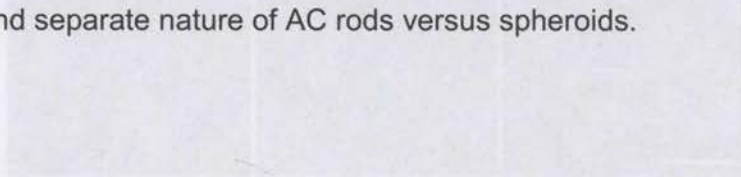
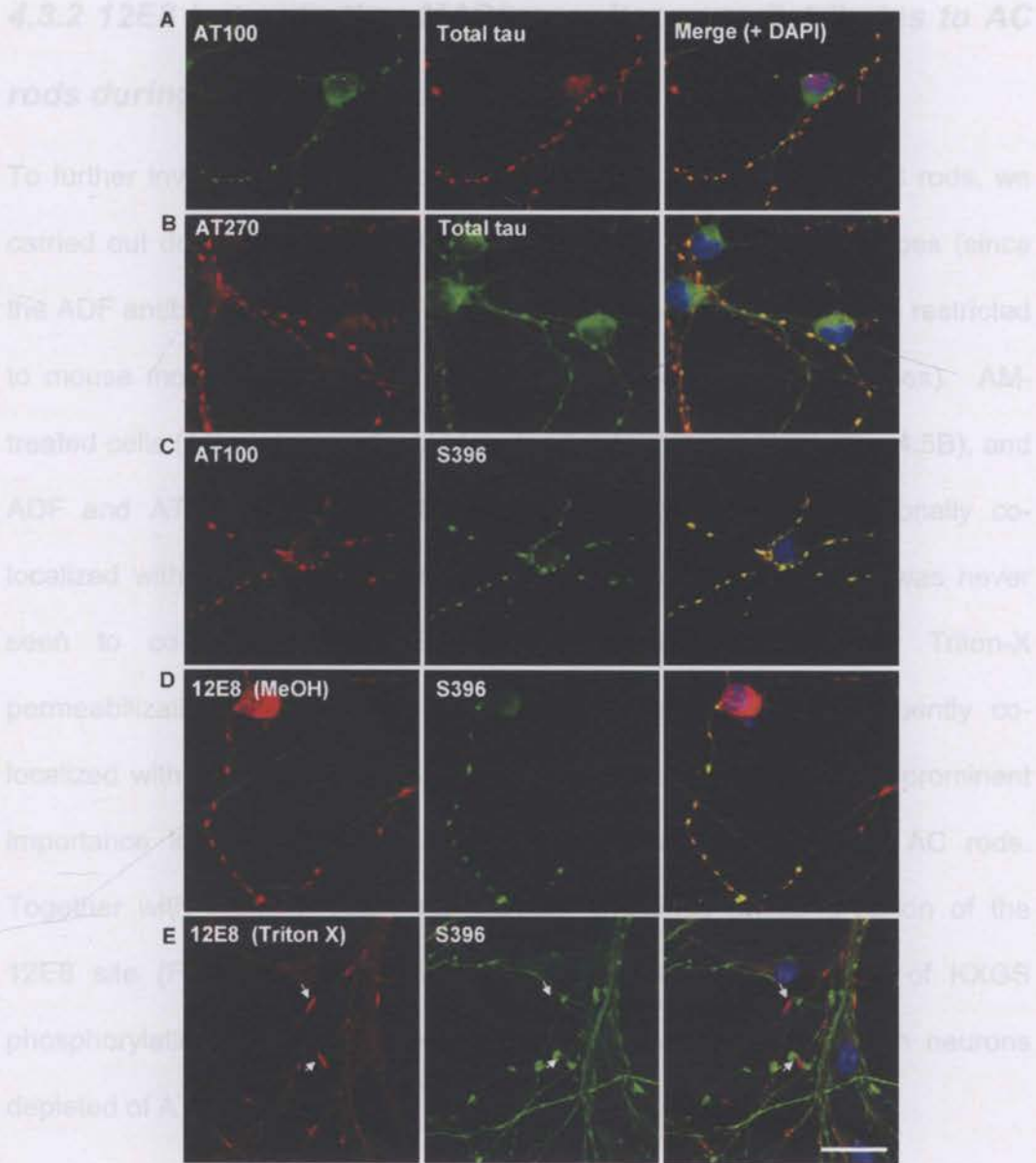


Figure 4.4 Distinct rod-shaped aggregates are specific to 12E8-MAP/tau and are best preserved with Triton-X permeabilization. ATP-depleted cells were permeabilized for 90 sec with 50% methanol or 0.05% Triton-X and co-labeled for epitopes of MAP/tau. Under both methanol and Triton-X methods, (shown here with methanol permeabilized cells in A-D), aggregations containing AT100 (A) and AT270 (B) epitopes co-labeled with total tau. In addition, aggregates containing S396 label also contained AT100 (C) and 12E8 (D), suggesting spheroid neuritic aggregates are comprised of a complex of MAP/tau phosphorylated at numerous epitopes. By contrast, distinct rod-shaped aggregates were only observed with 12E8-labeling and these did not co-label with S396 or any other tau epitope (E). 12E8-positive AC rods were best visualized following Triton-X permeabilization protocols. Scale bar = 20  $\mu$ m.



**Figure 4.4 Distinct rod-shaped aggregates are specific to 12E8-MAP/tau and are best preserved with Triton-X permeabilization.** ATP-depleted cells were permeabilized for 90 sec with 80% methanol or 0.05% Triton-X and co-labeled for epitopes of MAP/tau. Under both methanol and Triton-X methods, (shown here with methanol permeabilized cells in **A-D**), aggregations containing AT100 (**A**) and AT270 (**B**) epitopes co-labeled with total tau. In addition, aggregates containing S396 label also contained AT100 (**C**) and 12E8 (**D**), suggesting spheroid neuritic aggregates are comprised of a complex of MAP/tau phosphorylated at numerous epitopes. By contrast, distinct rod-shaped aggregates were only observed with 12E8-labeling and these did not co-label with S396 or any other tau epitope (**E**). 12E8-positive AC rods were best visualized following Triton-X permeabilization protocols. Scale bar = 20  $\mu$ m.



### 4.3.2 12E8 but not other MAP/tau epitopes redistributes to AC rods during mitochondrial inhibition

To further investigate whether other tau epitopes are present in AC rods, we carried out double-labeling for ADF and a variety of MAP/tau epitopes (since the ADF antibody central to this study was rabbit polyclonal, we were restricted to mouse monoclonal MAP/tau antibodies for double-labeling studies). AM-treated cells (15 min) were double-labeled for ADF and AT270 (Fig. 4.5B), and ADF and AT100 (Fig. 4.5C, D). AT270 aggregates only occasionally co-localized with AC rods (Fig. 4.5B, arrows), whereas AT100 label was never seen to co-localize with AC rods after either methanol or Triton-X permeabilization (Fig. 4.5C, D; arrows). By contrast, 12E8 frequently co-localized with AC rods (Fig. 4.5A), suggesting this epitope to be of prominent importance in the immediate stages of MAP/tau recruitment to AC rods. Together with Western blot data showing sustained phosphorylation of the 12E8 site (Fig. 4.1D, E) these results suggest the importance of KXGS phosphorylation in the rapid recruitment of MAP/tau to AC rods in neurons depleted of ATP.

Figure 4.5 Recruitment of MAP/tau to AC rods during ATP reduction is specific for 'KXGS' phosphorylated species. (A) Co-localization of 12E8-positive MAP/tau in AC rods during ATP reduction (Winters et al., 2009) (also Chapter 3). These inclusions often form in tandem arrays along neurites (arrows). Dual staining of (higher resolution) in lower panel of (A). Additional double-labeling was performed with AT270 (B) or AT100 (C) and ADF, to see if there was any relationship between these tau epitopes and AC rods. AC rods only sometimes overlapped with AT270 (B, arrows) and were never observed to co-localize with AT100, either after Triton-X or methanol permeabilization (C and D, arrows). These results suggest AC rods are derived from MAP/tau-containing neurofibrils and recruit only the 12E8-phosphorylated MAP/tau isoform into distinct rod structures during ATP reduction. (A, B and D) = Triton-X permeabilized. Scale bar = 20 µm; 5 µm (inset in A).

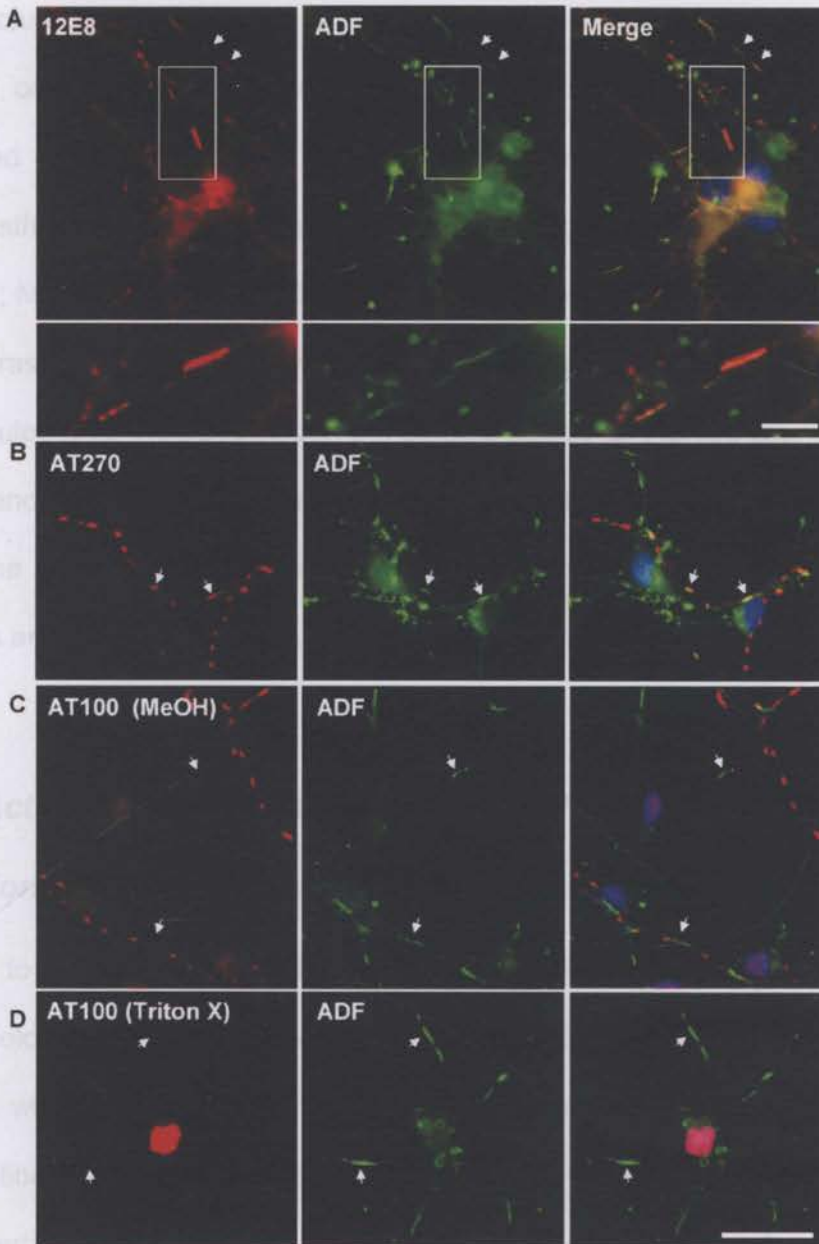


**Figure 4.5 Recruitment of MAP/tau to AC rods during ATP reduction is specific for 'KXGS' phosphorylated species.** (A) Confirmation of 12E8-positive MAP/tau in AC rods during ATP reduction (Whiteman et al., 2009) (also Chapter 3). These inclusions often form in tandem arrays along neurites (arrows). Inset shown at higher magnification in lower panel of (A). Additional double-labeling was performed with AT270 (B) or AT100 (C) and ADF, to see if there was any relationship between these tau epitopes and AC rods. AC rods only sometimes overlapped with AT270 (B, arrows) and were never observed to co-localize with AT100, under either Triton-X or methanol permeabilization (C and D, arrows). These results suggest AC rods are distinct from MAP/tau-containing neuritic spheroids and recruit only the 12E8-phosphorylated MAP/tau isoform into distinct rod structures during ATP reduction. (A, B and D) = Triton X permeabilized. Scale bar = 20  $\mu$ m; 5  $\mu$ m (inset in A).



Ultrastructural EM analysis of AC rods formed following ATP-reduction (Fig. 4.6A, B) corroborated previous results that demonstrated that AC rods are comprised of many individual parallel 10 nm filaments arranged into tightly bundled structures (Minamide et al., 2000; Bamburg and Bloom, 2009; Davis et al., 2009; Minamide et al., 2010), indicative of cofilin-saturated F-actin bundles. By contrast, unaffected neurites of treated cells contain evenly-spaced microtubules (Fig. 4.6C). Although the striated pattern of AC rod staining has a resemblance to what was observed for striated neuropil threads (Velasco et al., 1998), the neuropil threads from AD brain contain only 20 nm paired helical filaments and not actin-based AC rods (Bamburg and Bloom, 2009).

### ***4.3.3 Actin depolymerization mimics effects of mitochondrial inhibition on MAP/ tau phosphorylation and redistribution***

Similar to mitochondrial inhibition, we previously demonstrated that pharmacologically-induced depolymerization of actin induces the formation of AC rods which subsequently recruit phosphorylated MAP/tau labeled by the 12E8 antibody (Whiteman et al., 2009). In order to determine whether actin depolymerization induces aggregates of MAP/tau phosphorylated at other residues, as observed with AM-treated cultures, we treated primary neurons with Latrunculin B (Lat B) which induces AC-like depolymerization of actin filaments in the absence of ATP reduction. The formation and co-localization of AC rods with 12E8 under these conditions was confirmed (not shown). In contrast to AM-treated cells, staining for other epitopes including AT100 (Fig.

4.7A) and S396 (Fig. 4.3D) revealed an even distribution of immunolabel along neurites. Western blot analysis of Lat B-treated neurons revealed a 2.9-fold increase in 12E8 immunoreactivity after 2 min treatment while other epitopes such as S396 remained largely unchanged (Fig. 4.7B, C). These results confirm that 12E8 is the primary MAP/tau epitope recruited to Lat B-induced AC rods during actin reorganization, as was also found to be the case for AC rods induced by ATP-reduction. Together these results provide strong evidence for an important role of KXGS phosphorylation in the initial recruitment of MAP/tau to AC rods during times of cellular stress.

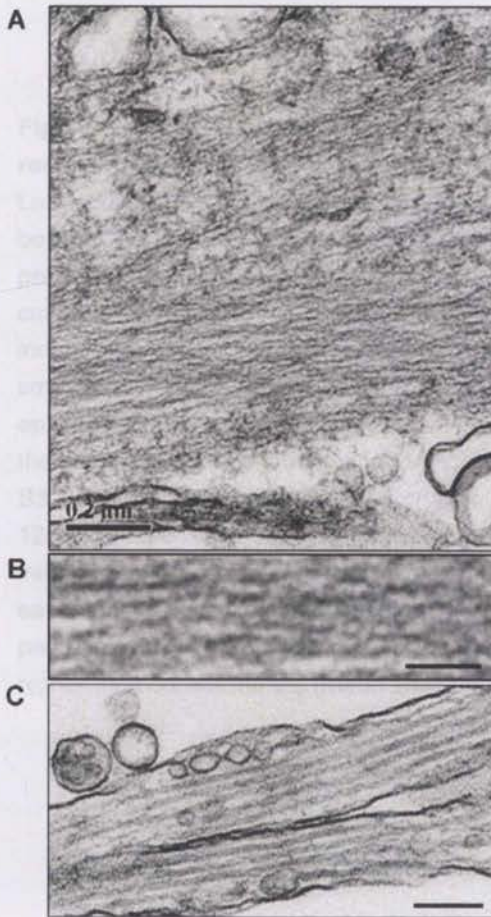


**Figure 4.6 Rod-like accumulations in neurites of primary neurons contain densely packed filaments.** Transmission electron micrograph of a primary chick neuron treated with 1  $\mu$ M AM for 15 min, fixed and processed for TEM as described in Methods. **(A)** A densely packed linear array of filaments occurs in the neurite, each filament approximately 8-10 nm in diameter, indicative of AC-saturated actin filaments. Higher magnification in **(B)**. In contrast, an unaffected neurite within the same treated cell **(C)** contains evenly-spaced microtubules approximately 24nm in diameter. Scale bars = 0.2  $\mu$ m **(A, C)**, 50 nm **(B)**. The author gratefully acknowledges De Lian Goh for EM experiments and images.



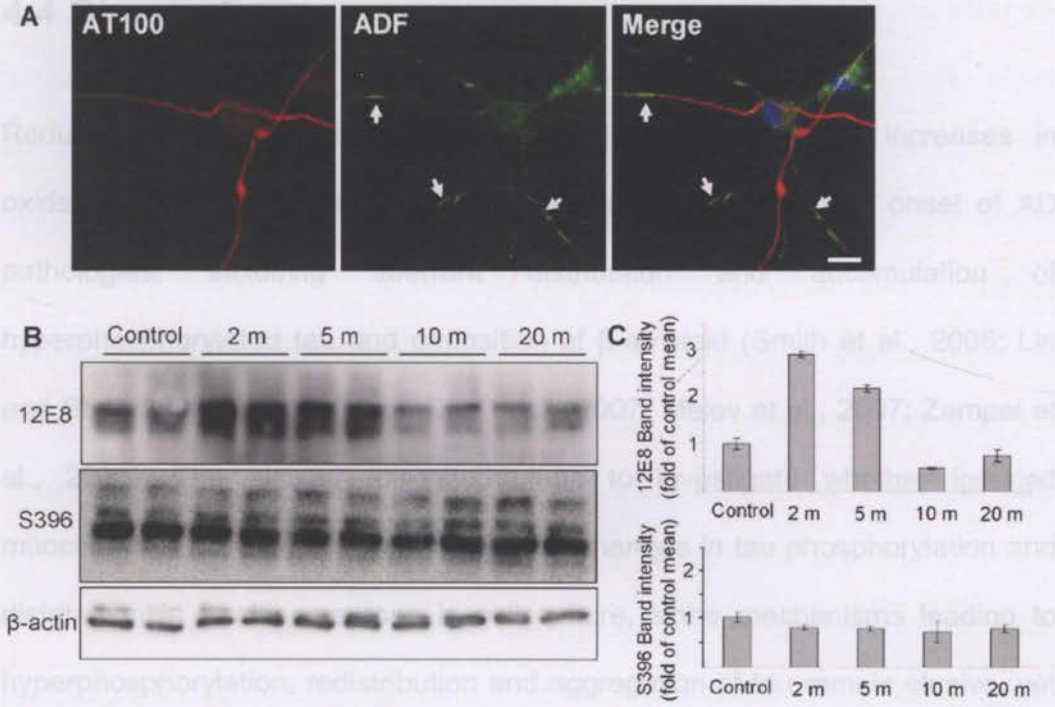


**Figure 4.7 12E8 MAP/tau but not other epitopes aggregates and co-localizes with AC rods during actin depolymerization.** Primary chick neurons were treated with 1 μg/ml Latrunculin B (Lat B) for 15 min, fixed and immunostained. We first confirmed formation of both AC and 12E8-MAP/tau positive rods in our cultures (data not shown), as has previously been observed (Whiteman et al., 2009) (see also Chapter 3) and then co-stained cultures for ADF with numerous tau epitopes. Whereas an abundance of AC rods were induced by Lat B (A, arrows), label for all tau epitopes, except 12E8, remained relatively smooth and evenly distributed throughout neurites, as shown here for AT100 (A) (other epitopes not shown). Western blots of lysates of Lat B-treated neurons were probed with the same battery of antibodies to MAP/tau phospho-epitopes. While most epitopes such as S396 (shown here) showed little change in phosphorylation during Lat B treatment, the 12E8 epitope was strongly phosphorylated within 2 min of treatment (B, C). Band intensities were quantified for each time-point for 12E8 and S396 immunoblots (C) with each lane normalized to individual β-actin loading controls and then calculated as a percentage of control band intensities. At 2 min, 12E8 phosphorylation was 2.9±0.1-fold higher than control means (mean ±min/max intensities). Scale bar = 10 μm.

## 4.4 Discussion

Reduced energy metabolism, mitochondrial dysfunction and increases in oxidative stress in the ageing brain have been linked with the onset of AD pathologies, including aberrant distribution and accumulation of hyperphosphorylated tau and deposition of  $\beta$ -amyloid (Smith et al., 2005; Lin and Beal, 2006; Escobar-Khondiker et al., 2007; Melov et al., 2007; Zempel et al., 2010). The aim of this study was to investigate whether induced mitochondrial dysfunction could elicit such changes in tau phosphorylation and distribution in healthy neurons in cell culture, since mechanisms leading to hyperphosphorylation, redistribution and aggregation of tau remain elusive, yet are central to understanding the pathogenesis of AD.

Here, we treated primary chick neuronal cell cultures with the mitochondrial inhibitor AM that rapidly depletes cellular ATP (Whiteman et al., 2009) and subsequently analyzed changes to phosphorylation and sub-cellular distribution of MAP/tau using Western blotting and immunolabeling. Since kinase activity is directly dependent on presence of ATP (unlike phosphatase activity which is dependent on hydrolysis), it follows that ATP depletion leads to an equilibrium shift toward phosphatase activity. As such, we were not surprised to see in this study rapid net dephosphorylation of the majority of MAP/tau epitopes upon mitochondrial inhibition. Interestingly however, we observed a substantial increase in phosphorylation at the 12E8 site, an 'early AD marker' antibody raised against the 'KXGS' motifs in the microtubule binding domain of human



MAP/tau (Seubert et al., 1995; Augustinack et al., 2002) (Fig. 4.1). Notably, we previously demonstrated that this epitope is incorporated into AC rods, which are also generated under ATP depleting conditions and closely resemble the neuropil threads characteristic of AD brain (Whiteman et al., 2009) (confirmed here in Fig. 4.5A). It is important to note that the MAP/tau protein family, including the vertebrate proteins tau, MAP2 and MAP4 (the latter of which is non-neuronal) all contain highly homologous carboxyl terminals, each with the conserved 'KXGS' motifs in MT-binding repeats (Lewis et al., 1988; Dehmelt and Halpain, 2004a). In light of this, we cannot discount that the 12E8-positivity we are observing in MAP/tau rods in the present study might be due at least in part, to presence of phospho-MAP2 in addition to phospho-tau. Recent studies in tau knock-out mice however suggest the contribution of MAP2 in these inclusions is negligible, and is discussed further in Chapter 5. Other phospho-MAP/tau epitopes including AT270, S422, AT100, S396 and S404 accumulated in small neuritic spheroid swellings, an effect that has previously been observed in pre-NFT neurons (so-called "pre-fibrillar punctate regions of tau") and proposed to be an early phenomenon in the development of AD tau pathology (Augustinack et al., 2002). Here, we found these epitopes to only occasionally form classic rod-shaped structures reminiscent of AC rods (Fig. 4.2 and 4.4), and furthermore, only some of these epitopes co-localized with ADF label in AC rods, albeit this observation was rare (Fig. 4.5). That some phospho-epitopes appeared to accrue into spheroids, others into rods and others still remained relatively evenly distributed in neurites further highlights

the complex regulation of MAP/tau protein via its many phosphorylation sites. Further involved studies would be required to adequately explain the differential distribution and phosphorylation patterns of these tau species. Nonetheless, we can conclude that recruitment of MAP/tau to AC rods during these conditions is primarily specific to KXGS-phosphorylated species in the initial stages. The occasional rod-shaped structure formed by S404 and AT270 label (Fig. 4.2) and rare co-localization of AT270 with ADF in AC rods, suggests that other phospho-epitopes of tau may appear in AC rods later, a subject of ongoing investigation. In primary neurons, Lat B-induced actin depolymerization also resulted in specific recruitment of KXGS-phosphorylated MAP/tau to AC rods, with a concomitant 2.9-fold increase phosphorylation of this site following 2 min Lat-B treatment (Fig. 4.7). By contrast, S396 was neither seen to redistribute into spheroid aggregates nor deviate from control levels of phosphorylation. These data suggest actin rearrangement triggered either by changes in cellular ATP levels or by actin depolymerizing drugs may be an upstream effector of KXGS phosphorylation and AD-like redistribution of MAP/tau into AC rods.

*converting structures in solution (Cleveland et al., 1977; Mukrasch et al., 2008).*

A predominant function of tau protein is to bind and stabilize axonal MTs – the tracks for cargo transport to synaptic terminals. Phosphorylation in the MTBD by microtubule affinity regulating kinase (MARK)/PAR1 decreases the binding affinity of tau, thus enabling MT dynamics (Biernat et al., 1993; Mandelkow et al., 1995; Drewes et al., 1997). Aberrant phosphorylation of tau in the MTBD gives rise to a destabilized MT network and concomitant self-aggregation of tau



by association of the hyperphosphorylated 'KXGS' repeat regions (Drewes et al., 1997; Alonso et al., 2001; Zhou et al., 2006). This self-aggregated tau is purported to serve as a seed for subsequent PHF assembly of redistributed tau along neurites (neuropil threads) and in the somatodendritic domain (neurofibrillary tangles) (Probst et al., 1996; Delacourte et al., 1998). Pertaining to this in the present study, we identify the KXGS-hyperphosphorylated epitope as a central player in the rapid recruitment and accumulation of MAP/tau into neuropil thread-like aggregates, reminiscent of those observed in AD (Augustinack et al., 2002; Whiteman et al., 2009). The important role of this site is underpinned by two findings. Firstly that this epitope is the only site to hyperphosphorylate during ATP-reduction (Fig. 4.1) or to Lat B treatment (Fig. 4.7), and secondly that under both conditions, only this phospho-epitope was seen to aggregate into distinct rod-shaped structures that frequently co-localized with AC (Fig. 4.5 and 4.7).

*In vivo*, tau is a natively unfolded protein that exists as a population of inter-converting structures in solution (Cleveland et al., 1977; Mukrasch et al., 2009). Nuclear magnetic resonance studies have shown that phosphorylation of various sites in tau cause changes in the local conformation and is proposed as an additional means through which tau can exert control over biological activity (Du et al., 2005). Specifically, pseudophosphorylation of KXGS motifs at S262 and S356 has been shown to induce selective conformational changes in the first and second repeats (Du et al., 2005; Fischer et al., 2009). Similar to our

observations of sustained KXGS phosphorylation over 120 min, enduring phosphorylation of the 12E8 epitope has been reported in a gerbil-model of brain ischaemia, a condition tantamount to reduced cellular metabolism in affected areas (Gordon-Krajcer et al., 2007). The increased and persistent phosphorylation of the S262/S356 site during mitochondrial stress in the present study may be explained by a conformational change to repeat region of MAP/tau that consequently 'masks' the residues from phosphatase access to the MTBD, such as has been previously suggested in relation to PHF conformation (Gordon-Krajcer et al., 2000). Likewise, we speculate that the rapid association of AC-actin and phospho-MAP/tau may also contribute to the masking of the residues. Another possible explanation for the persistent phosphorylation is that rapid depolymerization of the actin cytoskeleton may induce specific activation of MARK/Par-1, which has previously been implicated in conferring tau toxicity in *Drosophila* models (Drewes et al., 1997; Timm et al., 2003; Nishimura et al., 2004). Consistent with the latter, activation of MARK results in elevated phosphorylation and dendritic accumulation of tau in stressed primary hippocampal neurons (Zempel et al., 2010).

Extensive studies have demonstrated a role for tau and other MAPs in cross-linking and bundling of actin filaments (Griffith and Pollard, 1978; Nishida et al., 1981; Griffith and Pollard, 1982; Selden and Pollard, 1983; Correas et al., 1990; Yamauchi and Purich, 1993; Fulga et al., 2006). Some studies have additionally demonstrated that MAP-actin association is regulated by the



reversible phosphorylation of MAPs (Nishida et al., 1981; Selden and Pollard, 1983) and that furthermore, tau and MAP2 interactions with actin occur via their MT-binding domains (Correas et al., 1990; Ozer and Halpain, 2000). This actin-binding capacity of tau and MAP2 has been specifically attributed to the KXGS-containing motif in the repeat regions of the MTBD (Moraga et al., 1993; Ozer and Halpain, 2000). That 12E8-positive MAP/tau co-localized with AC rods in our study further supports a central role for this site in its rapid association with actin. Moreover, EM analysis of AC rods following 15 min AM treatment in primary neuron culture demonstrate presence of filamentous bundles consistent with F-actin (not MTs) (Fig. 5), and therefore we propose that AC-actin bundles form initially and serve as nucleation sites for subsequent recruitment of phosphorylated MAP/tau. A recent study of human AD brains provides support for this notion, which reported a strong correlation between increased cofilin expression and tau pathology in specific regions of the brain, including the temporal cortex (Nelson and Wang, 2010). Expression of the microRNA miR-107 has been shown to decrease in AD brain (Wang et al., 2008), which is associated with increased cofilin protein levels and formation of cofilin rod-like structures (Yao et al., 2011). In regions of AD brains with confirmed reduction of miR-107 expression, a significant increase ( $p < 0.02$ ) in NFTs was observed when compared with adjacent tissue expressing normal levels of miR-107 (Nelson and Wang, 2010).

et al., 1996; Mendelkovic et al., 2004; Bius and Qiang, 2005; Zempel et al., 2010). The present findings therefore suggest that targeting mitochondrial

Further investigations are required to delineate the mechanisms facilitating the interaction between MAP/tau and AC-actin and whether it is direct or indirect. Important questions that remain to be answered are whether the KXGS phosphorylation of MAP/tau is causative or correlative with its association with AC rods and what mechanism facilitates the interaction between MAP/tau and AC rods. Recent characterization of isolated AC rods demonstrated the presence of the scaffolding protein 14-3-3 $\zeta$  (Minamide et al., 2010) which was also shown to be associated with 12E8 within AC rods (unpublished observations LS Minamide and JR Bamburg), suggesting that 14-3-3 $\zeta$  may have a role either in rod structure or in a longer time-dependent maturation of MAP/tau phosphorylation, as has previously been suggested in other studies (Hashiguchi et al., 2000; Hernandez et al., 2004; Umahara et al., 2004). Answering these questions is the subject of ongoing studies.

In summary, we have shown that mitochondrial inhibition is associated with specific and sustained phosphorylation of the MTBD of MAP/tau, a site which we further identified as central to the recruitment of MAP/tau to AC rods and thus the formation of neuropil thread-like inclusions in neuronal cell culture. The combined effect of MT destabilization and deposition of hyperphosphorylated MAP/tau in the neurites is proposed to inhibit axonal transport, ultimately leading to synaptic pruning and neuronal death (Praprotnik et al., 1996; Ebner et al., 1998; Mandelkow et al., 2004; Baas and Qiang, 2005; Zempel et al., 2010). The present findings therefore suggest that targeting mitochondrial



dysfunction and down stream actin reorganization in aging cells may prevent neurodegeneration associated with aberrant phosphorylation, redistribution and aggregation of MAP/tau and thus provide further support for the development of antioxidants and pro-mitochondrial compounds targeting neurons as therapeutic strategies for AD and other tauopathies.

Elucidating pathogenic mechanisms of AD in  
tau transgenic mice:  
a role for ADF/cofilin in mediating  
 $\beta$ -amyloid and tau?

## 5.1 Introduction

Two neuropathological features of Alzheimer's disease (AD) are neuronal degeneration and decreased synaptic density, particularly in the hippocampus and neocortex. Synapse loss constitutes a strong anatomical correlate of the degree of clinical impairment and a number of studies have correlated axonal degeneration with synaptic decay and neuronal cell death (Mandelkow et al., 2003). Emerging evidence suggests an integral role of soluble A $\beta$  oligomers (dimers and trimers, but not monomers) in the earliest stages of AD pathogenesis owing, at least in part, to their direct effects at synapses. Both natural and synthetic A $\beta$  oligomers have been shown to impair synaptic

# 5

## Elucidating pathogenic mechanisms of AD in tau transgenic mice: a role for ADF/cofilin in mediating $\beta$ -amyloid and tau?

Shankar et al., 2008) and cerebral ventricles of transgenic mice injected into rat cerebral ventricles or dissociated neurons. Mechanistically, A $\beta$  oligomers interfere with post-synaptic excitatory N-Methyl-D-aspartate receptors (NMDA-R), structures critical for synaptic plasticity and long term potentiation (LTP) (Monyer et al., 1986; Bliss and Collingridge, 1993), leading to disruption of calcium homeostasis (Kelly and Ferreira, 2006), induction of neuronal oxidative stress (De Felice et al., 2007; Decker et al., 2010) and removal of NMDA-R from dendrites (Snyder et al., 2005; Lacor et al., 2007; Shankar et al., 2007). Studies in human AD brain and AD animal models have corroborated a 'synaptotoxic' role for A $\beta$ , demonstrating correlations between soluble A $\beta$  levels and synaptic and



## 5.1 Introduction

Two physiopathological features of Alzheimer's disease (AD) are axonal degeneration and decreased synaptic density, particularly in the hippocampus and neocortex. Synapse loss constitutes a strong anatomical correlate of the degree of clinical impairment and a number of studies have causally linked axonal degeneration with synaptic decay and neuronal cell death (Mandelkow et al., 2003). Burgeoning evidence suggests an integral role of soluble A $\beta$  oligomers (dimers and trimers, but not monomers) in the earliest stages of AD pathogenesis owing, at least in part, to their direct effects at synapses. Both natural and synthetic A $\beta$  oligomers have been shown to impair synaptic plasticity (Lambert et al., 1998; Walsh et al., 2002; Townsend et al., 2006; Shankar et al., 2008), memory (Cleary et al., 2005; Shankar et al., 2008) and cause loss of synapses (Lacor et al., 2007; Shankar et al., 2007) when injected into rat cerebral ventricles or applied exogenously to cultured rat brain slices or dissociated neurons. Mechanistically, A $\beta$  oligomers interfere with post-synaptic excitatory *N*-Methyl-*D*-aspartate receptors (NMDA-R), structures critical for synaptic plasticity and long term potentiation (LTP) (Morris et al., 1986; Bliss and Collingridge, 1993), leading to disruption of calcium homeostasis (Kelly and Ferreira, 2006), induction of neuronal oxidative stress (De Felice et al., 2007; Decker et al., 2010) and removal of NMDA-R from dendrites (Snyder et al., 2005; Lacor et al., 2007; Shankar et al., 2007). Studies in human AD brain and AD animal models have corroborated a 'synaptotoxic' role for A $\beta$ , demonstrating correlations between soluble A $\beta$  levels and synaptic and

cognitive impairment (Mucke et al., 2000; Gong et al., 2003; Cheng et al., 2007; Matsuyama et al., 2007).

A $\beta$  oligomers may also exert 'neurotoxic' effects by indirect mechanisms such as modulation of neuronal cytoskeletal proteins essential for axonal transport. However, our current understanding of the processes involved is relatively limited. A substantial body of evidence suggests an integral role of tau in mediating the neurotoxic effects of A $\beta$  (Goetz et al., 2001; Lewis et al., 2001; Oddo et al., 2003; Roberson et al., 2007; Ittner et al., 2010; Vossel et al., 2010; Roberson et al., 2011; Shipton et al., 2011), as was discussed in detail in Chapter 1.7. Tau hyperphosphorylation (De Felice et al., 2008; Tomiyama et al., 2010; Shipton et al., 2011), missorting and MT breakdown (Zempel et al., 2010) are some reported effects of A $\beta$  oligomer treatment in neurons. Similarly, detrimental effects of A $\beta$  may also be attributed to its influence on actin and ADF/cofilin (for more detail see Chapter 1.7.3) as evidenced by studies in rat primary neurons and organotypic brain slice culture showing that A $\beta$  oligomer treatment induces aggregation of actin (Hiruma et al., 2003) and AC into rod-shaped structures (Davis et al., 2009; Davis et al., 2011) similar to cofilin rods observed in AD brain and stressed primary neurons (Minamide et al., 2000). AC rod formation, together with A $\beta$ -induced F-actin reorganization has been shown to inhibit axonal transport of vesicles and organelles, including mitochondria and APP vesicles (Jang et al., 2005; Maloney et al., 2005; Maloney et al., 2008; Henriques et al., 2010), and is purported to contribute to



synaptic pruning of affected neurites by preventing transport of essential cargoes out to pre-synaptic terminals.

We recently showed that following mitochondrial inhibition, activated AC sequesters phosphorylated MAP/tau into rod-shaped structures in neurites, an effect which was also induced by treatment with synthetic A $\beta$  peptides (Whiteman et al., 2009). These AC-MAP/tau structures closely resemble the tau-containing neuropil threads observed in AD brain and implicate a disrupted cytoskeletal network within affected neurites which together we propose inhibit axonal transport and ultimately synaptic pruning of affected neurites. Indeed AC inclusions may therefore represent the mediating factor linking A $\beta$  secretion with tau pathology and thus serve to causally link several important features of AD.

Several important questions remain in delineating the mechanisms and interrelationships involved in initiation of AD cytopathology. Since sequestration of MAP/tau into thread-like inclusions has been shown to be dependent on the presence of AC (Whiteman et al., 2009) (see also Chapter 3), we asked four key questions:

(1) Is the reverse true, that is, is the formation of AC rods dependent on the presence of tau? (We refer to these as 'cofilin' rods in mice, see Chapter 1.5.2).

Although *in vitro* studies show purified actin and AC alone can aggregate into rods, we cannot assume that the same necessarily applies *in vivo*.

(2) If MAP/tau aggregation is dependent on cofilin, can induction of cofilin rods accelerate formation of MAP/tau early pathology (that is, neuropil threads) above the levels that occur naturally in well-characterized tau transgenic mouse models?

(3) In the absence of tau, is formation of KXGS-positive rods prevented? Answering this will further elucidate the role, if any, of other MAPs in formation of AC-MAP/tau rods.

(4) Finally, since synthetic A $\beta$  peptides have been shown to induce tau hyperphosphorylation, missorting and aggregation in primary neuron culture (De Felice et al., 2008; Whiteman et al., 2009; Zempel et al., 2010), can physiologically-relevant concentrations of naturally secreted A $\beta$  oligomers also induce these effects in organotypic brain slices? And if so, is this a time-dependent effect?

Answering these questions may indeed bring us a step closer to understanding the molecular neurodegenerative pathways involved in the true *in vivo* human AD brain.

We chose a tau transgenic mouse that best reflects the human profile of tau isoforms, expressing exclusively human tau (htau) wild type isoforms, in the absence of endogenous mouse tau (Duff et al., 2000; Andorfer et al., 2003). In htau mice, the first signs of spontaneous abnormal tau pathology (in the absence of any external stimuli) appear at 3 months, whereby extensive aggregates of phosphorylated tau appear throughout neuropil in the form of



thread-like 'distorted processes'. By 9 months of age, NFT-like somatodendritic accumulation of tau is identified with antibodies used to detect pathologic tau in human brain, including MC1, recognizing abnormal tau conformation, and PHF1, a marker for later stage tangles (Andorfer et al., 2003).

Organotypic brain slice culture is a powerful biological research tool that enables bridging of the expansive gap between *in vitro* dissociated neuron culture studies and the true *in vivo* nature of the whole organ. Previous studies have demonstrated that rat hippocampal brain slices retain intrinsic structure and organotypic cellular and connective organization for up to several weeks in culture (Zimmer and Gähwiler, 1984; Stoppini et al., 1991). In these studies, histochemical and immunohistochemical methods were performed on hippocampal tissue taken from 6-8-day-old rats maintained for 3-6 weeks in culture. Cresyl violet stains illustrated stable ultra-structure and morphology of cell layer organization throughout the dentate gyrus, hippocampus proper (cornu ammonis (CA) areas CA1, CA3 and CA4) and surrounding structures (Stoppini et al., 1991), while horse radish peroxidase (HRP) injections into individual granule and pyramidal cells revealed retention of connective organization throughout these structures, including axonal branching and termination of HRP-filled mossy fibres arising from HRP-injected granule cells (Zimmer and Gähwiler, 1984). Figure 5.1 illustrates these pathways in the rodent brain.

In elucidating answers to the three main aims of this study, we sought to closely recapitulate *in vivo* brain conditions by employing the organotypic slice

culture method using brains from tau transgenic mice, treated with physiologically-relevant concentrations of a highly potent form of human A $\beta$  oligomers (or dimer/trimers). Answers to these questions may give further clues to the complex relationship between cofilin, tau and A $\beta$  in initiating neurodegeneration.

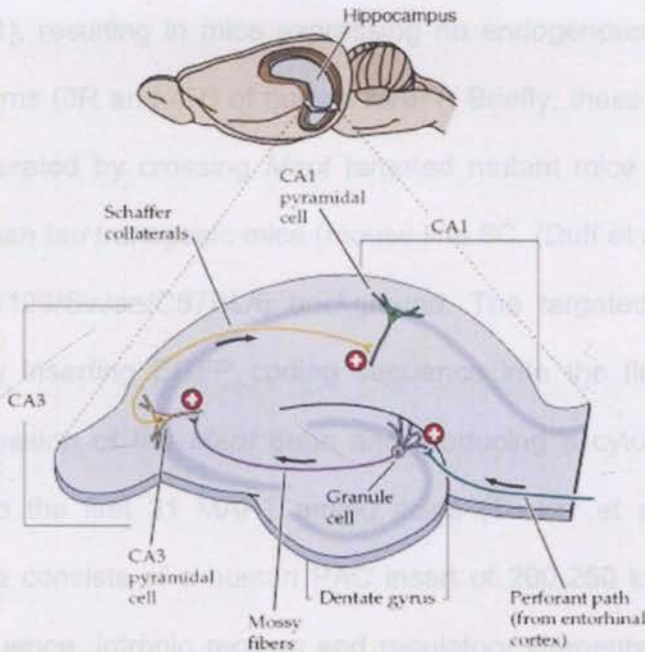


**Figure 5.1 The rodent hippocampus.** Diagram of section through the rodent hippocampus showing the major regions, excitatory pathways and synaptic connections. Source: (Purves et al., 2001).



## 5.2 Specific Materials and Methods

### 5.2.1 Transgenic MAPT mice

Breeding pairs of mice were acquired from The Jackson Laboratory (USA) and a working colony established at the Colorado State University Lab Animal Resources facility. The mouse strain B6.Cg-Mapt<sup>tm1(EGFP)Kit</sup> Tg(MAPT)8cPdav/J was generated as previously described (Andorfer et al., 2003) (Jackson Lab Stock # 005491), resulting in mice expressing no endogenous mouse MAPT but all six isoforms (3R and 4R) of human MAPT. Briefly, these double mutant mice were generated by crossing *Mapt* targeted mutant mice (Tucker et al., 2001) with human tau transgenic mice (mouse line 8C, (Duff et al., 2000)) on a Swiss Webster/129/SvJae/C57BL/6 background. The targeted mutant allele was created by inserting EGFP coding sequence into the first *Mapt* exon, disrupting expression of the *Mapt* gene and producing a cytoplasmic EGFP protein fused to the first 31 MAPT amino acids (Tucker et al., 2001). The transgenic allele consists of a human PAC insert of 200-250 kb that includes the coding sequence, intronic regions and regulatory elements of the human *MAPT* gene (Duff et al., 2000). The first generation (F1) of mice that contained the human tau gene was backcrossed to the KO mice to obtain a population of mice that were homozygous for the mouse tau disruption, but that also carried the human tau transgene (htau mice). Mice that are homozygous for the targeted *Mapt*<sup>tm1(EGFP)Kit</sup> allele and hemizygous for the human tau transgene are

viable and fertile. Mice from the colony that were noncarriers for the transgene (tau KO mice) were used as controls.

### **5.2.2 Transgene determination by Polymerase Chain Reaction**

#### **(PCR)**

2 mm of mouse tail was taken and lysed with 75  $\mu$ l alkaline lysis reagent (25 mM NaOH, 0.2 mM EDTA, pH 12) for 1 hour at 95°C. After briefly vortexing tubes, 75  $\mu$ l neutralizing buffer (40 mM Tris-HCl, pH 5) was added, left to stand for 1 min and then centrifuged for 3 min at 1500 x g at room temperature. Tail lysates were stored at 4 °C.

The genotype of the mice was determined by amplification of the target gene by polymerase chain reaction (PCR). The PCR mixture was prepared on ice to a final volume of 23  $\mu$ l per reaction comprised of 8.22  $\mu$ l RNase free ddH<sub>2</sub>O, 2.86  $\mu$ l PCR Buffer II (Fermentas, USA), 2 mM MgCl<sub>2</sub>, 0.5  $\mu$ l of 40 mM deoxyribonucleotide triphosphate mix (dNTPs; Roche, Switzerland), 1.43  $\mu$ l of each Forward and Reverse primer pair, 3.57  $\mu$ l loading dye and 0.14  $\mu$ l AmpliTaq Gold DNA Polymerase (Invitrogen). Human transgene PCR product = 187 base pairs (bp). Forward primer for human MAPT transgene: 5'-ACTTTGAACCAGGATGGCTGAGCCC-3'. Reverse primer for human MAPT transgene: 5'-CTGTGCATGGCTGTCCACTAACCTT-3'. Internal positive standard PCR product = 324 bp. Forward primer for internal positive control: 5'-



CTAGGCCACAGAATTGAAAGATCT-3'. Reverse primer for internal positive control: 5'-GTAGGTGGAAATTCTAGCATCATCC-3'.

For each sample, 2  $\mu$ l of tail lysate was combined with 23  $\mu$ l master PCR mix in PCR tubes and quickly spun down. PCR protocols were as follows: an initiation step of 94 °C for 3 min, followed by 38 cycles of denaturation at 94°C for 30 sec, annealing at 52°C for 1 min and elongation at 72°C for 1 min, with an end-hold temperature of 10°C. PCR DNA products were separated on a 1.5 % PCR grade agarose gel prepared with Tris-borate-EDTA. For the detection of the DNA fragments under UV-light, the DNA intercalating molecule ethidium bromide (0.5  $\mu$ g/ml) was added. Products were visualized in under UV light and images captured with a Kodak EDAS 290 camera.

### **5.2.3 Mouse brain preparation for Western blot**

Mice were euthanized by inhalation of isoflurane. Brains were immediately removed and frozen in liquid nitrogen. Anterior half of left cortex was solubilized by sonication in 0.5 ml 10 mM Tris pH 7.5, 1 % sodium dodecyl sulfate, 2 mM EGTA, 20 mM sodium fluoride, 0.5 mM dithiothreitol and placed in boiling water bath for 5 min. Proteins were precipitated (Wessel and Flügge, 1984) and then solubilized in 0.25 M Tris pH 6.8, 1% SDS, 10% 2-mercaptoethanol, 10% glycerol, and bromophenol blue. Protein concentrations were determined (Minamide and Bamberg, 1990) and 8  $\mu$ g loaded per lane on SDS-containing

10% isocratic polyacrylamide gels. Nitrocellulose membranes were probed with primary antibody raised against total tau (rabbit polyclonal antibody (1:200; Sigma-Aldrich) and GFP (mouse monoclonal 1:1000, Santa Cruz Biotechnology, USA). DyLight fluorescent secondary antibodies were used (Thermo Scientific, USA) and bands imaged with a Li-Cor Odyssey Infrared Imaging System.

### 5.2.3 human amyloid- $\beta$ dimer/trimer (hA $\beta$ d/T) purification

Chinese hamster ovary (CHO) cells stably expressing human APP<sub>695</sub> with the

### 5.2.4 Immunostaining of mouse brain slices

Following treatments, brain slices were fixed with warmed 4% PFA (EM-grade) in PBS for 2 h at RT, then washed three times with PBS. Since permeabilization conditions can significantly alter the preservation and ability to visualize different cytoskeletal proteins such as cofilin and MAP/tau (Whiteman et al., 2009) (see also Chapter 3), we carried out a variety of permeabilization methods using 0.05 % Triton X-100 (TX), 80% ice cold methanol (MeOH) (both diluted in PBS) or a combination of both for different lengths of time to compare results. Following permeabilization, slices were washed three times with PBS and non-specific antigens were blocked with 2 % goat serum/1 % BSA in TBS for 1.5 h at 4 °C. Slices were incubated overnight at 4 °C with primary antibodies diluted in 1 % BSA/TBS. For co-labeling studies, primary antibodies were incubated simultaneously. The following day, slices were washed in five changes of TBS over 1 h and incubated for 2.5 h at 4 °C with secondary antibody diluted 1 % BSA/TBS (1:200) and DAPI (1:500). Since B6.Cg-



*Mapt*<sup>tm1(EGFP)</sup> mice express GFP in all neurons, secondary antibodies used throughout this study were conjugated to 546 or 647 fluorophores. Slices were washed again in five changes of TBS over 1 h and coverslips mounted onto slides with ProLong Gold Antifade (Invitrogen).

### **5.2.5 Human amyloid- $\beta$ dimer/trimer (HA $\beta$ d/t) purification**

Chinese hamster ovary (CHO) cells stably expressing human APP<sub>751</sub> with the Val717Phe mutation (7PA2 cells) (Podlisny et al., 1995) secrete sub-nanomolar levels of low-*n* oligomers of human A $\beta$  (HA $\beta$ ), composed of heterogeneous A $\beta$  peptides that migrate on SDS/PAGE as dimers, trimers and tetramers. Size exclusion chromatography (SEC) to purify secreted HA $\beta$  dimer/trimers (HA $\beta$ d/t) in culture media of 7PA2 cells was kindly carried out by Ian T. Marsden at Colorado State University, USA, according to protocols adapted from Shankar and colleagues (Shankar et al., 2007), as described (Marsden et al., 2011).

Briefly, 7PA2 and CHO (control) cells were cultured in high glucose DMEM (Gibco, Invitrogen) with 10% fetal bovine serum (FBS) (Life Technologies, CA, USA). Cells were grown to near confluence and then conditioned in DMEM without FBS for ~16 h. The 7PA2 conditioned media (CM) and CHO non-conditioned (CN) media was cleared of cells by centrifuging (200 X *g* for 10 min) and concentrated ~10-fold using YM-3 Centriprep filters (Millipore, MA, USA). One milliliter of this concentrated CM and CN was injected onto a Superdex75 (10/30 HR) column (Amersham Biosciences, NJ, USA) and was

eluted in 1 ml fractions with 50 mM ammonium acetate, pH 8.5, at a flow rate of 1 ml/min. Fractions containing HA $\beta$  monomer (HA $\beta$ m) and HA $\beta$ d/t fractions (as previously identified (Shankar et al., 2007)) were removed, as were the identical fractions from CN, which served as a control. 800  $\mu$ l of the 1 ml fractions were stored at -80 °C and to confirm presence of HA $\beta$ m and HA $\beta$ d/t in the collected fractions, the remaining 200  $\mu$ l was lyophilized and re-suspended in 2x sample buffer (12  $\mu$ l), and electrophoresed on a 15-well 10–20% Tris-Tricine Criterion gel (Bio-Rad, CA, USA). Proteins were transferred onto 0.1  $\mu$ m nitrocellulose, blots boiled for 10 min and A $\beta$  detected by Western blotting (WB) with 6E10 mouse monoclonal antibody (1:2000; Covance, CA, USA) and DyLight secondary antibodies (Thermo Scientific, IL, USA). Bands were imaged with a Li-Cor Odyssey Infrared Imaging System and intensities quantified using TotalLab software (Nonlinear Dynamics, UK) (Fig. 5.2). SEC fractions enriched in SDS-stable low-*n* oligomers were pooled to generate the oligomer HA $\beta$ d/t preparation, divided into 200  $\mu$ l aliquots, lyophilized and stored at -80 °C. At 1x concentration, HA $\beta$ d/t preparations are equivalent to their secreted concentration in the culture medium, which is ~250 pM, as quantified by dot blots (Davis et al., 2011; Marsden et al., 2011).





**Figure 5.2 Western blot showing fractions of human  $A\beta$  monomers ( $HA\beta m$ ) and dimer/trimers ( $HA\beta d/t$ ) purified from 10x concentrated culture medium of 7PA2 cells.** Size exclusion chromatography (SEC) fractions 12 and 13 are enriched with dimers (D) and trimers (T) which run between 7.8–14.4 kDa on a 10–20% Tris-Tricine gel. Fractions 14 and 15 are enriched with monomers (M) (4kDa). Source: (Marsden et al., 2011). With thanks to the Bamberg Laboratory, Colorado State University, USA.

### 5.2.6 Testing $HA\beta d/t$ in rodent dissociated cell culture

Before treatment of organotypic brain slices, 1x concentrated  $HA\beta d/t$ ,  $HA\beta m$  and equivalent NC medium fractions were tested on dissociated E18 rat hippocampal neuron cultures to confirm cofilin rod-inducing properties. Experiments, data collection and analysis in Section 5.2.6 were carried out by members of the Bamberg Laboratory, Department of Biochemistry and Molecular Biology, Colorado State University, USA and are recently published

in (Davis et al., 2011). Results are therefore presented here in Materials and Methods.

Neurons were cultured for 4 days in Neurobasal culture media (containing supplements) on poly-D-lysine coated 8-well chamber slides or on 15 mm round coverslips in 24-well plates, with about 10-15,000 neurons per well. On day 4 lyophilized HA $\beta$ d/t, HA $\beta$ m or NC fraction aliquots were reconstituted in warmed Neurobasal media (containing supplements) and added to neurons. On day 5, neurons were fixed and stained for cofilin rods, as described in Chapter 2.4.

Treatment of dissociated hippocampal neurons with HA $\beta$ d/t at ~250 pM (1.1 ng/mL; equivalent to the concentration produced in the 7PA2 cell culture medium (Davis et al., 2011) induced the formation of cofilin-actin rods in many neurons, even more than treatment with 1 $\mu$ M of synthetic human A $\beta$ <sub>1-42</sub> oligomers (A $\beta$ syn) (Fig. 5.3). Significant rod induction did not occur in neurons treated with either the HA $\beta$ m or fractionated medium prepared from wild type CHO cells (non-conditioned (NC) medium). Incubation of HA $\beta$ d/t or A $\beta$ syn oligomers with 6E10 anti-A $\beta$  monoclonal antibody (as per (Cleary et al., 2005)) for 15 min prior to neuronal treatment reduced rod formation to control levels, implying it is A $\beta$  and not some other component in 7PA2 medium that is responsible for inducing rods.



The percentage of neurons with rods was quantified from each of the cultures treated with fractionated NC medium, HA $\beta$ m, HA $\beta$ d/t, or A $\beta$ syn oligomers (Fig. 5.3). Only HA $\beta$ d/t and A $\beta$ syn oligomers induced a significant ( $p < 0.01$ ) increase in the percentage of neurons with rods above control (combined data from untreated and synthetic scrambled A $\beta$  peptide-treated samples) and NC media (another control). Pretreatment with 6E10 antibody eliminated this increase. Furthermore, the percentage of HA $\beta$ d/t-treated neurons forming rods (about 30%) represents a significant ( $p < 0.05$ ) increase versus treatment with the 1  $\mu$ M A $\beta$ syn oligomers (18%).

### **5.2.7 Treating organotypic brain slices with HA $\beta$ d/t**

Prior to treatment, organotypic brain slices were maintained in culture for 2 weeks to allow stabilization and acclimatization. For treatments, 200  $\mu$ l aliquots of lyophilized HA $\beta$ d/t or CHO non-conditioned media (abbreviated to CN in these experiments) were reconstituted as above and immediately added to slices (0.6 ml per culture tube). Medium was replaced with freshly reconstituted HA $\beta$ d/t or CN fractions every 3 days for up to 9 days. Slices that were maintained in supplemented Neurobasal medium (changed every 3 days) served as one control, while slices treated with 2  $\mu$ M AM for 15 min (see Chapter 2) served as a positive control for rod analysis. Nine-day treatments were initiated first, followed by five-day treatments etc., such that all slices were fixed at the same time-point and were equal in number of days *ex vivo*.

### 5.2.8 Confocal Microscopy

An Olympus IX81 microscope equipped with an ASI piezo stage (Applied Scientific Instrumentation, OR, USA), CSU22 spinning disk confocal head (Yokogawa Instruments, Japan), 440 nm, 473 nm and 561 nm diode lasers, and a Cascade II EMCCD Camera (Roper Scientific, AZ, USA), all integrated and operated by SlideBook software (Intelligent Imaging Innovations, CO, USA), was used to obtain confocal sections through organotypic slices. The objectives used include a 4x Fluorite (0.13 NA), UAPO 40x/340W-DIC (1.35 NA), or Plan-APO 60x (1.42 NA). Image stacks were converted to TIFF for subsequent analysis in Image J. Since rods and neurites often extended through multiple sections within an image stack, consecutive optical sections were analyzed to confirm rod morphology before their inclusion for quantification. Brain slices labeled respectively with single antibodies and secondary-only were used to check background bleed-through between laser channels.

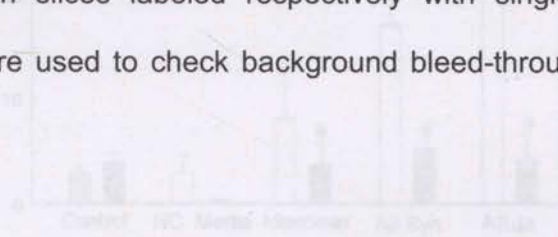
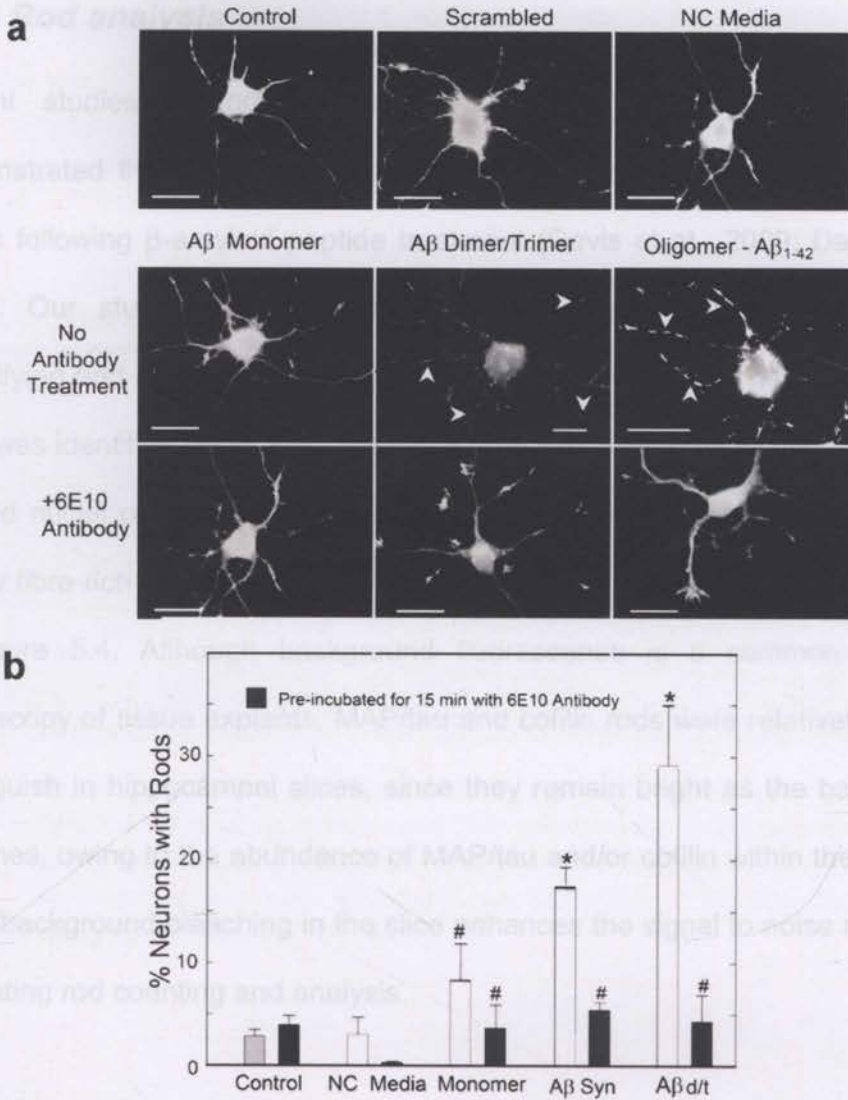


Figure 5.3. A $\beta$ 10 fraction from 7PA2 cells, but not monomer, induces rods in dissociated hippocampal neurons. Analysis by fluorescence microscopy of dissociated neurons treated with vehicle (control), scrambled A $\beta$  peptide (1  $\mu$ M), or non-conditioned media (NC media, 4% fetal bovine serum), as well as with the monomer and oligomers from 7PA2 cell culture medium and 1- $\mu$ M synthetic A $\beta$  oligomers (A $\beta$ 10). (a) Confocal fluorescence images of hippocampal neurons showing characteristic responses with cofilin rods (arrowheads) formed 24 h after treatment with A $\beta$ 10 and A $\beta$  oligomers. Preincubation of 24 h A $\beta$ -treated with an antibody (5E10) to A $\beta$  abrogates their rod-forming effects. Scale bars = 10  $\mu$ m. (b) Quantification of the rod-forming response showing the neutralizing effects of the 5E10 antibody and the non-significant changes in rod formation by A $\beta$  monomer ( $p < 0.01$  compared to control,  $p =$  not significantly different from control). Source: (Chen et al., 2011). With thanks to the Benberg Laboratory, Colorado State University, USA.





**Figure 5.3 Aβd/t fraction from 7PA2 cells, but not monomer, induces rods in dissociated hippocampal neurons.** Analysis by fluorescence microscopy of dissociated neurons treated with vehicle (control), scrambled Aβ peptide (1 μM), or non-conditioned media (NC media, d/t equivalent fraction), as well as with the monomer and d/t fractions from 7PA2 cell culture medium and 1 μM synthetic Aβ oligomers (Aβsyn). **(a)** Cofilin immunostained fluorescence images of hippocampal neurons showing representative responses with cofilin-actin rods (arrowheads) formed 24 h after treatment with Aβd/t and Aβsyn oligomers. Pretreatment of the Aβ-fractions with an antibody (6E10) to Aβ eliminates their rod-inducing effects. Scale bars = 10 μm. **(b)** Quantification of the rod forming response showing the neutralizing effects of the 6E10 antibody and the non-significant changes in rod formation by Aβ monomer. (\*p<0.01 compared to control; # = not significantly different from control). Source: (Davis et al., 2011). With thanks to the Bamburg Laboratory, Colorado State University, USA.

### 5.2.9 Rod analysis

Recent studies in rodent organotypic hippocampal slice culture have demonstrated the greatest density of cofilin rods occur in the dentate gyrus region following  $\beta$ -amyloid peptide treatment (Davis et al., 2009; Davis et al., 2011). Our study therefore focused on this region for the purposes of quantifying and comparing cofilin and MAP/tau pathologies. The dentate gyrus (DG) was identified under low magnification (4x objective) by locating the DAPI-stained nuclei of the granule cell layer. Three fields of view (FOV) within the mossy fibre-rich area of the DG were imaged at 60x magnification as illustrated in Figure 5.4. Although background fluorescence is a common issue in microscopy of tissue explants, MAP/tau and cofilin rods were relatively easy to distinguish in hippocampal slices, since they remain bright as the background bleaches, owing to the abundance of MAP/tau and/or cofilin within the rods. As such, background bleaching in the slice enhances the signal to noise ratio, thus facilitating rod counting and analysis.

Rods are not apparent at low magnification but become apparent and are relatively objectively distinguishable at 60x magnification, even in single confocal sections. For quantification, confocal image stacks of each FOV were analysed and only those structures clearly exhibiting classic 'rod-shaped' structure were counted (see Fig. 5.8a, b). Although an abundance of punctate/spheroid-like aggregates were observed and it may be argued that



these structures themselves form precursory 'seeds' or nucleation sites for the development of rods, they were omitted from counts in this study.

### 5.3.1 Preliminary work

Tau is expressed in htau mice but not tau KO mice

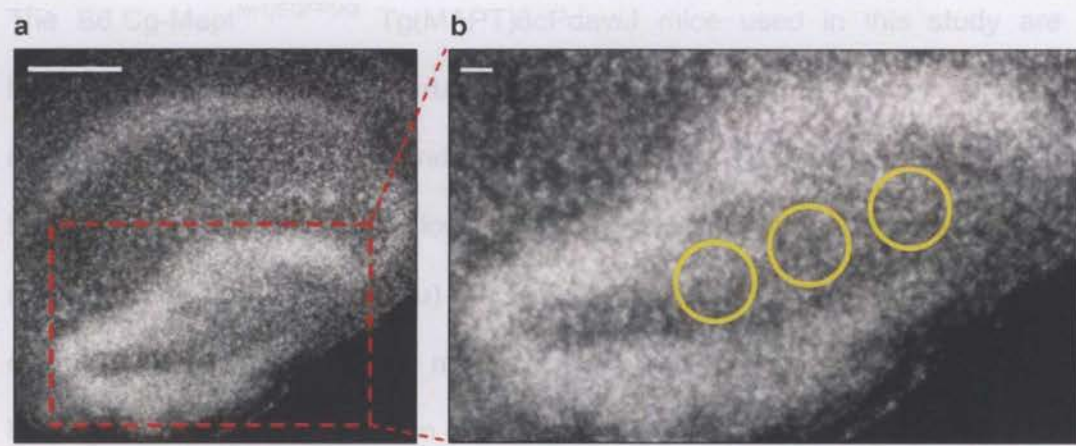


**Figure 5.4 Dentate gyrus fields of view (FOV) for imaging and analysis.** Granular layers of the dentate gyrus (DG) (identified with DAPI) were located under 4x magnification (a). Three FOVs were chosen within the mossy fibre-rich region within the DG (b, yellow circles) and imaged at 60x magnification. Scale bars = 100  $\mu$ m (a); 20  $\mu$ m (b).

## 5.3 Results

### 5.3.1 Preliminary work

#### Tau is expressed in htau mice but not tau KO mice

The B6.Cg-Mapt<sup>tm1(EGFP)Kit</sup> Tg(MAPT)8cPdav/J mice used in this study are homozygous for mouse tau disruption, such that all mice in this strain express no endogenous mouse tau (Andorfer et al., 2003). Those that express the human transgene express the longest isoform of human tau and hereafter are referred to as human tau (htau) mice. Those that do not carry the transgene express neither human tau nor mouse tau and are hereafter referred to as tau knockout (KO) mice. To confirm expression of tau in htau mice and its absence in tau KO mice, brain tissue lysates from genotyped htau and KO mice were immunoblotted for total tau (Fig. 5.5). Additionally, lysates were probed for tau-GFP to confirm GFP disruption of the gene.



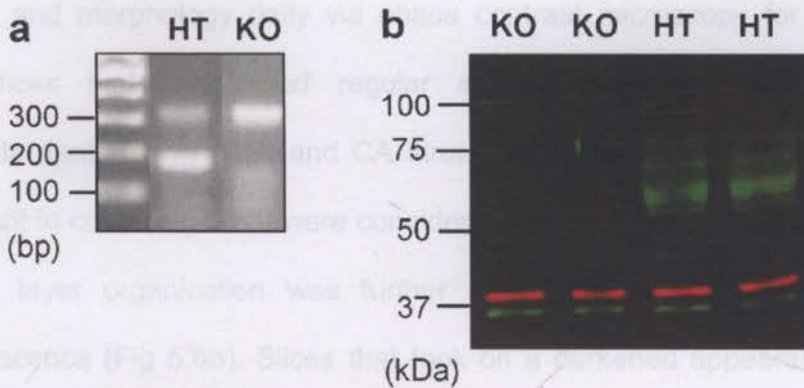


**Figure 5.5 Confirming expression of tau in human tau (htau) transgenic mice but not tau knockout (KO) mice.** (a) Genotyping was carried out via Polymerase Chain Reaction (PCR) using DNA extracted from mouse tail biopsies. The PCR product from mice carrying the htau transgene (HT) is 187 base pairs (bp) in size, as indicated by the lower band in the HT lane. The 'internal control' PCR product is 324 bp appearing as a fainter higher band in HT mice and is the only band appearing in PCR of KO (non-transgene-carrier) mice. (b) Brain lysates from KO and HT mice (2 per genotype) were immunoblotted for total tau (green) and GFP (red). Whereas the ~37 kilo Dalton (kDa) GFP band appears in lysates of both genotypes, indicating disruption of the gene for endogenous mouse tau, only HT mice express tau, as indicated by the bands ~55-75 kDa. The author gratefully acknowledges Laurie S. Minamide for Western blots in (b).

### Hippocampal brain slices retain organotypic organization for up to 48 days

#### *ex vivo*

In this study, we prepared mouse brain slice cultures using modified protocols from previous studies in rat brain, outlined above (Zimmer and Gähwiler, 1984; Stoppini et al., 1991) (also described in Chapter 2.9). Our first aim was to confirm viability of brain slices obtained from these methods. We prepared brain slices from wild-type C57BL/6 mice and monitored changes to gross

structure and morphology daily via phase contrast microscopy for up to 48 days. Slices that maintained regular shape and cytoarchitecture with discernible dentate gyri (DG) and CA structures and that appeared pale and translucent in color (Fig 5.6a) were considered viable. Organotypic morphology and cell layer organization was further confirmed by DAPI staining and epifluorescence (Fig 5.6b). Slices that took on a darkened appearance under the phase contrast microscope, showed degradation of DG/CA structures and exhibited 'spreading' across glass coverslips were considered not viable and removed from the study.

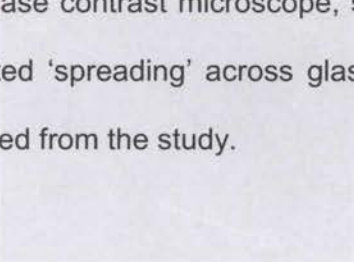
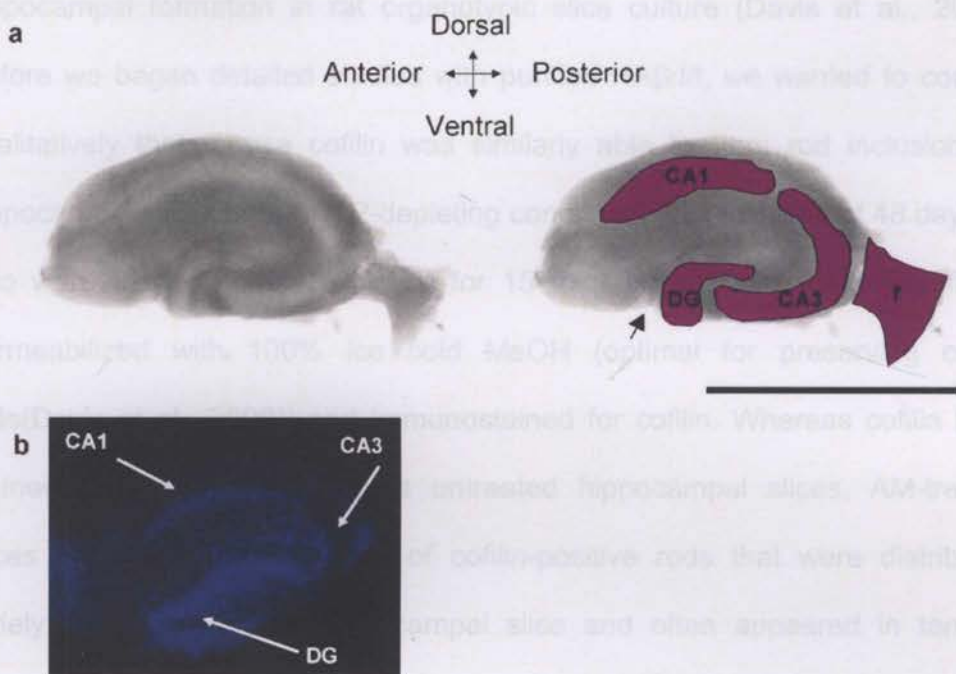


Figure 5.6 Organotypic rodent hippocampal brain slices. (a) An example of hippocampal ultra-structure in a slice from rat brain (approx. P7). Slices are typically oval in shape and exhibit clearly distinguishable cell body layers in CA1, CA3 and dentate gyrus (DG), as visualized by phase-contrast microscopy. (b) A reference slice obtained from CAST/EJ mice at 48 days in vitro. DAPI stain reveals cyto-architecture of DG and CA regions, as visualized with epifluorescence. Scale bar = 0.5 mm; image in (a) courtesy of the Stenberg Laboratory, Colorado State University, USA.

#### Endogenous mouse cofilin aggregates into rods during ATP depletion

Because cofilin concentrations in mammalian brain are 5-12 fold higher than ADF (Minamide et al., 2000; Garvalov et al., 2007), ADF/cofilin will henceforth be referred to only as 'cofilin' in these mouse experiments. ATP-depletion has been shown to induce cofilin rods that are evenly distributed across the





**Figure 5.6 Organotypic rodent hippocampal brain slices.** (a) An example of hippocampal ultra-structure in a slice from rat brain (approx. P7). Slices are typically oval in shape and exhibit clearly distinguishable cell body layers in CA1, CA3 and dentate gyrus (DG), as visualized by phase contrast microscopy. Fimbria (*f*) is retained in some slices. Arrow = hippocampal fissure. (b) A representative slice obtained from C57BL/6 mice at 48 days *ex vivo*. DAPI stain reveals cyto-architecture of DG and CA regions, as visualized with epifluorescence. Scale bar = 0.5 mm; Image in (a) courtesy of the Bamberg Laboratory, Colorado State University, USA.

### Endogenous mouse cofilin aggregates into rods during ATP depletion

Because cofilin concentrations in mammalian brain are 5-12 fold higher than ADF (Minamide et al., 2000; Garvalov et al., 2007), ADF/cofilin will henceforth be referred to only as 'cofilin' in these mouse experiments. ATP-depletion has been shown to induce cofilin rods that are evenly distributed across the

hippocampal formation in rat organotypic slice culture (Davis et al., 2009). Before we began detailed studies with purified HA $\beta$ d/t, we wanted to confirm qualitatively that mouse cofilin was similarly able to form rod inclusions in hippocampal slices under ATP-depleting conditions. Viable slices at 48 days *ex vivo* were treated with AM (2  $\mu$ M for 15 min) or left untreated, then fixed, permeabilized with 100% ice cold MeOH (optimal for preserving cofilin rods (Davis et al., 2009)) and immunostained for cofilin. Whereas cofilin label stained relatively evenly across untreated hippocampal slices, AM-treated slices exhibited an abundance of cofilin-positive rods that were distributed widely across the entire hippocampal slice and often appeared in tandem arrays throughout neurites (Fig. 5.7).

#### **Optimizing fixation and permeabilization protocols for cofilin and MAP/tau rods in organotypic brain slices**

The major aim of this study was to compare appearance and development of cofilin and MAP/tau rod pathologies in relation to each other in organotypic brain slices. Since preservation of each of these cytoskeletal protein aggregates are best optimized under different conditions in dissociated primary neuron culture (Whiteman et al., 2009) (see also Chapter 3.3) and since no studies simultaneously investigating both proteins in mouse brain slices have been previously reported, we conducted a combination of permeabilization procedures on AM-treated slices (2  $\mu$ M for 15 min) from htau mice and



qualitatively compared results to ascertain optimal conditions for preserving rod aggregates of both proteins in slice culture.

Based on results from previous studies (Chapter 3) (Davis et al., 2009; Whiteman et al., 2009) and general discussions, we chose six different permeabilization methods, incorporating ice cold methanol (MeOH) and/or Triton X-100 (TX), as tabled below. Slices were then blocked and immunostained for cofilin (1439 rabbit polyclonal antibody) and phosphorylated MAP/tau (12E8 mouse monoclonal) (as described above in 5.2.4) and analyzed via confocal microscopy. Overall, simultaneous preservation of MAP/tau and cofilin rods was observed best in slices permeabilized with 0.05% TX for 2 min (Condition 4). A large array of rods that stained well for phospho-MAP/tau and reasonably well for cofilin were observed across the whole hippocampal slice. By contrast, those slices permeabilized with MeOH or a combination of MeOH and TX either showed a large number of one rod type and only few of the other, or very few of each (Table 5.1).

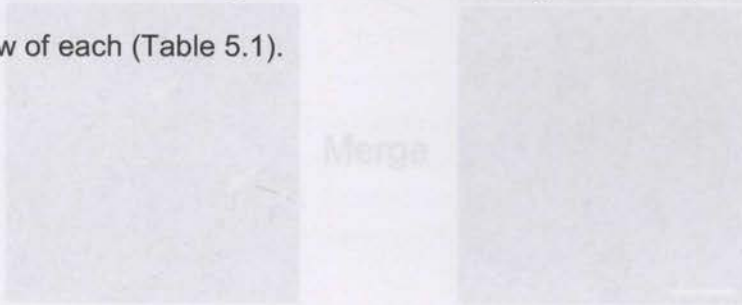
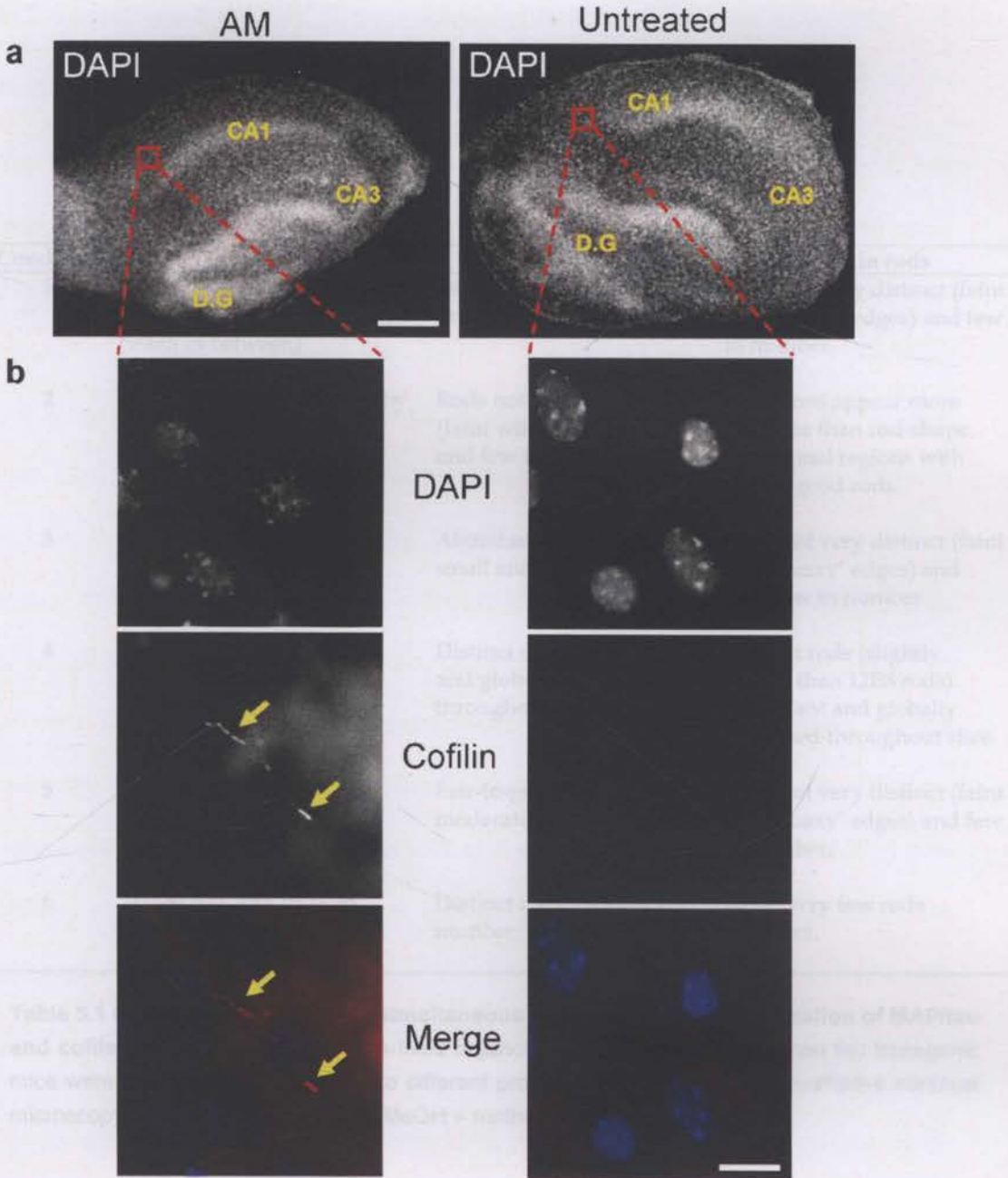


Figure 5.2 ATP-depletion induces cofilin rods in mouse organotypic hippocampal slices. 45 day-old (ex vivo) slices were treated with 2  $\mu$ M NM for 15 min, fixed and immunostained for cofilin. Many cofilin rods were observed which were fairly evenly distributed throughout the CA1, CA3, DG and surrounding regions in NM-treated slices. Here, comparable regions in treated and untreated slices illustrated in (a), were imaged at higher magnification (b). Cofilin rods were often observed in basket arrays throughout neurites of AM-treated slices (arrows). Scale bars = 100 $\mu$ m (a); 5  $\mu$ m (b).



**Figure 5.7 ATP-depletion induces cofilin rods in mouse organotypic hippocampal slices.** 48 day-old (*ex vivo*) slices were treated with 2  $\mu$ M AM for 15 min, fixed and immunostained for cofilin. Many cofilin rods were observed which were fairly evenly distributed throughout the CA1, CA3, DG and surrounding regions in AM-treated slices. Here, comparable regions in treated and untreated slices illustrated in (a), were imaged at higher magnification (b). Cofilin rods were often observed in tandem arrays throughout neurites of AM-treated slices (arrows). Scale bars = 100 $\mu$ m (a); 5  $\mu$ m (b).



### 5.3.2 Human amyloid- $\beta$ peptides induce cofilin and MAP/tau rods in the dentate gyrus

Tau transgenic mice expressing the longest isoform of human wild type tau (htau1) first exhibit abnormal tau aggregations in neuronal processes at 3

Condition	Protocol	MAP/tau rods	Cofilin rods
1	1 min 80% MeOH followed by 1 min 0.05% TX ( PBS wash in between)	Distinct rods, though few in number.	Rods not very distinct (faint with 'fuzzy' edges) and few in number.
2	1 min 0.05% TX followed by 1 min 80% MeOH (PBS wash in between)	Rods not very distinct (faint with 'fuzzy' edges) and few in number.	Inclusions appear more punctate than rod-shape. Occasional regions with fair-to-good rods.
3	5 min 80% MeOH	Abundant rods although small and grainy	Rods not very distinct (faint with 'fuzzy' edges) and very few in number.
4	2 min 0.05% TX	Distinct rods, abundant and globally dispersed throughout slice.	Distinct rods (slightly poorer than 12E8 rods). Abundant and globally dispersed throughout slice.
5	3 min 80% MeOH	Fair-to-good rods, moderate in number.	Rods not very distinct (faint with 'fuzzy' edges) and few in number.
6	90 sec 80% MeOH with 0.05% TX (final concentration)	Distinct rods, moderate in number.	None-very few rods apparent.

**Table 5.1 Optimization studies for simultaneous preservation and visualization of MAP/tau and cofilin rod inclusions.** 4% PFA-fixed organotypic brain slices from human tau transgenic mice were permeabilized according to different protocols described above. Qualitative confocal microscopy analysis was conducted. MeOH = methanol; TX = TritonX-100.

### 5.3.2 Human amyloid- $\beta$ peptides induce cofilin and MAP/tau rods in the dentate gyrus

Tau transgenic mice expressing the longest isoform of human wild type tau (htau) first exhibit abnormal tau aggregations in neuronal processes at 3 months of age (Andorfer et al., 2003). Since formation of ADF/cofilin rods is purported to be the preceding step before subsequent sequestering of MAP/tau into thread-like inclusions (Whiteman et al., 2009; Whiteman et al., 2011) (see also Chapter 4), we asked therefore whether 'premature' induction of cofilin rods in hippocampal slice culture could induce MAP/tau neuropil inclusions earlier than previously reported in these mice. To investigate the relationship between key constituents of AD pathology and to more closely recapitulate the *in vivo* state, we employed physiologically-relevant concentrations of the naturally secreted HA $\beta$ d/t peptide. Since oligomeric A $\beta$  occurs at sub-nanomolar (picomolar) concentrations in normal human cerebrospinal fluid and primary human neurons (Walsh et al., 2000), it is reasonable to assert that the picomolar concentrations (~250 pM) of secreted HA $\beta$ d/t employed in this study indeed constitute 'physiologically-relevant concentrations'.

At the endpoint of this study, brain slices prepared from P7 pups had been maintained in culture for 23 days, such that slices were effectively 30 days (1 month) of age at the point of fixing and immuno-labeling. Notwithstanding, we must be cautious in concluding that aging of slices *ex vivo* identically recapitulates the aging process *in vivo*. Figure 5.8a, b illustrates typical FOVs in



hippocampal slices from each genotype (htau or tau KO) under the different treatment conditions. Since phosphorylation of the KXGS motif of MAP/tau has been shown to be one of the first sites phosphorylated in pathogenesis of AD (Augustinack et al., 2002) and since AC rods predominantly recruit KXGS-phosphorylated MAP/tau during neurodegenerative stimuli in primary neurons (Whiteman et al., 2009; Whiteman et al., 2011) (see also Chapter 4), we focused exclusively on this epitope in the present study, labeling brain slices with the KXGS-specific antibody 12E8 (Seubert et al., 1995).

### ***5.3.3 The formation of cofilin rods is not dependent on the presence of tau but may be enhanced by human tau expression***

Several notable observations arose from this study. Firstly, since previous studies have demonstrated that formation of MAP/tau rod-like accumulations requires the presence of AC in primary neurons (Whiteman et al., 2009), we asked whether the reverse was true, that is, does cofilin require the presence of tau to form rods under neurodegenerative conditions? Indeed in tau KO hippocampal slices treated with A $\beta$ d/t and AM, many cofilin rods were evident (Fig. 5.8b, c), while 12E8 label only rarely appeared in rod structures (Fig. 5.8c), demonstrating that tau is not a necessary requirement per se in the formation of cofilin rods.

Notwithstanding, one of the most notable observations was the consistently higher number of MAP/tau rods than cofilin rods in brain slices under all treatment conditions (Fig. 5.8d), with the exception of 3D A $\beta$ d/t treatment. Additionally, tau expression was correlated to higher number of cofilin rods, whereby numbers of cofilin rods were consistently higher in htau brain slices compared to those from tau KO slices following A $\beta$ d/t and CN treatments (again with the exception of 3D d/t). Statistical analysis of pooled data from 1-5D treatments revealed higher number of cofilin rods in htau mice in both A $\beta$ d/t and CN treated slices (Fig. 5.8e). Cofilin rod numbers were significantly higher in htau mouse slices treated with CN ( $p < 0.05$ ) but not A $\beta$ d/t ( $p = 0.33$ ). To quantify this in another way, pooling all 1D-5D rod count data from dentate gyri of htau and tau KO slices (from both A $\beta$ d/t and CN treatments) revealed an increase in average number of cofilin rods in htau mice ( $24 \pm 5$ ) compared to tau KO ( $15 \pm 4$ ; average  $\pm$  SEM), although this did not quite reach statistical significance ( $p = 0.067$ ). Interestingly, acute mitochondrial inhibition with AM ( $1 \mu\text{M}$  for 15 min) induced abundant and equal numbers of cofilin rods in slices irrespective of tau expression (htau:  $46 \pm 6$ , tau KO:  $47 \pm 10$ ; average  $\pm$  min/max), although these were still fewer in number than MAP/tau rods in htau slices ( $65 \pm 8$ ). Together, these results suggest that a synergistic relationship may exist between tau and cofilin under physiologically-relevant neurodegenerative stimuli – that is, although the presence of tau is not necessary for cofilin rod formation, tau might somehow facilitate or enhance the development and accumulation of cofilin pathology when it is present. In the presence of more



acute cellular stress, such as AM, induction of cofilin pathology seems less influenced by the presence of tau.

### **5.3.4 Initiation of cofilin rods coincides with the generation of MAP/tau inclusions in transgenic tau mouse brain slices**

The present study also demonstrates the capacity for physiologically-relevant concentrations of HA $\beta$ d/t to induce cofilin and MAP/tau pathologies in mouse hippocampal brain slices. Moreover, HA $\beta$ d/t induces MAP/tau neuritic inclusions earlier than 'distorted neuropil processes' had been previously observed in this strain, with abundant numbers of MAP/tau inclusions evident after 1D d/t treatment, where slices were equivalent to 30 days old. Following 1D d/t, total numbers of both tau and cofilin rods in the DG of htau mice slices were elevated above control levels ( $45 \pm 2$  MAP/tau rods and  $32 \pm 14$  cofilin rods, compared to  $26 \pm 2$  MAP/tau and  $17 \pm 2$  cofilin rods in controls (NB media) and  $15 \pm 4$  MAP/tau and  $11 \pm 2$  cofilin in CHO non-conditioned (CN) media-treated slices; average  $\pm$  min/max) (Fig 5.8d).

MAP/tau and cofilin rod numbers peaked at 5D HA $\beta$ d/t treatment (htau:  $56 \pm 4$  MAP/tau and  $41 \pm 9$  cofilin rods; tau KO:  $19 \pm 17$  cofilin rods), above CN-treatment levels (htau:  $31 \pm 1$  MAP/tau and  $22 \pm 7$  cofilin rods; tau KO:  $13 \pm 6$  cofilin rods). However, 3D treatments gave rise to somewhat problematic results which prove difficult to interpret and explain. A substantial decrease in MAP/tau and cofilin rods was observed in HA $\beta$ d/t-treated slices at this time

point (htau:  $11.5 \pm 0.5$  MAP/tau and  $6 \pm 5$  cofilin; tau KO:  $19.5 \pm 11.5$  cofilin rods), while 3D CN treatments in htau slices induced a 3-fold higher number of rods (htau:  $35 \pm 6$  MAP/tau and  $31.5 \pm 8.5$  cofilin rods; tau KO:  $3 \pm 0.5$  cofilin rods).

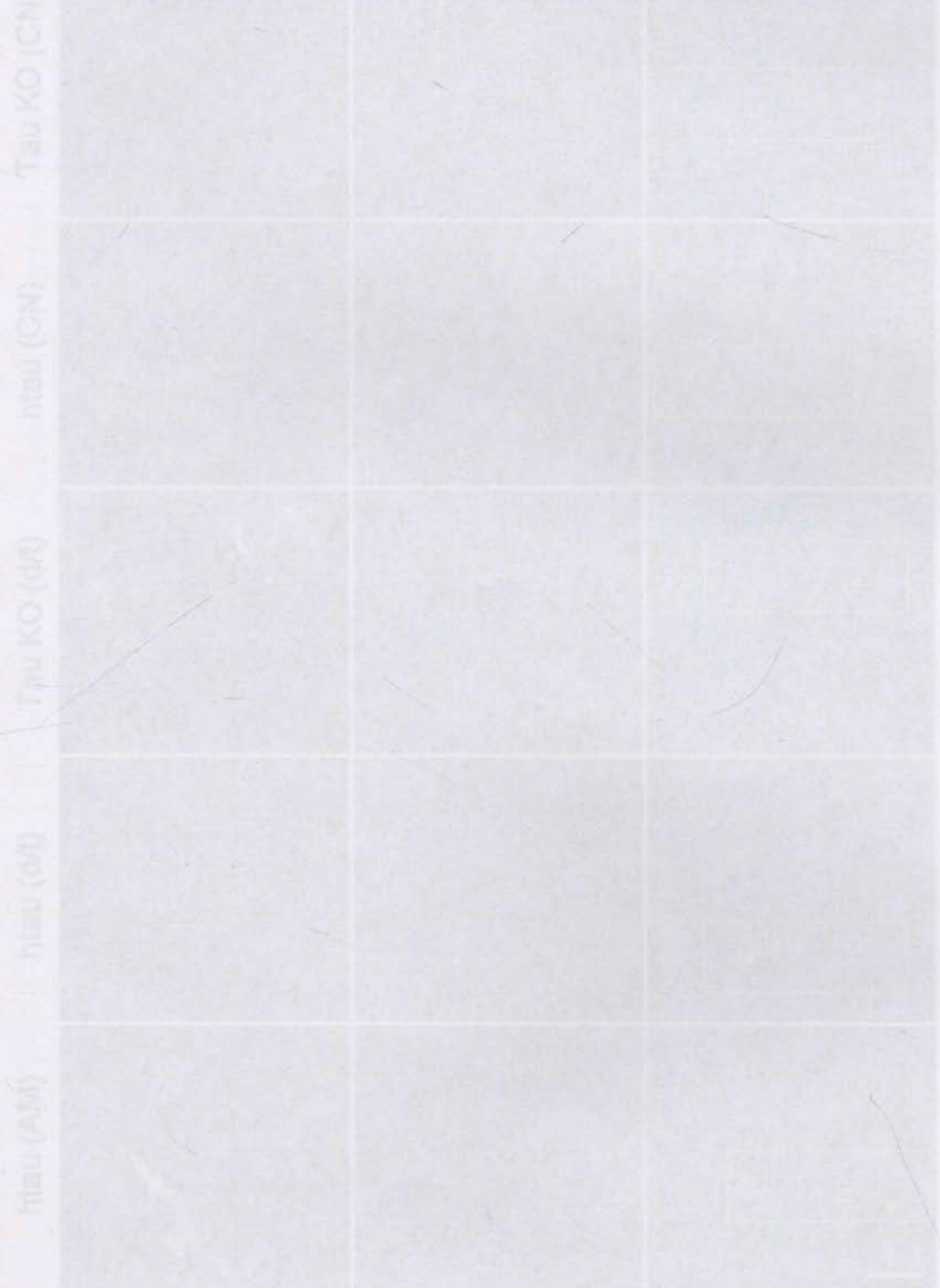
### ***5.3.5 Formation of KXGS-positive rods is markedly reduced in tau KO slices***

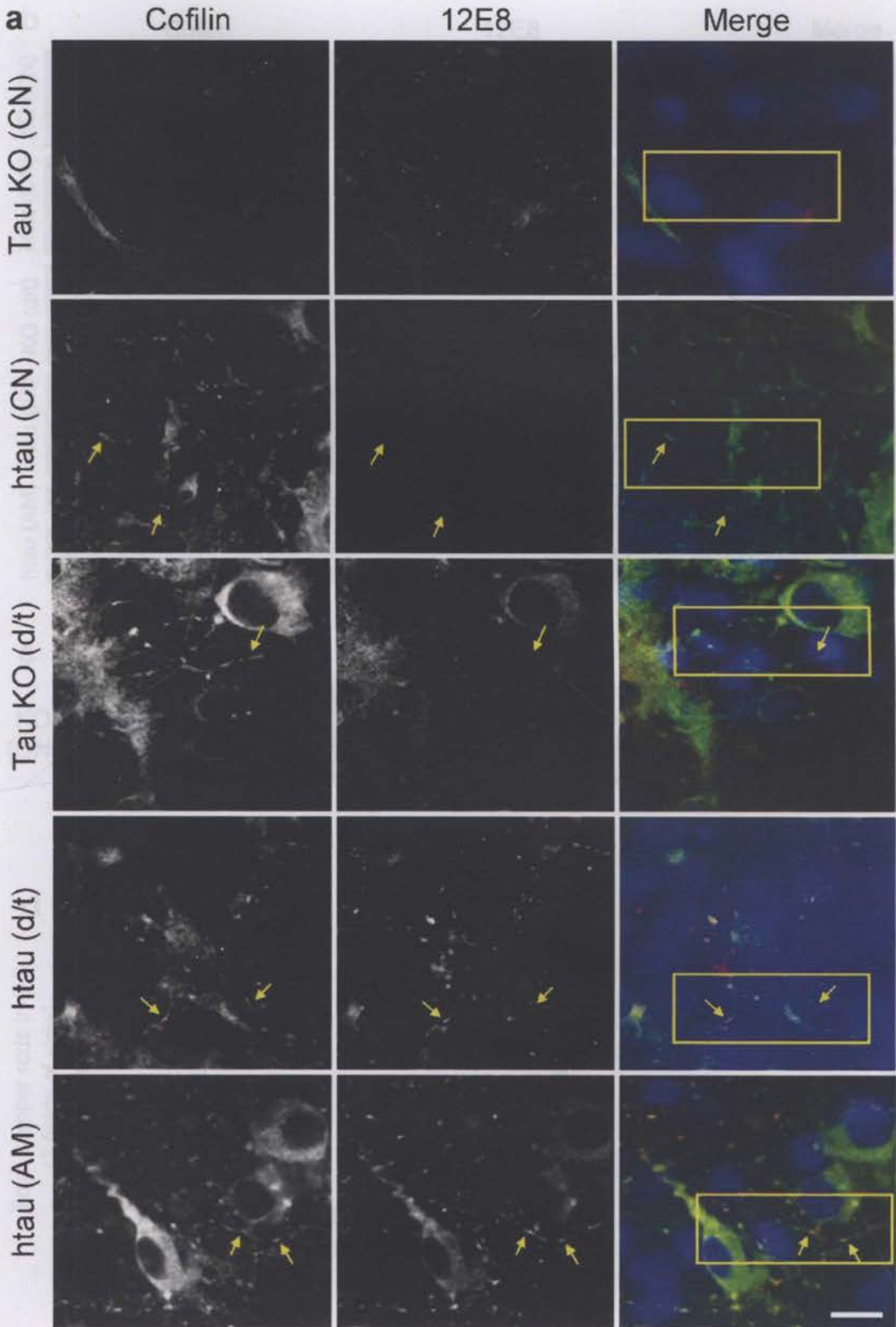
Tau KO mice slices only rarely exhibited MAP/tau rods under any treatment conditions (less than a total of 10 12E8-positive rods in all tau KO slices in this experiment), but contained elevated numbers of cofilin rods following 1D HA $\beta$ d/t ( $28 \pm 8$  cofilin rods) compared to controls ( $8 \pm 1$ ) and CN-treated slices ( $7 \pm 4$ ). Thus it appears from these experiments that the 12E8 antibody is recognizing mainly KXGS motifs of tau rather than significant amounts of other MAPs.

Nevertheless, since MAPs other than tau also contain the KXGS motifs recognized by the 12E8 antibody, it is possible that the 12E8-immunoreactivity we are observing in MAP/tau rods might be due to the presence of MAPs other than tau. To investigate further, we quantified and compared the number of 12E8-positive rods in htau and tau KO slices by pooling data for 1D, 3D and 5D treatments as above (Fig. 5.8f). The number of 12E8-positive rods was significantly lower in tau KO slices treated with d/t ( $0 \pm 0$  in tau KO,  $38 \pm 9$  in htau,  $p < 0.004$ ; average  $\pm$  SEM) and CN ( $3 \pm 1$  in tau KO,  $27 \pm 4$  in htau,  $p < 0.003$ ). Pooling all 1D-5D data from both HA $\beta$ d/t and CN treatments revealed a significant decrease ( $p < 0.00004$ ) in average number of 12E8 rods in tau KO

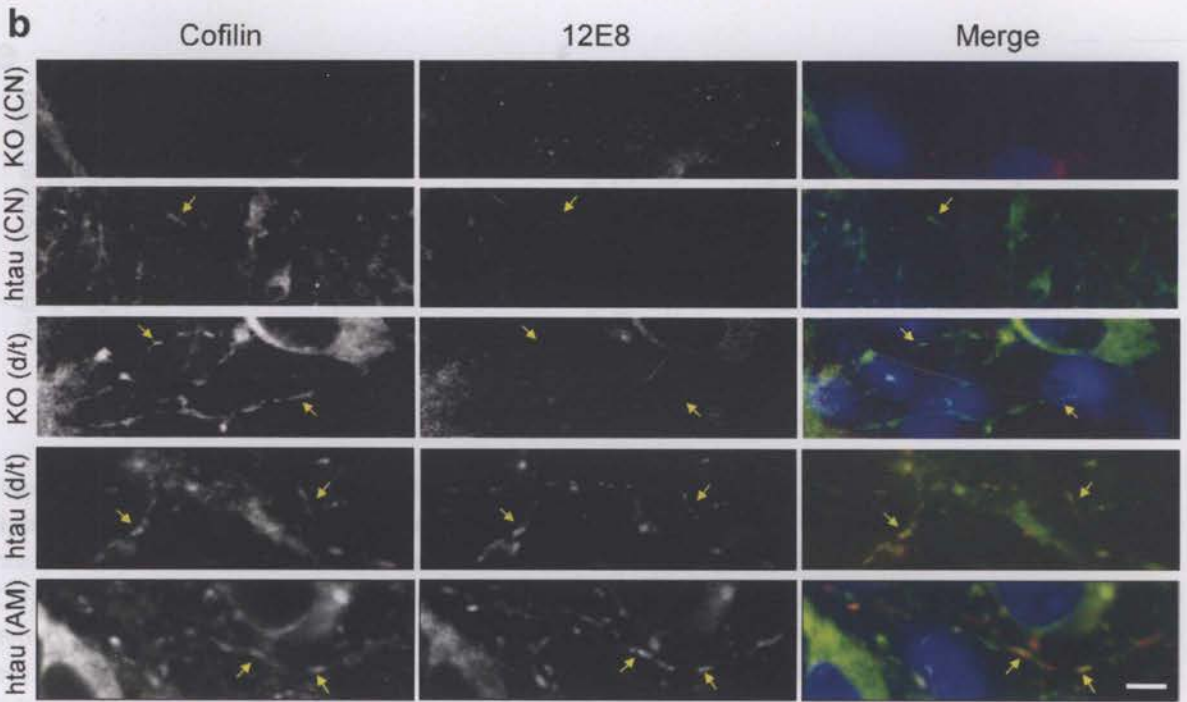


slices ( $1 \pm 1$ ) compared to htau ( $32 \pm 5$ ), suggesting that the contribution of MAPs other than tau to 12E8-immunoreactivity in MAP/tau rods is negligible.







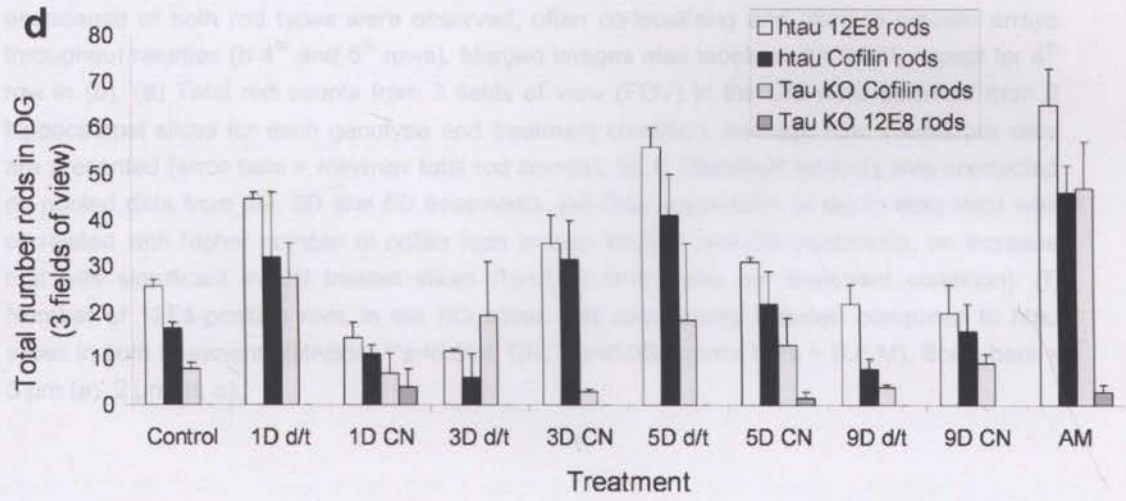


Representative single slice images from confocal stacks are shown in (b) (5-day KO mouse) and (c) (10-day htau mouse) with magnification of higher magnification (inset) indicated with CN marks only for htau (CN) mouse.



tau KO mouse slices generally exhibited fewer and thinner more faintly-labeled cofilin rods in response to the same treatment with the occasional 12E8 positive rod (example shown in c) although this was very rare. In htau mice treated with 3D d/t or AM, an average of both rod types were observed, often colocalizing.

Figure 5.10. Tau KO mouse slices generally exhibited fewer and thinner more faintly-labeled cofilin rods in response to the same treatment with the occasional 12E8 positive rod (example shown in c) although this was very rare. In htau mice treated with 3D d/t or AM, an average of both rod types were observed, often colocalizing.



## 5.4 Discussion

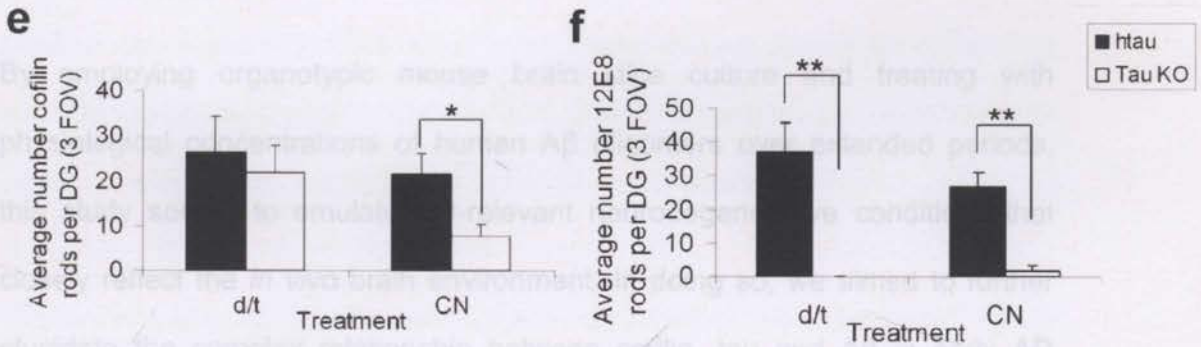


**Figure 5.8 Human A $\beta$  dimer/trimer (d/t) induces MAP/tau and cofilin rods in organotypic hippocampal slices of tau transgenic mice.** Hippocampal slices from human tau-expressing (htau) mice and tau knockout (KO) mice were treated with HA $\beta$ d/t (d/t) or CHO Non-conditioned (CN) medium for 1-9 days, such that all slices were fixed at the same time-point. Slices were immunostained for cofilin (depicted here in green) and KXGS-phosphorylated MAP/tau (12E8, red). Three fields of view were imaged within the mossy fibre-rich region of the dentate gyrus (DG) and number of cofilin-positive and 12E8-positive rods counted respectively. Representative single slice images from confocal stacks are shown in (a) (5-day (5D) treatments) with insets shown at higher magnification in (b). Treatment with CN media induced only few cofilin rods in slices from tau KO mice (a, b 1<sup>st</sup> row) however induced a number of both MAP/tau and cofilin rods in htai mouse slices (a, b 2<sup>nd</sup> row, arrows). htai mouse slices treated with d/t for 5D showed the greatest number of cofilin and MAP/tau rods (with the exception of AM-treated slices which served as a positive control), many of which co-localized (a, b 4<sup>th</sup> row, arrows). Tau KO mouse slices generally exhibited fewer and sometimes more faintly-labeled cofilin rods in response to the same treatment, and the occasional 12E8-positive rod (example shown in c) although this was very rare. In htai mice treated with 5D HA $\beta$ d/t or AM, an abundance of both rod types were observed, often co-localizing and often in tandem arrays throughout neurites (b 4<sup>th</sup> and 5<sup>th</sup> rows). Merged images also labeled with DAPI, except for 4<sup>th</sup> row in (b). (d) Total rod counts from 3 fields of view (FOV) in the DG were obtained from 2 hippocampal slices for each genotype and treatment condition. Average total counts per slice are presented (error bars = min/max total rod counts). (e, f) Statistical analysis was conducted on pooled data from 1D, 3D and 5D treatments. (e) Over-expression of tau in htai mice was correlated with higher number of cofilin rods in both HA $\beta$ d/t and CN treatments, an increase that was significant in CN treated slices (\* $p$ <0.05,  $n$ =6 slices per treatment condition). (f) Number of 12E8-positive rods in tau KO slices was significantly reduced compared to htai slices in both treatments (HA $\beta$ d/t: \*\* $p$ <0.004, CN: \*\* $p$ <0.003) (error bars = S.E.M). Scale bars = 5  $\mu$ m (a), 2  $\mu$ m (b, c).



## 5.4 Discussion

By employing organotypic mouse brain slice culture and treating with physiological concentrations of human A $\beta$  oligomers over extended periods, this study sought to emulate AD-relevant neurodegenerative conditions that closely reflect the *in vivo* brain environment. In doing so, we aimed to further elucidate the complex relationship between cofilin, tau and A $\beta$  in early AD pathogenesis. From the results of this preliminary study, we can make the following conclusions:

- (1) The formation of cofilin rods in this mouse model is not dependent on the presence of tau. However, the presence of tau might confer some synergistic effect, increasing the propensity for cofilin rod formation.
- (2) In part due to this enhancement of cofilin rod generation in htau mouse brain slices, we were so far unable to determine whether tau accumulation into rods fully depends on the induction of cofilin rods. Nevertheless, physiologically-relevant concentrations of human A $\beta$  oligomers in organotypic slice culture may be an effective inducer of two key AD-relevant pathologies: cofilin rods and MAP/tau neuropil thread-like inclusions. Whether this effect is time-dependent and whether cofilin rods serve as templates for subsequent recruitment of MAP/tau as hypothesized in brain slices remains somewhat ambiguous.
- (3) In the absence of tau, 12E8-positive rod formation is significantly reduced and therefore it is likely that tau, not other MAPs, makes up the

majority of MAP/tau protein in these rods. However, the presence of 12E8-positive rods in tau KO slices, albeit rare, means that we cannot yet completely exclude the possibility that other MAPs or MAP-like proteins are contributing to cofilin rod generation or maturation in tau KO brain slices

Additionally, important preliminary aspects of this study were three-fold. Firstly we ascertained optimal conditions for preparation and long-term maintenance of viable transgenic mouse hippocampal slices (Fig. 5.3), secondly we confirmed that mouse cofilin had the propensity to aggregate into neuritic inclusions under neurodegenerative stimuli (Fig 5.7) as had been previously observed in other animals models (Minamide et al., 2000; Maloney et al., 2005; Davis et al., 2009; Whiteman et al., 2009). Thirdly, we determined that optimal simultaneous preservation and visualization of both cofilin and MAP/tau rods in slices required 2 min TX permeabilization (Table 5.1).

Formation of cofilin rods does not require the presence of tau, since scores of cofilin rods were observed in tau KO slices under all treatment conditions (Fig. 5.8), which corroborates with results from a recent *in vitro* study (Minamide et al., 2010). However, if cofilin aggregation is the precursory event leading to subsequent sequestering of KXGS-phosphorylated MAP/tau in htau slices as hypothesized, we would expect to see an increase in the number of cofilin rods compared to 12E8-positive rods following neurodegenerative stimuli, at least in the earliest time-points. That we observed consistently higher numbers of



MAP/tau rods than cofilin rods under all but one treatment condition in htau slices (Fig 5.8) suggests the reverse is in fact true, that is, perhaps increased MAP/tau precedes aggregation of cofilin. This conclusion is supported by a previous study showing A $\beta$ -induced phosphorylation of wild type tau promoted bundling of F-actin in *Drosophila* and mouse models of tauopathy (Fulga et al., 2006). On the other hand, in both of these models tau overexpression could be causing neuronal stress, leading indirectly to an enhancement in cofilin rod generation (see below).

Our model may be problematic in that htau mice express very high levels of human tau (several-fold times higher than endogenous tau expression in wild-type mice) (Andorfer et al., 2003) which may increase the pool of free neuronal tau available for aggregation, whether spontaneous or otherwise. Moreover, whereas 3R and 4R tau isoforms typically exist in a 1:1 ratio in the normal human brain, htau mice express greater levels of 3R than 4R human tau and this shift in the ratio of normal tau isoforms may increase the propensity for tau to self-aggregate (Buee et al., 2000). Together, high levels of human tau expression and a shift in isoform ratio may account for consistently higher numbers of tau inclusions in htau mice and as such, impose limitations on using this model for examining the causal relationship between tau and endogenous mouse cofilin.

In interpreting the present data, we must also take into consideration the permeabilization methods employed for immunostaining cofilin and MAP/tau rods in this study. Although pilot studies in hippocampal slices indicated a mild (2 min) TX permeabilization produced best results among the six conditions tested (Table 5.1), it may be that these conditions are suboptimal for immunostaining of cofilin aggregates and therefore may account for the unexpectedly low numbers observed in slices. More recent studies employing a larger sample size have suggested that indeed 80% MeOH/PBS also produces optimal results for immunostaining of both tau and cofilin inclusions (personal communications with LS Minamide and JR Bamberg, discussed further in Chapter 6). It will be interesting to determine whether these conditions result in similar effects on the numbers of cofilin versus MAP/tau rods in these slices.

Since other MAPs share the 12EB 10XGS target sequence with tau (Sánchez  
Regardless of these caveats, one of the key findings of this study was that under all treatment conditions (with the exception of the AM positive-control treatment), the number of cofilin rods was consistently greater in htau slices than tau KO slices, suggesting a synergistic effect of tau in the generation of cofilin pathologies. As stated above, overexpression of tau in htau mice might in itself induce oxidative stress in the absence of any other neurodegenerative stimulus per se, thus inducing cofilin rods in a feed-forward manner. Age-dependent tau aggregation in transgenic mouse or *in vitro* models has been shown to induce mitochondrial dysfunction and increased ROS production (Stamer et al., 2002; David et al., 2005; Rhein et al., 2009) as well as retard



axonal transport of mitochondria and other vesicles (Ebner et al., 1998; Stamer et al., 2002; Mandelkow et al., 2003; Ittner et al., 2008; Ittner et al., 2009), effects of which might induce activation and rod-like accumulation of AC (Minamide et al., 2000; Maloney et al., 2005; Davis et al., 2009; Whiteman et al., 2009; Bamberg et al., 2010). At a local, individual neurite level, this feed-forward process is likely to be exacerbated. If organelles disappear from neurites of cells containing elevated MAP/tau and cofilin aggregates, one would expect major defects in their local metabolism due to reduction of ATP levels in the absence of mitochondria and a higher sensitivity to oxidative damage, caused by the absence of catalase in the transported peroxisomes (Mandelkow et al., 2003).

low that human-derived A $\beta$ 11 in picomolar concentrations induce both MAP/tau and cofilin pathologies, thus providing evidence for a 'triad' of AD

Since other MAPS share the 12E8 'KXGS' target sequence with tau (Sánchez et al., 2000; Dehmelt and Halpain, 2004) (see also Chapter 1), it is not surprising that some 12E8 immunoreactivity was observed in tau KO slices. However, since 12E8-positive rods were less frequently observed in tau KO slices (Fig. 5.8f) and generally, overall 12E8-labelling was considerably weaker, we can reasonably conclude that the major constituent of MAP/tau in rods is KXGS-phosphorylated tau.

preliminary results at hand. Likewise, whether A $\beta$ -induced tau pathology is mediated by cofilin per se as originally hypothesized

That physiologically-relevant concentrations of HA $\beta$ d/t induce both cofilin and MAP/tau rods, supports a causal relationship between A $\beta$  and these two cytopathologies in the *in vivo* brain. Indeed, synthetic A $\beta$  peptides in

micromolar ranges have been shown to elicit detrimental effects on tau including hyperphosphorylation at the KXGS motif and numerous other sites (De Felice et al., 2008; Tomiyama et al., 2010; Zempel et al., 2010; Shipton et al., 2011), missorting and aggregation along neurites (Zempel et al., 2010), tau-mediated MT disassembly (King et al., 2006) and in transgenic tau mouse models, A $\beta$  peptide treatment exacerbates tau pathology (Goetz et al., 2001; Lewis et al., 2001).. Similarly, A $\beta$  treatments *ex vivo* and *in vitro* detrimentally affect AC-actin by inducing F-actin remodeling and accumulation (Hiruma et al., 2003; Heredia et al., 2006) and formation of AC rods (Maloney et al., 2005; Davis et al., 2009), effects of which together inhibit fast axonal transport (FAT). Here we show that human-derived A $\beta$ d/t in picomolar concentrations induce both MAP/tau and cofilin pathologies, thus providing evidence for a 'triad' of AD pathology: A $\beta$ , tau and cofilin. It was recently shown that HA $\beta$ d/t treatment induces A $\beta$  secretion in primary neurons (Marsden et al., 2011) which may therefore be a potential feedforward mechanism exacerbating the detrimental effects of tau and cofilin pathologies in the aging brain over time. However, whether there are time-dependent effects of HA $\beta$ d/t on the development of MAP/tau and cofilin pathologies in our transgenic mouse model cannot be concluded based on the preliminary results at hand. Likewise, whether A $\beta$ -induced tau pathology is mediated by cofilin per se as originally hypothesized remains ambiguous and together, these questions remain the subject of ongoing studies.



This study suggests a synergistic relationship exists between the pathogenic 'triad' of cofilin, MAP/tau and  $A\beta$  in the initiation of AD. We propose that together, the  $A\beta$ -induced formation of MAP/tau and cofilin cytoskeletal inclusions may be one mechanism ultimately leading to neuronal death in the AD brain, through blockage of axonal transport of essential cargoes such as mitochondria. By contrast, it has been proposed that AC rods play a neuroprotective role during times of transient but not persistent neuronal insult (Bernstein et al., 2006). In the following chapter we discuss in more detail both the neuroprotective and neurotoxic roles of AC and MAP/tau cytoskeletal inclusions and address several vital questions pertaining to pathways that lead from the initial and early cytoskeletal pathologies to the destructive end-stage lesions of AD.

6

General Discussion

**PART IV**

Future Directions



## 6.1 General Discussion and Future Directions

Elucidating the mechanisms involved in the formation of cytoskeletal pathologies in sporadic AD and understanding how these pathologies are interrelated is essential for developing meaningful therapeutic strategies for this devastating and increasingly prevalent disease. Here, we provide evidence that mitochondrial dysfunction, a feature of aging, is central to the pathogenesis of AC-actin and MAP $\tau$  pathologies. Moreover, for the first time we show that these key histopathological features are closely interrelated and propose that aggregation and association of these proteins constitutes one of the earliest events in the initiation of AD.

### General Discussion

&

### Future Directions

Chapter 1 introduced the microtubule-associated protein  $\tau$  and another major cytoskeletal protein, actin and its associated protein AC. Both  $\tau$  and actin-cofilin are major constituents of AD histopathologies and a plethora of literature describes associations of these respective proteins with the three major AD pathology, A $\beta$  deposition. Surprisingly however, very few studies to date have investigated the relationship between MAP $\tau$  and AC in the AD brain. In Chapter 3, we describe for the first time an association between phosphorylated MAP $\tau$  and AC-actin aggregates that form following mitochondrial inhibition or synthetic A $\beta$  peptide treatment (see also Watters et al., 2009; Watters et al., 2011). In this study, we showed that AC-actin and phospho-MAP $\tau$  frequently co-localize throughout neurons in cytoskeletal protein complexes that often form in ordered arrays and closely resemble the

# 6

## 6.1 General Discussion and Future Directions

Elucidating the mechanisms involved in the formation of cytoskeletal pathologies in sporadic AD and understanding how these pathologies are interrelated is essential for developing meaningful therapeutic strategies for this devastating and increasingly prevalent disease. Here, we provide evidence that mitochondrial dysfunction, a feature of aging, is central to the pathogenesis of AC-actin and MAP/tau pathologies. Moreover, for the first time we show that these key histopathological features are closely interrelated and propose that aggregation and association of these proteins constitutes one of the earliest events in the initiation of sporadic AD.

Chapter 1 introduced the microtubule-associated protein tau and another major cytoskeletal protein, actin and its associated protein AC. Both tau and actin-cofilin are major constituents of AD histopathologies and a plethora of literature describes associations of these respective proteins with the third major AD pathology, A $\beta$  deposition. Surprisingly however, very few studies to date have investigated the relationship between MAP/tau and AC in the AD brain. In Chapter 3, we describe for the first time an association between phosphorylated MAP/tau and AC-actin aggregates that form following mitochondrial inhibition or synthetic A $\beta$  peptide treatment (see also (Whiteman et al., 2009; Whiteman et al., 2011)). In this study, we showed that AC-actin and phospho-MAP/tau frequently co-localize throughout neurites in cytoskeletal protein complexes that often form in tandem arrays and closely resemble the



striated tau neuropil threads observed in AD brain. Further, we demonstrated that presence of (activated) AC and a dynamic actin cytoskeleton is required for the recruitment of phospho-MAP/tau into these inclusions.

Since MAP/tau contains many physiological and AD-relevant phosphorylation sites, in Chapter 4 we further characterized the species of phospho-MAP/tau recruited into AC-actin inclusions. Whereas most phospho-epitopes were seen to aggregate into neuritic 'spheroid' inclusions, as has previously been reported in postmortem human AD brain (Velasco et al., 1998), we demonstrated that MAP/tau aggregation into classic rod-shaped structures reminiscent of AD neuropil threads was almost exclusively comprised of 'KXGS'-phosphorylated MAP/tau, as labeled with the mouse monoclonal antibody 12E8. Moreover, 12E8-positive MAP/tau was the only phospho-epitope observed to co-localize with AC (with the rare exception of one other epitope). This suggests that only MAP/tau phosphorylated in the MTBD is sequestered into AC rods during mitochondrial inhibition, at least in the earliest time-points, and as such, its recruitment to and co-localization with AC rods represents an early pathogenic process in generation of AD cytopathology.

In Chapter 5, we sought to move a step closer toward modeling and understanding pathogenic mechanisms in the AD brain *in vivo*. In previous chapters we employed relatively harsh ATP-reducing compounds or actin-modulating drugs in primary neuron culture, which served as useful and

accessible models for investigating more acute and rapid changes in isolated neurons. In Chapter 5, we established a more physiologically-relevant model using *ex vivo* mouse organotypic brain slice cultures. Here, we maintained viable brain slices for up to several weeks in culture and applied physiological (picomolar) concentrations of a naturally secreted human A $\beta$  peptide for extended periods to emulate conditions in the AD brain. We demonstrated that these conditions were sufficient to recapitulate the phenomena observed in our primary neuron culture models, that is, formation of both AC and phosphorylated MAP/tau rod-shaped aggregates which frequently co-localized. Although the precise nature of the causal relationship between these two lesions remains elusive based on this data, the results nonetheless implicate a role for A $\beta$  in initiation of these cytopathologies and for the first time place cofilin, tau and A $\beta$  in a common pathogenic pathway.

Together, results from this project suggest that actin-AC inclusions are most likely the initial aggregates to form following neurodegenerative stimuli and that subsequent to this, KXGS-phosphorylated MAP/tau is recruited as a secondary event. In other words, AC mediates the formation of MAP/tau pathology. Several lines of evidence from the current series of studies and others converge to support this hypothesis. Knocking down ADF expression in chick neurons (ADF constituting the vast majority of ADF/cofilin in these cells) prevents the formation of phospho-MAP/tau rods following mitochondrial inhibition (Chapter 3 and (Whiteman et al., 2009)). In addition, EM analysis



shows that immediately following mitochondrial inhibition, rod-shaped aggregates that form in neurites have an ultrastructure consistent with F-actin bundles (conferring the presence of AC), not filamentous MAP/tau (Chapter 4 and (Davis et al., 2009)). We propose that over time, KXGS phosphorylated MAP/tau which has the innate propensity to self-aggregate (Alonso et al., 2001; Zhou et al., 2006) is recruited to AC rods, followed by further phosphorylation additional sites, such that AC-actin bundles are eventually replaced by mature straight and twisted filaments of MAP/tau that later develop into PHFs (see Fig. 6.1). This corroborates with a previous study that identified marked cytoskeletal changes, specifically in actin and neurofilaments, as an early event in the cytopathology of AD, preceding appearance of neuropil threads and extensive PHF tau pathology (Perry et al., 1991). Finally, a recent study demonstrated that increases in cofilin protein levels in regions of the AD brain was significantly correlated to presence of tau pathologies and furthermore, elevation of cofilin levels due to decreases in regulating miRNAs was proposed to be an early event in the chronology of AD pathogenesis (Nelson and Wang, 2010). That results from Chapter 5 suggest MAP/tau recruitment might be the initial event in MAP/tau and AC co-aggregation may be explained by immunostaining protocols that favoured preservation and visualization of MAP/tau rather than AC. More recent studies employing 80% MeOH and TX together for permeabilization show cofilin rods forming before 12E8-positive rods in organotypic tau transgenic mouse brain slices. After 12 days in culture, around 30% of cofilin rods co-localize with 12E8, increasing to 50% around day

18 and 70% beyond 30 days in culture (personal communications with LS Minamide and JR Bamberg, Colorado State University). These latest data certainly corroborate well with our above hypothesis and further studies confirming these results are currently in progress.

Several major questions remain in delineating the apparently integral relationship between AC-actin and MAP/tau in the pathogenesis of AD. How do these cytoskeletal inclusions interact – directly or indirectly? Does the presence of MAP/tau confer any special property to AC rods? Do these interactions give clues as to how neuropil threads might transition to ‘end-stage’ NFTs in AD? What is the role of these inclusions in neurites – are they neuroprotective or neurotoxic? Each of these questions will be discussed in turn.

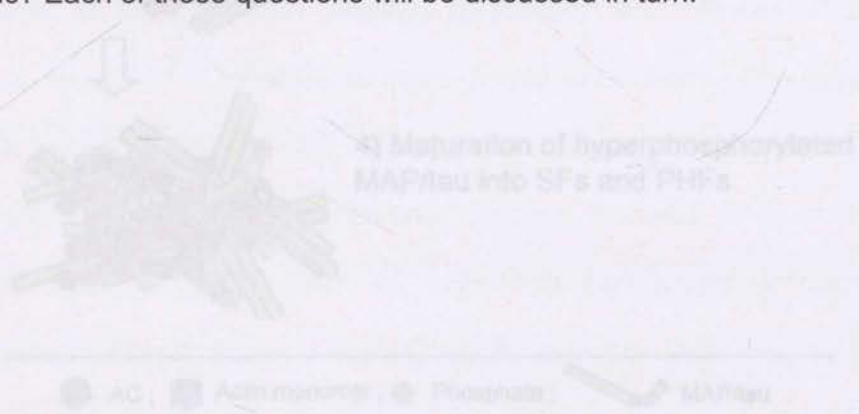
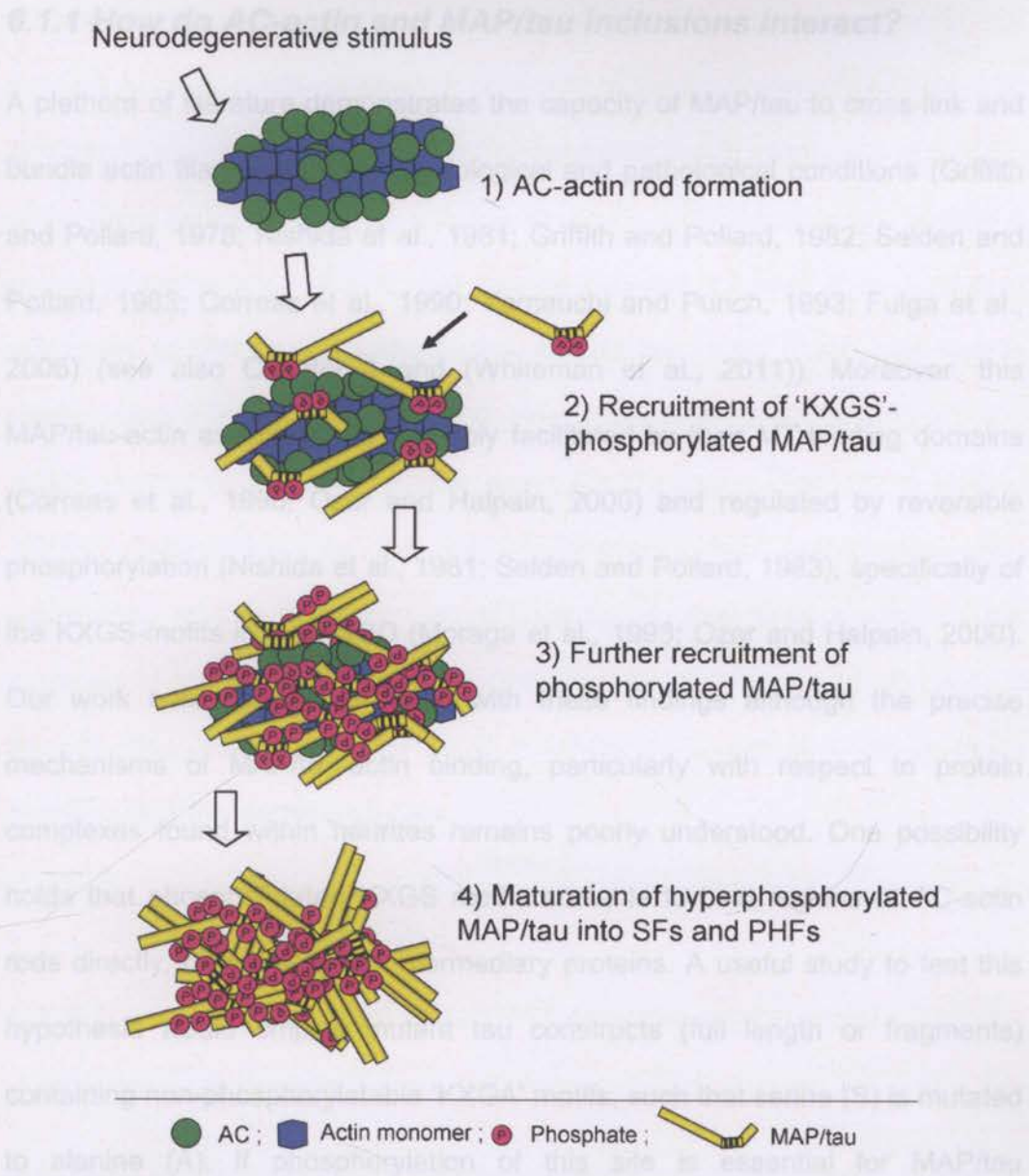


Figure 6.1 Proposed mechanism of how AC rods might facilitate formation of AD tau pathologies. (1) Neurodegenerative stimuli such as mitochondrial dysfunction induce formation of AC-rods, comprised of Aβ/actin (AC)-saturated bundles of F-actin (Minamide et al., 2009). (2) MAP/tau pre-associated at the ‘KQES’ motif in the microtubule binding domain (MTBD) is first recruited (Whitman et al., 2009; Whitman et al., 2011, probably binding AC-rods directly or indirectly via the ΔE AD prone region of tau). (3) Over time, more MAP/tau is recruited to AC-rods and phosphorylation is enhanced via kinases. (4) Eventually, AC-actin rods are completely occupied and released, and hyperphosphorylated MAP/tau enlists filaments (SFs) and paired helical filaments (PHFs), the primary constituents of neuropil threads and later neurofibrillary tangles (NFTs).





**Figure 6.1 Proposed mechanism of how AC rods might facilitate formation of AD tau pathologies.** (1) Neurodegenerative stimuli such as mitochondrial dysfunction induce formation of AC rods, comprised of ADF/cofilin (AC)-saturated bundles of F-actin (Minamide et al., 2000). (2) MAP/tau phosphorylated at the 'KXGS' motif in the microtubule binding domain (MTBD) is first recruited (Whiteman et al., 2009; Whiteman et al., 2011, probably binding AC rods directly or indirectly via the MTBD (black region of tau). (3) Over time, more MAP/tau is recruited to AC rods and phosphorylation at additional sites appears. (4) Eventually, AC-actin rods are completely occluded and replaced with phospho-MAP/tau straight filaments (SFs) and paired helical filaments (PHFs), the primary constituents of neuropil threads and later neurofibrillary tangles (NFTs).

### **6.1.1 How do AC-actin and MAP/tau inclusions interact?**

A plethora of literature demonstrates the capacity of MAP/tau to cross-link and bundle actin filaments under physiological and pathological conditions (Griffith and Pollard, 1978; Nishida et al., 1981; Griffith and Pollard, 1982; Selden and Pollard, 1983; Correas et al., 1990; Yamauchi and Purich, 1993; Fulga et al., 2006) (see also Chapter 4 and (Whiteman et al., 2011)). Moreover, this MAP/tau-actin association is probably facilitated by their MT-binding domains (Correas et al., 1990; Ozer and Halpain, 2000) and regulated by reversible phosphorylation (Nishida et al., 1981; Selden and Pollard, 1983), specifically of the KXGS-motifs in the MTBD (Moraga et al., 1993; Ozer and Halpain, 2000). Our work here corroborates well with these findings although the precise mechanisms of MAP/tau-actin binding, particularly with respect to protein complexes found within neurites remains poorly understood. One possibility holds that phosphorylated KXGS motifs are able to bind regions of AC-actin rods directly, or indirectly via intermediary proteins. A useful study to test this hypothesis would employ mutant tau constructs (full length or fragments) containing non-phosphorylatable 'KXGA' motifs, such that serine (S) is mutated to alanine (A). If phosphorylation of this site is essential for MAP/tau association with AC-actin, one would expect to see lack of immediate MAP/tau-positivity in AC rods induced under neurodegenerative stimuli.

Recent studies suggest that the scaffolding protein 14-3-3 $\zeta$  may play an intermediary role facilitating association of 12E8-positive MAP/tau with AC rods



(Minamide et al., 2010) (see also Chapter 4 Discussion). Characterization of isolated AC rods demonstrated the presence of the scaffolding protein 14-3-3 $\zeta$  and more recently, 14-3-3 $\zeta$  has also been shown to be associated with 12E8 within these rods (unpublished data LS Minamide and JR Bamburg). Beyond a simple structural role, 14-3-3 $\zeta$  may also be involved in longer time-dependent maturation of MAP/tau phosphorylation, as has previously been suggested in other studies (Hashiguchi et al., 2000; Hernandez et al., 2004; Umahara et al., 2004). In this regard, it is possible that 14-3-3 $\zeta$  plays a vital role in binding 12E8-phosphoMAP/tau to AC rods, facilitating further sequestration and aggregation of this and other phospho-epitopes, eventually leading to the formation of straight filaments and PHFs characteristic of matured AD neuropil threads. The precise role of 14-3-3 $\zeta$  in MAP/tau-AC rods is therefore being keenly pursued in ongoing studies.

### **6.1.2 Does the presence of MAP/tau confer any special property to AC rods?**

It is likely that association of MAP/tau, whether direct or indirect, serves to increase the stability of AC rods. AC rods induced by neurodegenerative stimuli are reversible when neurons are exposed to short, transient treatments (Minamide et al., 2000). Longer treatments in this study by Minamide and colleagues gave rise to so-called 'persistent' rods which remained 24 h after treatment washout (the longest time-point tested). Under EM, AC rods were

seen to span the width of affected neurites and were associated with complete loss of MTs in surrounding regions. We now propose that recruitment of MAP/tau to AC rods confers this persistence, preventing dissociation of AC-actin even after neurodegenerative stimuli have subsided. A study in tau-mutant *Drosophila* (Fulga et al., 2006) provides direct support for this hypothesis, which showed that *in vitro*, tau-associated F-actin bundles had a marked increase in resistance to the actin depolymerizing drug Swinholide-A, compared to non-tau containing preparations (Fulga et al., 2006).

Further reversibility studies are now required to test the extent to which MAP/tau confers stability to AC rods. Employing longer term (less harsh) treatments such as HA $\beta$  peptide treatment which induces phospho-MAP/tau accumulation at a slower, steady rate may be useful in determining whether a reversibility 'critical threshold' exists in level of MAP/tau recruited to AC rods. We hypothesize that to certain extent, washout of milder treatments may lead to dissociation of MAP/tau from AC rods and in turn, enable dissociation of AC rods, similar to those effects observed by Minamide and colleagues (Minamide et al., 2000). Beyond this threshold however, MAP/tau reversibility and rod dissociation may no longer be possible, thus conferring MAP-tau-AC rod persistence. This hypothesis is the subject of ongoing investigations.

Additionally, further studies are required to investigate the relationship between MAP/tau- AC rods and the formation of neuropil threads and NFTs in AD brain.



If, as we hypothesize, MAP/tau confers stability of these rods and eventually facilitates the transition of these inclusions to neuropil threads and NFTs, we can predict that recruitment of phosphorylated MAP/tau will follow a chronological pattern or 'hierarchy', as is observed in the generation of AD pathology. For example, whereas phosphorylation in the MTBD is an 'early marker' of AD tau pathology (neuropil threads), phosphorylation of S422 and S214 are indicative of 'intermediate' stages (pre-NFTs and NFTs) and phospho-sites S202/T205, S396/S404 and T212/S214 are indicative of late-stage tau pathology (NFTs and 'ghost-tangles'), as identified with antibodies AT8, PHF1 and AT100 (Augustinack et al., 2002). Characterizing phosphorylation profiles of MAP/tau in long term organotypic brain slice culture would therefore be a valuable model for investigating the relationship between MAP/tau and AC rods over time and importantly, may help to shed light on the processes involved in the transition from neuropil threads to somatodendritic NFTs in AD neurons (a question posed earlier).

### **6.1.3 What is the role of these inclusions in neurites?**

#### A neuroprotective effect?

Under normal physiological conditions, actin and MTs along with their respective associated proteins, AC and MAP/tau, function individually and in a coordinated manner to control essential neuronal processes such as regulating cell shape, polarity and movement and facilitating intracellular transport (for reviews see (Rodriguez et al., 2003; Dehmelt and Halpain, 2004) and also

Chapter 1). Neuronal actin subunit turnover depends largely on the availability of ATP (Bernstein and Bamberg, 2003) as does kinesin-dependant transport along MTs (Hirokawa, 1998; Hirokawa and Takemura, 2005). During times of mitochondrial stress in neurons formation of AC-actin rod inclusions have been shown to transiently retard the decline of ATP, suggesting these non-dynamic structures might have a neuroprotective role (Bernstein et al., 2006). Similarly, rapid recruitment of phosphorylated MAP/tau to AC rods during mitochondrial stress might also represent a neuroprotective mechanism. By binding and preventing dissociation of AC rods as discussed above, KXGS-phosphorylated MAP/tau may contribute to transiently preventing actin dynamics. This in turn, might increase the availability of limited ATP for kinesin motor activity, which requires ATP hydrolysis (Schnitzer and Block, 1997; Hirokawa and Takemura, 2005), and in doing so, enable ongoing transport of mitochondria to sites of oxidative stress, thus facilitating neuronal repair. A neuroprotective role for tau is not an entirely novel concept (Lee et al., 2005) and its role in energy preservation might be best supported by the numerous studies that show hyperphosphorylation and aggregation of tau occurs in hibernating animals (Arendt et al., 2003; Su et al., 2008; Stieler et al., 2011) or during transient ischemia (Gordon-Krajcer et al., 2007). Moreover, these studies demonstrate that tau is dephosphorylated, often back to normal physiological levels, upon arousal (in the case of hibernating animals) or reperfusion (following ischemia). Tau hyperphosphorylation has also been associated with hypothermia resulting from decreased glucose metabolism in animal models (Planel et al., 2004) and



again, suggests tau may play a neuroprotective role during times of transient neuronal stress.

### A neurotoxic effect?

On the other hand, neuritic tau aggregates and AC rods have been shown to block axonal transport (Ebner et al., 1998; Hiruma et al., 2003; Mandelkow et al., 2003; Maloney et al., 2005; Zhang et al., 2005; Ittner et al., 2009; Vossel et al., 2010). In AD brain, neuropil threads and dystrophic neurites are widely purported to prevent axonal transport of critical cellular cargoes such as mitochondria, owing to severe disruption of the cytoskeleton. Deleterious effects of this probably contribute to synaptic decay commonly observed in this disease (Perry et al., 1991; Praprotnik et al., 1996; Velasco et al., 1998; Mitchell et al., 2000; Stokin et al., 2005; Adalbert et al., 2009; Wang et al., 2009; Du et al., 2010). In *in vivo* and *in vitro* models, tau overexpression has been shown to induce tau accumulation and phosphorylation (especially in the MTBD), with the combined effect of inhibiting kinesin motor activity and axonal transport (Ebner et al., 1998; Seitz et al., 2002; Dixit et al., 2008; Ittner et al., 2009) (see also Chapter 1.4.2). Although axonal degeneration has been closely implicated with mitochondrial dysfunction and neuron death (Yahata et al., 2009), mechanisms involved in the destructive process have, until only recently, remained elusive. Recent studies in mouse optic (CNS) nerve explants have now showed that activation of the mitochondrial cyclophilin D (CypD) permeability transition pore (mPTP) triggers neurofilament disruption

and rapid axonal degeneration (Barrientos et al., 2011). Importantly, axonal degeneration was delayed when CypD-mediated activation of the mPTP was inhibited. Interestingly, mitochondrial abnormalities preceded axon degeneration by around 18 hours, suggesting an intermediary process might occur during this time (Barrientos et al., 2011). Although changes to AC-actin and MAP/tau were not investigated in this study, it is possible that mitochondrial dysfunction may induce axonal AC and phospho-MAP/tau rods in these cells and would be an interesting consideration for future work in this model.

Nonetheless, these apparently contradicting roles of MAP/tau and AC-actin aggregates can be reconciled and we propose that AC-MAP/tau rods may in fact represent both protective *and* toxic mechanisms in neurons. In the first instance, during times of transient mitochondrial dysfunction, we predict that AC rods form and recruit KXGS phospho-MAP/tau with the combined effect of preserving ATP by slowing actin dynamics and facilitating ongoing essential kinesin activity in a neuroprotective manner. However during persistent mitochondrial inhibition, a critical threshold of 'KXGS' phospho-MAP/tau may be recruited which renders AC rods and the resulting cytoskeletal complexes irreversible. As such, these inclusions become pathological, exerting deleterious and neurotoxic effects such as enduring inhibition of axonal transport and synaptic transmission.

This work has shown that mitochondrial dysfunction is a common mechanism giving rise to AD-like cytopathologies in neuronal and organotypic culture.



Together with an ever-growing body of literature that implicates mitochondrial dysfunction and oxidative stress as central to AD pathogenesis (as discussed in Chapter 1), the results presented in this thesis give credence to the notion that mitochondrial dysfunction is one of the key pathways – and perhaps even *the* key pathway – upon which formation of key human AD pathologies converge. Indeed several other stimuli independent of the ‘mitochondrial cascade’ theory, including excess glutamate leading to excitotoxicity or A $\beta$  interference at post-synaptic NMDA receptors, may also play important roles in the development of AD cytopathologies and such hypotheses are the subject of extensive ongoing research world-wide. With regards to A $\beta$  however and the question of how independent of the mitochondria it truly is in the pathogenesis of AD, it is poignant to note that oxidative damage initiates overexpression of APP in the brain and although considered a self-repair mechanism, formation and accumulation of A $\beta$  appears to be an end-product of this process (Aliiev et al., 2004; Aliyev et al., 2005). A $\beta$  has been shown to directly inhibit mitochondrial function and metabolism, as discussed in Chapter 1. We propose therefore that the detrimental effects of A $\beta$  also converge on mitochondrial dysfunction, thereby reconciling these seemingly disparate histopathological features of sporadic AD. Moreover, since A $\beta$  has recently been shown to induce further A $\beta$  secretion (Marsden et al., 2011), this may be a feed-forward mechanism that exacerbates mitochondrial dysfunction and development of cytopathologies with age.

Yet an interesting paradox arises. If mitochondrial dysfunction is a common part of aging, why don't more aging brains get AD? The "Mitochondrial Cascade Hypothesis" proposed by Swerdlow and colleagues answers this fairly simply. This theory postulates that genetic inheritance determines mitochondrial baseline function and durability, and that mitochondrial durability influences how mitochondria change with age in response to external influences (Swerdlow and Khan, 2004). In some individuals brain mitochondria are genetically more resilient to external influences such as decreased cerebral hypoperfusion commonly observed in aging brains (Aliev et al., 2009), while more 'genetically susceptible' individuals reach a critical threshold of mitochondrial changes that subsequently leads to pathogenesis of AD (Swerdlow and Khan, 2009).

## 6.2 Potential therapeutic avenues

### 6.2.1 Antioxidants and pro-mitochondrial compounds

AD treatments have yet to yield a successful therapy that addresses the underlying source of damage found in AD brain. Of the numerous etiologies proposed for sporadic AD etiology, oxidative damage and mitochondrial dysfunction is indeed cited as the leading risk factor and therefore efforts to address these abnormalities may indeed offer promising therapeutics, and perhaps even disease prevention.



Previous studies have demonstrated potential protective effects of selective mitochondrial antioxidant treatments (which prevent ROS) on brain mitochondria of aged rats (Liu et al., 2002a; Liu et al., 2002b; Ames, 2004) (for an excellent review see (Aliev et al., 2009)). Aged rats treated with antioxidants such as R-alpha-lipoic acid (LA), a coenzyme essential for energy homeostasis in mitochondria, or acetyl-L-carnitine (ALCAR), demonstrated a reduction in neuronal oxidative stress, decreased mitochondrial structural abnormalities and importantly, restored cognitive function compared to untreated, age-matched controls (Liu et al., 2002a; Liu et al., 2002b). Other promising therapeutic strategies may involve boosting a variety of major antioxidant defenses including coenzyme Q10, glutathione and enzymes manganese superoxide dismutase (MnSOD) and glutathione peroxidase (reviewed in (Lin and Beal, 2006)).

To date, human clinical trials of pro-mitochondrial compounds have been limited. A well-publicized pre-clinical (Phase II) study showed that Dimebon, a compound previously approved in Russia as a non-selective antihistamine, significantly improved the clinical course of patients with mild-to-moderate AD (Doody et al., 2008). One of the key therapeutic effects of the drug was attributed to its capacity to inhibit opening of the mitochondrial permeability transition pore and thereby attenuate, at least in part, neuronal mitochondrial dysfunction (Bachurin et al., 2001). However, Phase III trials of the drug failed dramatically to improve the clinical course of AD in subjects, reasons for which

are still being investigated by the drug companies who ran the study, Medivation and Pfizer (Miller, 2010). The therapeutic potential of this drug need not be ruled out. One explanation for the failure of Dimebon lies in the fact that subjects recruited to this study were already diagnosed with mild-moderate AD. If indeed one of the main effects of this drug is attenuating mitochondrial dysfunction, it may be reasonably assumed that major mitochondrial abnormalities and pathological cellular cascades were already widespread and beyond critical thresholds in these subjects at the time of recruitment. As such, Dimebon may have considerable 'preventative' potential, were it administered prior to the onset of significant mitochondrial changes.

### **6.2.2 The importance of diet and exercise in AD prevention**

With regards to preventing mitochondrial abnormalities and onset of sporadic AD, we cannot overlook the critical importance of diet and exercise. Diets rich in antioxidants and/or supplemented with antioxidant compounds discussed in 6.2.1 may be considered primary defenses against mitochondrial abnormalities associated with age. The 'Mediterranean Diet' (MeDi) is associated with low incidence of AD which may be indirectly related to prevention of mitochondrial abnormalities by reducing the risk of cardiovascular disease. The MeDi is characterized by high intake of vegetables, legumes, fruits, and cereals; high intake of unsaturated fatty acids (mostly in the form of olive oil), but low intake of saturated fatty acids; a moderately high intake of fish; a low-to-moderate intake of dairy products (mostly cheese or yogurt); a low intake of meat and



poultry; and a regular but moderate amount of ethanol, primarily in the form of wine (Scarmeas et al., 2006).

Maintenance of cerebrovascular function appears to be important for prevention of AD. Cardiovascular-based exercise may therefore constitute a second line of defense, contributing indirectly to the preservation of brain mitochondria. Hypoperfusion is common in aging brains and is associated with oxidative stress in a feed-forward manner, such that oxidative stress due to hypoperfusion leads to formation of ROS which in turn contributes significantly to the deleterious effects of aging on the vascular endothelium and further enhances hypoperfusion (reviewed in (Aliev et al., 2004; Aliev et al., 2009)). As such, vascular abnormalities are cited as a risk factor for sporadic AD. Physical exercise has been shown to improve cognitive and memory function in humans (Hillman et al., 2004) as well as rodents (Uda et al., 2006; Reisi et al., 2009) and is probably due, at least in part, to increases in blood flow throughout cerebrovasculature. Similarly, mental exercise might be important for preventing AD. Recent studies have suggested mental activity such as reading books, playing games or participating in computer activities in middle age or later life is associated with decreased risk of mild cognitive impairment, a transitional state between normal aging and early AD (Roberts et al., 2008).

### **6.2.3 Preventing development of cytoskeletal pathologies**

Downstream from mitochondrial dysfunction, effective therapeutic strategies might include those that prevent formation of persistent AC-actin rods (since transient AC rods may be neuroprotective, as discussed above), by preventing hyperphosphorylation and association of 'KXGS' phosphorylated MAP/tau. Preventing phosphorylation and subsequent MAP/tau self-aggregation may be best effected through compounds that inhibit activity of the KXGS-targeted MARK2/Par1 kinase or its upstream regulators, or by upregulation of PP2A activity.

Production of quinolinic acid (QA), an excitotoxic catabolite of the kynurenine pathway production, is elevated in AD brain particularly in hippocampal regions (Guillemin and Brew, 2002). QA has been shown to co-localize in dystrophic neurites and NFTs (Guillemin et al., 2005) and interestingly, induces tau hyperphosphorylation due to its effects on decreasing PP2A activity (Rahman et al., 2009). One therapeutic avenue for reducing tau hyperphosphorylation might lie in developing compounds that combat excess QA production by targeting the kynurenine pathway.

Further downstream, compounds that prevent binding of phospho-MAP/tau to AC-actin by disrupting putative binding sites on either protein or on the proposed intermediary protein 14-3-3 $\zeta$  might indeed attenuate the persistent



nature of these MAP/tau-AC rods, rendering them reversible and thus preventing the ensuing neurotoxic effects of such neuritic inclusions.

In summary, this collection of studies has demonstrated that initiation of the major pathological hallmarks of sporadic AD may converge on the common mechanism of mitochondrial dysfunction. Moreover, it has brought to light some important and complex interactions between the key cytopathologies and as such, provides valuable and tangible therapeutic targets that may help to combat this disease in its earliest stages.

## PART V

## PART V



- Adalbert R, Nogradi A, Babelis E, Janeczkova L (2009) Severely dystrophic axons at amyloid plaques remain continuous and connected to viable cell bodies. *Brain* 132:402-416.
- Al-Bassam J, Czer RS, Safer D, Helpain S, Milligan RA (2002) MAP2 and tau bind longitudinally along the outer ridges of microtubule protofilaments. *Journal of Cell Biology* 157:1187-1196.
- Aliev G, Smith MA, de la Torre JC, Perry G (2004) Mitochondria as a primary target for vascular hypoperfusion and oxidative stress in Alzheimer's disease. *Mitochondrion* 4:549-563.
- Aliev G, Palacios HH, Wotrzen B, Lipari AE, Obozovitch ME, Morales L (2009) Brain mitochondria as a primary target in the development of treatment strategies for Alzheimer disease. *The International Journal of Biochemistry & Cell Biology* 41:1989-2004.
- Aliev A, Czer BG, Seyidova D, Smith MA, Perry G, De La Torre J, Aliev G (2005) Mitochondria DNA deletions in atherosclerotic hypoperfused brain microvessels as a primary target for the development of Alzheimer's disease. *Journal of the Neurological Sciences* 229-230:285-292.

## References

- Alonso AC, Zandi T, Novak M, Grundke-Iqbal I, Iqbal K (2001) Hyperphosphorylation induces self-assembly of tau into tangles of paired helical filaments/straight filaments. *Proceedings of the National Academy of Science USA* 98:6923-6928.
- Amadoro G, Corselli V, Ciotti MT, Fiorinzano F, Caporin S, Arnold G, Calissano P (2008) Endogenous A $\beta$  causes cell death via early tau hyperphosphorylation. *Neurobiology of Aging* 22:969-90.
- Ames BN (2004) Delaying the mitochondrial decay of aging. *Annals of the New York Academy of Sciences* 1019:406-411.
- Andorfer C, Kress Y, Espinoza M, Silva Rd, Tucker KL, Barde Y-A, Duff K, Davies P (2003) Hyperphosphorylation and aggregation of tau in mice expressing normal human tau isoforms. *Journal of Neurochemistry* 86:582-590.
- Andriantsoloandro E, Pollard TD (2006) Mechanism of actin filament turnover by severing and nucleation at different concentrations of ADF/cofilin. *Mol Cell* 24:13-23.

- Adalbert R, Nogradi A, Babetto E, Janeckova L (2009) Severely dystrophic axons at amyloid plaques remain continuous and connected to viable cell bodies. *Brain* 132: 402-416.
- Al-Bassam J, Ozer RS, Safer D, Halpain S, Milligan RA (2002) MAP2 and tau bind longitudinally along the outer ridges of microtubule protofilaments. *Journal of Cell Biology* 157:1187-1196.
- Aliev G, Smith MA, de la Torre JC, Perry G (2004) Mitochondria as a primary target for vascular hypoperfusion and oxidative stress in Alzheimer's disease. *Mitochondrion* 4:649-663.
- Aliev G, Palacios HH, Walrafen B, Lipsitt AE, Obrenovich ME, Morales L (2009) Brain mitochondria as a primary target in the development of treatment strategies for Alzheimer disease. *The International Journal of Biochemistry & Cell Biology* 41:1989-2004.
- Aliyev A, Chen SG, Seyidova D, Smith MA, Perry G, De La Torre J, Aliev G (2005) Mitochondria DNA deletions in atherosclerotic hypoperfused brain microvessels as a primary target for the development of Alzheimer's disease. *Journal of the Neurological Sciences* 229-230:285-292.
- Alonso AC, Zaidi T, Novak M, Grundke-Iqbal I, Iqbal K (2001) Hyperphosphorylation induces self-assembly of tau into tangles of paired helical filaments/straight filaments. *Proceedings of the National Academy of Science USA* 98:6923-6928.
- Amadoro G, Corsetti V, Ciotti MT, Florenzano F, Capsoni S, Amato G, Calissano P (2009) Endogenous A $\beta$  causes cell death via early tau hyperphosphorylation. *Neurobiology of Aging* 32:969-90
- Ames BN (2004) Delaying the mitochondrial decay of aging. *Annals of the New York Academy of Sciences* 1019:406-411.
- Andorfer C, Kress Y, Espinoza M, Silva Rd, Tucker KL, Barde Y-A, Duff K, Davies P (2003) Hyperphosphorylation and aggregation of tau in mice expressing normal human tau isoforms. *Journal of Neurochemistry* 86:582-590.
- Andrianantoandro E, Pollard TD (2006) Mechanism of actin filament turnover by severing and nucleation at different concentrations of ADF/cofilin. *Mol Cell* 24:13-23.



- Arendt T, Stieler J, Strijkstra AM, Hut RA, Rudiger J, Van der Zee EA, Harkany T, Holzer M, Hartig W (2003) Reversible Paired Helical Filament-Like Phosphorylation of Tau Is an Adaptive Process Associated with Neuronal Plasticity in Hibernating Animals. *Journal of Neuroscience* 23:6972-6981.
- Arnold SE, Hyman BT, Flory J, Damasio AR, Van Hoesen GW (1991) The Topographical and Neuroanatomical Distribution of Neurofibrillary Tangles and Neuritic Plaques in the Cerebral Cortex of Patients with Alzheimer's Disease. *Cerebral Cortex* 1:103-116.
- Augustinack J, Schneider A, Mandelkow E, Hyman B (2002) Specific tau phosphorylation sites correlate with severity of neuronal cytopathology in Alzheimer's disease. *Acta Neuropathologica* 103:26-35.
- Avila J, Lucas JJ, Perez MAR, Hernandez F (2004) Role of Tau Protein in Both Physiological and Pathological Conditions. *Physiological Reviews* 84:361-384.
- Baas PW, Qiang L (2005) Neuronal microtubules: when the MAP is the roadblock. *Trends in Cell Biology* 15:183-187.
- Bachurin S, Bukatina E, Lermontova N, Tkachenko S, Afanasiev A, Grigoriev V, Grigorieva I, Ivanov Y, Sablin S, Zefirov N (2001) Antihistamine agent dimebon as a novel neuroprotector and a cognition enhancer. *Annals of the New York Academy of Sciences* 939:425-435.
- Bamburg J, Bernstein B, Davis R, Flynn K, Goldsberry C, Jensen J, Maloney M, Marsden I, Minamide L, Pak C, Shaw A, Whiteman I, Wiggan O (2010) ADF/Cofilin-actin rods in neurodegenerative diseases. *Current Alzheimer Research* 7:241-250.
- Bamburg JR (1999) Proteins of the ADF/cofilin Family: Essential Regulators of Actin Dynamics. *Annual Review of Cell and Developmental Biology* 15:185-230.
- Bamburg JR, Wiggan OP (2002) ADF/cofilin and actin dynamics in disease. *Trends in Cell Biology* 12:598-605.
- Bamburg JR, Bernstein BW (2008) ADF/Cofilin. *Current Biology* 18:R273-R275.
- Bamburg JR, Bloom GS (2009) Cytoskeletal pathologies of Alzheimer disease. *Cell Motility and the Cytoskeleton* 66:635-649.

- Bamburg JR, Harris HE, Weeds AG (1980) Partial purification and characterization of an actin depolymerizing factor from brain. *FEBS Letters* 121:178-182.
- Barrientos SA, Martinez NW, Yoo S, Jara JS, Zamorano S, Hetz C, Twiss JL, Alvarez J, Court FA (2011) Axonal Degeneration Is Mediated by the Mitochondrial Permeability Transition Pore. *Journal of Neuroscience* 31:966-978.
- Baumann K, Mandelkow EM, Biernat J, Piwnica-Worms H, Mandelkow E (1993) Abnormal Alzheimer-like phosphorylation of tau-protein by cyclin-dependent kinases cdk2 and cdk5. *FEBS Letters* 336:417-424.
- Bernstein BW, Bamburg JR (2003) Actin-ATP hydrolysis is a major energy drain for neurons. *J Neurosci* 23:1-6.
- Bernstein BW, Chen H, Boyle JA, Bamburg JR (2006) Formation of actin-ADF/cofilin rods transiently retards decline of mitochondrial potential and ATP in stressed neurons. *Am J Physiol Cell Physiol* 291:C828-839.
- Biernat J, Gustke N, Drewes G, Mandelkow E, Mandelkow E (1993) Phosphorylation of Ser262 strongly reduces binding of tau to microtubules: Distinction between PHF-like immunoreactivity and microtubule binding. *Neuron* 11:153-163.
- Biernat J, Wu Y-Z, Timm T, Zheng-Fischhofer Q, Mandelkow E, Meijer L, Mandelkow E-M (2002) Protein Kinase MARK/PAR-1 Is Required for Neurite Outgrowth and Establishment of Neuronal Polarity. *Molecular Biology of the Cell* 13:4013-4028.
- Blass JP (2000) The Mitochondrial Spiral: An Adequate Cause of Dementia in the Alzheimer's Syndrome. *Annals of the New York Academy of Sciences* 924:170-183.
- Blennow K, de Leon MJ, Zetterberg H (2006) Alzheimer's disease. *The Lancet* 368:387-403.
- Bliss TVP, Collingridge GL (1993) A synaptic model of memory: long-term potentiation in the hippocampus. *Nature* 361:31-39.
- Boveris A, Navarro A (2008) Brain mitochondrial dysfunction in aging. *IUBMB Life* 60:308-314.
- Braak F, Braak H, Mandelkow E (1994) A sequence of cytoskeleton changes related to the formation of neurofibrillary tangles and neuropil threads. *Acta Neuropathologica* 87:554-567.



- Braak H, Braak E (1991) Neuropathological staging of Alzheimer-related changes. *Acta Neuropathologica* 82:239-259.
- Braak H, Braak E (1995) Staging of alzheimer's disease-related neurofibrillary changes. *Neurobiology of Aging* 16:271-278.
- Braak H, Braak E (1997) Diagnostic Criteria for Neuropathologic Assessment of Alzheimer's Disease. *Neurobiology of Aging* 18:S85-S88.
- Braak H, Duyckaerts C, Braak E, Piette F (1993) Neuropathological staging of Alzheimer-related changes correlates with psychometrically assessed intellectual status. in B Corain et al *Alzheimer's Disease Advances in Clinical and Basic Research* John Wiley:131-137.
- Braak H, Alafuzoff I, Arzberger T, Kretschmar H, Tredici K (2006) Staging of Alzheimer disease-associated neurofibrillary pathology using paraffin sections and immunocytochemistry. *Acta Neuropathologica* 112:389-404.
- Brandt R, Lee G (1993) The Balance Between Tau Protein's Microtubule Growth and Nucleation Activities: Implications for the Formation of Axonal Microtubules. *Journal of Neurochemistry* 61:997-1005.
- Brookmeyer R, Johnson E, Ziegler-Graham K, Arrighi HM (2007) Forecasting the global burden of Alzheimer's disease. *Alzheimer's & Dementia: the Journal of the Alzheimer's Association* 3:186-191.
- Brummelkamp TR, Bernards R, Agami R (2002) A system for stable expression of short interfering RNAs in mammalian cells. *Science* 296:550-553.
- Bubb MR, Senderowicz AM, Sausville EA, Duncan KL, Korn ED (1994) Jasplakinolide, a cytotoxic natural product, induces actin polymerization and competitively inhibits the binding of phalloidin to F-actin. *J Biol Chem* 269:14869-14871.
- Buee-Scherrer V, Goedert M (2002) Phosphorylation of microtubule-associated protein tau by stress-activated protein kinases in intact cells. *FEBS Letters* 515:151-154.
- Buee L, Bussiere T, Buee-Scherrer V, Delacourte A, Hof PR (2000) Tau protein isoforms, phosphorylation and role in neurodegenerative disorders. *Brain Research Reviews* 33:95-130.
- Carlier M-F, Pantaloni D (1997) Control of actin dynamics in cell motility. *Journal of Molecular Biology* 269:459-467.

- Carlier M-F, Ressad F, Pantaloni D (1999) Control of Actin Dynamics in Cell Motility. *Journal of Cell Biology* 274:33827-33830.
- Carlier M-F, Laurent V, Santolini J, Melki R, Didry D, Xia G-X, Hong Y, Chua N-H, Pantaloni D (1997) Actin Depolymerizing Factor (ADF/Cofilin) Enhances the Rate of Filament Turnover: Implication in Actin-based Motility. *Journal of Cell Biology* 136:1307-1322.
- Chan C, Beltzner CC, Pollard TD (2009) Cofilin dissociates Arp2/3 complex and branches from actin filaments. *Curr Biol* 19:537-545.
- Chen H, Chan DC (2005) Emerging functions of mammalian mitochondrial fusion and fission. *Human Molecular Genetics* 14:R283-R289.
- Chen H, Chan DC (2006) Critical dependence of neurons on mitochondrial dynamics. *Current Opinion in Cell Biology* 18:453-459.
- Chen H, Bernstein BW, Bamburg JR (2000) Regulating actin-filament dynamics in vivo. *Trends in Biochemical Sciences* 25:19-23.
- Cheng IH, Scearce-Levie K, Legleiter J, Palop JJ, Gerstein H, Bien-Ly N, Puoliväli J, Lesné S, Ashe KH, Muchowski PJ, Mucke L (2007) Accelerating Amyloid- $\beta$  Fibrillization Reduces Oligomer Levels and Functional Deficits in Alzheimer Disease Mouse Models. *Journal of Biological Chemistry* 282:23818-23828.
- Cho DH, Nakamura T, Fang J, Cieplak P, Godzik A, Gu Z, Lipton SA (2009) S-nitrosylation of Drp1 mediates  $\beta$ -amyloid-related mitochondrial fission and neuronal injury. *Science* 324:102-105.
- Cingolani LA, Goda Y (2008) Actin in action: the interplay between the actin cytoskeleton and synaptic efficacy. *Nat Rev Neurosci* 9:344-356.
- Cleary J, Walsh D, Hofmeister J, Shankar G, Kuskowski M, Selkoe D, Ashe K (2005) Natural oligomers of the amyloid- $\beta$  protein specifically disrupt cognitive function. *Nature Neuroscience* 8:79-84.
- Cleveland DW, Hwo S-Y, Kirschner MW (1977) Physical and chemical properties of purified tau factor and the role of tau in microtubule assembly. *Journal of Molecular Biology* 116:227-247.
- Corder E, Saunders A, Strittmatter W, Schmechel D, Gaskell P, Small G, Roses A, Haines J, Pericak-Vance M (1993) Gene dose of apolipoprotein E type 4 allele and the risk of Alzheimer's disease in late onset families. *Science* 261:921-923.



- Correas I, Padilla R, Avila J (1990) The tubulin-binding sequence of brain microtubule-associated proteins, tau and MAP-2, is also involved in actin binding. *Journal of Biochemistry* 269:61-64.
- Coue M, Brenner SL, Spector I, Korn ED (1987) Inhibition of actin polymerization by latrunculin A. *FEBS Letters* 213:316-318.
- Crowther RA (1991) Straight and paired helical filaments in Alzheimer disease have a common structural unit. *Proceedings of the National Academy of Science USA* 88:2288-2292.
- Crowther RA, Goedert M (2000) Abnormal Tau-Containing Filaments in Neurodegenerative Diseases. *Journal of Structural Biology* 130:271-279.
- Cullen KM, Kócsi Z, Stone J. (2005) Vascular relationships of haem-rich deposits in the aging cerebral cortex. *J Cereb Blood Flow Metab* 25:1656-1667.
- David DC, Hauptmann S, Scherping I, Schuessel K, Keil U, Rizzu P, Ravid R, Droese S, Brandt U, Mueller WE, Eckert A, Goetz J (2005) Proteomic and Functional Analyses Reveal a Mitochondrial Dysfunction in P301L Tau Transgenic Mice. *Journal of Biological Chemistry* 280:23802-23814.
- Davis R, Marsden I, Maloney M, Minamide L, Podlisny M, Selkoe D, Bamberg J (2011) Amyloid- $\beta$  dimers/trimers potently induce cofilin-actin rods that are inhibited by maintaining cofilin phosphorylation. *Molecular Neurodegeneration* 6:10.
- Davis RC, Maloney MT, Minamide LS, Flynn KC, Stonebraker MA, Bamberg JR (2009) Mapping Cofilin-Actin Rods in Stressed Hippocampal Slices and the Role of cdc42 in Amyloid- $\beta$ -Induced Rods. *Journal of Alzheimer's Disease*.
- De Felice FG, Velasco PT, Lambert MP, Viola K, Fernandez SJ, Ferreira ST, Klein WL (2007) A $\beta$  Oligomers Induce Neuronal Oxidative Stress through an N-Methyl-D-aspartate Receptor-dependent Mechanism That Is Blocked by the Alzheimer Drug Memantine. *Journal of Biological Chemistry* 282:11590-11601.
- De Felice FG, Wu D, Lambert MP, Fernandez SJ, Velasco PT, Lacor PN, Bigio EH, Jerecic J, Acton PJ, Shughrue PJ, Chen-Dodson E, Kinney GG, Klein WL (2008) Alzheimer's disease-type neuronal tau hyperphosphorylation induced by A $\beta$  oligomers. *Neurobiology of Aging* 29:1334-1347.

- Decker H, Jürgensen S, Adrover MF, Brito-Moreira J, Bomfim TR, Klein WL, Epstein AL, De Felice FG, Jerusalinsky D, Ferreira ST (2010) N-Methyl-D-aspartate receptors are required for synaptic targeting of Alzheimer's toxic amyloid- $\beta$  peptide oligomers. *Journal of Neurochemistry* 115:1520-1529.
- Dehmelt L, Halpain S (2004a) The MAP2/Tau family of microtubule-associated proteins. *Genome Biology* 6:204.
- Dehmelt L, Halpain S (2004b) Actin and microtubules in neurite initiation: Are MAPs the missing link? *Journal of Neurobiology* 58:18-33.
- Delacourte A, Sergeant N, Wattez A, Gauvreau D, Robitaille Y (1998) Vulnerable neuronal subsets in Alzheimer's and Pick's disease are distinguished by their tau isoform distribution and phosphorylation. *Annals of Neurology* 43:193-204.
- Devineni N, Minamide LS, Niu M, Safer D, Verma R, Bamburg JR, Nachmias VT (1999) A quantitative analysis of G-actin binding proteins and the G-actin pool in developing chick brain. *Brain Research* 823:129-140.
- Dixit R, Ross JL, Goldman YE, Holzbaur ELF (2008) Differential Regulation of Dynein and Kinesin Motor Proteins by Tau. *Science* 319:1086-1089.
- Doody RS, Gavrilova SI, Sano M, Thomas RG, Aisen PS, Bachurin SO, Seely L, Hung D (2008) Effect of dimebon on cognition, activities of daily living, behaviour, and global function in patients with mild-to-moderate Alzheimer's disease: a randomised, double-blind, placebo-controlled study. *The Lancet* 372:207-215.
- Drechsel DN, Hyman AA, Cobb MH, Kirschner MW (1992) Modulation of the dynamic instability of tubulin assembly by the microtubule-associated protein tau. *Molecular Biology of the Cell* 3:1141-1154.
- Drewes G, Ebner A, Preuss U, Mandelkow E-M, Mandelkow E (1997) MARK, a Novel Family of Protein Kinases That Phosphorylate Microtubule-Associated Proteins and Trigger Microtubule Disruption. *Cell* 89:297-308.
- Drewes G, Mandelkow EM, Baumann K, Goris J, Merlevede W, Mandelkow E (1993) Dephosphorylation of tau protein and Alzheimer paired helical filaments by calcineurin and phosphatase-2A. *FEBS Letters* 336:425-432.
- Ehelt IM, Pasquale EB (2008) Molecular mechanisms of dendritic spine development and remodeling. *Progress in Neurobiology* 77:181-205.



- Drewes G, Lichtenberg-Kraag B, Döring F, Mandelkow E, Biernat J, Goris J, Dorée M, Mandelkow E (1992) Mitogen activated protein (MAP) kinase transforms tau protein into an Alzheimer-like state. *EMBO Journal* 11:2131-2138.
- Du H, Guo L, Yan S, Sosunov AA, McKhann GM, ShiDu Yan S (2010) Early deficits in synaptic mitochondria in an Alzheimer's disease mouse model. *Proceedings of the National Academy of Science USA* 107:18670-18675.
- Du H, Guo L, Fang F, Chen D, Sosunov AA, McKhann GM, Yan Y, Wang C, Zhang H, Molkentin JD, Gunn-Moore FJ, Vonsattel JP, Arancio O, Chen JX, Yan SD (2008) Cyclophilin D deficiency attenuates mitochondrial and neuronal perturbation and ameliorates learning and memory in Alzheimer's disease. *Nat Med* 14:1097-1105.
- Du J-T, Li Y-M, Ma Q-F, Qiang W, Zhao Y-F, Abe H, Kanazawa K, Qin X-R, Aoyagi R, Ishizuka Y, Nemoto T, Nakanishi H (2005) Synthesis and conformational properties of phosphopeptides related to the human tau protein. *Regulatory Peptides* 130:48-56.
- Duff K, Knight H, Refolo LM, Sanders S, Yu X, Picciano M, Malester B, Hutton M, Adamson J, Goedert M, Burki K, Davies P (2000) Characterization of Pathology in Transgenic Mice Over-Expressing Human Genomic and cDNA Tau Transgenes. *Neurobiology of Disease* 7:87-98.
- Ebneth A, Godemann R, Stamer K, Illenberger B, Trinczek B, Mandelkow E (1998) Overexpression of tau protein inhibits kinesin-dependent trafficking of vesicles, mitochondria and endoplasmic reticulum: implications for Alzheimer's disease. *Journal of Cell Biology* 143:777-794.
- Edison P, Archer HA, Hinz R, Hammers A, Pavese N, Tai YF, Hotton G, Cutler D, Fox N, Kennedy A, Rossor M, Brooks DJ (2007) Amyloid, hypometabolism, and cognition in Alzheimer disease. *Neurology* 68:501-508.
- Escobar-Khondiker M, Hollerhage M, Muriel M-P, Champy P, Bach A, Depienne C, Respondek G, Yamada ES, Lannuzel A, Yagi T, Hirsch EC, Oertel WH, Jacob R, Michel PP, Ruberg M, Hoglinger GU (2007) Annonacin, a Natural Mitochondrial Complex I Inhibitor, Causes Tau Pathology in Cultured Neurons. *Journal of Neuroscience* 27:7827-7837.
- Ethell IM, Pasquale EB (2005) Molecular mechanisms of dendritic spine development and remodeling. *Progress in Neurobiology* 75:161-205.





- Giannakopoulos P, von Gunten A, Kovari E, Gold G, Herrmann FR, Hof PR, Bouras C (2007) Stereological analysis of neuropil threads in the hippocampal formation: relationships with Alzheimer's disease neuronal pathology and cognition. *Neuropathology and Applied Neurobiology* 33:334-343.
- Goedert M (1993) Tau protein and the neurofibrillary pathology of Alzheimer's disease. *Trends in Neurosciences* 16:460-465.
- Goedert M, Spillantini MG (2006) A Century of Alzheimer's Disease. *Science* 314:777-781.
- Goedert M, Jakes R, Crowther RA (1994) Epitope mapping of monoclonal antibodies to the paired helical filaments of Alzheimer's disease: identification of phosphorylation sites in tau protein. *Journal of Biochemistry* 301:871-877.
- Goedert M, Spillantini MG, Potier MC, Ulrich J, Crowther RA (1989) Cloning and sequencing of the cDNA encoding an isoform of microtubule-associated protein tau containing four tandem repeats: differential expression of tau protein mRNAs in human brain. *EMBO Journal* 8:393-399.
- Goedert M, Jakes R, Qi Z, Wang JH, Cohen P (1995) Protein Phosphatase 2A Is the Major Enzyme in Brain that Dephosphorylates  $\tau$  Protein Phosphorylated by Proline-Directed Protein Kinases or Cyclic AMP-Dependent Protein Kinase. *Journal of Neurochemistry* 65:2804-2807.
- Goetz J, Chen F, van Dorpe J, Nitsch RM (2001) Formation of Neurofibrillary Tangles in P301L Tau Transgenic Mice Induced by A $\beta$ 42 Fibrils. *Science* 293:1491-1495.
- Goldsbury CS, Wirtz S, Müller SA, Sunderji S, Wicki P, Aebi U, Frey P (2000) Studies on the in vitro assembly of A $\beta$ 1-40: implications for the search for A $\beta$  fibril formation inhibitors. *J Struct Biol* 130:217-231.
- Goldsbury C, Whiteman IT, Jeong EV, Lim Y-A (2008) Oxidative stress increases levels of endogenous amyloid- $\beta$  peptides secreted from primary chick brain neurons. *Aging Cell* 7:771-775.
- Gong C-X, Lidsky T, Wegiel J, Zuck L, Grundke-Iqbal I, Iqbal K (2000) Phosphorylation of Microtubule-associated Protein Tau Is Regulated by Protein Phosphatase 2A in Mammalian Brain. Implications for neurofibrillary degeneration in Alzheimer's Disease. *Journal of Biological Chemistry* 275:5535-5544.

- Gong Y, Chang L, Viola KL, Lacor PN, Lambert MP, Finch CE, Krafft GA, Klein WL (2003) Alzheimer's disease-affected brain: Presence of oligomeric A $\beta$  ligands (ADDLs) suggests a molecular basis for reversible memory loss. *Proceedings of the National Academy of Science USA* 100:10417-10422.
- Gordon-Krajcer W, Yang LS, Ksiezak-Reding H (2000) Conformation of paired helical filaments blocks dephosphorylation of epitopes shared with fetal tau except Ser199/202 and Ser202/Thr205. *Brain Research* 856:163-175.
- Gordon-Krajcer W, Kozniowska E, Lazarewicz J, Ksiezak-Reding H (2007) Differential Changes in Phosphorylation of Tau at PHF-1 and 12E8 Epitopes During Brain Ischemia and Reperfusion in Gerbils. *Neurochemical Research* 32:729-737.
- Griffith LM, Pollard TD (1978) Evidence for actin filament-microtubule interaction mediated by microtubule-associated proteins. *Journal of Cell Biology* 78:958-965.
- Griffith LM, Pollard TD (1982) The interaction of actin filaments with microtubules and microtubule-associated proteins. *Journal of Biological Chemistry* 257:9143-9151.
- Gu J, Lee CW, Fan Y, Komlos D, Tang X, Sun C, Yu K, Hartzell HC, Chen G, Bamberg JR, Zheng JQ (2010) ADF/cofilin-mediated actin dynamics regulate AMPA receptor trafficking during synaptic plasticity. *Nat Neurosci* 13:1208-1215.
- Guillemin GJ, Brew BJ (2002) Implications of the kynurenine pathway and quinolinic acid in Alzheimer's disease. *Redox Report* 7:199-206.
- Guillemin GJ, Brew BJ, Noonan CE, Takikawa O, Cullen KM (2005) Indoleamine 2,3 dioxygenase and quinolinic acid Immunoreactivity in Alzheimer's disease hippocampus. *Neuropathology and Applied Neurobiology* 31:395-404.
- Guillemin GJ, Cullen KM, Lim CK, Smythe GA, Garner B, Kapoor V, Takikawa O, Brew BJ (2007) Characterization of the Kynurenine Pathway in Human Neurons. *J Neurosci* 27:12884-12892.
- Haass C, Koo EH, Mellon A, Hung AY, Selkoe DJ (1992) Targeting of cell-surface  $\beta$ -amyloid precursor protein to lysosomes: alternative processing into amyloid-bearing fragments. *Nature* 357:500-503.



- Haass C, Selkoe DJ (2007) Soluble protein oligomers in neurodegeneration: lessons from the Alzheimer's amyloid  $\beta$ -peptide. *Nat Rev Mol Cell Biol* 8:101-12.
- Hardy J, Selkoe DJ (2002) The Amyloid Hypothesis of Alzheimer's Disease: Progress and Problems on the Road to Therapeutics. *Science* 297:353-356.
- Harvey RJ, Skelton-Robinson M, Rossor MN (2003) The prevalence and causes of dementia in people under the age of 65 years. *Journal of Neurology, Neurosurgery and Psychiatry* 74:1206-1209.
- Hashiguchi M, Sobue K, Paudel H (2000) 14-3-3-zeta is an effector of tau protein phosphorylation. *Journal of Biological Chemistry* 275:25247-25254.
- He H, Wang X, Pan R, Wang D, Liu M, He R (2009) The proline-rich domain of tau plays a role in interactions with actin. *BMC Cell Biology* 10:81.
- He TC, Zhou S, da Costa LT, Yu J, Kinzler KW, Vogelstein B (1998) A simplified system for generating recombinant adenoviruses. *Proc Natl Acad Sci U S A* 95:2509-2514.
- Henriques AG, Vieira SI, Da Cruz e Silva EF, Da Cruz e Silva OAB (2010) A $\beta$  promotes Alzheimer's disease-like cytoskeleton abnormalities with consequences to APP processing in neurons. *Journal of Neurochemistry* 113:761-771.
- Hernandez F, Cuadros R, Avila J (2004) Zeta 14-3-3 protein favours the formation of human tau fibrillar polymers. *Neuroscience Letters* 357:143-146.
- Heredia L, Helguera P, de Olmos S, Kedikian G, Sola Vigo F, LaFerla F, Staufenbiel M, de Olmos J, Busciglio J, Caceres A, Lorenzo A (2006) Phosphorylation of Actin-Depolymerizing Factor/Cofilin by LIM-Kinase Mediates Amyloid  $\beta$ -Induced Degeneration: A Potential Mechanism of Neuronal Dystrophy in Alzheimer's Disease. *Journal of Neuroscience* 26:6533-6542.
- Hillman CH, Belopolsky AV, Snook EM, Kramer AF, McAuley E (2004) Physical activity and executive control: Implications for increased cognitive health during older adulthood. *Research Quarterly for Exercise and Sport* 75:176-185.
- Hirokawa N (1998) Kinesin and dynein superfamily proteins and the mechanisms of organelle transport *Science* 279:519-526.

- Hirokawa N, Takemura R (2005) Molecular motors and mechanisms of directional transport in neurons. *Nat Rev Neurosci* 6:201-214.
- Hiruma H, Katakura T, Takahashi S, Ichikawa T, Kawakami T (2003) Glutamate and Amyloid  $\beta$ -Protein Rapidly Inhibit Fast Axonal Transport in Cultured Rat Hippocampal Neurons by Different Mechanisms. *Journal of Neuroscience* 23:8967-8977.
- Hock C, Villringer K, MÜLLer-Spahn F, Hofmann M, Schuh-Hofer S, Heekeren H, Wenzel R, Dirnagl U, Villringer A (1996) Near Infrared Spectroscopy in the Diagnosis of Alzheimer's Disease. *Annals of the New York Academy of Sciences* 777:22-29.
- Holtmaat A, Svoboda K (2009) Experience-dependent structural synaptic plasticity in the mammalian brain. *Nat Rev Neurosci* 10:647-658.
- Hotulainen P, Hoogenraad CC (2010) Actin in dendritic spines: connecting dynamics to function. *Journal of Cell Biology* 189:619-629.
- Hotulainen P, Llano O, Smirnov S, Tanhuanpää K, Faix J, Rivera C, Lappalainen P (2009) Defining mechanisms of actin polymerization and depolymerization during dendritic spine morphogenesis. *J Cell Biol* 185:323-339.
- Hsia AY, Masliah E, McConlogue L, Yu G-Q, Tatsuno G, Hu K, Kholodenko D, Malenka RC, Nicoll RA, Mucke L (1999) Plaque-independent disruption of neural circuits in Alzheimer's disease mouse models. *Proceedings of the National Academy of Science USA* 96:3228-3233.
- Huang TY, Minamide LS, Bamburg JR, Bokoch GM (2008) Chronophin Mediates an ATP-Sensing Mechanism for Cofilin Dephosphorylation and Neuronal Cofilin-Actin Rod Formation. *Developmental Cell* 15:691-703.
- International AD (2010) World Alzheimer Report 2010: The Global Impact of Dementia. In: Alzheimer's Disease International
- Ittner LM, Fath T, Ke YD, Bi M, van Eersel J, Li KM, Gunning P, Goetz J (2008) Parkinsonism and impaired axonal transport in a mouse model of frontotemporal dementia. *Proceedings of the National Academy of Science USA* 105:15997-16002.
- Ittner LM, Ke YD, Goetz J (2009) Phosphorylated Tau Interacts with c-Jun N-terminal Kinase-interacting Protein 1 (JIP1) in Alzheimer Disease. *Journal of Biological Chemistry* 284:20909-20916.



- Ittner LM, Ke YD, Delerue F, Bi M, Gladbach A, van Eersel J, Wölfing H, Chieng BC, Christie MJ, Napier IA, Eckert A, Staufenbiel M, Hardeman E, Götz J (2010) Dendritic Function of Tau Mediates Amyloid- $\beta$  Toxicity in Alzheimer's Disease Mouse Models. *Cell* 142:387-397.
- Jang D, Han J, Lee S, Lee Y, Park H, Lee S, Kim H, Kaang B (2005) Cofilin expression induces cofilin-actin rod formation and disrupts synaptic structure and function in *Aplysia* synapses. *Proceedings of the National Academy of Science USA* 102:16072-16077.
- Kamal A, Goldstein LSB (2002) Principles of cargo attachment to cytoplasmic motor proteins. *Current Opinion in Cell Biology* 14:63-68.
- Kasai H, Fukuda M, Watanabe S, Hayashi-Takagi A, Noguchi J (2003) Structural dynamics of dendritic spines in memory and cognition. *Trends in Neurosciences* 33:121-129.
- Kelly BL, Ferreira A (2006)  $\beta^2$ -Amyloid-induced Dynamin 1 Degradation Is Mediated by N-Methyl-D-Aspartate Receptors in Hippocampal Neurons. *Journal of Biological Chemistry* 281:28079-28089.
- Kerr SJ, Armati PJ, Guillemin GJ, Brew BJ (1998) Chronic exposure of human neurons to quinolinic acid results in neuronal changes consistent with AIDS dementia complex. *AIDS* 12:355-363.
- Kim JS, Huang TY, Bokoch GM (2009) Reactive oxygen species regulate a slingshot-cofilin activation pathway. *Mol Biol Cell* 20:2650-2660.
- Kindler S, Garner CC (1994) Four repeat MAP2 isoforms in human and rat brain. *Molecular Brain Research* 26:218-224.
- King ME, Kan H-M, Baas PW, Erisir A, Glabe CG, Bloom GS (2006) Tau-dependent microtubule disassembly initiated by prefibrillar  $\beta$ -amyloid. *Journal of Cell Biology* 175:541-546.
- Klyubin I, Walsh DM, Lemere CA, Cullen WK, Shankar GM, Betts V, Spooner ET, Jiang L, Anwyl R, Selkoe DJ, Rowan MJ (2005) Amyloid- $\beta$  protein immunotherapy neutralizes A $\beta$  oligomers that disrupt synaptic plasticity in vivo. *Nat Med* 11:556-561.
- Lacor PN, Buniel MC, Furlow PW, Sanz Clemente A, Velasco PT, Wood M, Viola KL, Klein WL (2007) A $\beta$  Oligomer-Induced Aberrations in Synapse Composition, Shape, and Density Provide a Molecular Basis for Loss of Connectivity in Alzheimer's Disease. *Journal of Neuroscience* 27:796-807.

- Lambert MP, Barlow AK, Chromy BA, Edwards C, Freed R, Liosatos M, Morgan TE, Rozovsky I, Trommer B, Viola KL, Wals P, Zhang C, Finch CE, Krafft GA, Klein WL (1998) Diffusible, nonfibrillar ligands derived from A $\beta$ 42 are potent central nervous system neurotoxins. *Proceedings of the National Academy of Science USA* 95:6448-6453.
- Lee G, Neve RL, Kosik KS (1989) The microtubule binding domain of tau protein. *Neuron* 2:1615-1624.
- Lee H-G, Perry G, Moreira PI, Garrett MR, Liu Q, Zhu X, Takeda A, Nunomura A, Smith MA (2005) Tau phosphorylation in Alzheimer's disease: pathogen or protector? *Trends in Molecular Medicine* 11:164-169.
- Lee VMY, Goedert M, Trojanowski JQ (2001) Neurodegenerative Tauopathies. *Annual Review of Neuroscience* 24:1121-1159.
- Lewis J, Dickson DW, Lin W-L, Chisholm L, Corral A, Jones G, Yen S-H, Sahara N, Skipper L, Yager D, Eckman C, Hardy J, Hutton M, McGowan E (2001) Enhanced Neurofibrillary Degeneration in Transgenic Mice Expressing Mutant Tau and APP. *Science* 293:1487-1491.
- Lewis SA, Wang DH, Cowan NJ (1988) Microtubule-associated protein MAP2 shares a microtubule binding motif with tau protein. *Science* 242:936-939.
- Lin MT, Beal MF (2006) Mitochondrial dysfunction and oxidative stress in neurodegenerative diseases. *Nature* 443:787-795.
- Lindwall G, Cole RD (1984) Phosphorylation affects the ability of tau protein to promote microtubule assembly. *Journal of Biological Chemistry* 259:5301-5305.
- Liu J, Atamna H, Kuratsune H, Ames BN (2002a) Delaying brain mitochondrial decay and aging with mitochondrial antioxidants and metabolites. *Annals of the New York Academy of Sciences* 959:133-166.
- Liu J, Head E, Gharib AM, Yuan W, Ingersoll RT, Hagen TM, Cotman CW, Ames BN (2002b) Memory loss in old rats is associated with brain mitochondrial decay and RNA/DNA oxidation: Partial reversal by feeding acetyl-L-carnitine and/or R- $\alpha$ -lipoic acid. *Proceedings of the National Academy of Sciences of the United States of America* 99:2356-2361.
- Lowry OH, Rosebrough NJ, Farr AL, Randall RJ (1951) Protein measurement with the folin phenol reagent. *Journal of Biological Chemistry* 193:265-275.



- Lucotte G, Visvikis S, Leininger-Möler B, David F, Berriche S, Revéilleau S, Couderc R, Babron MC, Aguillon D, Siest G (1994) Association of apolipoprotein E allele  $\epsilon$ 4 with late-onset sporadic Alzheimer's disease. *American Journal of Medical Genetics* 54:286-288.
- Luo L (2002) Actin Cytoskeleton Regulation in Neuronal Morphogenesis and Structural Plasticity. *Annual Review of Cell and Developmental Biology* 18:601-635.
- Maekawa S, Nishida E, Ohta Y, Sakai H (1984) Isolation of Low Molecular Weight Actin-Binding Proteins from Porcine Brain. *The Journal of Biochemistry* 95:377-385.
- Maloney M, Bamburg J (2007) Cofilin-mediated neurodegeneration in alzheimer's disease and other amyloidopathies. *Molecular Neurobiology* 35:21-43.
- Maloney MT, Kinley AW, Pak C, Bamburg JR (2008) ADF/cofilin, actin dynamics and disease. *Protein Reviews* 8:83-187.
- Maloney MT, Minamide LS, Kinley AW, Boyle JA, Bamburg JR (2005)  $\beta$ -Secretase-Cleaved Amyloid Precursor Protein Accumulates at Actin Inclusions Induced in Neurons by Stress or Amyloid  $\beta$ : A Feedforward Mechanism for Alzheimer's Disease. *Journal of Neuroscience* 25:11313-11321.
- Mandelkow E-M, Thies E, Trinczek B, Biernat J, Mandelkow E (2004) MARK/PAR1 kinase is a regulator of microtubule-dependent transport in axons. *Journal of Cell Biology* 167:99-110.
- Mandelkow EM, Biernat J, Drewes G, Gustke N, Trinczek B, Mandelkow E (1995) Tau domains, phosphorylation, and interactions with microtubules. *Neurobiology of Aging* 16:355-362.
- Mandelkow EM, Stamer K, Vogel R, Thies E, Mandelkow E (2003) Clogging of axons by tau, inhibition of axonal traffic and starvation of synapses. *Neurobiology of Aging* 24:1079-1085.
- Marsden I, Minamide LS, Bamburg JR (2011) Amyloid- $\beta$ -induced amyloid- $\beta$  secretion: A possible feed-forward mechanism in Alzheimer disease. *Journal of Alzheimer's Disease* Feb 4 [Epub ahead of print].
- Matsuyama S, Teraoka R, Mori H, Tomiyama T (2007) Inverse correlation between amyloid precursor protein and synaptic plasticity in transgenic mice. *Neuroreport* 18:1083-1087.

- Matus A (2000) Actin-Based Plasticity in Dendritic Spines. *Science* 290:754-758.
- McGough A, Pope B, Chiu W, Weeds A (1997) Cofilin Changes the Twist of F-Actin: Implications for Actin Filament Dynamics and Cellular Function. *Journal of Cell Biology* 138:771-781.
- McLean CA, Cherny RA, Fraser FW, Fuller SJ, Smith MJ, Konrad V, Bush AI, Masters CL (1999) Soluble pool of A $\beta$  amyloid as a determinant of severity of neurodegeneration in Alzheimer's disease. *Annals of Neurology* 46:860-866.
- Melov S, Adlard PA, Morten K, Johnson F, Golden TR, Hinerfeld D, Schilling B, Mavros C, Masters CL, Volitakis I, Li Q-X, Laughton K, Hubbard A, Cherny RA, Gibson B, Bush AI (2007) Mitochondrial Oxidative Stress Causes Hyperphosphorylation of Tau. *PLoS ONE* 2:e536.
- Miller G (2010) The Puzzling Rise and Fall of a Dark-Horse Alzheimer's Drug. *Science* 327:1309.
- Minamide LS, Bamberg JR (1990) A filter paper dye-binding assay for quantitative determination of protein without interference from reducing agents or detergents. *Analytical Biochemistry* 190:66-70.
- Minamide L, Striegl A, Boyle J, Meberg P, Bamberg J (2000) Neurodegenerative stimuli induce persistent ADF/cofilin-actin rods that disrupt distal neurite function. *Nature Cell Biology* 2:628-636.
- Minamide LS, Maiti S, Boyle JA, Davis RC, Coppinger JA, Bao Y, Huang TY, Yates J, Bokoch GM, Bamberg JR (2010) Isolation and Characterization of Cytoplasmic Cofilin-Actin Rods. *Journal of Biological Chemistry* 285:5450-5460.
- Mitchell TW, Nissanov J, Han L-Y, Mufson EJ, Schneider JA, Cochran EJ, Bennett DA, Lee VMY, Trojanowski JQ, Arnold SE (2000) Novel Method to Quantify Neuropil Threads in Brains from Elders With or Without Cognitive Impairment. *Journal of Histochemistry and Cytochemistry* 48:1627-1638.
- Mitchison TJ, Kirschner MW (1984) Dynamic instability of microtubule growth. *Nature* 312:237-242.
- Moraga DM, Nuñez P, Garrido J, Maccioni RB (1993) A Tau Fragment Containing a Repetitive Sequence Induces Bundling of Actin Filaments. *Journal of Neurochemistry* 61:979-986.



- Moreira PI, Zhu X, Wang X, Lee H-g, Nunomura A, Petersen RB, Perry G, Smith MA (2010) Mitochondria: A therapeutic target in neurodegeneration. *Biochimica et Biophysica Acta (BBA) - Molecular Basis of Disease* 1802:212-220.
- Morris RGM, Anderson E, Lynch GS, Baudry M (1986) Selective impairment of learning and blockade of long-term potentiation by an N-methyl-D-aspartate receptor antagonist, AP5. *Nature* 319:774-776.
- Mosconi L (2005) Brain glucose metabolism in the early and specific diagnosis of Alzheimer's disease. *European Journal of Nuclear Medicine and Molecular Imaging* 32:486-510.
- Mucke L, Masliah E, Yu G-Q, Mallory M, Rockenstein EM, Tatsuno G, Hu K, Kholodenko D, Johnson-Wood K, McConlogue L (2000) High-Level Neuronal Expression of A $\beta$ 1-42 in Wild-Type Human Amyloid Protein Precursor Transgenic Mice: Synaptotoxicity without Plaque Formation. *Journal of Neuroscience* 20:4050-4058.
- Mukrasch MD, Bibow S, Korukottu J, Jeganathan S, Biernat J, Griesinger C, Mandelkow E, Zweckstetter M (2009) Structural Polymorphism of 441-Residue Tau at Single Residue Resolution. *PLoS Biol* 7:e1000034.
- Navarro A, Boveris A (2007) The mitochondrial energy transduction system and the aging process. *American Journal of Physiology and Cell Physiology* 292:C670-C686.
- Nelson P, Wang W-X (2010) MiR-107 is Reduced in Alzheimer's Disease Brain Neocortex: Validation Study *Journal of Alzheimer's Disease* 21:75-79.
- Nishida E, Kuwaki T, Sakai H (1981) Phosphorylation of Microtubule-Associated Proteins (MAPs) and pH of the Medium Control Interaction between MAPs and Actin Filaments. *Journal of Biochemistry* 90:575-578.
- Nishimura I, Yang Y, Lu B (2004) PAR-1 kinase plays an initiator role in a temporally ordered phosphorylation process that confers tau toxicity in *Drosophila*. *Cell* 116:671-682.
- Nunomura A, Perry G, Aliev G, Hirai K, Takeda A, Balraj E, Jones P, Ghanbari H, Wataya T, Shimohama S, Chiba S, Atwood C, Petersen R, Smith M (2001) Oxidative damage is the earliest event in Alzheimer disease. *Journal of Neuropathology and Experimental Neurology* 60:759-767.

- Oddo S, Caccamo A, Tran L, Lambert MP, Glabe CG, Klein WL, LaFerla FM (2006) Temporal Profile of Amyloid- $\beta$  (A $\beta$ ) Oligomerization in an in Vivo Model of Alzheimer Disease. *Journal of Cell Biology* 281:1599-1604.
- Oddo S, Caccamo A, Shepherd JD, Murphy MP, Golde TE, Kaye R, Metherate R, Mattson MP, Akbari Y, LaFerla FM (2003) Triple-Transgenic Model of Alzheimer's Disease with Plaques and Tangles: Intracellular A $\beta$  and Synaptic Dysfunction. *Neuron* 39:409-421.
- Ozer RS, Halpain S (2000) Phosphorylation-dependent Localization of Microtubule-associated Protein MAP2c to the Actin Cytoskeleton. *Molecular Biology of the Cell* 11:3573-3587.
- Pendleton A, Pope B, Weeds A, Koffer A (2003) Latrunculin B or ATP Depletion Induces Cofilin-dependent Translocation of Actin into Nuclei of Mast Cells. *J Biol Chem* 278:14394-14400.
- Perry G, Kawai M, Tabaton M, Onorato M, Mulvihill P, Richey P, Morandi A, Connolly JA, Gambetti P (1991) Neuropil threads of Alzheimer's disease show a marked alteration of the normal cytoskeleton. *J Neurosci* 11:1748-1755.
- Pettmann B, Louis JC, Sensenbrenner M (1979) Morphological and biochemical maturation of neurones cultured in the absence of glial cells. *Nature* 281:378-380.
- Planel E, Miyasaka T, Launey T, Chui D-H, Tanemura K, Sato S, Murayama O, Ishiguro K, Tatebayashi Y, Takashima A (2004) Alterations in Glucose Metabolism Induce Hypothermia Leading to Tau Hyperphosphorylation through Differential Inhibition of Kinase and Phosphatase Activities: Implications for Alzheimer's Disease. *Journal of Neuroscience* 24:2401-2411.
- Planel E, Sun X, Takashima A (2002) Role of GSK-3 $\beta$  in Alzheimer's Disease pathology. *Drug Development Research* 56:491-510.
- Podlisny MB, Ostaszewski BL, Squazzo SL, Koo EH, Rydell RE, Teplow DB, Selkoe DJ (1995) Aggregation of Secreted Amyloid  $\beta$ -Protein into Sodium Dodecyl Sulfate-stable Oligomers in Cell Culture. *Journal of Biological Chemistry* 270:9564-9570.
- Posse de Chaves EI (2006) Sphingolipids in apoptosis, survival and regeneration in the nervous system. *Biochimica et Biophysica Acta (BBA) - Biomembranes* 1758:1995-2015.



- Praprotnik D, Smith M, Richey P, Vinters H, Perry G (1996) Filament heterogeneity within the dystrophic neurites of senile plaques suggests blockage of fast axonal transport in Alzheimer's disease. *Acta Neuropathologica* 91:226-235.
- Praticò D, Uryu K, Leight S, Trojanowski JQ, Lee VMY (2001) Increased Lipid Peroxidation Precedes Amyloid Plaque Formation in an Animal Model of Alzheimer Amyloidosis. *Journal of Neuroscience* 21:4183-4187.
- Probst A, Tolnay M, Langui D, Goedert M, Spillantini MG (1996) Pick's disease: hyperphosphorylated tau protein segregates to the somatoaxonal compartment. *Acta Neuropathologica* 92:588-596.
- Purves D, Augustine G, Fitzpatrick D, Katz L, LaMantia A, McNamara J, Williams S, Eds (2001) *Neuroscience*, 2nd Edition: Sunderland (MA): Sinauer Associates.
- Rahman A, Ting K, Cullen KM, Braidy N, Brew BJ, Guillemin GJ (2009) The Excitotoxin Quinolinic Acid Induces Tau Phosphorylation in Human Neurons. *PLoS ONE* 4:e6344.
- Rapoport M, Dawson HN, Binder LI, Vitek MP, Ferreira A (2002) Tau is essential to  $\beta$ -amyloid-induced neurotoxicity. *Proceedings of the National Academy of Science USA* 99:6364-6369.
- Reddy PH, McWeeney S, Park BS, Manczak M, Gutala RV, Partovi D, Jung Y, Yau V, Searles R, Mori M, Quinn J (2004) Gene expression profiles of transcripts in amyloid precursor protein transgenic mice: up-regulation of mitochondrial metabolism and apoptotic genes is an early cellular change in Alzheimer's disease. *Human Molecular Genetics* 13:1225-1240.
- Reisi P, Alaei H, Babri S, Sharifi MR, Mohaddes G (2009) Effects of treadmill running on spatial learning and memory in streptozotocin-induced diabetic rats. *Neuroscience Letters* 455:79-83.
- Renner M, Specht CG, Triller A (2008) Molecular dynamics of postsynaptic receptors and scaffold proteins. *Current Opinion in Neurobiology* 18:532-540.
- Rhein V, Song X, Wiesner A, Ittner LM, Baysang G, Meier F, Ozmen L, Bluethmann H, Droese S, Brandt U, Savaskan E, Czech C, Goetz J, Eckert A (2009) Amyloid- $\beta$  and tau synergistically impair the oxidative phosphorylation system in triple transgenic Alzheimer's disease mice. *PNAS* 106:20057-62.

- Riederer B, Matus A (1985) Differential expression of distinct microtubule-associated proteins during brain development. *Proceedings of the National Academy of Science USA* 82:6006-6009.
- Roberson ED, Scearce-Levie K, Palop JJ, Yan F, Cheng IH, Wu T, Gerstein H, Yu G-Q, Mucke L (2007) Reducing Endogenous Tau Ameliorates Amyloid  $\beta$ -Induced Deficits in an Alzheimer's Disease Mouse Model. *Science* 316:750-754.
- Roberson ED, Halabisky B, Yoo JW, Yao J, Chin J, Yan F, Wu T, Hamto P, Devidze N, Yu GQ, Palop JJ, Noebels JL, Mucke L (2011) Amyloid- $\beta$ -induced synaptic, network, and cognitive impairments depend on tau levels in multiple mouse models of Alzheimer's disease. *Journal of Neuroscience* 31:700-711.
- Roberts R, Geda Y, Knopman D, Cha R, Pankratz VS, Boeve BF, Ivnik RJ, Tangalos EG, Petersen RC, Rocca WA (2008) The Mayo Clinic Study of Aging: Design and Sampling, Participation, Baseline Measures and Sample Characteristics. *Neuroepidemiology* 30:58-69.
- Rodriguez OC, Schaefer AW, Mandato CA, Forscher P, Bement WM, Waterman-Storer CM (2003) Conserved microtubule-actin interactions in cell movement and morphogenesis. *Nat Cell Biol* 5:599-609.
- Roger B, Al-Bassam J, Dehmelt L, Milligan RA, Halpain S (2004) MAP2c, but Not Tau, Binds and Bundles F-Actin via Its Microtubule Binding Domain. *Current Biology* 14:363-371.
- Sánchez C, Díaz-Nido J, Avila J (2000) Phosphorylation of microtubule-associated protein 2 (MAP2) and its relevance for the regulation of the neuronal cytoskeleton function. *Progress in Neurobiology* 61:133-168.
- Saraiva LM, Seixas da Silva GS, Galina A, da-Silva WS, Klein WL, Ferreira SrT, De Felice FG (2011) Amyloid- $\beta$  Triggers the Release of Neuronal Hexokinase 1 from Mitochondria. *PLoS ONE* 5:e15230.
- Scarmeas N, Stern Y, Tang M-X, Mayeux R, Luchsinger JA (2006) Mediterranean diet and risk for Alzheimer's disease. *Annals of Neurology* 59:912-921.
- Schaar BT, Kinoshita K, McConnell SK (2004) Doublecortin Microtubule Affinity Is Regulated by a Balance of Kinase and Phosphatase Activity at the Leading Edge of Migrating Neurons. *Neuron* 41:203-213.
- Schlager M, Hoogenraad C (2009) Basic mechanisms for recognition and transport of synaptic cargos. *Molecular Brain* 2:25.



- Schmidt M, Murray J, Trojanowski J (1993) Continuity of neuropil threads with tangle-bearing and tangle-free neurons in Alzheimer disease cortex. *Molecular and Chemical Neuropathology* 18:299-312.
- Schnitzer MJ, Block SM (1997) Kinesin hydrolyses one ATP per 8-nm step. *Nature* 388:386-390.
- Schubert V, Dotti CG (2007) Transmitting on actin: synaptic control of dendritic architecture. *Journal of Cell Science* 120:205-212.
- Seitz A, Kojima H, Oiwa K, Mandelkow E, Song YH, Mandelkow E (2002) Single-molecule investigation of the interference between kinesin, tau and MAP2c. *EMBO Journal* 21:4896-4905.
- Selden CS, Pollard TD (1986) Interaction of Actin Filaments with Microtubules Is Mediated by Microtubule-Associated Proteins and Regulated by Phosphorylation. *Annals of the New York Academy of Sciences* 466:803-812.
- Selden SC, Pollard TD (1983) Phosphorylation of microtubule-associated proteins regulates their interaction with actin filaments. *Journal of Biological Chemistry* 258:7064-7071.
- Selkoe DJ (1998) The cell biology of  $\beta$ -amyloid precursor protein and presenilin in Alzheimer's disease. *Trends in Cell Biology* 8:447-453.
- Sensenbrenner M, Maderspach K, Latzkovits L, Jaros GG (1978) Neuronal Cells from Chick Embryo Cerebral Hemispheres Cultivated on Polylysine-Coated Surfaces. *Developmental Neuroscience* 1:90-101.
- Seubert P, Mawal-Dewan M, Barbour R, Jakes R, Goedert M, Johnson G, W, Litsky JM, Schenk D, Lieberburg I, Trojanowski JQ, Lee VMY (1995) Detection of Phosphorylated Ser262 in Fetal Tau, Adult Tau, and Paired Helical Filament Tau. *Journal of Biological Chemistry* 270:18917-18922.
- Shankar GM, Bloodgood BL, Townsend M, Walsh DM, Selkoe DJ, Sabatini BL (2007) Natural Oligomers of the Alzheimer Amyloid- $\beta$  Protein Induce Reversible Synapse Loss by Modulating an NMDA-Type Glutamate Receptor-Dependent Signaling Pathway. *Journal of Neuroscience* 27:2866-2875.
- Shankar GM, Li SM, Mehta TH, Garcia-Munoz A, Shepardson NE, Smith I, Brett FM, Farrell MA, Rowan MJ, Lemere CA, Regan CM, Walsh DM, Sabatini BL, Selkoe DJ (2008) Amyloid- $\beta$  protein dimers isolated directly from Alzheimer's brains impair synaptic plasticity and memory. *Nature Medicine* 14:837-842.

- Shaw AE, Minamide LS, Bill CL, Funk JD, Maiti S, Bamberg JR (2004) Cross-reactivity of antibodies to actin-depolymerizing factor/cofilin family proteins and identification of the major epitope recognized by a mammalian actin-depolymerizing factor/cofilin antibody. *Electrophoresis* 25:2611-2620.
- Sheng M, Hoogenraad CC (2007) The Postsynaptic Architecture of Excitatory Synapses: A More Quantitative View. *Annual Review of Biochemistry* 76:823-847.
- Shipton OA, Leitz JR, Dworzak J, Acton CEJ, Tunbridge EM, Denk F, Dawson HN, Vitek MP, Wade-Martins R, Paulsen O, Vargas-Caballero M (2011) Tau Protein Is Required for Amyloid  $\beta$ -Induced Impairment of Hippocampal Long-Term Potentiation. *Journal of Neuroscience* 31:1688-1692.
- Smith MA, Nunomura A, Lee H-g, Zhu X, Moreira PI, Avila J, Perry G (2005) Chronological primacy of oxidative stress in Alzheimer disease. *Neurobiol Aging* 26:579-580.
- Snyder EM, Nong Y, Almeida CG, Paul S, Moran T, Choi EY, Nairn AC, Salter MW, Lombroso PJ, Gouras GK, Greengard P (2005) Regulation of NMDA receptor trafficking by amyloid- $\beta$ . *Nat Neurosci* 8:1051-1058.
- Sontag E, Nunbhakdi-Craig V, Lee G, Bloom GS, Mumby MC (1996) Regulation of the Phosphorylation State and Microtubule-Binding Activity of Tau by Protein Phosphatase 2A. *Neuron* 17:1201-1207.
- Squire LR, Knowlton B, Musen G (1993) The Structure and Organization of Memory. *Annual Review of Psychology* 44:453-495.
- Stamer K, Vogel R, Thies E, Mandelkow E, Mandelkow EM (2002) Tau blocks traffic of organelles, neurofilaments, and APP vesicles in neurons and enhances oxidative stress. *Journal of Cell Biology* 156:1051-1063.
- Stieler JT, Bullmann T, Kohl F, Tøien Ø, Brückner MK, Härtig W, Barnes BM, Arendt T (2011) The Physiological Link between Metabolic Rate Depression and Tau Phosphorylation in Mammalian Hibernation. *PLoS ONE* 6:e14530.
- Stokin GB, Lillo C, Falzone TL, Brusch RG, Rockenstein E, Mount SL, Raman R, Davies P, Masliah E, Williams DS, Goldstein LSB (2005) Axonopathy and Transport Deficits Early in the Pathogenesis of Alzheimer's Disease. *Science* 307:1282-1288.



- Stoppini L, Buchs PA, Muller D (1991) A simple method for organotypic cultures of nervous tissue. *Journal of Neuroscience Methods* 37:173-182.
- Su B, Wang X, Drew KL, Perry G, Smith MA, Zhu X (2008) Physiological regulation of tau phosphorylation during hibernation. *Journal of Neurochemistry* 105:2098-2108.
- Su B, Wang X, Zheng L, Perry G, Smith MA, Zhu X (2010) Abnormal mitochondrial dynamics and neurodegenerative diseases. *Biochimica et Biophysica Acta (BBA) - Molecular Basis of Disease* 1802:135-142.
- Swerdlow RH, Khan SM (2004) A "mitochondrial cascade hypothesis" for sporadic Alzheimer's disease. *Medical Hypotheses* 63:8-20.
- Swerdlow RH, Khan SM (2009) The Alzheimer's disease mitochondrial cascade hypothesis: An update. *Experimental Neurology* 218:308-315.
- Tada T, Sheng M (2006) Molecular mechanisms of dendritic spine morphogenesis. *Current Opinion in Neurobiology* 16:95-101.
- Terada S, Hirokawa N (2000) Moving on to the cargo problem of microtubule-dependent motors in neurons. *Current Opinion in Neurobiology* 10:566-573.
- Terry R (1998) The cytoskeleton in Alzheimer disease. *J Neural Transm Supp* 53: 141-145.
- Terry R, Masliah E, Salmon D, Butters N, DeTeresa R, Hill R, Hansen L, Katzman R (1991) Physical basis of cognitive alterations in Alzheimer's disease: synapse loss is the major correlate of cognitive impairment. *Annals of Neurology* 30:572-580.
- Tillement L, Lecanu L, Papadopoulos V (2011) Further Evidence on Mitochondrial Targeting of  $\beta$ -Amyloid and Specificity of  $\beta$ -Amyloid-Induced Mitotoxicity in Neurons. *Neurodegenerative Diseases* ePub ahead of print.
- Timm T, Li XY, Biernat J, Jiao J, Mandelkow E, Vandekerckhove J, Mandelkow EM (2003) MARKK, a Ste20-like kinase, activates the polarity-inducing kinase MARK/PAR-1. *EMBO J* 22:5090-5101.
- Vossel KA, Zhang K, Brodbeck J, Daub AC, Sharma P, Finkbeiner S, Cui B, Mucha L (2010) Tau Reduction Prevents A $\beta$ -induced Defects in Axonal Transport. *Science* 333:186.

- Tomiyama T, Matsuyama S, Iso H, Umeda T, Takuma H, Ohnishi K, Ishibashi K, Teraoka R, Sakama N, Yamashita T, Nishitsuji K, Ito K, Shimada H, Lambert MP, Klein WL, Mori H (2010) A Mouse Model of Amyloid  $\beta$  Oligomers: Their Contribution to Synaptic Alteration, Abnormal Tau Phosphorylation, Glial Activation, and Neuronal Loss In Vivo. *Journal of Neuroscience* 30:4845-4856.
- Townsend M, Shankar GM, Mehta T, Walsh DM, Selkoe DJ (2006) Effects of secreted oligomers of amyloid  $\beta$ -protein on hippocampal synaptic plasticity: a potent role for trimers. *The Journal of Physiology* 572:477-492.
- Trinczek B, Ebner A, Mandelkow EM, Mandelkow E (1999) Tau regulates the attachment/detachment but not the speed of motors in microtubule-dependent transport of single vesicles and organelles. *Journal of Cell Science* 112:2355-2367.
- Tucker KL, Meyer M, Barde Y-A (2001) Neurotrophins are required for nerve growth during development. *Nat Neurosci* 4:29-37.
- Tucker RP (1990) The roles of microtubule-associated proteins in brain morphogenesis: a review. *Brain Research Reviews* 15:101-120.
- Uda M, Ishido M, Kami K, Masuhara M (2006) Effects of chronic treadmill running on neurogenesis in the dentate gyrus of the hippocampus of adult rat. *Brain Research* 1104:64-72.
- Umahara T, Uchihara T, Tsuchiya K, Nakamura A, Iwamoto T, Ikeda K, Takasaki M (2004) 14-3-3 proteins and zeta isoform containing neurofibrillary tangles in patients with Alzheimer's disease. *Acta Neuropathologica* 108:279-286.
- Velasco ME, Smith MA, Siedlak SL, Nunomura A, Perry G (1998) Striation is the characteristic neuritic abnormality in Alzheimer disease. *Brain Research* 813:329-333.
- Vickers JC, King AE, Woodhouse A, Kirkcaldie MT, Staal JA, McCormack GH, Blizzard CA, Musgrove REJ, Mitew S, Liu Y, Chuckowree JA, Bibari O, Dickson TC (2009) Axonopathy and cytoskeletal disruption in degenerative diseases of the central nervous system. *Brain Research Bulletin* 80:217-223.
- Vossel KA, Zhang K, Brodbeck J, Daub AC, Sharma P, Finkbeiner S, Cui B, Mucke L (2010) Tau Reduction Prevents A $\beta$ -Induced Defects in Axonal Transport. *Science* 330:198.



- Walsh DM, Lomakin A, Benedek GB, Condron MM, Teplow DB (1997) Amyloid  $\beta$ -Protein Fibrillogenesis. *Journal of Biological Chemistry* 272:22364-22372.
- Walsh DM, Tseng BP, Rydel RE, Podlisny MB, Selkoe DJ (2000) The Oligomerization of Amyloid- $\beta$ -Protein Begins Intracellularly in Cells Derived from Human Brain. *Biochemistry* 39:10831-10839.
- Walsh DM, Klyubin I, Fadeeva JV, Cullen WK, Anwyl R, Wolfe MS, Rowan MJ, Selkoe DJ (2002) Naturally secreted oligomers of amyloid  $\beta$  protein potently inhibit hippocampal long-term potentiation in vivo. *Nature* 416:535-539.
- Wang H-W, Pasternak JF, Kuo H, Ristic H, Lambert MP, Chromy B, Viola KL, Klein WL, Stine WB, Krafft GA, Trommer BL (2002) Soluble oligomers of  $\beta$ -amyloid (1-42) inhibit long-term potentiation but not long-term depression in rat dentate gyrus. *Brain Research* 924:133-140.
- Wang W-X, Rajeev BW, Stromberg AJ, Ren N, Tang G, Huang Q, Rigoutsos I, Nelson PT (2008a) The Expression of MicroRNA miR-107 Decreases Early in Alzheimer's Disease and May Accelerate Disease Progression through Regulation of  $\beta$ -Site Amyloid Precursor Protein-Cleaving Enzyme 1. *Journal of Neuroscience* 28:1213-1223.
- Wang X, Su B, Zheng L, Perry G, Smith MA, Zhu X (2009a) The role of abnormal mitochondrial dynamics in the pathogenesis of Alzheimer's disease. *Journal of Neurochemistry* 109:153-159.
- Wang X, Su B, Lee H-g, Li X, Perry G, Smith MA, Zhu X (2009b) Impaired Balance of Mitochondrial Fission and Fusion in Alzheimer's Disease. *Journal of Neuroscience* 29:9090-9103.
- Wang X, Su B, Siedlak SL, Moreira PI, Fujioka H, Wang Y, Casadesus G, Zhu X (2008b) Amyloid- $\beta$  overproduction causes abnormal mitochondrial dynamics via differential modulation of mitochondrial fission/fusion proteins. *Proceedings of the National Academy of Science USA* 105:19318-19323.
- Wegner A (1982) Treadmilling of actin at physiological salt concentrations : An analysis of the critical concentrations of actin filaments. *Journal of Molecular Biology* 161:607-615.
- Weingarten MD, Lockwood AH, Hwo SY, Kirschner MW (1975) A protein factor essential for microtubule assembly. *Proceedings of the National Academy of Science USA* 72:1858-1862.

- Wessel D, Flügge UI (1984) A method for the quantitative recovery of protein in dilute solution in the presence of detergents and lipids. *Analytical Biochemistry* 138:141-143.
- Whiteman IT, Minamide LS, Goh DL, Bamberg JR, Goldsberry C (2011) Rapid changes in phospho-MAP/tau epitopes during neuronal stress: cofilin-actin rods primarily recruit microtubule binding domain epitopes. *PLoS ONE* 6:e20878.
- Whiteman IT, Gervasio OL, Cullen KM, Guillemin GJ, Jeong EV, Witting PK, Antao ST, Minamide LS, Bamberg JR, Goldsberry C (2009) Activated Actin-Depolymerizing Factor/Cofilin Sequesters Phosphorylated Microtubule-Associated Protein during the Assembly of Alzheimer-Like Neuritic Cytoskeletal Striations. *Journal of Neuroscience* 29:12994-13005.
- Wirhans O, Weis J, Kaye R, Saido TC, Bayer TA (2007) Age-dependent axonal degeneration in an Alzheimer mouse model. *Neurobiology of Aging* 28:1689-1699.
- Woodhouse A, Shepherd C, Sokolova A, Carroll V, King A, Halliday G, Dickson T, Vickers J (2009) Cytoskeletal alterations differentiate presenilin-1 and sporadic Alzheimer's disease. *Acta Neuropathologica* 117:19-29.
- Yahata N, Yuasa S, Araki T (2009) Nicotinamide Mononucleotide Adenylyltransferase Expression in Mitochondrial Matrix Delays Wallerian Degeneration. *Journal of Neuroscience* 29:6276-6284.
- Yamauchi PS, Purich DL (1993) Microtubule-Associated Protein Interactions with Actin Filaments: Evidence for Differential Behavior of Neuronal MAP-2 and Tau in the Presence of Phosphatidylinositol. *Biochemical and Biophysical Research Communications* 190:710-715.
- Yao J, Hennessey T, Flynt A, Lai E, Beal MF, Lin MT (2011) MicroRNA-Related Cofilin Abnormality in Alzheimer's Disease. *PLoS ONE* 5:e15546.
- Yoshida H, Goedert M (2002) Molecular cloning and functional characterization of chicken brain tau: isoforms with up to five tandem repeats. *Biochemistry* 41:15203-15211.
- Yoshida H, Goedert M (2006) Sequential phosphorylation of tau protein by cAMP-dependent protein kinase and SAPK4/p38[alpha]; or JNK2 in the presence of heparin generates the AT100 epitope. *Journal of Neurochemistry* 99:154-164.



- Zempel H, Thies E, Mandelkow E, Mandelkow E-M (2010) A $\beta$  Oligomers Cause Localized Ca<sup>2+</sup> Elevation, Missorting of Endogenous Tau into Dendrites, Tau Phosphorylation, and Destruction of Microtubules and Spines. *Journal of Neuroscience* 30:11938-11950.
- Zhang B, Maiti A, Shively S, Lakhani F, McDonald-Jones G, Bruce J, Lee EB, Xie SX, Joyce S, Li C, Toleikis PM, Lee VMY, Trojanowski JQ (2005) Microtubule-binding drugs offset tau sequestration by stabilizing microtubules and reversing fast axonal transport deficits in a tauopathy model. *Proceedings of the National Academy of Science USA* 102:227-231.
- Zhao L, Ma Q-L, Calon F, Harris-White ME, Yang F, Lim GP, Morihara T, Ubeda OJ, Ambegaokar S, Hansen JE, Weisbart RH, Teter B, Frautschy SA, Cole GM (2006) Role of p21-activated kinase pathway defects in the cognitive deficits of Alzheimer disease. *Nat Neurosci* 9:234-242.
- Zhou L-X, Zeng Z-Y, Du J-T, Zhao Y-F, Li Y-M (2006) The self-assembly ability of the first microtubule-binding repeat from tau and its modulation by phosphorylation. *Biochemical and Biophysical Research Communications* 348:637-642.
- Zimmer J, Gähwiler BH (1984) Cellular and connective organization of slice cultures of the rat hippocampus and fascia dentata. *The Journal of Comparative Neurology* 228:432-446.

## Publications

Whitman IT, Minamide LS, Guillemain GJ, Goh DL, Bamburg JR, and Goldsbury C (2011) Rapid Changes in Phospho-MAPtau Epitopes During Neuronal Stress: Cofilin-Actin Rods Primarily Recruit Microtubule Binding Domain Epitopes. *PLoS ONE* 6(6):e20878.

Bamburg JR, Bernstein BW, Davis RG, Flynn KC, Goldsbury C, Jensen JR, Maloney MT, Maraden IT, Minamide LS, Pak CW, Show AE, Whitman I, Wiggan J, Woodgett JR, and Wozniak DA (2011) ADF/cofilin rods in neurodegenerative disease. *Current Alzheimer Research* 7(3):241-50.

## Appendix

Whitman IT, Gervasio OL, Cullen KM, Guillemain GJ, Jeong EV, Waring RK, Anthon ST, Minamide LS, Bamburg JR and Goldsbury C (2009) Activated Actin-Depolymerizing Factor/Cofilin Sequesters Phosphorylated Microtubule-Associated Protein during the Assembly of Alzheimer-Like Neuronal Cytoskeletal Scaffolds. *Journal of Neuroscience* 29(41):12964-13005.

Goldsbury C, Whitman IT, Jeong E and Lim YA (2008) Oxidative stress increases levels of endogenous amyloid- $\beta$  peptides secreted from primary chick brain neurons. *Aging Cell* 7:771-775.



# Rapid Changes in Phospho-MAP/Tau Epitopes during Neuronal Stress: Cofilin-Actin Rods Primarily Recruit Microtubule Binding Domain Epitopes

Itzhack T. Whiteman<sup>1,2</sup>, Laurie S. Minamide<sup>1</sup>, Guillemin GJ, James R. Bamburg<sup>1</sup>, Claire Goldsbury<sup>1,2</sup>

## Publications

<sup>1</sup>City State and West England Institute for Health Research, University of Exeter, Exeter, UK; <sup>2</sup>Department of Molecular Biology, University of Exeter, Exeter, UK

**Abstract**

**Background:** Cofilin-actin rods are a prominent feature of Alzheimer's disease pathology. These structures are thought to be involved in the sequestration of microtubule-binding domain (MTBD) epitopes of phosphorylated microtubule-associated protein (MAP) and tau. However, the precise mechanism of recruitment of MTBD epitopes to cofilin-actin rods remains unclear. We investigated the recruitment of MTBD epitopes to cofilin-actin rods in primary chick brain neurons under conditions of neuronal stress.

**Results:** We found that cofilin-actin rods primarily recruit MTBD epitopes of phosphorylated MAP and tau. This recruitment is dependent on the presence of phosphorylated MAP and tau, and is mediated by the interaction of the MTBD epitopes with the cofilin-actin rods. We also found that the recruitment of MTBD epitopes to cofilin-actin rods is dependent on the presence of phosphorylated MAP and tau, and is mediated by the interaction of the MTBD epitopes with the cofilin-actin rods.

**Conclusion:** Our findings suggest that cofilin-actin rods primarily recruit MTBD epitopes of phosphorylated MAP and tau. This recruitment is dependent on the presence of phosphorylated MAP and tau, and is mediated by the interaction of the MTBD epitopes with the cofilin-actin rods.

- **Whiteman IT**, Minamide LS, Guillemin GJ, Goh DL, Bamburg JR and Goldsbury C (2011) Rapid Changes in Phospho-MAP/tau Epitopes During Neuronal Stress: Cofilin-Actin Rods Primarily Recruit Microtubule Binding Domain Epitopes. *PLoS ONE* 6(6):e20878.
- Bamburg JR, Bernstein BW, Davis RC, Flynn KC, Goldsbury C, Jensen JR, Maloney MT, Marsden IT, Minamide LS, Pak CW, Shaw AE, **Whiteman I**, Wiggan O. (2010) ADF/cofilin-actin rods in neurodegenerative disease. *Current Alzheimer Research* 7(3):241-50.
- **Whiteman IT**, Gervasio OL, Cullen KM, Guillemin GJ, Jeong EV, Witting PK, Antao ST, Minamide LS, Bamburg JR and Goldsbury C (2009) Activated Actin-Depolymerizing Factor/Cofilin Sequesters Phosphorylated Microtubule-Associated Protein during the Assembly of Alzheimer-Like Neuronal Cytoskeletal Striations. *Journal of Neuroscience* 29(41):12994-13005.
- Goldsbury C, **Whiteman IT**, Jeong E and Lim YA (2008) Oxidative stress increases levels of endogenous amyloid- $\beta$  peptides secreted from primary chick brain neurons. *Aging Cell* 7:771-775.



# Rapid Changes in Phospho-MAP/Tau Epitopes during Neuronal Stress: Cofilin-Actin Rods Primarily Recruit Microtubule Binding Domain Epitopes

Ineka T. Whiteman<sup>1,2</sup>, Laurie S. Minamide<sup>3</sup>, De Lian Goh<sup>1,2</sup>, James R. Bamberg<sup>3</sup>, Claire Goldsbury<sup>1,2\*</sup>

<sup>1</sup>The Brain and Mind Research Institute, University of Sydney, Sydney, Australia, <sup>2</sup>Bosch Institute, School of Medical Sciences, University of Sydney, Sydney, Australia, <sup>3</sup>Department of Biochemistry and Molecular Biology, Colorado State University, Fort Collins, Colorado, United States of America

## Abstract

Abnormal mitochondrial function is a widely reported contributor to neurodegenerative disease including Alzheimer's disease (AD), however, a mechanistic link between mitochondrial dysfunction and the initiation of neuropathology remains elusive. In AD, one of the earliest hallmark pathologies is neuropil threads comprising accumulated hyperphosphorylated microtubule-associated protein (MAP) tau in neurites. Rod-like aggregates of actin and its associated protein cofilin (AC rods) also occur in AD. Using a series of antibodies - AT270, AT8, AT100, S214, AT180, 12E8, S396, S404 and S422 - raised against different phosphoepitopes on tau, we characterize the pattern of expression and re-distribution in neurites of these phosphoepitope labels during mitochondrial inhibition. Employing chick primary neuron cultures, we demonstrate that epitopes recognized by the monoclonal antibody 12E8, are the only species rapidly recruited into AC rods. These results were recapitulated with the actin depolymerizing drug Latrunculin B, which induces AC rods and a concomitant increase in the 12E8 signal measured on Western blot. This suggests that AC rods may be one way in which MAP redistribution and phosphorylation is influenced in neurons during mitochondrial stress and potentially in the early pathogenesis of AD.

**Citation:** Whiteman IT, Minamide LS, Goh DL, Bamberg JR, Goldsbury C (2011) Rapid Changes in Phospho-MAP/Tau Epitopes during Neuronal Stress: Cofilin-Actin Rods Primarily Recruit Microtubule Binding Domain Epitopes. *PLoS ONE* 6(6): e20878. doi:10.1371/journal.pone.0020878

**Editor:** Mark P. Mattson, National Institute on Aging Intramural Research Program, United States of America

**Received:** March 30, 2011; **Accepted:** May 11, 2011; **Published:** June 28, 2011

**Copyright:** © 2011 Whiteman et al. This is an open-access article distributed under the terms of the Creative Commons Attribution License, which permits unrestricted use, distribution, and reproduction in any medium, provided the original author and source are credited.

**Funding:** The Sir Zelman Cowen Universities Fund, The Judith Jane Mason and Harold Stannett Williams Memorial Foundation, The Rebecca Cooper Foundation, The NHMRC, Sydney Medical School and the National Institutes of Health grant N540371 (JRB). The funders had no role in study design, data collection and analysis, decision to publish, or preparation of the manuscript.

**Competing Interests:** The authors have declared that no competing interests exist.

\* E-mail: claire.goldsbury@sydney.edu.au

## Introduction

Neuronal histopathological hallmarks of AD include neurofibrillary tangles (NFT) and neuropil threads both comprised of hyperphosphorylated microtubule-associated protein (MAP) tau. NFTs and neuropil threads assemble in cell bodies and neurites respectively. Comprising a reported >85% of end-stage cortical tau pathology, neuropil threads correlate with cognitive decline [1–6]. The major known function of tau, like other MAPs, is its stabilization and regulation of microtubule (MT) dynamics necessary for neurite outgrowth, morphogenesis and since tau is predominantly an axonal protein, it plays an important role in facilitating MT-dependent axonal transport (for reviews see [7,8]). Tau can also interact with the plasma membrane and may play roles in relaying signals to the cytoskeleton from the cell surface or scaffolding signaling complexes [9]. The MT directed activity of tau is regulated by phosphorylation/dephosphorylation cycles, such that phosphorylation at specific sites detaches tau from MTs and allows MT depolymerization, while tau dephosphorylation enables it to bind and stabilize MT via its MT binding domain (MTBD) [10,11]. In AD, tau is hyperphosphorylated, the MT network is destabilized and tau self-assembles into paired helical filaments (PHFs) that form the NFT and neuropil thread structures. Over 20 phosphorylation sites have been characterized for tau, two of these are located in the MTBD at two 'KXGS' amino acid motifs corresponding to residues S262 and S356 [11–

13]. Phosphorylation of these KXGS motifs is one of the earliest markers of AD pathology, readily detectable in neuropil threads with the monoclonal antibody 12E8 that recognizes these conserved motifs in both tau as well as in other MAPs [14]. In the case of tau, phosphorylation of the MTBD sites has been shown to induce MT disassembly whereby the new unbound pool of tau is susceptible to self-assembly into PHFs [12,15–17].

Neuropil threads generally precede the appearance of extensive NFTs, suggesting tau first accumulates in neurites during the development of AD pathology before the proliferation of cell body NFTs [1,4,18,19]. An *in vitro* cell model for neuropil thread assembly may therefore help mimic early cellular events relevant to the disease mechanism. To this end, we recently demonstrated in primary neuronal cell culture and organotypic slice culture that mitochondrial dysfunction initiates formation of 12E8-positive neuritic inclusions that co-localize with actin depolymerizing factor (ADF)/cofilin-actin rods (AC rods) [20]. These inclusions bear some morphological resemblance to inclusions observed in AD brain which also include punctuate and rod-like linear arrays of cofilin and actin aggregates throughout the neuropil [21] (reviewed in [22]). The relevance of this model lies in an increasing body of evidence that implicates disrupted energy metabolism and mitochondrial dysfunction in AD (for reviews see [23–27]). Reduced mitochondrial function and increased oxidative stress are reported to occur early in disease progression, suggesting that these factors could play an integral role in initiating pathological



cascades that result in the varied cytopathology of AD [23]. AC rods are independently induced in cell culture by the inhibition of mitochondrial ATP generation, thus potentially linking the formation and co-localization of AC rods and MAP inclusions to mitochondrial dysfunction [20]. Moreover, interaction of MAPs and actin in the organization of the cytoskeletal network is well-documented [28–35] and emerging evidence suggests that these interactions may be central to the processes involved in the initiation and development of early AD pathology [20,22,36,37].

Since AD neuropathology involves hyperphosphorylation and accumulation of numerous phosphoepitopes of tau and not just those in the MTBD recognized by 12E8, the aim of this study was to investigate the phosphorylation pattern and re-distribution of several other key phospho-tau epitopes in the primary neuronal culture model. We utilized the chick model since chick neurons express five forms of tau that are homologous to human tau isoforms and exhibit conserved phosphoepitopes recognized by antibodies against human tau [38]. Using a series of commercially available phospho-tau antibodies, we measured time-dependent effects of mitochondrial dysfunction on the levels and distribution patterns of these phosphoepitopes. We found that cellular ATP reduction gave rise to rapid overall dephosphorylation at most epitopes with the exception of the 12E8 epitope that exhibited persistent phosphorylation over the 120 min treatment time. Further, 12E8 was the only epitope predominantly recruited to AC rods generated under these conditions within the time frame investigated. These results highlight the MTBD of MAP/tau as a potential early player in the initiation of neuropil threads in neurons of the AD brain.

## Methods

### Ethics Statement

Donated frontal cortex and hippocampal brain tissue from normal adult and confirmed Alzheimer's disease patients were obtained from the Alzheimer Disease Research Center, University of California, San Diego, USA and approved for use by the Institutional Review Board (formerly the Human Research Committee), Colorado State University, USA (Approval ID: JR Bamberg 2001).

Experiments involving the use of animals (cell cultures derived from chicken embryos) were approved by the Animal Ethics Committee, University of Sydney, Australia (Approval ID: CS Goldsury K00/5-2008/3/4786).

### Antibodies and reagents

Mouse monoclonal antibodies against phosphorylated tau epitopes were as follows: AT8 (which recognizes S202/T205 in the longest isoform of human tau and S193/T196 in the longest isoform of chick tau; Pierce USA), AT100 (T212/S214 in human, T203/S205 in chick; Sigma-Aldrich), AT180 (T231/S235 in human, T222/S226 in chick; Sigma-Aldrich), AT270 (T181 in human, T155 in chick; Sigma-Aldrich), 12E8 ('KXGS' motifs in MTBDs of tau and other MAPs. For tau, these motifs correspond to S262/S356 in human, S253/S378 in chick; Elan USA) [14]. Other mouse monoclonal antibodies included GAPDH and  $\beta$ -actin (Sigma-Aldrich). Rabbit polyclonal antibodies against phosphorylated tau epitopes were S214 (S205 in chick; GenScript USA), S396 (S418 in chick; Biosource), S404 (S426 in chick; Biosource), S422 (S444 in chick; Sigma-Aldrich), total tau (Dako, USA) and against chick ADF and mammalian ADF and cofilin (1439) [39]. Anti-mouse and anti-rabbit secondary antibodies included Alexa Fluor-conjugated 488, 555, 594 and 647 (Invitrogen) for immunofluorescence and horseradish peroxidase-conjugated (Amersham) for chemiluminescence detection of immunoblots.

### Cell culture and treatments

Primary chick tectal neurons were prepared from freshly dissected chicken embryos (E7), as previously described and cultured for 7 days *in vitro* (d.i.v) on poly-D-lysine-coated 30 mm culture dishes or glass coverslips [40]. For reduction of ATP, cells were treated with 1–2  $\mu$ M antimycin (AM; a mitochondrial complex III inhibitor; Sigma-Aldrich) in warm phosphate buffered saline (PBS). The actin depolymerizing drug Latrunculin B (Calbiochem 428020, CA) and actin stabilizing drug Jasplakinolide (Calbiochem 420127, CA) were used at 1  $\mu$ g/ml in warm PBS. Cells left without a medium change served as controls. After treatments, cells were immediately fixed for immunostaining (cells on coverslips) or lysed, harvested and prepared for Western blot analysis (cells on tissue culture dishes).

### Immunoblotting

Primary neurons were treated in duplicate and prepared for SDS-PAGE. For equal gel loading, protein concentrations were determined by the Lowry assay (BioRad). Proteins transferred to nitrocellulose membranes were detected with an ECL Western Blotting Detection System (Amersham) on a ChemiDoc XRS (BioRad). For analysis, band densities were measured using Image J (v1.38x, National Institutes of Health freeware; <http://rsb.info.nih.gov/ij/>), background intensity was subtracted for each individual lane and normalized to GAPDH or  $\beta$ -actin loading controls. For quantification, blots within the linear range of detection were selected by plotting the band density versus exposure time. An average for each treatment condition was determined with error bars representing min/max intensities (where  $n=2$ ) or SEM (where  $n=4$ ). Results are presented as a percentage of the mean control band intensities.

### Microscopy

Cells were fixed with 4% paraformaldehyde at 37°C for 35 minutes, permeabilized for 90 sec with 0.05% Triton X-100 in PBS or ice-cold 80% methanol/20% PBS (1 $\times$ ), blocked in 5% goat serum and immunostained using primary antibodies and fluorescent secondary antibodies described above. Epifluorescence images were obtained on a Zeiss Axioplan 2 microscope, captured with a CCD camera driven by AxioVision software. Single labeled cells/sections were used to check for bleed-through in all double-label immunofluorescence studies. Confocal images were obtained on a Zeiss LSM 510 Meta driven by LSM 510 software. All captured images were converted to Tagged Image Files for subsequent analysis and presentation.

### Nuclear accumulation analysis

For quantification of cells containing nuclear accumulation of AT100 label in control, AM- and Lat B-treated conditions, a number of randomly selected fields on each coverslip were selected and cells containing nuclear tau were counted and expressed as a percentage of the total number of counted cells. Inclusion criteria for nuclear accumulation were (i) general neuron morphology appeared normal (including intact nucleus) (ii) neuron exhibited obvious co-localization of AT100 label with DAPI nuclear label and (iii) nucleus exhibited AT100 fluorescence intensity  $>1.5\times$  the intensity of nuclei of surrounding, unaffected cells, as measured using Image J. Over 200 cells were counted for each condition in duplicate experiments using independently prepared cell cultures.

### Human tissue preparation

Post-mortem time to fixation in formalin (for immunofluorescence) was 3 h. For immunofluorescence, paraffin sections (6–



7  $\mu\text{m}$ ) were deparaffinized for 20 min in Hemo-De (Fisher Scientific), rehydrated to distilled water through decreasing concentrations of ethanol, microwaved in water for 8 min, blocked with 5% goat serum for one hour and immunostained.

### Transmission Electron Microscopy

Primary chick neurons were grown on glass coverslips, treated, washed with warm PBS and fixed for 30 min with 2.5% glutaraldehyde (Electron Microscopy Sciences, USA) in 0.1 M sodium cacodylate buffer (Sigma-Aldrich). Cells were rinsed with buffer and post-fixed for 30 min in cold 1% osmium tetroxide (Sigma-Aldrich). Cells were rinsed again and stained for 2 h with 1% uranyl acetate (Sigma-Aldrich), filtered through 0.22  $\mu\text{m}$  Biofil Syringe filter in 0.05 M sodium acetate (Sigma-Aldrich). To prepare TEM grids, cells were dehydrated through increasing concentrations of ethanol (v/v) (50%, 70%, 95% and ultra-dry 100%), then infiltrated with Spurr's resin in increasing ratios to 100% ethanol (1:1, 2:1 and 3:1). Cells on coverslips were embedded in 100% Spurr's resin and cured at 60°C overnight. To remove coverslips, resin blocks were placed in liquid nitrogen for ~15 sec, transferred to warm water and carefully removed. Resin blocks were section using a diamond knife (70 nm) and placed on 200-mesh copper TEM grids that were subsequently post-stained for 10 min with uranyl acetate and lead citrate. Images were acquired with a Phillips CM 120 Biofilter TEM at 120 kV.

## Results

### Mitochondrial inhibition induces rapid dephosphorylation at all MAP/tau phosphoepitopes except for 12E8

In AD neurons, tau is hyperphosphorylated and abnormally redistributed to NFTs and neuropil threads in cell bodies and neurites respectively. The mechanisms by which these processes occur are not fully understood. The aim of this study was to test the hypothesis that inhibiting mitochondrial function influences the phosphorylation state and localization of tau protein. Primary neuronal cultures (prepared from E7 chick tectum) were treated for 10, 30, 60 or 120 min with the mitochondrial complex III inhibitor AM which has previously been shown to reduce the level of ATP in these neurons by 60% within 10 min [20]. Cells were then lysed or fixed for immunostaining and probed with a battery of phospho-tau antibodies - AT270, AT8, AT100, S214, AT180, 12E8, S396, S404 or S422 - that have been raised against different phosphoepitopes on human tau and have analogous corresponding epitopes in chicken tau (Fig. 1A) The 12E8 antibody recognizes phosphorylated KXGS motifs in the conserved MTBDs of both tau and other MAPs [14]. Western blot analysis of lysates revealed that compared to untreated (control) cells, ATP reduction leads to dephosphorylation of epitopes S396, AT8, AT270, AT180, S404 and S422 over the 120 min treatment time when normalized for loading to GAPDH (Fig. 1B, C). Total tau was observed to decrease transiently before returning to control levels at 120 min. By contrast, the blots revealed a strong and sustained signal for the epitopes recognized by the 12E8 antibody (Fig. 1D, E). Consistent with this, the ratio of 12E8 to total tau band intensities increased >2-fold by 60 min whereas the AT8 to total tau ratio declined over the same time frame to near zero (Fig. 1D). This trend of persistence of the 12E8 epitope signal was reproducible in a second independent experiment and combined ( $n = 4$ ), these data reveal a peak increase to  $232 \pm 69\%$  at 60 min and sustained phosphorylation at 120 min ( $155 \pm 4\%$ ,  $p < 0.05$ ) (mean  $\pm$  SEM) (Fig. 1E).

### Redistribution of MAP/tau phosphoepitopes to rod-like or spheroid inclusions in neurites

Next, we conducted immunofluorescence imaging of the same phosphoepitopes in AM-treated (15 min.) neurons to investigate distribution patterns of these antibody labels throughout neurons following mitochondrial inhibition. While some phosphoepitope labeling remained relatively smoothly distributed throughout neurites of AM-treated cells, other labels were aggregated into spheroid inclusions in affected processes (Fig. 2A-J). Cell body staining intensity, indicative of phosphorylation state, of phosphoepitopes AT8, S214 and AT180 was somewhat reduced (AT8 = ~30% intensity of control cells after 15 min AM treatment), but otherwise comparable to control cells with regards to its smooth distribution. By contrast, AT270, AT100, S396, S404, S422 and total tau labeling aggregated into spheroids that were rarely seen in untreated control cells. Overall cell body staining intensity for some of these epitopes was also found to be reduced (AT270 ~40% intensity compared to control cells). Although the 12E8 antibody labeled some spheroids, it predominantly labeled rod-shaped aggregates throughout neurites (Fig. 2F) which were previously shown to be AC rods [20]. The insets in Fig. 2 illustrate the appearance of spheroids and rods respectively. Rod-shaped structures were observed less often with the S404, S422 and AT270 phosphoepitope labels (Fig. 2A and G, insets). As shown for AT270 below, these structures only rarely co-localized with AC which was in contrast to 12E8 label which largely colocalized with AC rods.

In AM-treated cells, in addition to labeling neuritic inclusions that co-localized with total tau immunolabeling, AT100 revealed a redistribution into cell nuclei in a subset of neurons (~36%), as indicated by colocalization with the nuclear stain DAPI (Fig. 2D, asterisks), which was never observed for any other tau epitope (Supplementary Fig. S1). However, further analysis demonstrated that this nuclear epitope does not represent tau protein as AT100 also labeled nuclei of mouse tau knockout neurons (LSM, ITW and JRB unpublished observations). Moreover, neither S214 (which shares the serine-214 recognition site of AT100) nor total tau labels were ever seen to accumulate in nuclei of AM-treated cells further suggesting this AT100 accumulation to be non-tau related. Interestingly however, the same nuclear localization of the AT100 label was seen in post mortem AD tissue (Supplementary Fig. S1F).

Co-labeling studies of spheroids in AM-treated cells revealed colocalization of phospho-tau epitopes with total tau (Fig. 3A and results not shown), suggesting that these observed aggregates in ATP-depleted cells are comprised of tau phosphorylated at many sites. By contrast, rod-like structures immunolabeled for the 12E8 epitope did not co-label with other phosphoepitopes (Fig. 3B). We had previously demonstrated 12E8 label in AC rods [20], which we confirm here in both Triton X and methanol permeabilized cells (Fig. 4A and data not shown). We found that the 12E8 labeling of AC rods in AM treated cells was best preserved under Triton X permeabilization (Fig. 3B) whereas methanol permeabilization resulted mostly in spheroid labeling (Fig. 3C). Further, 12E8-labeled AC rods did not co-localize with S396 label (Fig. 3B) which by contrast only localized to spheroid structures in the same cells (arrows Fig. 3B). This further documents the distinct and separate nature of AC rods versus spheroids.

### 12E8 but not other phosphoepitopes redistributes to AC rods during mitochondrial inhibition

To further investigate whether other tau epitopes are present in AC rods, we carried out double-labeling for ADF and a variety of



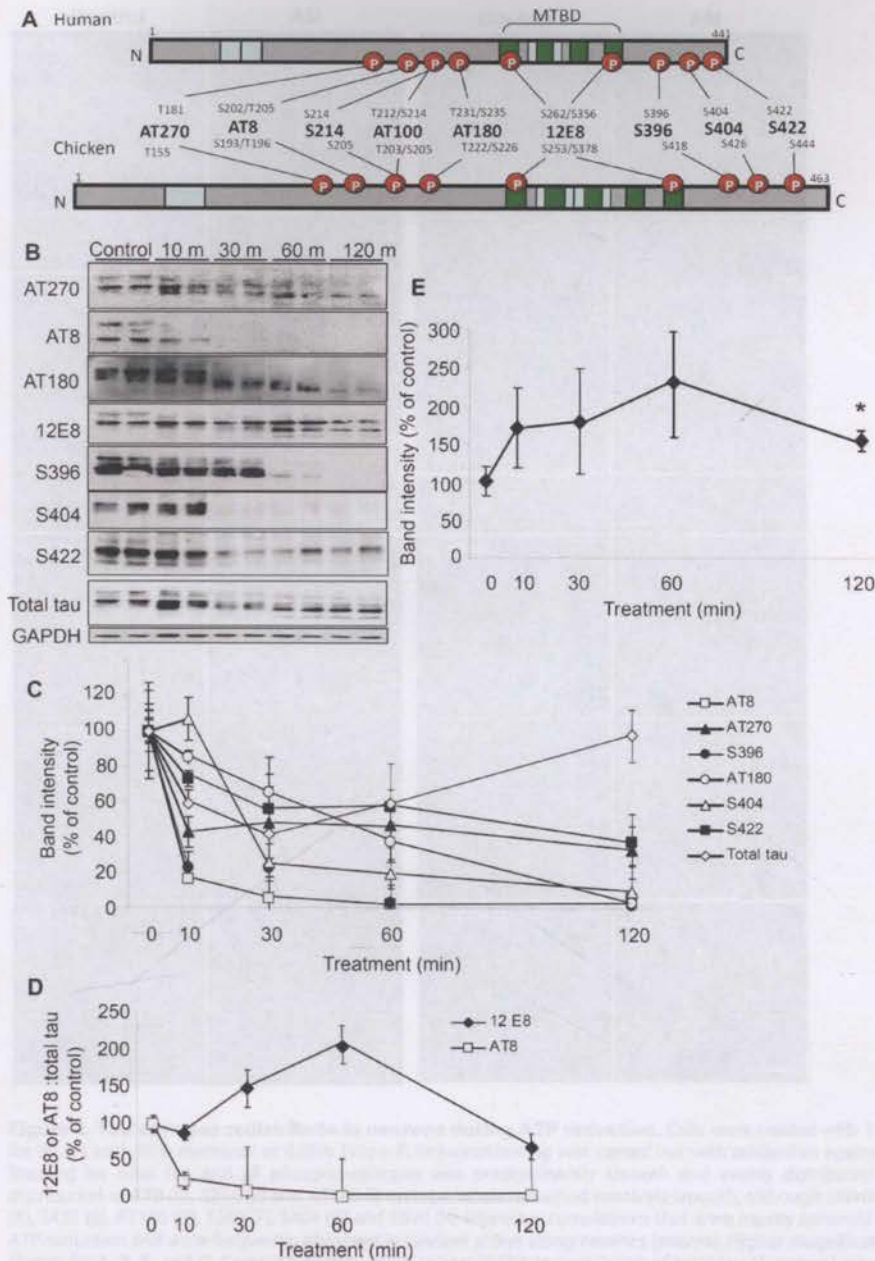


**Figure 1. ATP reduction causes persistent phosphorylation of 12E8 epitope and dephosphorylation at other sites.** (A) Epitope map of tau antibodies in human and chicken brain [38]. Schematic representations of the longest tau isoforms are shown (441 amino acid residues in human tau, 463 in chicken). The phosphorylation-dependent anti-tau antibodies (AT270, AT8, S214, AT100, AT180, 12E8, S396, S404 and S422) are shown with their corresponding target residues (S = Serine, T = Threonine). Positions of the various alternatively spliced inserts which give rise to 6 different isoforms in humans and 5 in chick are shown in blue. Green boxes denote tandem amino acid sequence repeats, which constitute the MTBD. (B) Representative Western blots of extracts from cell cultures treated in duplicate with 1  $\mu$ M AM for 10, 30, 60 or 120 min. (C) Quantification of the Western blots shown in (B) reveal rapid dephosphorylation of AT8, S396 and AT270 epitopes (respectively declining to  $16 \pm 0.03\%$ ,  $23 \pm 9\%$  and  $43 \pm 9\%$  of control values; mean  $\% \pm$  min/max intensities). By 30 min, phosphorylation at epitope S404 had also markedly declined ( $25 \pm 11\%$ ) while epitopes S422 and AT180 exhibited a more moderate decline in phosphorylation (reduced to  $55 \pm 3\%$  and  $65 \pm 20\%$  at 30 min). Total tau was observed to decrease transiently ( $41 \pm 5\%$  at 30 min) before returning to control levels ( $98 \pm 19\%$ ) at 120 min. All antibodies were probed on fresh blots and normalized to GAPDH loading control bands. (D) By contrast, phosphorylation of the 12E8 epitope increased markedly. To ascertain a phosphorylation:total tau ratio, blots probed for 12E8 or AT8 (for comparison) were stripped and reprobed for total tau (polyclonal rabbit antibody). Whereas the AT8:total tau ratio decreased rapidly, the 12E8:total tau ratio increased at 30 min and peaked at  $\sim 200\%$  after 60 min. Error bars in (C and D) indicate the maximum and minimum intensities. (E) Quantification of persistent phosphorylation at the 12E8 epitope (normalized to GAPDH) was significant with a peak of  $>200\%$  at 60 min and sustained phosphorylation ( $\sim 150\%$ ) at 120 min ( $n=4$ ;  $*p<0.05$ ). Error bars = SEM.

doi:10.1371/journal.pone.0020878.g001

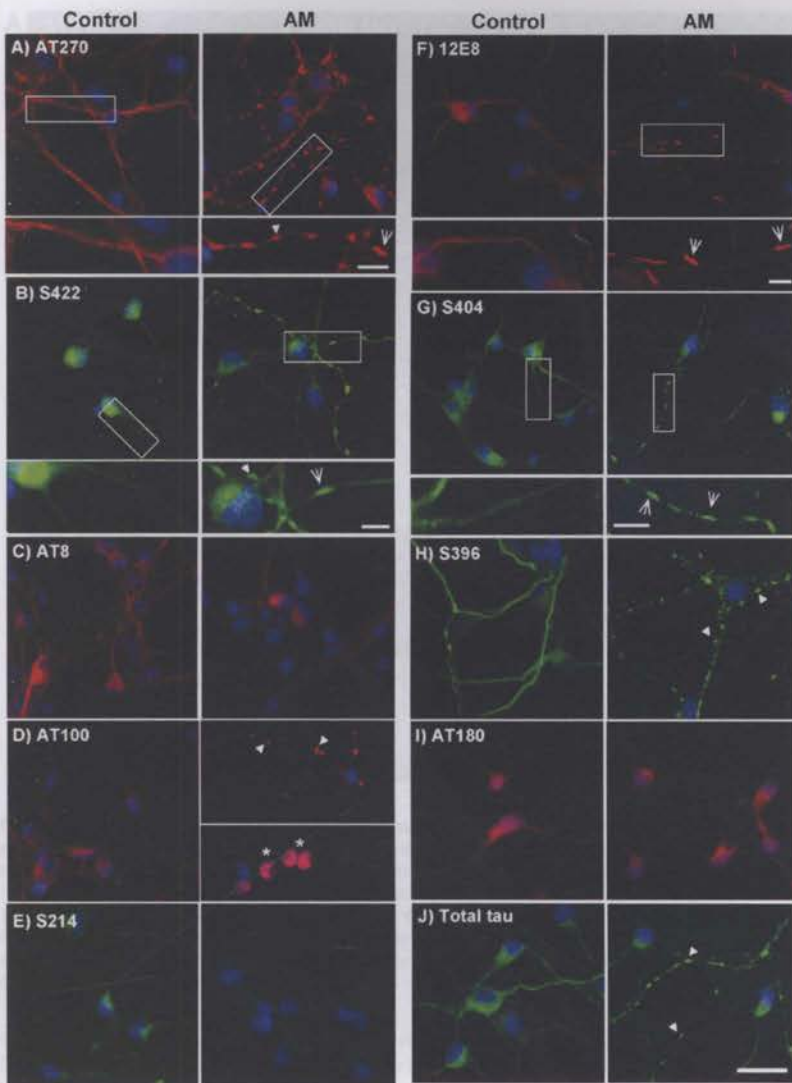


**Figure 2. Tau epitopes redistribute in neurons during ATP reduction.** Cells were treated with 1  $\mu$ M AM for 15 min, fixed and permeabilized for 90 sec with 80% methanol or 0.05% Triton-X. Immunostaining was carried out with antibodies against phosphorylated tau epitopes, as indicated. Staining for total tau and all phospho-epitopes was predominantly smooth and evenly distributed in control cells. Following ATP reduction, distribution of AT8 (C), S214 (E) and AT180 (I) epitope labels remained relatively smooth, although staining intensity was reduced. By contrast, AT270 (A), S422 (B), AT100 (D), 12E8 (F), S404 (G) and S396 (H) labeled accumulations that were mostly spheroid in shape, but occasionally rod-like, following ATP-reduction and were frequently observed in tandem arrays along neurites (arrows). Higher magnification insets of controls vs. AM-treated cells are shown for A, B, F, and G. Correspondingly, some spheroid-like accumulation of total tau (J, arrows) was also evident in neurites of AM-treated cells. Interestingly, only aggregates labeled with 12E8 (F) consistently showed classic and distinct rod-shaped structure throughout AM-treated cells, which is better observed at higher magnification (inset in F, arrows). Additionally, ATP reduction led to the redistribution and nuclear-accumulation of AT100 label (D, arrows), a phenomenon that was observed neither in control cultures stained with AT100, nor in treated cells labeled with any other MAP/tau phospho-epitope. However, nuclear AT100 label is unlikely to represent tau (see text). Nuclei were labeled with DAPI (blue). While most epitopes (except for 12E8 – see Fig. 3) appeared identical under methanol and Triton X permeabilization conditions, images in this figure represent a combination of both protocols. Methanol: (A, B, E, G, J). Triton X: (C, D, F, H, I). Scale bar = 20  $\mu$ m for all images except insets in (A, B, F, and G) = 5  $\mu$ m. doi:10.1371/journal.pone.0020878.g002

tau epitopes (since the ADF antibody was rabbit polyclonal, we were restricted to mouse monoclonal MAP/tau antibodies for double-labeling studies). AM-treated cells (15 min) were double-labeled for ADF and AT270 (Fig. 4B), and ADF and AT100 (Fig. 4C, D). AT270 aggregates only occasionally co-localized with AC rods (Fig. 4B, arrows), whereas AT100 label was never seen to co-localize with AC rods after either methanol or Triton-X permeabilization (Fig. 4C, D; arrows). By contrast, as previously

shown, 12E8 frequently co-localized with AC rods (Fig. 4A and reference [20]), suggesting this epitope to be of prominent importance in the immediate stages of MAP recruitment to AC rods.

Ultrastructural EM analysis of AC rods formed in chick neurons following ATP-reduction (Fig. 5A, B) corroborated previous results that demonstrated that AC rods are comprised of many individual parallel filaments arranged into tightly bundled structures [21,41–



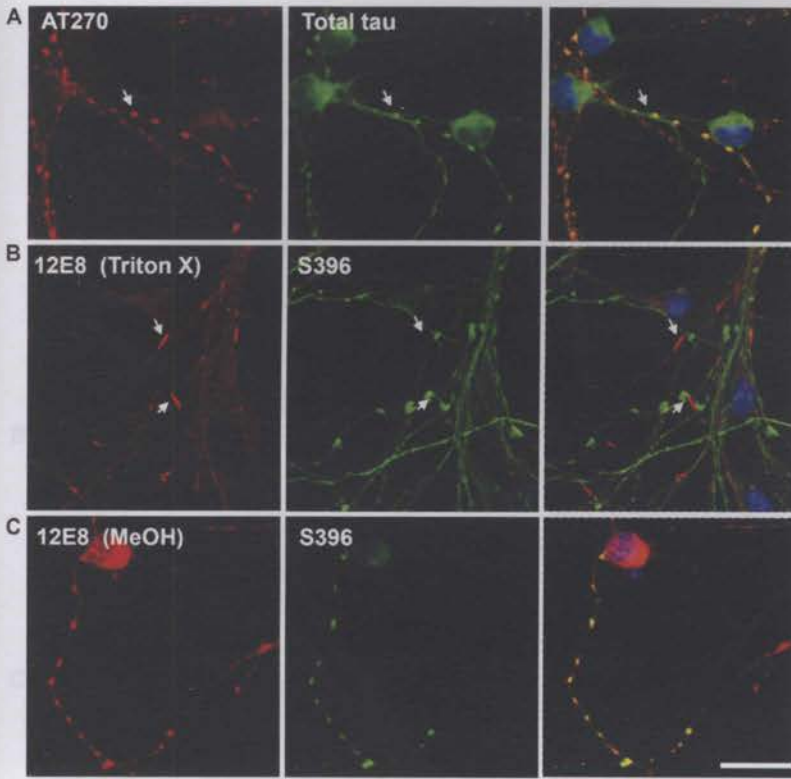


**Figure 3. Distinct rod-shaped aggregates are specific to 12E8 and are best preserved with Triton-X permeabilization.** ATP-depleted cells were permeabilized for 90 sec with 80% methanol or 0.05% Triton-X and co-labeled for epitopes of tau. (A) Under both methanol and Triton-X methods, aggregations containing AT270 epitopes co-labeled with total tau (shown here with methanol permeabilized cells) suggesting spheroid neuritic aggregates are comprised of tau phosphorylated at numerous epitopes. (B) By contrast, 12E8-labeling was predominantly in distinct rod-shaped aggregates that did not co-label with other phospho-tau epitopes (shown here for S396). 12E8-positive AC rods were best visualized following Triton-X permeabilization. (C) Using methanol permeabilization protocols, 12E8 by contrast more often labeled spheroid structures that as described above could be co-labeled with many other tau epitopes (shown here for S396). Scale bar = 20  $\mu$ m. doi:10.1371/journal.pone.0020878.g003

43]. By contrast, unaffected neurites of treated cells contain individually spaced microtubules approximately 24 nm in diameter (Fig. 5C).

#### Actin depolymerization mimics effects of mitochondrial inhibition on 12E8 epitope redistribution but does not affect the distribution of other phosphoepitopes

Similar to mitochondrial inhibition, we previously demonstrated that pharmacologically-induced depolymerization of actin induces the formation of AC rods which subsequently recruit 12E8 epitopes [20]. In order to determine whether actin depolymerization induces redistribution of other phosphoepitopes, we treated primary neurons with Latrunculin B (Lat B) which induces depolymerization of actin filaments in the absence of ATP reduction. The formation and co-localization of AC rods with 12E8 label under these conditions was confirmed (not shown). In contrast to AM-treated cells, staining for other phosphoepitopes including AT100 (Fig. 6A) and S396 (Supplementary Fig. S1D) in Lat B treated cells revealed an even distribution along neurites. Western blot analysis of Lat B-treated neurons revealed a 2.9-fold increase in 12E8 immunoreactivity after 2 min treatment while other phosphoepitopes such as S396 remained largely unchanged (Fig. 6B, C). These results confirm that 12E8 is the primary epitope recruited to Lat B-induced AC rods during actin

reorganization, as was also found to be the case for AC rods induced by ATP-reduction. Together these results provide evidence for an important role of KXGS phosphorylation in the initial recruitment of tau or other MAPs to AC rods during times of cellular stress.

#### Discussion

Disrupted energy metabolism, mitochondrial dysfunction and increases in oxidative stress in the ageing brain have been linked with the onset of AD pathologies, including aberrant distribution and accumulation of hyperphosphorylated tau and deposition of amyloid- $\beta$  [24,44–47]. The aim of this study was to investigate whether induced mitochondrial dysfunction could elicit changes in tau phosphorylation and distribution in healthy neurons in cell culture, since mechanisms leading to hyperphosphorylation and redistribution of tau remain elusive, yet are central to understanding the pathogenesis of AD.

Here, we treated primary neuronal cell cultures derived from chick tecta with the mitochondrial inhibitor AM that rapidly depletes cellular ATP [20] and subsequently analyzed changes to phosphorylation and sub-cellular distribution of tau using Western blotting and immunolabeling. Whereas dephosphorylation was observed for every other epitope over 120 min, we observed a substantial increase in phosphorylation at the 12E8 site, an 'early

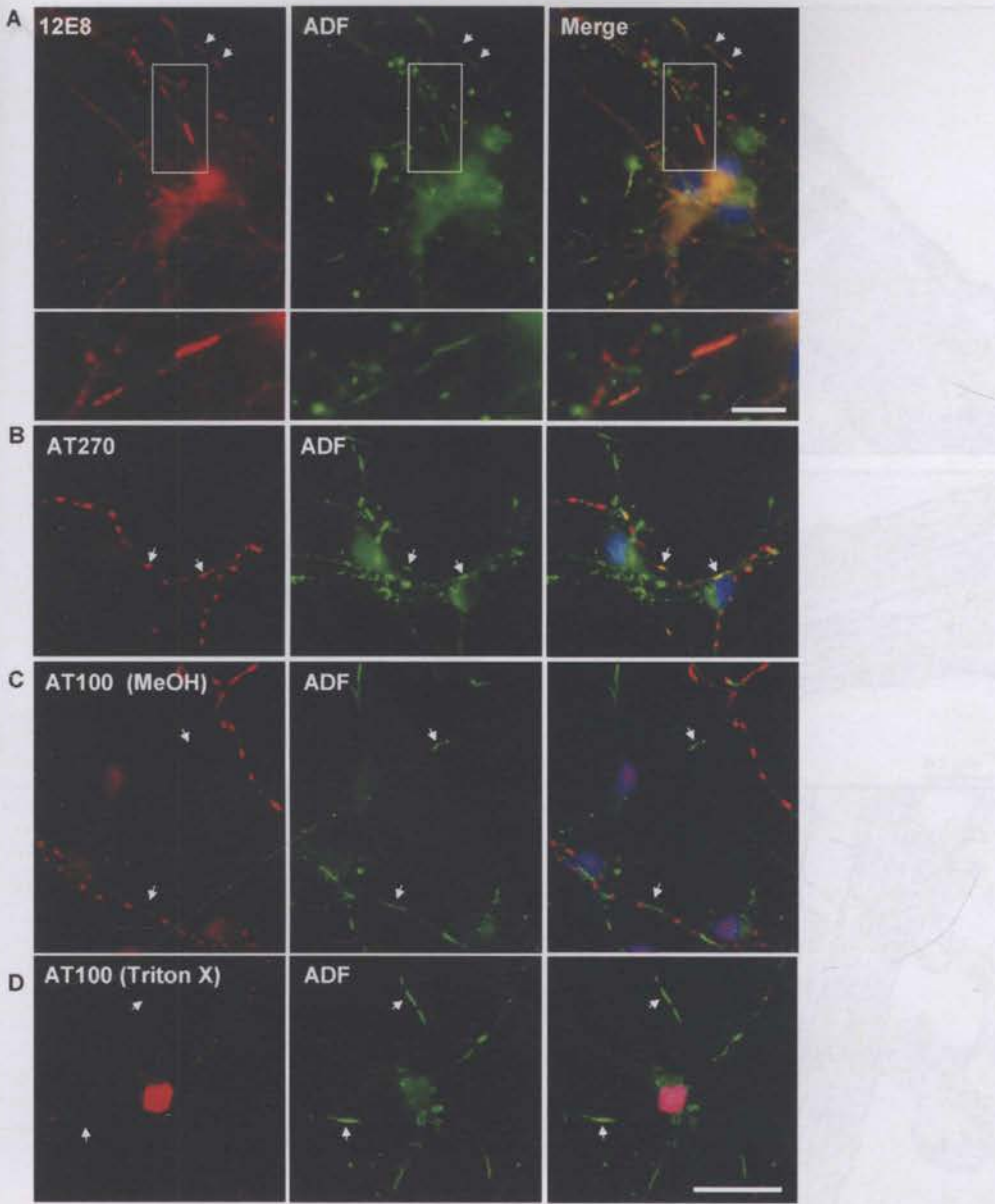


**Figure 4. Recruitment to AC rods during ATP reduction is specific for 'KXGS' phosphorylated species.** (A) Confirmation of 12E8-positive MAP/tau in AC rods during ATP reduction [20]. These inclusions often form in tandem arrays along neurites (arrows). Inset shown at higher magnification in lower panel of (A). Additional double-labeling was performed with AT270 (B) or AT100 (C) and ADF, to see if there was any relationship between these tau epitopes and AC rods. AC rods only sometimes overlapped with AT270 (B, arrows) and were never observed to colocalize with AT100, under either Triton-X or methanol permeabilization (C and D, arrows). These results suggest AC rods are distinct from MAP/tau-containing neuritic spheroids and recruit only the 12E8-phosphorylated MAP/tau isoform into distinct rod structures during ATP reduction. (A, B and D) = Triton X permeabilized. Scale bar = 20  $\mu$ m; 5  $\mu$ m (inset in (A)).  
doi:10.1371/journal.pone.0020878.g004

AD marker' antibody raised against 'KXGS' motifs in the MTBD of human tau [1,14] (Fig. 1). Notably, we previously demonstrated that this epitope is incorporated into AC rods, which are also generated under ATP depleting conditions [20] (confirmed here in Fig. 4A). The MAP protein family, including the vertebrate proteins tau, MAP2, doublecortin and MAP4 (the latter of which is non-neuronal) contain homologous conserved 'KXGS' repeat motifs in MTBDs [8,48,49]. In light of this, although tau is

probably the most predominant protein recognized by 12E8, we cannot completely discount that the 12E8-immunoreactivity we are observing in AC rods might be due to the presence of other MAPs in addition to tau.

In animal models of ischemia-reperfusion, rapid dephosphorylation of tau occurs during the initial ischemia and we have confirmed in our primary neuronal cell culture model that tau dephosphorylation not hyperphosphorylation is the immediate



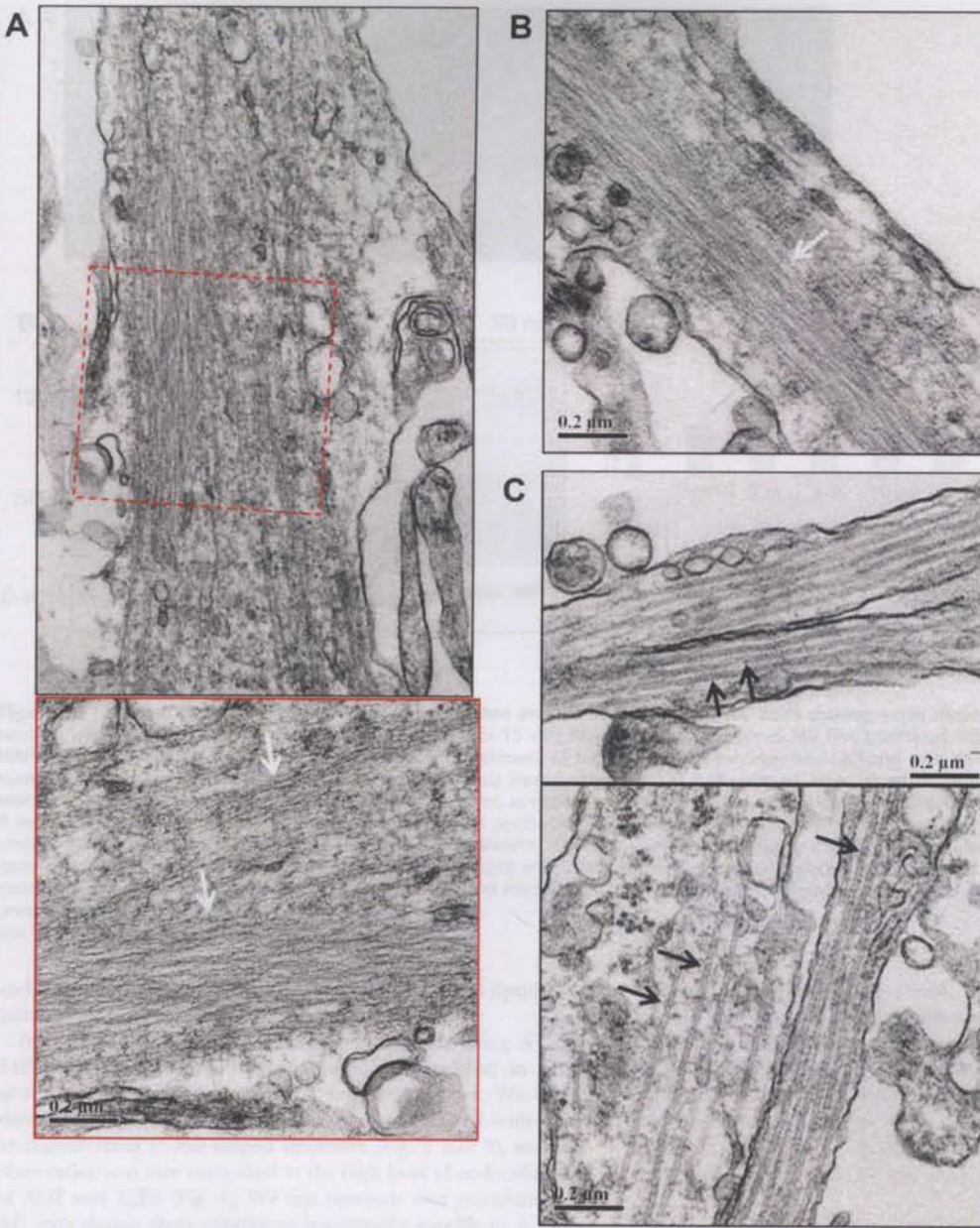


**Figure 5. Rod-like accumulations in neurites of primary chick neurons contain densely packed filaments.** Transmission electron micrographs of primary chick neurons treated with  $1 \mu\text{M}$  AM for 15 min, fixed and processed for TEM as described in Methods. (A) Densely packed linear arrays of filaments occur in the neurite (white arrows). The lower panel shows a higher magnification view of the boxed region above. (B) Another example of densely packed filaments within a neurite (white arrow). Here the filament bundle spans a large proportion of the width of the neurite. (C) In contrast, unaffected neurites contain individual separated microtubules approximately 24 nm in diameter (black arrows). Scale bars =  $0.2 \mu\text{m}$ .

doi:10.1371/journal.pone.0020878.g005

cellular response to ischemia (mimicked by transient ATP depletion) [50]. An interesting exception to this, consistent in both cell culture and in an animal model, is the enduring phosphorylation of the 12E8 epitope that has been reported in a gerbil-model of brain ischemia [51]. However after reperfusion, tau proteins are slowly phosphorylated and accumulate, resulting in hyperphosphorylation days after the initial ischemic event in the animal potentially due to the down-regulation of phosphatases or

induction of specific kinases, although the mechanism remains to be determined [50]. Importantly, our cell culture model is consistent with the animal models and mimics early signaling events directed to tau during transient brain ischemia. While we are not saying that such a large scale global ischemic event is directly relevant to AD, it is interesting that stroke is a significant risk factor for the later development of dementia and AD [50]. More commonly in AD, smaller less severe microischemic events



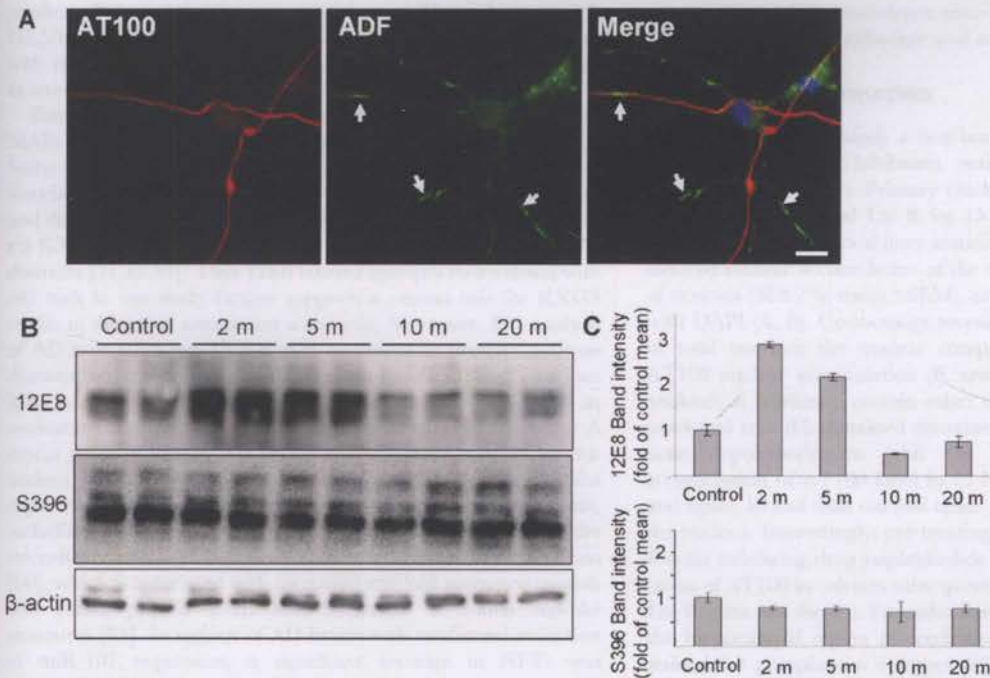


**Figure 6. 12E8 but not other tau epitopes aggregates and co-localizes with AC rods during actin depolymerization.** Primary chick neurons were treated with 1 μg/ml Latrunculin B (Lat B) for 15 min, fixed and immunostained. We first confirmed formation of both AC and 12E8-MAP/tau positive rods in Lat B treated cultures (data not shown), as has previously been observed [20] and then co-stained cultures for ADF with numerous tau epitopes. Whereas an abundance of AC rods were induced by Lat B (A, arrows), label for all tau epitopes, except 12E8, remained relatively smooth and evenly distributed throughout neurites, as shown here for AT100 (A) (other epitopes not shown). Western blots of lysates of Lat B-treated neurons were probed with the same battery of antibodies to tau phospho-epitopes. While most epitopes such as S396 (shown here) showed little change in phosphorylation during Lat B treatment, the 12E8 epitope was strongly phosphorylated within 2 min of treatment (B, C). Band intensities were quantified for each time-point for 12E8 and S396 immunoblots (C) with each lane normalized to individual β-actin loading controls and then calculated as a percentage of control band intensities. At 2 min, 12E8 phosphorylation was  $2.9 \pm 0.1$ -fold higher than control means (mean  $\pm$  min/max intensities). Scale bar = 10 μm. doi:10.1371/journal.pone.0020878.g006

and highly localized cytopathology could reflect a sub-optimal or failing local microvasculature [52].

In contrast to 12E8, other phosphoepitopes including AT270, S422, AT100, S396 and S404 mostly accumulated in small neuritic spheroid swellings in ATP depleted neurons. We found these phosphoepitopes only occasionally co-localized with ADF immunostaining in rod-shaped structures (Fig. 2 and 3), and this observation was rare compared to the high level of co-localization of ADF and 12E8 (Fig. 4). We can conclude that recruitment to AC rods during these conditions is primarily specific to KXGS-phosphorylated species in the initial stages. The occasional rod-shaped structure formed by S404 and AT270 label (Fig. 2) and rare co-localization of AT270 with ADF in AC rods, suggests that other phosphoepitopes of tau may appear in AC rods later, a subject of ongoing investigation. In primary neurons, Lat B-induced actin depolymerization also resulted in specific recruitment of 12E8 epitopes to AC rods, with a concomitant ~3-fold increase in the signal of the band recognized by 12E8 on immunoblots following 2 min Lat-B treatment (Fig. 6). By contrast, S396 was neither seen to redistribute into spheroid or rod-like aggregates nor deviate from control levels of phosphorylation. These data suggest that actin rearrangement in this cell model triggered either by changes in cellular ATP levels or directly by actin depolymerizing drugs may be an upstream effector of KXGS phosphorylation and redistribution of MAP into AC rods. Converging or independent signaling mechanisms triggered by

mitochondrial dysfunction, excess glutamate, oxidative stress, calcium deregulation or other effectors leading to AC rods and MAP/tau redistribution *in vivo* are potentially multifold [22,43,47,53]. Oxidative stress and calcium have previously been implicated in the cytoskeletal pathology of AD and studies have shown both calcium-dependent and -independent pathways leading to AC rods in various model systems [22,43,53]. More work is needed to delineate the involvement of these pathways in AD.

A predominant function of tau protein is to bind and stabilize axonal MTs – the tracks for cargo transport to synaptic terminals. Hyperphosphorylation of tau in the MTBD by microtubule affinity regulating kinase (MARK)/PAR1 or other kinases gives rise to a destabilized MT network and concomitant self-assembly of the increased concentration of unbound tau [13,15,16]. This self-assembled tau is purported to serve as a seed for further assembly of redistributed tau into PHFs along neurites (neuropil threads) and in the somatodendritic domain (neurofibrillary tangles) [1,2,54,55]. Albeit in a cell model and not demonstrated *in situ* in brain tissue, our results suggest that AC rods may contribute to the sequestration and accumulation of unbound tau via its phosphorylated MTBD in neurites leading to neuropil thread-like inclusions and potentially PHFs. We speculate that rapid depolymerization and rearrangement of the actin cytoskeleton during rod assembly may induce activation of MARK/Par-1 or other kinases, the former of which has previously been



implicated in conferring tau toxicity in *Drosophila* models [15,56,57]. Consistent with this, activation of MARK correlates with elevated phosphorylation and dendritic accumulation of tau in stressed primary hippocampal neurons [47].

Extensive studies have demonstrated a role for tau and other MAPs in cross-linking and bundling of actin filaments [28–37]. Some studies have additionally demonstrated that MAP-actin association is regulated by the reversible phosphorylation of MAPs and that furthermore, tau and MAP2 interactions with actin occur via KXGS-containing motifs in the repeat regions of their MTBD domains [31,32,58]. That 12E8 labeled epitopes co-localized with AC rods in our study further supports a central role for KXGS motifs in the rapid association with actin. Moreover, EM analysis of AC rods following 15 min AM treatment in primary neurons demonstrate the presence of filamentous bundles (Fig. 5), and we speculate that AC-actin bundles form initially and serve as nucleation sites for subsequent recruitment of 12E8 epitopes. A recent study of human AD brains provides some support for this notion, which reported a correlation between increased cofilin expression and tau pathology in specific regions of the brain, including the temporal cortex [59–61]. Expression of the microRNA miR-107 has been shown to decrease in AD brain [60], which is associated with increased amyloid precursor protein and cofilin protein levels and formation of cofilin rod-like structures [61]. In regions of AD brains with confirmed reduction of miR-107 expression, a significant increase in NFTs was observed when compared with adjacent tissue expressing normal levels of miR-107 [59].

Further investigations are required to delineate the mechanisms facilitating the interaction between MAP and AC-actin rods and whether it is direct or indirect. Important questions that remain to be answered are whether the KXGS phosphorylation of tau or other MAPs is causative or correlative with its association with actin or AC rods and what mechanism facilitates the interaction between 12E8 epitopes and AC rods. Recent characterization of isolated AC rods demonstrated the presence of the scaffolding protein 14-3-3 $\zeta$  [42] which was also shown to be associated with 12E8 within AC rods (unpublished observations LSM and JRB), suggesting that 14-3-3 $\zeta$  may have a role either in rod structure or in a longer time-dependent maturation of MAP/tau phosphorylation, as has previously been suggested in other studies [62–64]. Answering these questions is the subject of ongoing studies.

In summary, we have shown that mitochondrial inhibition is associated with specific and sustained detection of 12E8 epitopes indicative of MAP phosphorylation in MTBD KXGS motifs, but a concomitant dephosphorylation of other phospho-tau epitopes. The combined effects of MT destabilization and accumulation of MAP/tau and cofilin-actin rods in the neurites is proposed to inhibit axonal transport, ultimately leading to synaptic pruning and neuronal death [47,65–68]. The present findings therefore suggest that targeting disrupted energy metabolism, mitochondrial dysfunction and downstream actin reorganization in aging cells

may help prevent neurodegeneration associated with aberrant phosphorylation, redistribution and self-assembly of tau.

## Supporting Information

**Figure S1** AT100 labels a non-tau component in the nucleus during mitochondrial inhibition, actin depolymerization and in postmortem AD brain. Primary chick neurons were treated with 1  $\mu$ M AM or 1  $\mu$ g/ml Lat B for 15 min, fixed, immunostained and analyzed via confocal laser scanning. ATP reduction with AM induced nuclear accumulation of the AT100 label in a proportion of neurons ( $36 \pm 2\%$ ; mean  $\pm$  SEM), as indicated by co-localization with DAPI (A, B). Co-stainings revealed no obvious translocation of total tau into the nuclear compartment in cells exhibiting AT100 nuclear accumulation (B, arrows), suggesting the AT100 antibody is labeling a protein other than tau. AT100 labeling in untreated cells (C) remained contained in the neurites. Similarly, actin depolymerization with Lat B gave rise to nuclear accumulation of AT100 label in  $22 \pm 2\%$  cells (mean  $\pm$  SEM) (D) and again, lack of total tau and other epitopes such as S396 (D) in the nucleus. Interestingly, pre-treating cultures for 2 min with the F-actin stabilizing drug jasplakinolide prevented nuclear accumulation of AT100 in cultures subsequently treated with either AM or Lat-B (data not shown). Formalin-fixed 7  $\mu$ m brain sections from the hippocampal region of confirmed AD cases were immunostained for phospho-tau epitopes. S396 label (E) and other tau epitopes (data not shown) often accumulated in flame-shaped tangles, though remained largely absent from the nucleus (E, arrows). By contrast, double-labeling studies showed AT100 label frequently appearing in the nuclear compartment as evidenced by its co-localization with DAPI (F, arrowhead). In the same neurons, S396 was exclusively contained within the somal compartment (F, arrow). Although characterization and identification of this AT100-positive protein is beyond the scope of the present study, further investigation of this stress-induced response would be valuable as the appearance of the epitope in the nucleus specifically occurs in stressed cells (ATP depleted) or AD brain and not control cells. Images in (A–D): confocal microscope; (E, F): optical microscope. Scale bars = 10  $\mu$ m (A, F); 20  $\mu$ m (B–E). (TIF)

## Acknowledgments

We thank Prof. Peter Seubert, Elan Pharmaceuticals for providing the 12E8 antibody. We also thank Denise Nergensau for help with the TEM and Dr O'Neil Wiggan for valuable discussions and suggestions in the development of this manuscript.

## Author Contributions

Conceived and designed the experiments: CG ITW LSM JRB. Performed the experiments: ITW DG LSM. Analyzed the data: ITW CG JRB LSM. Wrote the paper: ITW CG JRB.

## References

1. Augustinack J, Schneider A, Mandelkow E, Hyman B (2002) Specific tau phosphorylation sites correlate with severity of neuronal cytopathology in Alzheimer's disease. *Acta Neuropathologica* 103: 26–35.
2. Braak H, Alafuzoff I, Arzberger T, Kretschmar H, Tredici K (2006) Staging of Alzheimer disease-associated neurofibrillary pathology using paraffin sections and immunocytochemistry. *Acta Neuropathologica* 112: 389–404.
3. Giannakopoulos P, von Gunten A, Kovari E, Gold G, Herrmann FR, et al. (2007) Stereological analysis of neuropil threads in the hippocampal formation: relationships with Alzheimer's disease neuronal pathology and cognition. *Neuropathology and Applied Neurobiology* 33: 334–343.
4. Velasco ME, Smith MA, Siedlak SL, Numomura A, Perry G (1998) Striation is the characteristic neuritic abnormality in Alzheimer disease. *Brain Research* 813: 329–333.
5. Mitchell TW, Nisanov J, Han L-Y, Mufson EJ, Schneider JA, et al. (2000) Novel Method to Quantify Neuropil Threads in Brains from Elders With or Without Cognitive Impairment. *Journal of Histochemistry and Cytochemistry* 48: 1627–1638.
6. Schmidt M, Murray J, Trojanowski J (1993) Continuity of neuropil threads with tangle-bearing and tangle-free neurons in Alzheimer disease cortex. *Molecular and Chemical Neuropathology* 18: 299–312.



7. Garcia ML, Cleveland DW (2001) Going new places using an old MAP: tau, microtubules and human neurodegenerative disease. *Current Opinion in Cell Biology* 13: 41–48.
8. Dehmelt L, Halpain S (2004) The MAP2/Tau family of microtubule-associated proteins. *Genome Biology* 6: 204.
9. Gauthier-Kemper A, Weissmann C, Golovayshkina N, Sebó-Lemke Z, Drewes G, et al. (2011) The frontotemporal dementia mutation R406W blocks tau's interaction with the membrane in an annexin A2-dependent manner. *Journal of Cell Biology* 192: 647–646.
10. Lindvall G, Cole RD (1984) Phosphorylation affects the ability of tau protein to promote microtubule assembly. *Journal of Biological Chemistry* 259: 5301–5305.
11. Mandelkow EM, Biernat J, Drewes G, Gustke N, Trinczek B, et al. (1995) Tau domains, phosphorylation, and interactions with microtubules. *Neurobiology of Aging* 16: 355–362.
12. Biernat J, Gustke N, Drewes G, Mandelkow E, Mandelkow E (1993) Phosphorylation of Ser262 strongly reduces binding of tau to microtubules: Distinction between PHF-like immunoreactivity and microtubule binding. *Neuron* 11: 153–163.
13. Zhou L-X, Zeng Z-Y, Du J-T, Zhao Y-F, Li Y-M (2006) The self-assembly ability of the first microtubule-binding repeat from tau and its modulation by phosphorylation. *Biochemical and Biophysical Research Communications* 348: 637–642.
14. Seubert P, Mawal-Dewan M, Barbour R, Jakes R, Goedert M, et al. (1995) Detection of Phosphorylated Ser262 in Fetal Tau, Adult Tau, and Paired Helical Filament Tau. *Journal of Biological Chemistry* 270: 18917–18922.
15. Drewes G, Ebneth A, Preuss U, Mandelkow E-M, Mandelkow E (1997) MARK, a Novel Family of Protein Kinases That Phosphorylate Microtubule-Associated Proteins and Trigger Microtubule Disruption. *Cell* 89: 297–308.
16. Alonso AD, Zaidi T, Novak M, Grundke-Iqbal I, Iqbal K (2001) Hyperphosphorylation induces self-assembly of tau into tangles of paired helical filaments/straight filaments. *Proceedings of the National Academy of Science USA* 98: 6923–6928.
17. Fischer D, Mukrasch MD, Biernat J, Bibow S, Blackledge M, et al. (2009) Conformational changes specific for pseudo-phosphorylation at Ser262 selectively impair binding of tau to microtubules. *Biochemistry* 48: 10047–10055.
18. Goedert M (1993) Tau protein and the neurofibrillary pathology of Alzheimer's disease. *Trends in Neurosciences* 16: 460–465.
19. Braak H, Braak E (1995) Staging of Alzheimer's disease-related neurofibrillary changes. *Neurobiology of Aging* 16: 271–278.
20. Whiteman IT, Gervasio OL, Cullen KM, Guillemin GJ, Jeong EV, et al. (2009) Activated Actin-Depolymerizing Factor/Cofilin Sequesters Phosphorylated Microtubule-Associated Protein during the Assembly of Alzheimer-Like Neuritic Cytoskeletal Striations. *Journal of Neuroscience* 29: 12994–13005.
21. Minamide L, Striegl A, Boyle J, Meberg P, Bamberg J (2000) Neurodegenerative stimuli induce persistent ADF/cofilin-actin rods that disrupt distal neurite function. *Nature Cell Biology* 2: 628–636.
22. Bamberg J, Bernstein B, Davis R, Flynn K, Goldsburgy C, et al. (2010) ADF/Cofilin-actin rods in neurodegenerative diseases. *Current Alzheimer Research* 7: 241–250.
23. Blass JP (2000) The Mitochondrial Spiral: An Adequate Cause of Dementia in the Alzheimer's Syndrome. *Annals of the New York Academy of Sciences* 924: 170–183.
24. Lin MT, Beal MF (2006) Mitochondrial dysfunction and oxidative stress in neurodegenerative diseases. *Nature* 443: 787–795.
25. Wang X, Su B, Zheng L, Perry G, Smith MA, et al. (2009) The role of abnormal mitochondrial dynamics in the pathogenesis of Alzheimer's disease. *Journal of Neurochemistry* 109: 153–159.
26. Su B, Wang X, Zheng L, Perry G, Smith MA, et al. (2010) Abnormal mitochondrial dynamics and neurodegenerative diseases. *Biochimica et Biophysica Acta (BBA) - Molecular Basis of Disease* 1802: 135–142.
27. Kapogiannis D, Mattson M (2010) Disrupted energy metabolism and neuronal circuit dysfunction in cognitive impairment and Alzheimer's disease. *Lancet Neurology* 10: 187–198.
28. Griffith LM, Pollard TD (1978) Evidence for actin filament-microtubule interaction mediated by microtubule-associated proteins. *Journal of Cell Biology* 78: 958–965.
29. Griffith LM, Pollard TD (1982) The interaction of actin filaments with microtubules and microtubule-associated proteins. *Journal of Biological Chemistry* 257: 9143–9151.
30. Selden SC, Pollard TD (1983) Phosphorylation of microtubule-associated proteins regulates their interaction with actin filaments. *Journal of Biological Chemistry* 258: 7064–7071.
31. Correas I, Padilla R, Avila J (1990) The tubulin-binding sequence of brain microtubule-associated proteins, tau and MAP-2, is also involved in actin binding. *Journal of Biochemistry* 269: 61–64.
32. Moraga DM, Nuñez P, Garrido J, Maccioni RB (1993) A Tau Fragment Containing a Repetitive Sequence Induces Bundling of Actin Filaments. *Journal of Neurochemistry* 61: 979–986.
33. Yamauchi PS, Purich DL (1993) Microtubule-Associated Protein Interactions with Actin Filaments: Evidence for Differential Behavior of Neuronal MAP-2 and Tau in the Presence of Phosphatidylinositol. *Biochemical and Biophysical Research Communications* 190: 710–715.
34. Dehmelt L, Halpain S (2004) Actin and microtubules in neurite initiation: Are MAPs the missing link? *Journal of Neurobiology* 50: 18–33.
35. He H, Wang X, Pan R, Wang D, Liu M, et al. (2009) The proline-rich domain of tau plays a role in interactions with actin. *BMC Cell Biology* 10: 81.
36. Fulga T, Elson-Schwab I, Khurana V, Steinbilb M, Spiers T, et al. (2006) Abnormal bundling and accumulation of F-actin mediates tau-induced neuronal degeneration in vivo. *Nat Cell Biol* 9: 139–148.
37. Gallo G (2007) Tau is actin up in Alzheimer's disease. *Nat Cell Biol* 9: 133–134.
38. Yoshida H, Goedert M (2002) Molecular Cloning and Functional Characterization of Chicken Brain Tau: Isoforms with up to Five Tandem Repeats. *Biochemistry* 41: 15203–15211.
39. Shaw AE, Minamide LS, Bill CL, Funk JD, Maiti S, et al. (2004) Cross-reactivity of antibodies to actin-depolymerizing factor/cofilin family proteins and identification of the major epitope recognized by a mammalian actin-depolymerizing factor/cofilin antibody. *Electrophoresis* 25: 2611–2620.
40. Goldsburgy C, Whiteman IT, Jeong EV, Lin Y-A (2008) Oxidative stress increases levels of endogenous amyloid- $\beta$  peptides secreted from primary chick brain neurons. *Aging Cell* 7: 771–775.
41. Davis RC, Maloney MT, Minamide LS, Flynn KC, Stonebraker MA, et al. (2009) Mapping Cofilin-Actin Rods in Stressed Hippocampal Slices and the Role of cdc42 in Amyloid- $\beta$ -Induced Rods. *Journal of Alzheimer's Disease* 18(1): 35–50.
42. Minamide LS, Maiti S, Boyle JA, Davis RC, Coppinger JA, et al. (2010) Isolation and Characterization of Cytoplasmic Cofilin-Actin Rods. *Journal of Biological Chemistry* 285: 5450–5460.
43. Bamberg JR, Bloom GS (2009) Cytoskeletal pathologies of Alzheimer disease. *Cell Motility and the Cytoskeleton* 66: 635–649.
44. Smith MA, Nunomura A, Lee H-g, Zhu X, Moreira PI, et al. (2005) Chronological primacy of oxidative stress in Alzheimer disease. *Neurobiology of Aging* 26: 579–580.
45. Melov S, Adlard PA, Morten K, Johnson F, Golden TR, et al. (2007) Mitochondrial Oxidative Stress Causes Hyperphosphorylation of Tau. *PLoS ONE* 2: e536.
46. Escobar-Khondiker M, Hollerhage M, Muriel M-P, Champy P, Bach A, et al. (2007) Annonacin, a Natural Mitochondrial Complex I Inhibitor, Causes Tau Pathology in Cultured Neurons. *Journal of Neuroscience* 27: 7827–7837.
47. Zempel H, Thies E, Mandelkow E, Mandelkow E-M (2010)  $\beta$  Oligomers Cause Localized Ca<sup>2+</sup> Elevation, Missorting of Endogenous Tau into Dendrites, Tau Phosphorylation, and Destruction of Microtubules and Spines. *Journal of Neuroscience* 30: 11938–11950.
48. Lewis SA, Wang DH, Cowan NJ (1988) Microtubule-associated protein MAP2 shares a microtubule binding motif with tau protein. *Science* 242: 936–939.
49. Schaar B, Kinoshita K, McConnell S (2004) Doublecortin microtubule affinity is regulated by a balance of kinase and phosphatase activity at the leading edge of migrating neurons. *Neuron* 41: 203–213.
50. Wen Y, Yang S, Liu R, Simpkins J (2004) Transient cerebral ischemia induces site-specific hyperphosphorylation of tau protein. *Brain Research* 1022: 30–38.
51. Gordon-Krajcar W, Kozniowska E, Lazarewicz J, Ksiazek-Reding H (2007) Differential Changes in Phosphorylation of Tau at PHF-1 and 12E8 Epitopes During Brain Ischemia and Reperfusion in Gerbils. *Neurochemical Research* 32: 729–737.
52. Cullen KM, Kocsi Z, Stone J (2006) Microvascular pathology in the aging human brain: Evidence that senile plaques are sites of microhaemorrhages. *Neurobiology of Aging* 27: 1786–1796.
53. Mattson MP (2010) ER calcium and Alzheimer's disease: in a state of flux. *Science Signaling* 3: pe10.
54. Probst A, Tolnay M, Langui D, Goedert M, Spillantini MG (1996) Pick's disease: hyperphosphorylated tau protein segregates to the somatoaxonal compartment. *Acta Neuropathologica* 92: 588–596.
55. Delacourte A, Sergeant N, Wattez A, Gauvreau D, Robitaille Y (1998) Vulnerable neuronal subsets in Alzheimer's and Pick's disease are distinguished by their tau isoform distribution and phosphorylation. *Annals of Neurology* 43: 193–204.
56. Timm T, Li XY, Biernat J, Jiao J, Mandelkow E, et al. (2003) MARKK, a Ste20-like kinase, activates the polarity-inducing kinase MARK/PAR-1. *EMBO Journal* 22: 5090–5101.
57. Nishimura I, Yang Y, Lu B (2004) PAR-1 Kinase Plays an Initiator Role in a Temporally Ordered Phosphorylation Process that Confers Tau Toxicity in *Drosophila*. *Cell* 116: 671–682.
58. Ozer RS, Halpain S (2000) Phosphorylation-dependent Localization of Microtubule-associated Protein MAP2c to the Actin Cytoskeleton. *Molecular Biology of the Cell* 11: 3573–3587.
59. Nelson P, Wang W-X (2010) MiR-107 is Reduced in Alzheimer's Disease Brain Neocortex: Validation Study. *Journal of Alzheimer's Disease* 21: 75–79.
60. Wang W-X, Rajeev BW, Stromberg AJ, Ren N, Tang G, et al. (2008) The Expression of MicroRNA miR-107 Decreases Early in Alzheimer's Disease and May Accelerate Disease Progression through Regulation of  $\beta$ -Site Amyloid Precursor Protein-Cleaving Enzyme 1. *Journal of Neuroscience* 28: 1213–1223.
61. Yao J, Hennessey T, Flynt A, Lai E, Beal MF, et al. (2011) MicroRNA-Related Cofilin Abnormality in Alzheimer's Disease. *PLoS ONE* 5: e15346.
62. Hashiguchi M, Sobue K, Paudel H (2000) 14-3-3-zeta is an effector of tau protein phosphorylation. *Journal of Biological Chemistry* 275: 25247–25254.
63. Hernandez F, Cuadros R, Avila J (2004) Zeta 14-3-3 protein favours the formation of human tau fibrillar polymers. *Neuroscience Letters* 357: 143–146.



64. Umahara T, Uchihara T, Tsuchiya K, Nakamura A, Iwamoto T, et al. (2004) 14-3-3 proteins and zeta isoform containing neurofibrillary tangles in patients with Alzheimer's disease. *Acta Neuropathologica* 108: 279-286.

65. Praprotnik D, Smith M, Richey P, Vinters H, Perry G (1996) Filament heterogeneity within the dystrophic neurites of senile plaques suggests blockage of fast axonal transport in Alzheimer's disease. *Acta Neuropathologica* 91: 226-235.

66. Ebner A, Godemann R, Stamer K, Illenberger B, Trinczek B, et al. (1998) Overexpression of tau protein inhibits kinesin-dependent trafficking of vesicles,

mitochondria and endoplasmic reticulum: implications for Alzheimer's disease. *Journal of Cell Biology* 143: 777-794.

67. Mandelkow E-M, Thies E, Trinczek B, Biernat J, Mandelkow E (2004) MARK/PAR1 kinase is a regulator of microtubule-dependent transport in axons. *Journal of Cell Biology* 167: 99-110.

68. Baas PW, Qiang L (2005) Neuronal microtubules: when the MAP is the roadblock. *Trends in Cell Biology* 15: 183-187.

*Department of Pharmacology and Molecular Biology and Behavioral, Cognitive and Integrative Neurosciences, The George Washington University, 2201 Reservoir Road, NW, Washington, DC 20057, United States; Department of Neurobiology, Georgetown University, 3900 Reservoir Road, NW, Washington, DC 20057, United States; Department of Neurobiology and Behavioral, Cognitive and Integrative Neurosciences, The George Washington University, 2201 Reservoir Road, NW, Washington, DC 20057, United States*

**Abstract:** Dysregulation of microtubule dynamics in axons leading to growth cone collapse is associated with neuronal dysfunction and degeneration including Alzheimer's disease, Parkinson's disease, Huntington's disease, and multiple forms of frontotemporal dementia. Alzheimer's disease brain pathology is characterized by neurofibrillary tangles (NFTs) composed of hyperphosphorylated tau protein. We used a mouse model of Alzheimer's disease to study the role of tau in axonal transport. Normal cytoplasmic tau is essential for axonal transport of synaptic vesicles and other organelles. In contrast, hyperphosphorylated tau is a major cause of synaptic loss without disruption of axonal transport in dystrophic neurites. We used a mouse model of Alzheimer's disease to study the role of tau in axonal transport. Normal cytoplasmic tau is essential for axonal transport of synaptic vesicles and other organelles. In contrast, hyperphosphorylated tau is a major cause of synaptic loss without disruption of axonal transport in dystrophic neurites. We used a mouse model of Alzheimer's disease to study the role of tau in axonal transport. Normal cytoplasmic tau is essential for axonal transport of synaptic vesicles and other organelles. In contrast, hyperphosphorylated tau is a major cause of synaptic loss without disruption of axonal transport in dystrophic neurites.

**Keywords:** Cytoskeleton, Alzheimer's disease, hippocampus, axonal transport, amyloid beta, oxidative stress, Huntington's disease, protein and gene expression analysis

**ALZHEIMER DISEASE PATHOLOGY AND PRESUMPTIVE MECHANISMS**

Alzheimer disease (AD) is diagnosed post mortem when the classical pathological hallmarks are extracellular plaques containing amyloid beta (Aβ) peptide [1] and intracellular neurofibrillary tangles of the hyperphosphorylated microtubule-associated protein tau [2]. One of the major challenges in AD research is to identify the mechanisms that prevent the whole nervous system from neuronal and synaptic AD brain damage. AD is an age-related disease, and early onset forms are associated with autosomal dominant inheritance [3]. Mitochondrial defects (e.g. beta-amyloid and amyloidosis) have been implicated in progressive dementia [4] and also could contribute to sporadic AD. Mitochondrial dysfunction produces reactive oxygen species, following oxidative stress, or indirectly, other forms of oxidative stress could lead to neurofibrillary dysfunction. Regardless of the nature, mitochondrial insufficiency decreases cellular ATP. Another possible AD disease mechanism is microtubule dysfunction, the

major cell cytoskeleton component [5, 6]. Disturbance microtubule likely occurs as a result of decreased glutamate and neuronal ATP decline. Any of these mechanisms for AD disease could be associated by a falling rate of microtubule that impacts transport and exchange mechanisms.

**COFFIN PATHOLOGY IN AD**

A widely increased neuronal pathology of AD brain, axonal cytoskeleton pathology because of the abnormal localization of coffinin [7, 8], may help explain the accumulation of sporadic AD and light in pathology of familial AD. Axonal dysregulation factor (ADF) and coffinin are two members of an essential vesicle family that enhance the rapid assembly and disassembly dynamics of actin, which is critical to many cell behaviors. The two proteins share 75% sequence identity, have the same single phosphorylation site and crystal nuclear localization sequence, and have evolutionarily similar but quantitatively different effects on actin in vivo and in vitro [9-11]. The proteins have together with actin in the same compartment of axonal transport [12, 13], suggesting a role for ADF/coffinin in transport and maturation of axons and cytoskeletal structures during neuronal development. ADF/coffinin expression patterns and function

† Author contributions: The author(s) conceived and designed the experiments, performed the experiments, analyzed the data, contributed reagents and materials, wrote the paper, and approved the final version of the manuscript. All authors contributed equally and significantly to writing this paper. All authors read and approved the final manuscript.

## ADF/Cofilin-Actin Rods in Neurodegenerative Diseases

J.R. Bamburg<sup>1,\*</sup>, B.W. Bernstein<sup>1</sup>, R.C. Davis<sup>1</sup>, K.C. Flynn<sup>2</sup>, C. Goldsbury<sup>3</sup>, J.R. Jensen<sup>1</sup>, M.T. Maloney<sup>4</sup>, I.T. Marsden<sup>1</sup>, L.S. Minamide<sup>1</sup>, C.W. Pak<sup>1</sup>, A.E. Shaw<sup>1</sup>, I. Whiteman<sup>3</sup> and O. Wiggan<sup>1</sup>

<sup>1</sup>Department of Biochemistry and Molecular Biology and Molecular, Cellular and Integrative Neuroscience Program, Colorado State University, Fort Collins, CO 80523, USA; <sup>2</sup>Axon Growth and Regeneration, Max Planck Institute of Neurobiology, Martinsried, Germany; <sup>3</sup>The Brain & Mind Research Institute, School of Medical Sciences, University of Sydney, 100 Mallet Street, Camperdown, NSW 2006, Australia; <sup>4</sup>Department of Neurology and Neurological Sciences, Stanford University School of Medicine, Stanford, CA, USA

**Abstract:** Dephosphorylation (activation) of cofilin, an actin binding protein, is stimulated by initiators of neuronal dysfunction and degeneration including oxidative stress, excitotoxic glutamate, ischemia, and soluble forms of  $\beta$ -amyloid peptide ( $A\beta$ ). Hyperactive cofilin forms rod-shaped cofilin-saturated actin filament bundles (rods). Other proteins are recruited to rods but are not necessary for rod formation. Neuronal cytoplasmic rods accumulate within neurites where they disrupt synaptic function and are a likely cause of synaptic loss without neuronal loss, as occurs early in dementias. Different rod-inducing stimuli target distinct neuronal populations within the hippocampus. Rods form rapidly, often in tandem arrays, in response to stress. They accumulate phosphorylated tau that immunostains for epitopes present in "striated neuropil threads," characteristic of tau pathology in Alzheimer disease (AD) brain. Thus, rods might aid in further tau modifications or assembly into paired helical filaments, the major component of neurofibrillary tangles (NFTs). Rods can occlude neurites and block vesicle transport. Some rod-inducing treatments cause an increase in secreted  $A\beta$ . Thus rods may mediate the loss of synapses, production of excess  $A\beta$ , and formation of NFTs, all of the pathological hallmarks of AD. Cofilin-actin rods also form within the nucleus of heat-shocked neurons and are cleared from cells expressing wild type huntingtin protein but not in cells expressing mutant or silenced huntingtin, suggesting a role for nuclear rods in Huntington disease (HD). As an early event in the neurodegenerative cascade, rod formation is an ideal target for therapeutic intervention that might be useful in treatment of many different neurological diseases.

**Keywords:** Cytoskeleton, Alzheimer disease, hippocampus, vesicle transport, amyloid beta, oxidative stress, Huntington disease, peptidomimetics, phosphorylated tau

### ALZHEIMER DISEASE PATHOLOGY AND PRESUMPTIVE INITIATORS

Alzheimer Disease (AD) is diagnosed post mortem where the classical pathological hallmarks are extracellular plaques containing amyloid beta ( $A\beta$ ) peptides [1] and intra-neuronal neurofibrillary tangles of the hyperphosphorylated microtubule-associated protein tau [2]. One of the major challenges in AD research is to identify the mechanisms that generate the same common pathologies in sporadic and familial AD brains. Because AD is an age-related disorder, one early focus for its cause was mitochondrial dysfunction due to aging [3]. Mitochondrial poisons (e.g. herbicides and insecticides) have been implicated in Parkinson disease [4] and also could contribute to sporadic AD. Mitochondrial dysfunction produces reactive oxygen species, initiating oxidative stress, or reciprocally, other initiators of oxidative stress could lead to mitochondrial dysfunction. Regardless of the initiator, mitochondrial insufficiency decreases cellular ATP. Another potential AD initiator is excessive extracellular glutamate, the

major CNS excitatory neurotransmitter [5, 6]. Glutamate excitotoxicity likely occurs as a result of decreased glial uptake and neuronal ATP decline. Any of these mechanisms for AD initiation could be exacerbated by a failing cerebrovasculature that impacts clearance and exchange mechanisms.

### COFILIN PATHOLOGY IN AD

A seldom examined molecular pathology of AD brains, named cofilin pathology because of the abnormal immunostaining of cofilin [7, 8], may help explain the development of sporadic AD and link its pathology to familial AD. Actin depolymerizing factor (ADF) and cofilin are two members of an essential protein family that enhances the rapid assembly and/or disassembly (dynamics) of actin, which is critical to many cell behaviors. The two proteins share 70% sequence identity, have the same single phosphoregulatory site and cryptic nuclear localization sequence, and have qualitatively similar but quantitatively different effects on actin *in vitro* and *in vivo* [9-11]. The proteins travel together with actin in the same component of slow axonal transport [12, 13], suggesting a role for ADF/cofilin in the transport and exchange of actin into cytoskeletal structures during neuronal development. Rodent hippocampal neurons and human

\*Address correspondence to this author at the Department of Biochemistry and Molecular Biology, Colorado State University, Fort Collins, CO 80523, USA; Tel: 970-491-6096; Fax: 970-491-0494; E-mail: jbamburg@lamar.colostate.edu



brain contain 5-12 fold more cofilin than ADF [7, 14]; hence we will hereafter just refer to cofilin unless studies have been done specifically to express or examine ADF.

At low ratios (<1:100) to actin subunits in filamentous actin (F-actin), cofilin severs filaments forming more filament ends that can either nucleate filament growth or more rapidly depolymerize filaments, depending on the amount of available actin monomers [15]. At higher ratios, cofilin severing is rapid but transient as its binding to F-actin stabilizes a twisted form of actin, eliminating the phalloidin binding site and allowing filaments to bundle [15, 16] (reviewed in [17]). Cofilin's ability to bind to actin and dynamize filament assembly/disassembly is inhibited by phosphorylation of its ser3 by LIM kinase and other kinases (reviewed in [11]). Active cofilin, generated by specific and highly regulated phosphatases in the slingshot [18] and chronophin [19] families, binds ADP-actin with higher affinity than ATP-actin [20, 21]. In stressed cells, ATP declines, oxidative potential increases, and these effects activate cofilin phosphatases [22, 23]. ATP-actin levels decrease [24], and cofilin binds ADP-actin generating cofilin-saturated ADP-actin filaments, which aggregate *in vivo* [7] or *in vitro* (Minamide *et al.*, submitted) to form rods. Many rod-inducing stresses decrease the primary cellular reducing agent reduced glutathione, and the four free sulfhydryl groups of cofilin are prime targets for oxidation [25, 26], which can enhance actin bundling into rods *in vitro*.

Cofilin immunostaining (IHC and IF) was observed in ovoid aggregates and in rod-like tandem arrays in AD brain [7]. Recently, Sandra Siedlak and George Perry found electron micrographs that showed a rod-like bundle of actin-

sized filaments in a human AD brain section [17]. The similarities between the ultrastructure of this bundle and that of cofilin-actin rods induced experimentally in organotypic slices of rodent brain (see below) are striking.

**ISOLATION AND CHARACTERIZATION OF RODS**

Cofilin-actin rods induced by ATP-depletion have been isolated from non-neuronal cell lines expressing a human cofilin-GFP or Xenopus ADF/cofilin-GFP, and from non-neuronal cells and cultured rat cortical neurons in which rods are composed only of endogenously expressed proteins (Minamide *et al.*, submitted). Rods are stable in DTT, EGTA and ATP but not in non-ionic detergents. Rods formed from endogenous proteins contain cytoplasmic actins ( $\beta$ - and  $\gamma$ -actin) and cofilin-1 identified by proteomic analysis. Immunoblot and silver staining analysis of neuronal rod proteins show a 1:1 ADF/cofilin:actin ratio based upon standard curves of purified proteins. Several other proteins were identified in rods, some of which are contaminants (*e.g.* tubulin and keratins) and others whose roles in rod formation have been investigated by immunostaining. Only actin and cofilin are in rods during all stages of rod formation. Thus, core rod components are ADF/cofilin and  $\beta$ - and  $\gamma$ -actins, confirmed by *in vitro* rod assembly from these purified proteins (Minamide *et al.*, submitted).

**SIGNALING TO ADF/COFILIN-ACTIN RODS FORMATION**

Several pathways leading to cofilin activation from externally applied stress agents have been characterized (Fig. 1). Disruption of mitochondrial electron transport causes

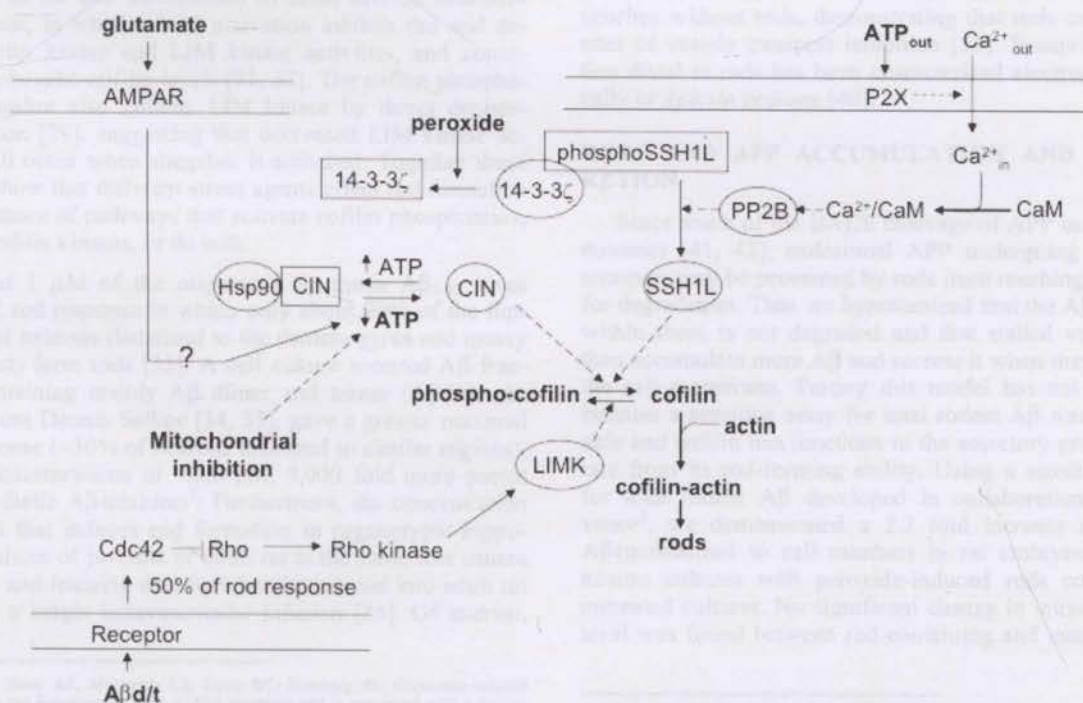


Fig. (1). Summary of signaling pathways discussed in text for stress-induced cofilin-activation leading to rod formation.



ATP-depletion and release of chronophin from inhibition by its intracellular complex with Hsp90 [22]. Because silencing of chronophin by siRNA significantly, but only partially, delays rod formation and cofilin dephosphorylation, slingshot phosphatase may play a secondary role [22]. Since most neuronal stress agents induce a decline in ATP, chronophin activation may often be involved.

Externally applied ATP induces rods in some neurons through activation of the P2X receptor and calcium influx [27]. Elevated calcium binds to calmodulin and the complex stimulates calcineurin, which dephosphorylates slingshot, releasing it from its inhibitory binding partner 14-3-3 $\zeta$  [23, 28]. 14-3-3 $\zeta$  also is involved in peroxide induced rods, but in this case it is through sulfhydryl oxidation of 14-3-3 $\zeta$  and its release of active slingshot [23]. Full activation of slingshot after release from 14-3-3 $\zeta$  requires F-actin binding [28, 29].

Because glutamate activates several different receptor types in neurons, one of which is the calcium permeable ionotropic NMDA receptor, we anticipated glutamate would activate slingshot via the calcium/calmodulin/calcineurin-mediated pathway. Surprisingly, glutamate-induced rod formation in cultured rat embryonic hippocampal neurons (5-7 days *in vitro*) is mediated entirely by AMPA receptors and is calcium-independent<sup>1</sup>; how the AMPA-induced depolarization mediates cofilin dephosphorylation has not been determined. Whether AMPA receptors alone mediate rod formation in older neurons is currently being investigated.

A $\beta$ -induced rod formation is inhibited in ~50% of the neurons in which *cdc42* is missing or a dominant negative *cdc42* is expressed [30], suggesting that about half the hippocampal neurons that form rods in response to A $\beta$  utilize a *cdc42*-dependent pathway. This pathway may be similar or identical to the one downstream of brain derived neurotrophic factor, in which *cdc42* activation inhibits rho and decreases rho kinase and LIM kinase activities, and consequently phospho-cofilin levels [31, 32]. The cofilin phosphatase slingshot also inhibits LIM kinase by direct dephosphorylation [29], suggesting that decreased LIM kinase activity will occur when slingshot is activated. Together these studies show that different stress agents effect rod formation by a plethora of pathways that activate cofilin phosphatases, inhibit cofilin kinases, or do both.

About 1  $\mu$ M of the oligomeric synthetic A $\beta$ <sub>1-42</sub> gives maximal rod response in which only about 20% of the hippocampal neurons (localized to the dentate gyrus and mossy fiber tract) form rods [33]. A cell culture secreted A $\beta$  fraction, containing mainly A $\beta$  dimer and trimer (A $\beta$ d/t), obtained from Dennis Selkoe [34, 35], gave a greater maximal rod response (~30% of neurons localized to similar regions), but at concentrations of ~200 pM, 5,000 fold more potent than synthetic A $\beta$  mixtures<sup>2</sup>. Furthermore, the concentration of A $\beta$ d/t that induces rod formation in organotypic hippocampal slices of juvenile or adult rat is the same that causes memory and learning deficits when introduced into adult rat brain by a single intraventricular infusion [35]. Of interest,

cognitive deficits in adult rats occur between 1-4 h after infusion and completely disappear by 24 h [35]. Rod formation induced in organotypic slices by A $\beta$ d/t is twice control levels within 1 h and becomes highly significant ( $p < 0.001$ ) by 2 h<sup>2</sup>. Rods are fully reversible, disappearing 24 h after washout of the A $\beta$  [30].

These findings led to our hypothesis that in familial AD, caused by mutations in pathways that lead to excessive A $\beta$ d/t production, rods form primarily from the effects of A $\beta$ d/t, whereas in sporadic AD other stress stimuli, e.g. cardiovascular insufficiency, oxidative stress, or excitotoxic glutamate, initiate rod formation [36, 37]. The rods then block transport and enhance the formation and release of A $\beta$ , some of which forms plaques and some of which, presumably as A $\beta$  dimer or A $\beta$ d/t [38], spreads the degenerative zone. This model explains the similar pathologies found in familial and sporadic AD.

### COFILIN-ACTIN RODS FORM IN NEURITES AND BLOCK VESICULAR TRANSPORT AND DISTAL SYNAPTIC ACTIVITY

Transport inhibition is one of the earliest defects in a human mutant APP transgenic mouse model for AD and in human AD brain [39]. Defects consist of axonal swellings containing organelles, vesicles and microtubule-associated proteins including motor molecules. Cofilin-actin rods form in axons and dendrites of cultured neurons treated with A $\beta$ , where they inhibit vesicular transport and accumulate vesicles containing APP and A $\beta$  peptides [33, 37]. Although some rod-inducing agents block vesicle transport throughout the neurites of cells that form rods, probably due to a more global drop in ATP, other agents cause vesicle accumulation at sites of rod formation and vesicles remain dispersed in neurites without rods, demonstrating that rods can serve as sites of vesicle transport inhibition [33]. Synaptic dysfunction distal to rods has been characterized electrophysiologically in *Aplysia* neurons [40].

### RODS AND APP ACCUMULATION AND A $\beta$ SECRETION

Since much of the BACE cleavage of APP occurs in endosomes [41, 42], endosomal APP undergoing retrograde transport may be prevented by rods from reaching lysosomes for degradation. Thus we hypothesized that the A $\beta$  produced within them is not degraded and that stalled vesicles will then accumulate more A $\beta$  and secrete it when they fuse with the cell membrane. Testing this model has not been easy because a sensitive assay for total rodent A $\beta$  was not available and cofilin has functions in the secretory process separate from its rod-forming ability. Using a sensitive ELISA for total rodent A $\beta$  developed in collaboration with Covance<sup>3</sup>, we demonstrated a 2.2 fold increase in secreted A $\beta$  (normalized to cell number) in rat embryonic cortical neuron cultures with peroxide-induced rods compared to untreated cultures. No significant change in intracellular A $\beta$  level was found between rod-containing and untreated neu-

<sup>1</sup> Pak CW, Shaw AE, Minamide LS, Davis RC, Bamberg JR. Glutamate-induced cofilin-actin rod formation requires AMPA receptors and is associated with a disruption in APP-YFP transport. *Mol Biol Cell Suppl.* (abstract in press) (2009)

<sup>2</sup> Davis RC, Maloney MT, Minamide LS, Podlisky M, Selkoe DJ and Bamberg JR. Manuscript in preparation.

<sup>3</sup> Marsden IT, Pak CW, Maloney MT, Davis RC, Minamide LS, Bamberg JR. Feed-forward mechanisms of A $\beta$  production and secretion in cortical neurons. *Mol Biol Cell Suppl.* (abstract in press) (2009)



rons and the extracellular A $\beta$  gradually increased each day suggesting that enhanced secretion of the contents of stalled vesicles takes place. These results lend support to our feed-forward hypothesis that A $\beta$  induction of rods will potentiate secretion of A $\beta$  in a positive loop [33]. A nearly identical increase in A $\beta$  secretion (2.4 fold) from chicken tectal neurons treated with peroxide was quantified using immunoprecipitation and western blotting [43]. Some rod-inducing stimuli (ATP-depletion, glutamate stimulation) do not increase A $\beta$ -secretion but freeze vesicle transport blocking accumulation at rods<sup>3</sup>. This finding suggests that interactions between different vesicle populations at rods may be required to bring about enhanced A $\beta$  formation and/or secretion.

#### DIFFERENT STIMULI TARGETING DIFFERENT POPULATIONS IN HIPPOCAMPUS

We developed a mapping method for hippocampal organotypic slices with rod formation as a measured end point; our data demonstrate that discrete neuronal populations are sensitive to different stress-inducing agents [30]. Glutamate-induced rods are prevalent in the hippocampal CA3 region, whereas rods induced by synthetic amyloid beta (A $\beta$ <sub>1-42</sub>) peptide oligomers and especially the A $\beta$ d/t occur mostly in the dentate gyrus and mossy fiber tract [30]. This location suggests a major impact on cognitive function.

The dentate gyrus, with input from the perforant pathway axons and cholinergic neurons from the basal forebrain, plays a central role in associative memory [44], where dentate granule cells play a crucial role in pattern separation [45, 46]. The CA3 pyramidal cells receive the granule cell output via the mossy fibers and aid in pattern completion [47] required for rapid one-trial contextual learning and pattern completion-based memory recall [48]. Because of its central role in associative memory, the dentate gyrus has been extensively studied in AD brain [46]. There is an early loss of synapses (48% decrease) before a measurable loss of neurons is detected [49, 50]. Synaptic loss correlates with cognitive dysfunction during AD progression with early, mild and severe AD cases showing a decline in staining of the synaptic marker synaptophysin of about 25, 45 and 65%, respectively [51]. Because they block neurite transport and cause atrophy distal to them without killing neurons [7, 40], A $\beta$ -induced rods provide a plausible mechanism for synaptic loss in these regions. Thus they represent a novel target for therapeutic intervention.

#### COFILIN-ACTIN RODS AS MEDIATORS OF ISCHEMIC INJURY

Time-lapse imaging in cofilin-GFP expressing cells shows that rod formation begins within 4-8 min of anoxia in hippocampal slices [30] and plateaus by 10 min, suggesting a role in synaptic dysfunction during hypoxic/ischemic injury or traumatic brain injury. During early phases of rod formation induced by overexpression of cofilin-GFP, rods form transiently and may move both anterogradely and retrogradely within processes before undergoing disassembly. Transient rods can fuse to form larger structures that still move, and sometimes larger rods give rise to smaller ones that eventually disappear. When rods reach a certain size, as

determined by the intensity of the cofilin-GFP, their motility ceases and they inhibit transport of other materials within the neurite<sup>2</sup>.

#### ROLE OF COFILIN-ACTIN RODS IN FORMATION OF STRIATED NEUROFIL THREADS.

In Alzheimer's disease, cofilin-actin rods and thread-like inclusions containing phosphorylated microtubule-associated protein tau form in the neuropil of the brain. The tau-containing structures have been referred to as striated neuropil threads [52], which comprise >85% of cortical tau pathology [53] and are directly correlated to cognitive decline and disease progression [54-56]. However, the mechanism leading to their assembly has remained elusive.

The 12E8 monoclonal antibody, which recognizes human tau phosphorylated on ser262 and ser356, immunostains tau in a pattern that co-localizes with cofilin-actin rods in chicken, rat and human neurons (Fig. 2) [57]. The rod-like staining for tau is induced by several treatments that cause cofilin-actin rod formation, including cofilin overexpression, but does not occur in neurons similarly treated but in which cofilin expression is silenced. Furthermore, cofilin-actin rods precede tau immunostaining, suggesting cofilin-actin rods form a tau-binding matrix. FRET experiments show that cofilin and tau are in close proximity. Bundling and accumulation of F-actin was previously observed to mediate tau induced degeneration in mice expressing mutant forms of tau associated with Frontal Temporal Dementia [58]. These results combined with our observations suggest a common pathway for phospho-tau and cofilin accumulation in neurites that can be initiated by oxidative stress, mitochondrial dysfunction or A $\beta$ , all suspected initiators of synaptic loss in AD. We hypothesize that tau binding to cofilin-actin rods aids in its assembly into paired helical filaments, the main component of neurofibrillary tangles.

#### NUCLEAR COFILIN-ACTIN RODS

Nuclear inclusion bodies, in the form of rods and sheets, were observed as long ago as the late 19th century [59]; reviewed in [60]. Although their function is unclear, their frequent appearance in neurons from normal aged brain (as well as other tissues) suggests that they serve some physiological purpose. There is evidence that the formation of nuclear inclusion bodies *in vivo* can be a response to aging or stress. For example, none of the neurons of the cochlear nucleus in 12-day postnatal rats contained nuclear inclusions, but in adult and aged rats up to 23% of these neurons contained these structures [60]. Nuclear rods also appear spontaneously in sympathetic neuron explants after 2-3 weeks and increase in size with increasing time in culture [61]. The percentage of neurons with nuclear inclusions can be increased *in vivo* by intense electrical stimulation or local perfusion of agents that increase concentrations of intracellular cAMP [62, 63].

In 1978, Fukui demonstrated that intranuclear rods, composed of actin, could be induced in *Dictyostelium* by treatment of the cells with 7-15% dimethylsulfoxide (DMSO) [64]. Nuclear actin rods have been induced in cultured mammalian cells with DMSO [65, 66], heat shock [67, 68] cytochalasin D [69], trifluoperazine, a calmodulin inhibitor, [70], forskolin, a cAMP inducing agent [71], and the



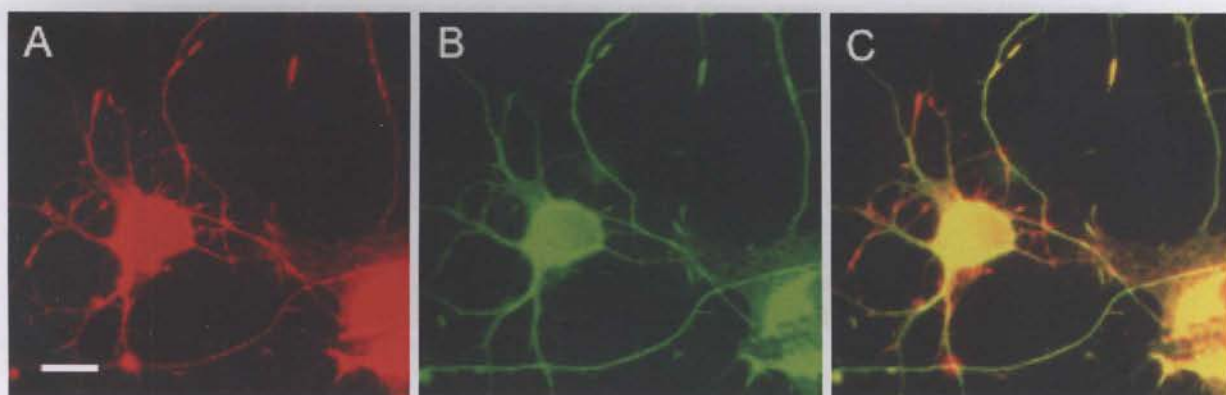


**Fig. (2).** Accumulation of (B) phosphorylated tau (12E8 antibody staining) at (A) cofilin-actin rods in antimycin A-treated hippocampal neurons. (C) Overlay of images. E18 rat hippocampal neurons were cultured 5 days and then treated with antimycin A for 30 min. Cells were fixed with 4% formaldehyde for 45 min and permeabilized for 90 s in 0.05% Triton X-100. Higher concentrations of Triton X-100 or treatment for longer periods reduces immunostaining of cofilin in rods. Methanol permeabilization, which is ideal for cofilin-actin rod immunostaining, destroys the 12E8 epitope. Bar=10  $\mu$ m.

$Ca^{2+}/Mg^{2+}$  ionophore A23187 in the presence of 100 mM  $Mg^{2+}$  [72]. The rods are formed from actin derived from the disassembly of cytoplasmic F-actin and the subsequent movement of actin into the nucleus [66]. Neuronal nuclear rods can be immunostained with antibodies against actin and cofilin (Fig. 3), but not typically with fluorescent derivatives of phalloidin [73], suggesting they have a similar structure to cytoplasmic rods.

Other than actin, the only components that have been positively identified in these rods are ADF and cofilin. Ohta *et al.* [74] showed that dephosphorylation of phospho-cofilin occurred in fibroblasts prior to nuclear translocation in response to DMSO, suggesting that the phosphorylation state may regulate nuclear uptake. Dephosphorylation of ADF/cofilins also has been observed prior to nuclear translocation in T-cells in response to co-stimulatory signals [75]. However, Saito *et al.* [76] showed that both ADF and cofilin were totally dephosphorylated in thyroid cells in response to thyrotropin, but formed nuclear rods in these cells only after exposure to DMSO. Taken together, these data suggest that dephosphorylation of ADF/cofilin is necessary but not sufficient for nuclear uptake.

Both ADF and cofilin contain an identical nuclear localization sequence (NLS) P-X-X-X-K-K-R-K-K [77, 78], which is necessary for nuclear translocation resulting from heat shock [79]. A synthetic peptide containing this NLS rapidly accumulates in nuclei when injected into the cytoplasm of myotubes [80], suggesting that the exposure of the NLS in ADF and cofilin is regulated. Since actin lacks a NLS, ADF and cofilin may serve as chaperones to transport actin into the nucleus under conditions that induce rod formation.

Although no specific role for nuclear rods is known, actin has roles in chromatin remodeling, formation of heterogeneous nuclear ribonucleoprotein complexes, and in transcription from all three RNA polymerases (reviewed in [81]). Thus, sequestering actin into nuclear rods with cofilin could have major effects on gene expression.

## NUCLEAR RODS IN HUNTINGTON DISEASE

Huntington disease (HD) is caused by a CAG triplet-repeat expansion in the gene encoding huntingtin, which results in an expanded polyglutamine tract in the protein [82]. Although the biological function of the entire 350 kDa huntingtin protein has remained elusive, it has been implicated in vesicular trafficking, nucleocytoplasmic transport, and transcription modulation [83-86]. Huntingtin is normally found associated with the endoplasmic reticulum (ER) surface, but under cell stress, including temperature shock and reduced ATP, huntingtin is released from the ER and undergoes nuclear entry. Huntingtin associates with nuclear cofilin-actin rods in cultured heat-shocked cells from a striatal neuron-derived cell line<sup>4</sup>. Upon removal of the stress, rods normally disappear. However, silencing huntingtin expression with siRNA or expressing a human HD mutant form of huntingtin with a large (111 amino acid) polyglutamine tract in place of wild type huntingtin inhibits clearance of nuclear cofilin-actin rods, suggesting that one role of normal huntingtin is clearing cofilin-actin nuclear rods.

## RODS AS A TARGET FOR THERAPEUTIC INTERVENTION

Because cofilin modulates actin in many different cellular processes [11, 87], it has been difficult to determine if the sequestering of cofilin into rods has detrimental effects in cells due to the rod formation *per se*, or whether it is the alteration of cofilin activity at some other place that is having the detrimental effect. Thus, for example, when we treat neurons with a rod inducing stimulus and see a decline in synaptic activity, we could be observing effects on delivery of synaptic material required for maintenance of activity or we could be observing a direct effect on local cofilin-actin dynamics within the synapse (or both). To get around this problem, we have taken two approaches. The first approach is to

<sup>4</sup> Munsie L, Atwal RS, Marsden I, Wild EJ, Bamberg JR, Tabrizi SJ and Truant R. Manuscript submitted.



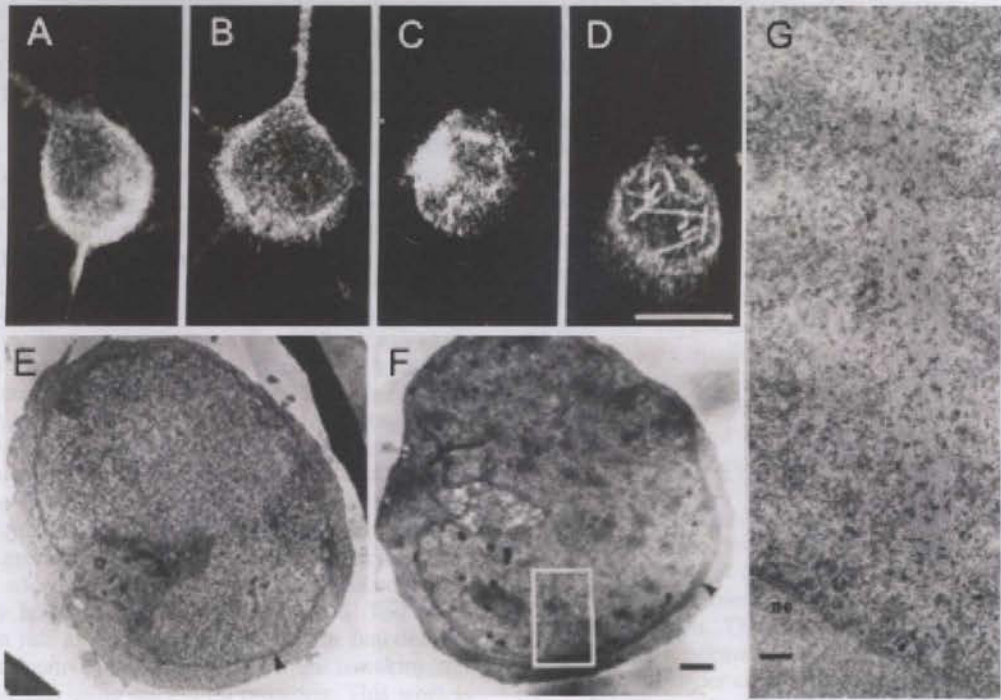


**Fig. (3).** Nuclear ADF/cofilin-actin rods induced in hippocampal neurons by 10% DMSO. (A-D) Time-course of rod formation after addition of 10% DMSO. A=0 time; B=15 min; C=30 min; D=90 min. Cells were fixed in 4% paraformaldehyde for 30 min, permeabilized with  $-20^{\circ}$  methanol for 3 min and stained for ADF/cofilin with affinity purified rabbit 1439 antibody [98]. Bar for A-D= 10  $\mu$ m. Transmission electron micrographs of sections through the cell body of hippocampal neurons that were untreated (E) or treated 90 min with 10% DMSO (F). Rods in longitudinal section and cross-section are present around the nucleus but are also within white box. Bar for E and F= 1  $\mu$ m. (G) Nuclear rod from another cell that was stained with immunogold for ADF/cofilin. Virtually all of the ADF/cofilin immunogold staining lies over rods. Bar=0.1  $\mu$ m.

identify surface mutations on cofilin that do not alter normal cofilin-dependent actin dynamics but do prevent the mutant cofilin from incorporating into rods, especially in cells in which endogenous cofilin expression is silenced. Such a mutant cofilin could be used to make a knock-in mouse which should be resistant to forming rods and thus useful for testing directly the importance of rods in the degenerative response and synaptic loss. However, we also have shown that the ability of cells to form rods is transiently neuroprotective [88]. By tying up virtually all the cofilin but only a small fraction of the actin in rods, cells spare ATP that normally is consumed in actin filament dynamics [89], which can help maintain ionic homeostasis for several minutes giving the cell a chance to recover from its stress. Thus, there is no guarantee that a viable mouse which never forms rods can be obtained. The second approach is to identify peptides that will disrupt the surface interface between adjacent cofilin-actin filaments in the rod but not normal cofilin-actin binding. These peptides could then be made cell permeable and used to inhibit rod formation in acute experiments in cultured neurons or organotypic slices.

#### Studies on Mutant Cofilins

We examined several mutations of cofilin on the non-actin binding surface. Mutant cofilin-RFP chimeras were expressed from plasmids transfected into different cell lines that express only cofilin and not ADF. Cofilin-actin rods

were induced in the cytoplasm upon ATP depletion and in the nucleus upon 10% DMSO treatment. Many of the mutant cofilin-RFPs incorporated into cytoplasmic and nuclear rods nearly identically to wild type (wt) cofilin-RFP. However, several mutants showed > 50% decrease in cells forming both nuclear and cytoplasmic rods. Since residual rods could be due to mutant incorporation into rods initiated by endogenous proteins, we retested their ability to form rods in cells in which endogenous cofilin was silenced. One mutant did not form any rods and a second gave significantly reduced rod formation. Both mutant cofilins were phosphorylated to the same extent as wt cofilin in cells expressing an active form of LIM kinase and were dephosphorylated in cells expressing wt slingshot, suggesting the proteins folded correctly and served as LIM kinase and slingshot substrates. Bacterial expression and isolation of each of these mutant proteins allowed us to characterize their actin binding and dynamizing activities. One of the mutants (R21Q) had about a 10 fold weaker binding to F-actin, explaining its inability to incorporate into rods. The other mutant behaved similarly to wt cofilin in actin binding assays suggesting it might be useful in generating a knock-in mouse if it rescued normal actin dynamics in cofilin silenced cells.

We initially used a variety of functional assays to see if the mutants could rescue some cofilin-dependent activity in cofilin-silenced cells. Major assays used include: 1) cell division (cytokinesis) in which cofilin-silenced cells accumulate



as a multinucleated phenotype; 2) Golgi organization in which cofilin-silenced cells exhibit a dispersed Golgi vesicle array; and 3) cell polarization/migration in which cofilin-silenced cells have a poor ability to undergo polarized migration either in wound healing (time to wound closure) or in spontaneously polarized migrating cells (chick cardiac fibroblasts [90]). Each of these assays has its strengths in trying to identify a non-rod forming mutant cofilin that maintains its essential actin dynamizing capability. Unfortunately, none of the assays performed as expected when we rescued with vectors expressing wt cofilin. For example the multinucleated cell type decreased from 24% in the cofilin-silenced cells to about 11% in cells expressing wt cofilin-RFP, significantly above the 3% average multinucleated phenotype in the parental cell cultures. We reasoned that the RFP might be inhibiting full cofilin activity so we expressed untagged wt cofilin from vectors expressing a fluorescent protein from a separate promoter (to identify expressing cells) but obtained about the same level of rescue. Another possibility that could explain the limited rescue, even with wt cofilin, is that cofilin overexpression from a strong CMV promoter might not create an adequate time window during which optimal cofilin activity required for rescue is expressed. Too much cofilin may be just as inhibitory to some actin functions as too little. To circumvent this problem we are remaking our expression plasmids using the cofilin promoter. This work is in progress.

#### Testing Peptidomimetics to Block Rod Formation

Although the structure of the cofilin-actin complex has not been directly determined, both NMR and X-ray crystal structures have been determined for several ADF/cofilin family members from across phylogeny. All have a very similar core structure, called the ADF-homology domain, also found in some other actin binding proteins where it may be repeated more than once [91]. Models of the complex between cofilin and F-actin (based on the F-actin model of Holmes *et al.* [92]) have been built using molecular dynamics simulations, structural homology considerations, and synchrotron radiolytic footprinting data [93-96]. In addition, the crystal structure of one ADF-H domain of twinfilin in complex with actin was recently determined [97]. We considered residues exposed on the surface of the cofilin bound to F-actin to be likely candidates for interaction between adjacent cofilin-saturated filaments in forming rods. Thus we prepared synthetic peptides corresponding to the entire exposed surface regions and tested their ability to block rod formation when injected into cells expressing human cofilin-GFP. Peptides were injected with rhodamine-dextran so that injected cells could be scored for rods following ATP-depletion. Initial injections were performed with peptides made at 2 mg/ml. Assuming injection volumes of about 10% of the cell volume the final intracellular concentrations of most of the peptides should be approximately 100  $\mu$ M, or about 5 times the estimated 20  $\mu$ M concentration of cofilin. At this concentration, one peptide gave ~20% decrease in rod formation.

While these studies were in progress we completed the characterization of rods isolated from cells expressing cofilin-GFP and cells where rods formed from endogenous proteins. Rods formed from endogenous proteins were more

unstable in 0.5 M salt than were rods formed from cofilin-GFP, suggesting that the interface between the adjacent cofilin-actin filaments will differ in the two cases. Thus, we are now retesting the peptides used above for their abilities to inhibit endogenous rod formation in A431 cells subjected to ATP-depletion.

#### CONCLUSIONS

Cofilin's ability to enhance F-actin severing and subunit turnover when at low stoichiometry to F-actin subunits and to bind and stabilize F-actin when at high stoichiometry is a form of self-regulation, which when coupled to its phosphorylation by a number of upstream regulators, provides an exquisite mechanism for spatial and temporal control of actin filament dynamics. The reversible stress-induced bundling of the cofilin-saturated F-actin into rods, which occurs in all cells expressing adequate levels of ADF/cofilin proteins, is possibly just an additional regulatory layer to further conserve ATP for other processes. However, in neurons, where ADF/cofilin is distributed within the neurites and forms rods that inhibit transport and thus inhibit their own ability to recover, additional complications arise that can compromise synaptic function. The transport of actin into the nucleus may also be a normal cellular function of cofilin that gets compromised under certain types of stress leading to formation of nuclear rods. These might also have a transient protective effect through changes in the transcriptome but might be detrimental to long-term neuronal function. Developing new tools to test the role of rods in different aspects of neurodegenerative diseases is critical to further our understanding of rods and how their manipulation might be of therapeutic significance.

#### ACKNOWLEDGEMENTS

We gratefully acknowledge support from the Alzheimer Drug Discovery Foundation (grant 281201 to JRB), the National Institutes of Health, National Institute of Neurological Diseases and Stroke (grants NS43115, NS40371 to JRB), and The Sir Zelman Cowen Universities Fund, The Judith Jane Mason and Harold Stannet Williams Memorial Foundation, and the Rebecca Cooper Foundation (to CG). We are indebted to Marcia DeWit for electron micrographs of nuclear rods.

#### REFERENCES

- [1] Haass C, Selkoe DJ. Soluble protein oligomers in neurodegeneration: lessons from the Alzheimer's amyloid beta-peptide. *Nat Rev Mol Cell Biol* 8: 101-112 (2007).
- [2] Goedert M, Spillantini MG. A century of Alzheimer's disease. *Science* 314: 777-781 (2006).
- [3] Fukui H, Moraes CT. The mitochondrial impairment, oxidative stress and neurodegeneration connection: reality or just an attractive hypothesis. *Trends Neurosci* 31: 251-256 (2008).
- [4] Hatcher JM, Pennell KD, Miller GW. Parkinson's disease and pesticides: a toxicological perspective. *Trends Pharmacol* 29: 322-329 (2008).
- [5] Arias C, Becerra-Garcia F, Tapia R. Glutamic acid and Alzheimer's disease. *Neurobiol* 6: 33-43 (1998).
- [6] Lancelot E and Beal MF. Glutamate toxicity in chronic neurodegenerative disease. *Prog Brain Res* 116, 331-347 (1998).
- [7] Minamide LS, Striegl AM, Boyle JA, Meberg PJ, Bamburg JR. Neurodegenerative stimuli induce persistent ADF/cofilin-actin rods that disrupt distal neurite function. *Nat Cell Biol* 2: 628-636 (2000).



- [8] Zhao L, Ma QL, Calon F, Harris-White ME, Yang F, Lim GP, et al. Role of p21-activated kinase pathway defects in the cognitive deficits of Alzheimer disease. *Nat Neurosci* 9: 234-242 (2006).
- [9] Bamburg JR. Proteins of the ADF/cofilin family: essential regulators of actin dynamics. *Annu Rev Cell Dev Biol* 15: 185-230 (1999).
- [10] Chen H, Bernstein BW, Sneider J, Boyle JA, Minamide LS, Bamburg JR. *In vitro* activity differences between proteins of the ADF/cofilin family define two distinct subgroups. *Biochemistry* 43: 7127-7142 (2004).
- [11] Van Troys M, Huyck L, Leyman S, Dhaese S, Vandekerckhove J, Ampe C. Ins and outs of ADF/cofilin activity and regulation. *Eur J Cell Biol* 87: 649-667 (2008).
- [12] Mills RG, Minamide LS, Yuan A, Bamburg JR, Bray JJ. Slow axonal transport of soluble actin with actin depolymerizing factor, cofilin, and profilin suggests actin moves in an unassembled form. *J Neurochem* 67: 1225-1234 (1996).
- [13] Flynn KC, Pak CW, Shaw AE, Bradke F, Bamburg JR. Growth cone-like waves transport actin and promote axonogenesis and neurite branching. *Dev Neurobiol* 69: 761-779 (2009).
- [14] Garvalov BK, Flynn KC, Neukirchen D, Meyn L, Teusch N, Wu X, et al. Cdc42 regulates cofilin during the establishment of neuronal polarity. *J Neurosci* 27: 13117-13129 (2007).
- [15] Andrianantoandro E, Pollard TD. Mechanism of actin filament turnover by severing and nucleation at different concentrations of ADF/cofilin. *Molecular Cell* 24: 13-23 (2006).
- [16] McGough A, Pope B, Chiu W, Weeds A. Cofilin changes the twist of F-actin: implications for actin filament dynamics and cellular function. *J Cell Biol* 138: 771-781 (1997).
- [17] Bamburg JR, Bloom GS. Cytoskeletal pathologies of Alzheimer disease. *Cell Motil Cytoskel* 66: 635-649 (2009).
- [18] Niwa R, Nagata-Ohashi K, Takeichi M, Mizuno K, Uemura T. Control of actin reorganization by Slingshot, a family of phosphatases that dephosphorylate ADF/cofilin. *Cell* 108: 233-246 (2002).
- [19] Gohla A, Birkenfeld J, Bokoch GM. Chronophin, a novel HAD-type serine protein phosphatase, regulates cofilin-dependent actin dynamics. *Nat Cell Biol* 7: 21-29 (2005).
- [20] Maciver SK, Weeds AG. Actophorin preferentially binds monomeric ADP-actin over ATP-bound actin: consequences for cell locomotion. *FEBS Lett* 347: 251-256 (1994).
- [21] Ressay F, Didry D, Egile C, Pantaloni D, Carlier MF. Control of actin filament length and turnover by actin depolymerizing factor (ADF/cofilin) in the presence of capping proteins and ARP2/3 complex. *J Biol Chem* 274: 20970-20976 (1999).
- [22] Huang TY, Minamide LS, Bamburg JR, Bokoch GM. Chronophin serves as an ATP-sensing mechanism for cofilin dephosphorylation and neuronal cofilin-actin rod formation. *Dev Cell* 15: 691-703 (2008).
- [23] Kim JS, Huang TY, Bokoch GM. Reactive oxygen species regulate a slingshot-cofilin activation pathway. *Mol Biol Cell* 20: 2650-2660 (2009).
- [24] Atkinson SJ, Hosford MA, Molitoris BA. Mechanism of actin polymerization in cellular ATP-depletion. *J Biol Chem* 279: 5194-5199 (2004).
- [25] Pfannstiel J, Cyrklaff M, Habermann A, Stoeva S, Griffiths G, Shoeman R, et al. Human cofilin forms oligomers exhibiting actin bundling activity. *J Biol Chem* 276: 49476-49484 (2001).
- [26] Fratelli M, Demol H, Puype M, Casagrande S, Eberini I, Salmona M, et al. Identification by redox proteomics of glutathionylated proteins in oxidatively stressed human T lymphocytes. *Proc Natl Acad Sci USA* 99: 3505-3510 (2002).
- [27] Homma K, Niino Y, Hotta K, Oka K. Ca(2+) influx through P2X receptors induces actin cytoskeleton reorganization by the formation of cofilin rods in neurites. *Mol Cell Neurosci* 37: 261-270 (2008).
- [28] Wang Y, Shibasaki F, Mizuno K. Calcium signal-induced cofilin dephosphorylation is mediated by Slingshot via calcineurin. *J Biol Chem* 280: 12683-12689 (2005).
- [29] Soosairajah J, Maiti S, Wiggan O, Sarmiere P, Moussi N, Sarcevic R, et al. Interplay between components of a novel LIM kinase1-slingshot phosphatase complex regulate ADF/cofilin activity. *EMBO J* 24: 473-486 (2005).
- [30] Davis RC, Maloney MT, Minamide LS, Flynn KC, Stonebraker MA, Bamburg JR. Mapping cofilin-actin rods in stressed hippocampal slices and the role of cdc42 in amyloid  $\beta$ -induced rods. *J Alzheimers Dis* 18: 35-50 (2009).
- [31] Gehler S, Shaw AE, Sarmiere PD, Bamburg JR, Letourneau PC. Brain derived neurotrophic factor regulation of growth cone filopodial dynamics is mediated through actin depolymerizing factor/cofilin. *J Neurosci* 24: 10741-10749 (2004).
- [32] Chen T-j, Gehler S, Shaw AE, Bamburg JR, Letourneau PC. Cdc42 participates in the regulation of ADF/cofilin and retinal growth cone filopodial dynamics by Brain Derived Neurotrophic Factor. *J Neurobiol* 66: 103-114 (2006).
- [33] Maloney MT, Minamide LS, Kinley AW, Boyle JA, Bamburg JR. Beta-secretase-cleaved amyloid precursor protein accumulates at actin inclusions induced in neurons by stress or amyloid beta: a feedforward mechanism for Alzheimer's disease. *J Neurosci* 25: 11313-11321 (2005).
- [34] Walsh DM, Klyubin I, Fadeeva JV, Cullen WK, Anwyl R, Wolfe MS, et al. Naturally secreted oligomers of amyloid beta protein potently inhibit hippocampal long-term potentiation *in vivo*. *Nature* 416: 535-539 (2002).
- [35] Cleary JP, Walsh DM, Hofmeister JJ, Shankar GM, Kuskowski MA, Selkoe DJ, et al. Natural oligomers of the amyloid-beta protein specifically disrupt cognitive function. *Nat Neurosci* 8: 79-84 (2005).
- [36] Maloney MT and Bamburg JR. Cofilin-mediated neurodegeneration in Alzheimer's disease and other amyloidopathies. *Mol Neurobiol* 35: 21-44 (2007).
- [37] Maloney MT, Kinley A, Pak C, Bamburg JR. ADF/cofilin, actin dynamics and disease. *Protein Reviews* 8: 83-187 (2008).
- [38] Shankar GM, Li S, Mehta TH, Garcia-Munoz A, Shepardson NE, Smith I, et al. Amyloid-beta protein dimers isolated directly from Alzheimer's brain impair synaptic plasticity and memory. *Nat Med* 14: 837-842 (2008).
- [39] Stokin GB, Lillo C, Falzone TL, Brusch RG, Rockenstein E, Mount SL, et al. Axonopathy and transport defects early in the pathogenesis of Alzheimer's disease. *Science* 307: 1282-1288 (2005).
- [40] Jang DH, Han JH, Lee SH, Lee YS, Park H, Lee SH, et al. Cofilin expression induces cofilin-actin rod formation and disrupts synaptic structure and function in *Aplysia* synapses. *Proc Natl Acad Sci USA* 102: 16072-16077 (2005).
- [41] Ehehalt R, Keller P, Haass C, Thiele C, Simons K. Amyloidogenic processing of the Alzheimer beta-amyloid precursor protein depends on lipid rafts. *J Cell Biol* 160: 113-123 (2003).
- [42] Thomas RS, Liddell JE, Murphy LS, Pache DM, Kidd EJ. An antibody to the beta-secretase cleavage site on amyloid-beta-protein precursor inhibits amyloid-beta production. *J Alzheimers Dis* 10: 379-390 (2006).
- [43] Goldsby C, Whiteman IT, Jeong EV, Lim Y-A. Oxidative stress increases levels of endogenous amyloid-beta peptides secreted from primary chick brain neurons. *Aging Cell* 7: 771-775 (2008).
- [44] Morris RG. Elements of a neurobiological theory of hippocampal function: the role of synaptic plasticity, synaptic tagging and schemas. *Eur J Neurosci* 23: 2829-2846 (2006).
- [45] McHugh TJ, Jones MW, Quinn JJ, Balthasar N, Coppari R, Elmquist JK, et al. Dentate gyrus NMDA receptors mediate rapid pattern separation in the hippocampus. *Science* 317: 94-99 (2007).
- [46] Ohm TG. The dentate gyrus in Alzheimer's disease. *Prog Brain Res* 163: 723-740 (2007).
- [47] Nakazawa K, Quirk MC, Chitwood RA, Watanabe M, Yeckel MF, Sun LD, et al. Requirement for hippocampal CA3 NMDA receptors in associative memory recall. *Science* 297: 211-218 (2002).
- [48] Nakashiba T, Young JZ, McHugh TJ, Buhl DL, Tonegawa S. Transgenic inhibition of synaptic transmission reveals role of CA3 output in hippocampal learning. *Science* 319: 1260-1264 (2008).
- [49] Bertoni-Freddari C, Fattoretti P, Casoli T, Caselli U, Meier-Ruge W. Deterioration threshold of synaptic morphology in aging and senile dementia of Alzheimer's type. *Anal Quant Cytol Histol* 18: 209-213 (1996).
- [50] Scheff SW, Price DA. Synaptic pathology in Alzheimer's disease: a review of ultrastructural studies. *Neurobiol Aging* 24: 1029-1046 (2003).
- [51] Masliah E, Mallory M, Hansen L, De Teresa R, Alford M, Terry R. Synaptic and neuritic alterations during the progression of Alzheimer's disease. *Neurosci Lett* 174: 67-72 (1994).
- [52] Velasco ME, Smith MA, Siedlak SL, Nunomura A, Perry G. Striation is the characteristic neuritic abnormality in Alzheimer disease. *Brain Res* 813: 329-333 (1998).



- [53] Mitchell TW, Nissanov J, Han LY, Mufson EJ, Schneider JA, Cochran EJ, *et al.* Novel method to quantify neuropil threads in brains from elders with or without cognitive impairment. *J Histochem Cytochem* 48: 1627-1638 (2000).
- [54] Braak H, Alafuzoff I, Arzberger T, Kretschmar H, Tredici K. Staging of Alzheimer disease-associated neurofibrillary pathology using paraffin sections and immunocytochemistry. *Acta Neuropathol* 112: 389-404 (2006).
- [55] Augustinack J, Schneider A, Mandelkow E, Hyman B. Specific tau phosphorylation sites correlate with severity of neuronal cytopathology in Alzheimer's disease. *Acta Neuropathol* 103: 26-35 (2002).
- [56] Giannakopoulos P, von Gunten A, Kovari E, Gold G, Herrman FR, Hof PR, *et al.* Stereological analysis of neuropil threads in the hippocampal formation: relationships with Alzheimer's disease neuronal pathology and cognition. *Neuropath Appl Neurobiol* 33: 334-343 (2007).
- [57] Whiteman IT, Gervasio OL, Cullen KM, Guillemain GJ, Jeong EV, Wittig PK, *et al.* Activated ADF/cofilin sequesters phosphorylated microtubule-associated protein during the assembly of Alzheimer-like neuronal cytoskeletal striations. *J Neurosci* 29: 12994-13005 (2009).
- [58] Fulga T, Elson-Schwab I, Khurana V, Steinhilb M, Spire T, Hyman B, *et al.* Abnormal bundling and accumulation of F-actin mediates tau-induced neuronal degeneration *in vivo*. *Nat Cell Biol* 9: 139-148 (2006).
- [59] Mann G. Histological changes induced in sympathetic, motor, and sensory nerve cells by functional activity. *J Anat Physiol* 29: 100-108 (1894).
- [60] Feldman ML, Peters A. Intranuclear rods and sheets in rat cochlear nucleus. *J Neurocytol* 1: 109-127 (1972).
- [61] Masurovsky EB, Benitez HH, Kim SU, Murray MR. Origin, development, and nature of intranuclear rodlets and associated bodies in chicken sympathetic neurons. *J Cell Biol* 44: 172-191 (1970).
- [62] Seite R, Mei N, Vuillet-Luciani J. Effect of electrical stimulation on nuclear microfilaments and microtubules of sympathetic neurons submitted to cycloheximide. *Brain Res* 50: 419-423 (1973).
- [63] Seite R, Leonetti J, Luciani-Vuillet J, Vio M. Cyclic AMP and ultrastructural organization of the nerve cell nucleus: stimulation of nuclear microtubules and microfilaments assembly in sympathetic neurons. *Brain Res* 124: 41-51 (1977).
- [64] Fukui Y. Intranuclear actin bundles induced by dimethyl sulfoxide in interphase nucleus of Dictyostelium. *J Cell Biol* 76: 146-157 (1978).
- [65] Fukui Y, Katsumaru H. Dynamics of nuclear actin bundle induction by dimethyl sulfoxide and factors affecting its development. *J Cell Biol* 84: 131-140 (1980).
- [66] Sanger JW, Sanger JM, Kreis TE, Jockusch BM. Reversible translocation of cytoplasmic actin into the nucleus caused by dimethyl sulfoxide. *Proc Natl Acad Sci USA* 77: 5268-5272 (1980).
- [67] Welch WJ, Suhan JP. Morphological study of the mammalian stress response: characterization of changes in cytoplasmic organelles, cytoskeleton, and nucleoli, and appearance of intranuclear actin filaments in rat fibroblasts after heat-shock treatment. *J Cell Biol* 101: 1198-1211 (1985).
- [68] Iida K, Iida H, Yahara I. Heat shock induction of intranuclear actin rods in cultured mammalian cells. *Exp Cell Res* 165: 207-215 (1986).
- [69] Yahara I, Harada F, Sekita S, Yoshihira K, Natori S. Correlation between effects of 24 different cytochalasins on cellular structure and cellular events and those on actin *in vitro*. *J Cell Biol* 92: 69-78 (1982).
- [70] Osborn M, Weber K. Damage of cellular functions by trifluoperazine, a calmodulin-specific drug. *Exp Cell Res* 130: 484-488 (1980).
- [71] Osborn M, Weber K. Actin paracrystal induction by forskolin and by db-cAMP in CHO cells. *Exp Cell Res* 150: 408-418 (1984).
- [72] Osborn M, Weber K. Dimethylsulfoxide and the ionophore A23187 affect the arrangement of actin and induce nuclear actin paracrystals in PtK2 cells. *Exp Cell Res* 129: 103-114 (1980).
- [73] Nishida E, Iida K, Yonezawa N, Koyasu S, Yahara I, Sakai H. Cofilin is a component of intranuclear and cytoplasmic actin rods induced in cultured cells. *Proc Natl Acad Sci USA* 84: 5262-5266 (1987).
- [74] Ohta Y, Nishida E, Sakai H, Miyamoto E. Dephosphorylation of cofilin accompanies heat shock-induced nuclear accumulation of cofilin. *J Biol Chem* 264: 16143-16148 (1989).
- [75] Samstag Y, Eckerskorn C, Wesselborg S, Henning S, Wallich R, Meuer SC. Costimulatory signals for human T-cell activation induce nuclear translocation of pp19/cofilin. *Proc Natl Acad Sci USA* 91: 4494-4498 (1994).
- [76] Saito T, Lamy F, Roger PP, Lecocq R, Dumont JE. Characterization and identification as cofilin and destrin of two thyrotropin- and phorbol ester-regulated phosphoproteins in thyroid cells. *Exp Cell Res* 212: 49-61 (1994).
- [77] Matsuzaki F, Matsumoto S, Yahara I, Yonezawa N, Nishida E, Sakai H. Cloning and characterization of porcine brain cofilin cDNA. *J Biol Chem* 263: 11564-11568 (1988).
- [78] Abe H, Endo T, Yamamoto K, Obinata T. Sequence of cDNAs encoding actin depolymerizing factor and cofilin of embryonic chicken skeletal muscle: two functionally distinct actin regulatory proteins exhibit high structural homology. *Biochemistry* 29: 7420-7425 (1990).
- [79] Iida K, Matsumoto S, Yahara I. The KKRKK sequence is involved in heat shock-induced nuclear translocation of the 18-kDa actin-binding protein, cofilin. *Cell Struct Funct* 17: 39-46 (1992).
- [80] Abe H, Nagaoka R, Obinata T. Cytoplasmic localization and nuclear transport of cofilin in cultured myotubes. *Exp Cell Res* 206: 1-10 (1993).
- [81] Zheng B, Han M, Bernier M, Wen J-k. Nuclear actin and actin-binding proteins in the regulation of transcription and gene expression. *FEBS J* 276: 2669-2685 (2009).
- [82] MacDonald ME, Ambrose CM, Duyao MP, Myers RH, Lin C, Srinidhi L, *et al.* A novel gene containing a trinucleotide repeat that is expanded and unstable on Huntington's disease chromosomes. *Cell* 72: 971-983 (1993).
- [83] Truant R, Atwal R, Burtnik A. Hypothesis: Huntingtin may function in membrane association and vesicular trafficking. *Biochem Cell Biol* 84: 912-917 (2006).
- [84] Truant R, Atwal RS, Burtnik A. Nucleocytoplasmic trafficking and transcription effects of huntingtin in Huntington's disease. *Prog Neurobiol* 83: 211-227 (2007).
- [85] Trushina E, Dyer RB, Badger JD 2<sup>nd</sup>, Ure D, Eide L, Tran DD, *et al.* Mutant huntingtin impairs axonal trafficking in mammalian neurons *in vivo* and *in vitro*. *Mol Cell Biol* 24: 8195-8209 (2004).
- [86] Xia J, Lee DH, Taylor J, Vandelft M, Truant R. Huntingtin contains a highly conserved nuclear export signal. *Hum Mol Genet* 12: 1393-1403 (2003).
- [87] Bamberg JR, Wiggan O. ADF/cofilin and actin dynamics in disease. *Trends Cell Biol* 12: 598-605 (2002).
- [88] Bernstein BW, Chen H, Boyle JA and Bamberg JR. Formation of actin-ADF/cofilin rods transiently retards decline of mitochondrial potential and ATP in stressed neurons. *Am J Physiol Cell Physiol* 291: C828-C839 (2006).
- [89] Bernstein BW and Bamberg JR. Actin-ATP hydrolysis is a major energy drain for neurons. *J Neurosci* 23: 1-6 (2003).
- [90] Dawe HR, Minamide LS, Bamberg JR, Cramer LP. ADF/cofilin controls cell polarity during fibroblast migration. *Curr Biol* 13: 252-257 (2003).
- [91] Lappalainen P, Kessels MM, Cope MJTV, Drubin DG. The ADF homology (ADF-H) domain: a highly exploited actin-binding module. *Mol Biol Cell* 9: 1951-1959 (1998).
- [92] Holmes KC, Popp D, Gebhard W, Kabsch W. Atomic model of the actin filament. *Nature* 347: 44-49 (1990).
- [93] Lappalainen P, Fedorov EV, Fedorov AA, Almo SC, Drubin DG. Essential functions and actin-binding surfaces of yeast cofilin revealed by systematic mutagenesis. *EMBO J* 16: 5520-5530 (1997).
- [94] Pope BJ, Gonsior SM, Yeoh S, McGough A, Weeds AG. Uncoupling actin filament fragmentation by cofilin from increased subunit turnover. *J Mol Biol* 298: 649-661 (2000).
- [95] Kamal JK, Benchaar SA, Takamoto K, Reisler E, Chance MR. Three-dimensional structure of cofilin bound to monomeric actin derived by structural mass spectrometry data. *Proc Natl Acad Sci USA* 104: 7910-7915 (2007).
- [96] Grintsevich EE, Benchaar SA, Warshaviak D, Boontheung P, Halgand F, Whitelegge JP, *et al.* Mapping the cofilin binding site on yeast G-actin by chemical cross-linking. *J Mol Biol* 377: 395-409 (2008).



- [97] Paavilainen VO, Oksanen E, Goldman A, Lappalainen P. Structure of the actin-depolymerizing factor homology domain in complex with actin. *J Cell Biol* 182: 51-59 (2009).
- [98] Shaw AE, Minamide LS, Bill CL, Funk JD, Maiti S, Bamburg JR. Cross-reactivity of antibodies to actin-depolymerizing factor/cofilin

family proteins and identification of the major epitope recognized by a mammalian actin-depolymerizing factor/cofilin antibody. *Electrophoresis* 25: 2611-2620 (2004).

Received: September 5, 2009 Revised: November 13, 2009 Accepted: November 24, 2009

# Activated Actin-Depolymerizing Factor/Cofilin Sequesters Cytoskeletal-Associated Protein during the Assembly of Alzheimer-Like Neuritic Cytoskeletal Striations

Leena T. Whitten<sup>1,2\*</sup>, Nathan L. Garrad<sup>1</sup>, Ewan M. Collins<sup>1</sup>, Gillian J. Griffiths<sup>1</sup>, Erica V. Joung<sup>1,3</sup>, Paul K. Wright<sup>1</sup>, Diane T. Armes<sup>1</sup>, Laurio K. Minamide<sup>1</sup>, James P. Bamburg<sup>4</sup>, and Claire C. Chikley<sup>1,4</sup>

<sup>1</sup>The Peter D. MacLeod Research Institute and <sup>2</sup>Neuro Sciences, School of Medical Sciences, University of Western Australia, Nedlands, Western Australia; <sup>3</sup>Department of Cell Biology, University of New South Wales, Sydney, New South Wales 2052, Australia, and <sup>4</sup>Department of Pathology and Immunology, Monash Medical Centre, Parkville, Victoria 3046, Australia

Alzheimer's disease (AD) and the related aggressive tauopathies (tau) and frontotemporal lobar degeneration containing phosphorylated microtubule-associated protein (pMTA) tau form in the brain (neuritic tangles), and the extent of these processes correlates with cognitive decline and disease progression. The assembly mechanisms of these respective pathological lesions and the relationship between them is poorly understood, yet critical to understanding the causes of sporadic AD. We demonstrate that, during widespread inhibition, activated actin-depolymerizing factor (ADF/cofilin) sequesters tau in cell cycle processes of cultured primary neurons that express pMTA tau and exhibit neurofibrillary tangles. Phosphorylation sequesters tau by its essential interaction with actin-cofilin (green fluorescent protein) and pMTA in vivo, suggesting their close proximity within a cytoskeletal inclusion complex. The relationship between pMTA and cofilin-actin rods was further investigated using genetic screening, drug and small interfering RNA knockdown of ADF/cofilin primary neurons. The results suggest that activation of ADF/cofilin and generation of cofilin-actin rods is required for the subsequent recruitment of pMTA into the formation. Additionally, we were able to induce the formation of pMTA-positive ADF/cofilin rods by exposing cells to oxidative stress. A pMTA pathway that results from a common pathway for pMTA and cofilin accumulation in neuronal processes. The recruitment of pMTA to the neurofibrillary tangle suggests an important structural role for pMTA in the formation of neurofibrillary tangles and pMTA in the formation of neurofibrillary tangles. The recruitment of pMTA to the neurofibrillary tangle suggests an important structural role for pMTA in the formation of neurofibrillary tangles and pMTA in the formation of neurofibrillary tangles.

## INTRODUCTION

Alzheimer's disease (AD) is a genetically dependent neurodegenerative disorder characterized by neurofibrillary tangles of an intracellular protein, tau (plaque) (Garrad and Garrad, 2007; Garrad and Garrad, 2007). In early stages of AD, neurofibrillary tangles (neurofibrillary tangles) (NFT) are formed through the striations in what are called "neurofibrillary tangles" (Garrad et al., 1998; Garrad et al., 2007). The striations with cognitive decline and neuropathology in 80% of end-stage clinical AD pathology (Garrad et al., 1998; Garrad et al., 2007; Garrad and Garrad, 2007).

The tau-like other MTA, microtubule-associated protein (MTA) and tubulin MTA systems through its phosphorylation and

dephosphorylation (Garrad et al., 2007; Garrad and Garrad, 2007). Although several other various cellular levels of tau phosphorylation, activation of AD tau and other tau-related neurodegenerative diseases show high levels of tau phosphorylation in both physiological and pathological disease models. The tau hyperphosphorylation in primary neurons and inhibition of MTA and causes abnormal translocation of tau from axonal MTA, leads to cytoskeletal tangle formation, dendritic processes, and cell bodies in which it accumulates and aggregates (Garrad, 1998; Garrad and Garrad, 2007). The phosphorylation of tau at Ser202 in the microtubule binding domain is one of the earliest markers of AD neuropathology, readily observed in "neurofibrillary tangles" (Garrad et al., 2007).

Another prominent feature widespread in the AD brain is hyperphosphorylation of the actin-associated protein cofilin, which forms part of the actin-cofilin rods through the neurofibrillary tangles (Minamide et al., 2007). Neurofibrillary tangles play important roles in learning and memory pathways by sequestering actin-rich dendritic spine to the tau (Minamide et al., 2007) (in review; see Bamburg and Nieren, 2009). The activity of cofilin and related protein with-depolymerizing factor (ADF) is negatively regulated by phosphorylation of the conserved Ser3 by LIM-kinase 1, 2, and 3 and other kinases and sequestered

\*Correspondence: Leena T. Whitten, The Peter D. MacLeod Research Institute, University of Western Australia, Nedlands, Western Australia. E-mail: leena.whitten@uwa.edu.au  
 Received: September 5, 2009; Accepted: November 24, 2009  
 Copyright © 2009 Bentham Science Publishers. ISSN 1567-2051  
 DOI: 10.2196/1567-2051.70301

# Activated Actin-Depolymerizing Factor/Cofilin Sequesters Phosphorylated Microtubule-Associated Protein during the Assembly of Alzheimer-Like Neuritic Cytoskeletal Striations

Ineka T. Whiteman,<sup>1,2</sup> Othon L. Gervasio,<sup>2</sup> Karen M. Cullen,<sup>2</sup> Gilles J. Guillemin,<sup>3</sup> Erica V. Jeong,<sup>1,2</sup> Paul K. Witting,<sup>2</sup> Shane T. Antao,<sup>2</sup> Laurie S. Minamide,<sup>4</sup> James R. Bamburg,<sup>4</sup> and Claire Goldsbury<sup>1,2</sup>

<sup>1</sup>The Brain & Mind Research Institute, and <sup>2</sup>Bosch Institute, School of Medical Sciences, University of Sydney, Camperdown, New South Wales 2006, Australia, <sup>3</sup>Neuroinflammation Group, Department of Pharmacology, University of New South Wales, Sydney, New South Wales 2052, Australia, and <sup>4</sup>Department of Biochemistry and Molecular Biology, Colorado State University, Fort Collins, Colorado 80523

In Alzheimer's disease (AD), rod-like cofilin aggregates (cofilin-actin rods) and thread-like inclusions containing phosphorylated microtubule-associated protein (pMAP) tau form in the brain (neuropil threads), and the extent of their presence correlates with cognitive decline and disease progression. The assembly mechanism of these respective pathological lesions and the relationship between them is poorly understood, yet vital to understanding the causes of sporadic AD. We demonstrate that, during mitochondrial inhibition, activated actin-depolymerizing factor (ADF)/cofilin assemble into rods along processes of cultured primary neurons that recruit pMAP/tau and mimic neuropil threads. Fluorescence resonance energy transfer analysis revealed colocalization of cofilin-GFP (green fluorescent protein) and pMAP in rods, suggesting their close proximity within a cytoskeletal inclusion complex. The relationship between pMAP and cofilin-actin rods was further investigated using actin-modifying drugs and small interfering RNA knockdown of ADF/cofilin in primary neurons. The results suggest that activation of ADF/cofilin and generation of cofilin-actin rods is required for the subsequent recruitment of pMAP into the inclusions. Additionally, we were able to induce the formation of pMAP-positive ADF/cofilin rods by exposing cells to exogenous amyloid- $\beta$  ( $\beta$ ) peptides. These results reveal a common pathway for pMAP and cofilin accumulation in neuronal processes. The requirement of activated ADF/cofilin for the sequestration of pMAP suggests that neuropil thread structures in the AD brain may be initiated by elevated cofilin activation and F-actin bundling that can be caused by oxidative stress, mitochondrial dysfunction, or  $\beta$  peptides, all suspected initiators of synaptic loss and neurodegeneration in AD.

## Introduction

Alzheimer's disease (AD) is a progressive, degenerative dementia histopathologically characterized by neurofibrillary tangles of tau protein and amyloid- $\beta$  ( $\beta$ ) plaques (Goedert and Spillantini, 2006; Haass and Selkoe, 2007). In early stages of AD, hyperphosphorylated microtubule-associated protein (pMAP) tau forms striated thread-like structures in neurites, so-called "neuropil threads" (Velasco et al., 1998; Augustinack et al., 2002), that correlate with cognitive decline and comprise >85% of end-stage cortical tau pathology (Velasco et al., 1998; Braak et al., 2006; Giannakopoulos et al., 2007).

Tau, like other MAPs, stabilizes neuronal microtubules (MTs) and facilitates MT dynamics through its phosphorylation and

dephosphorylation (Timm et al., 2003) (for review, see Garcia and Cleveland, 2001). Although normal adult neurons exhibit low levels of tau phosphorylation, neurons of AD brain and other tau-related neurodegenerative diseases show high levels of tau phosphorylation at both physiological and pathological disease-specific residues. This tau hyperphosphorylation prevents binding and stabilization of MTs and causes abnormal translocation of tau from axonal MT tracks to neuropil thread inclusions, dendritic processes, and cell bodies in which it accumulates and aggregates (Terry, 1998; Garcia and Cleveland, 2001). The phosphorylation of tau at Ser262 in the microtubule-binding domain is one of the earliest markers of AD neuropathology, readily detected in "pretangle" neuropil threads (Augustinack et al., 2002).

Another prominent feature widespread in the AD brain is abnormal aggregates of the actin-associated protein cofilin, which forms punctate and rod-like linear arrays through the neuropil (Minamide et al., 2000). Neuronal cofilin plays important roles in learning and memory pathways by modulating actin-rich dendritic spine architecture (Hotulainen et al., 2009) (for review, see Bamburg and Bloom, 2009). The activity of cofilin and related protein actin-depolymerizing factor (ADF) is negatively regulated by phosphorylation of the conserved Ser3 by LIM (Lin-11, Isl-1, and Mec-3) and other kinases and reactivated on

Received July 21, 2009; revised Aug. 12, 2009; accepted Aug. 27, 2009.

This work was supported by The Sir Zelman Cowen Universities Fund, The Judith Jane Mason and Harold Starnett Williams Memorial Foundation, The Rebecca Cooper Foundation, Sydney Medical School (C.G.), Alzheimer Drug Delivery Foundation Grant 281201 (J.R.B.), and National Institutes of Health—National Institute of Neurological Diseases and Stroke Grants NS43115 and NS40371 (J.R.B.). We thank Prof. Peter Seubert (Eli Lilly Pharmaceuticals, South San Francisco, CA) for providing the 12E8 antibody.

Correspondence should be addressed to either of the following: James R. Bamburg, Department of Biochemistry and Molecular Biology, Colorado State University, Fort Collins, CO 80523, E-mail: james.bamburg@colostate.edu; or Claire Goldsbury, The Brain & Mind Research Institute, School of Medical Sciences, University of Sydney, 100 Mallett Street, Camperdown, NSW 2006, Australia, E-mail: cgoldsbury@usyd.edu.au.

DOI:10.1523/JNEUROSCI.3531-09.2009

Copyright © 2009 Society for Neuroscience 0270-6474/09/2912994-12\$15.00/0



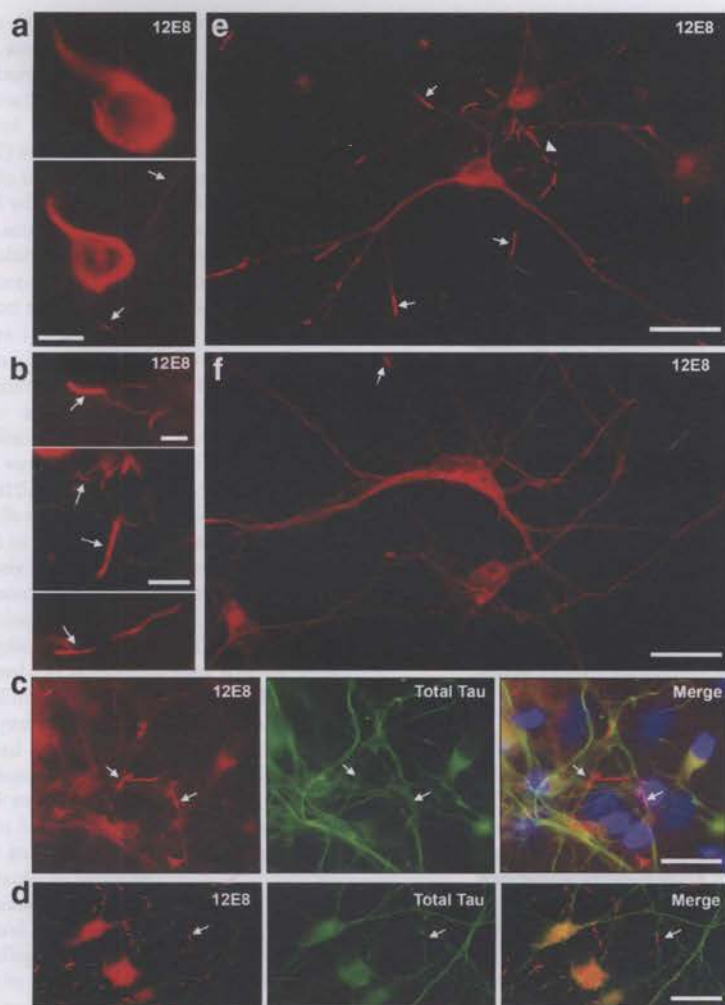


**Figure 1.** Neuropathological hallmarks of human AD can be recapitulated in ATP-depleted human and chick primary neurons. **a, b**, Hyperphosphorylation of tau at Ser262/356 (immunolabeled with the 12E8 antibody) and striated neurites are early markers of AD. Immunofluorescent staining of sections of frontal cortex from human AD brain show strong 12E8 reactivity in neurofibrillary tangles in individual neurons (**a**) and abundant linear arrays of 12E8-labeled inclusions in neurites (**a, b**, arrows). **c**, Human primary neuronal cell cultures labeled with the 12E8 antibody (red) and total tau antibody (green), after 30 min AM treatment (plus DAPI in blue in merged image). Tapered pMAP-positive rods were observed throughout the neurites (arrows). **d, e**, Primary chick neurons (7 div) treated with AM for 15 min also rapidly accumulate rod-like 12E8-positive inclusions (red) that frequently form linear striations within single neurites (**e**, arrowhead). Rods were not enriched with total tau (**c, d**, green), indicating that inclusions contain MAP/tau specifically phosphorylated within the microtubule-binding KXGS motifs, as immunostained with 12E8 (red). **f**, Control chick neurons show evenly distributed 12E8 staining along neurites with only the occasional rod-like accumulation (arrow). Scale bars: **a, b**, 10  $\mu$ m; **c–f**, 20  $\mu$ m.

its dephosphorylation by slingshot or chronophin phosphatases (Huang et al., 2008) (for review, see Bamberg and Bloom, 2009), allowing it to actively bind and sever filamentous actin (F-actin), thus regulating actin turnover (Carlier et al., 1997; Bamberg and Bloom, 2009).

ADF/cofilin–actin rods comparable with those observed in the AD brain are inducible in neuronal cell culture through inhibition of mitochondrial ATP generation and other neurodegenerative stimuli such as oxidative stress or exposure to A $\beta$  peptides (Minamide et al., 2000; Maloney et al., 2005; Davis et al., 2009). Since actin dynamics in neurons are purported to use ~50% of total cellular ATP (Bernstein and Bamberg, 2003), ADF/cofilin–actin rods have been proposed to represent an early neuroprotective mechanism during times of transient stress since virtually all ADF/cofilin is sequestered into nondynamic polymers of

ADF/cofilin–actin, inhibiting actin turnover and thereby preserving ATP (Bernstein et al., 2006). Although mitochondrial dysfunction has been linked to AD (Smith et al., 2005; Wang et al., 2009), the relationship between mitochondrial dysfunction, the generation of tau inclusions, and their relationship to cofilin aggregates remains elusive.

In this study, we aimed to determine the effects of mitochondrial dysfunction on cellular pMAP/tau distribution compared with ADF/cofilin–actin rod distribution (Minamide et al., 2000; Huang et al., 2008). Using primary neuronal cell culture models, we demonstrate that cytoskeletal rods containing ADF/cofilin sequester and bind pMAP. The resulting striated pMAP-positive rods bear striking resemblance to neuropil threads observed in postmortem AD brain labeled with the same pMAP antibody. This process may well represent an early pathogenic event in AD leading to synaptic loss and neurodegeneration.

## Materials and Methods

**Antibodies and reagents.** Mouse monoclonal antibodies are actin (1A4; Dako),  $\beta$ -actin (Abcam),  $\beta$ (III)-tubulin (Abcam), tau phosphorylated at Ser202/Thr205 (AT8; Pierce), and Ser262/356 (12E8; Elan) (Seubert et al., 1995). The monoclonal antibody 12E8, raised against Ser262-phosphorylated tau, is known to cross-react with other phosphorylated MAPs such as MAP2c, MAP4 (Timm et al., 2003), and doublecortin (Schaar et al., 2004) since these MAPs also contain the 12E8-specific KXGS motifs in their microtubule-binding domains. However, 12E8 has strong affinity for tau, in which the microtubule-binding domain contains several KXGS motifs, the target sequence for 12E8 (Seubert et al., 1995; Yoshida and Goedert, 2002; Timm et al., 2003; Schaar et al., 2004). Rabbit polyclonal antibodies are ADF (1439), ADF (D8815; Sigma-Aldrich), Ser3-phosphorylated ADF/cofilin (Shaw et al., 2004), cofilin (C8736; Sigma-Aldrich), actin (A2066; Sigma-Aldrich), and total tau (A0024; Dako). Phalloidin 488 (Invitrogen) was used to visualize F-actin (Invitrogen). Anti-mouse and anti-rabbit secondary antibodies included Alexa Fluor (488, 555, and 647)-conjugated (Invitrogen) for immunofluorescence and horseradish peroxidase-conjugated (GE Healthcare) for immunoblotting. Lyophilized amyloid peptides were from Bachem.

**Cell culture and treatments.** Primary chick neurons were prepared from freshly dissected chicken embryos [embryonic day 7 (E7)], as previously described, and cultured for 7 d *in vitro* (div) on polylysine-coated 30 mm culture dishes or glass coverslips (Goldsbury et al., 2008). Primary human neurons were prepared and cultured for 14–20 d as previously described (Guillemin et al., 2007). Primary (E18) rat hippocampal neurons were cultured for 5 d as previously described (Minamide et al., 2000). For ATP depletion studies, cells were treated with 1–2  $\mu$ M antimycin (AM) (a mitochondrial complex III inhibitor; Sigma-Aldrich), 3  $\mu$ M carbonyl cyanide 3-chlorophenylhydrazone (CCCP) (a mitochondrial uncoupling agent; Sigma-Aldrich), or 100  $\mu$ M hydrogen peroxide



(Sigma-Aldrich) in PBS containing 0.5 mM  $\text{CaCl}_2$  and 1 mM  $\text{MgSO}_4$ . For ADF/cofilin phosphorylation studies, cells were treated for 15 min with 1  $\mu\text{M}$  AM. Actin drugs were used at 1  $\mu\text{g/ml}$  jaspalaginolide (Jasp) (Calbiochem; 420127) or latrunculin B (Lat B) (Calbiochem; 428020). Cells left without a medium change or treated with PBS or DMSO acted as controls. Stock solutions of lyophilized  $\text{A}\beta$  peptides were solubilized to 2 mM in DMSO, aliquoted, and stored at  $-20^\circ\text{C}$ . Immediately before application to cells, the stock solutions were diluted to 100  $\mu\text{M}$  in PBS and agitated at 1200 rpm on a laboratory shaker for 30 min to generate mixtures of polymorphic oligomeric and fibrillar aggregates as previously described (Goldsbury et al., 2000). The peptide assemblages were then applied to cells in 24-well plates at final concentrations of 1 or 2  $\mu\text{M}$ . Control wells were treated with the same volume of DMSO in PBS. After treatments, cells were immediately fixed (cells on coverslips) or prepared for Western blot analysis (plated cells).

**Luminescent measurements.** After treatments (in triplicate), primary chick neurons were harvested and assessed for total ATP (ATPLite; PerkinElmer) using a Victor III Multilabel plate reader. Protein measurements were determined using the identical samples and the bicinchoninic acid assay (Sigma-Aldrich). Total ATP was normalized against total protein to account for any difference in cell density. Statistical analysis used Prism software (version 3.0; GraphPad Software).

**Immunoblotting.** After treatments, cells were lysed and prepared for SDS-PAGE. For equal gel loading, protein concentrations were determined by the Lowry assay (Bio-Rad). Proteins transferred to nitrocellulose membranes were detected with ECL Western Blotting Detection System (GE Healthcare) on a ChemiDoc XRS (Bio-Rad). For analysis, band densities were measured using ImageJ (version 1.38x; National Institutes of Health freeware; <http://rsb.info.nih.gov/ij/>), and background intensity was subtracted and normalized to individual  $\beta$ -actin or tubulin loading controls. An average and SEM for each treatment condition was determined, and results are presented as a percentage of the mean control band intensities.

**Plasmids and transfection.** Plasmid-mediated expression of wild-type human cofilin has been previously described (Davis et al., 2009). Human cofilin cDNA in a pET vector (a gift from Alan Weeds, Medical Research Council Laboratory of Molecular Biology, Cambridge, UK) was modified by PCR with a 5'-PCR primer containing an EcoRI site and a 3'-primer that removed the stop codon and introduced an XmaI site at the 3'-end. EcoRI and XmaI were then used to cut the PCR product and the cDNA was ligated into pEGFP-N1 (Clontech) in-frame with the green fluorescent protein (GFP) to encode cofilin-GFP. A plasmid vector for expressing small interfering RNAs (siRNAs) for chick ADF was made by inserting DNA oligonucleotides (Macromolecular Resources) into a plasmid expression vector (pSuper) (Brummelkamp et al., 2002) containing the H1 polymerase III promoter. The oligonucleotide product from the pol III promoter is a double-stranded hairpin RNA (antisense-linker-sense) that is processed into a functional siRNA in the cell. The modified inserts including the H1 pol III promoter from

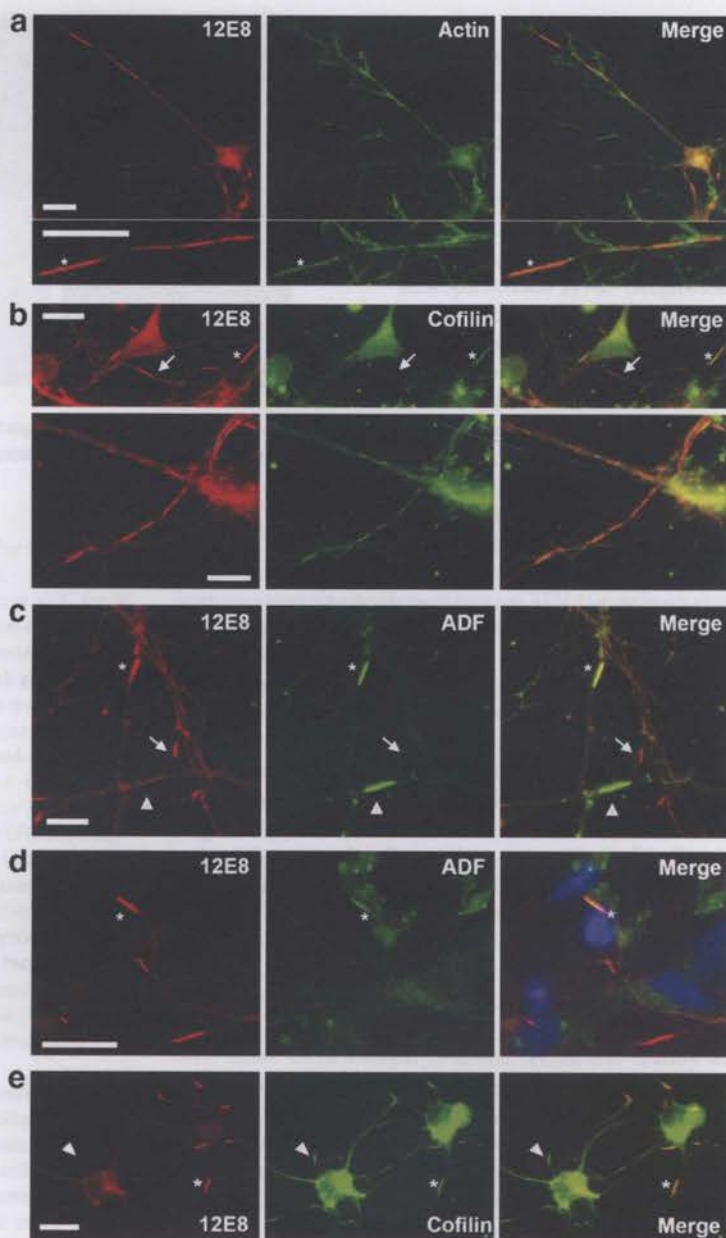


**Figure 2.** Colocalization of actin, cofilin, and ADF occurs in pMAP inclusions after ATP depletion. Chick neurons treated with AM were double-labeled with 12E8 (red) and actin (**a**), cofilin (C8736; Sigma-Aldrich) (**b**), or ADF (D8815; Sigma-Aldrich) (**c**) antibodies as indicated (green). Merged images are shown on the right. Rods containing pMAP also stained positively for actin (**a**, asterisk), cofilin (**b**, asterisk in top panel), and ADF (**c**, asterisk). Double-labeled strings of rods were often observed within single neurites (**b**, bottom panel). pMAP inclusions in primary human (**d**) and rat (**e**) hippocampal (5 div) neurons also colabeled with ADF (D8815) (**d**) and cofilin (1439) (**e**). Some rods contained pMAP but were weakly labeled or negative for cofilin or ADF (**b**, **c**, arrows), whereas others stained strongly for ADF or cofilin but only weakly or negatively for pMAP (**c**, **e**, arrowheads). This is suggestive of a heterogeneous population of rod-like structures and/or suboptimal immunostaining conditions for the respective structures (see text). Scale bars, 10  $\mu\text{m}$ .

the pSuper vector were excised and ligated into the pAdTrack vector (He et al., 1998). The siRNA sequence contained within the hairpin used for chick ADF is 5'-GTGGAAGAAGGCCAAAAGAGATT-3'. A plasmid made identically but that makes a hairpin RNA to silence human Pak2 (5'-GTCTCTGGGTATCATGGCTAT-3') was used as a transfection control in the chick cells. The ability of the small hairpin RNA (shRNA)-expressing plasmid to effectively knock down ADF in chick cells was tested in cultures of chick skin fibroblasts (B. M. Marsick, K. C. Flynn, J. R. Bamberg, and P. C. Letourneau, unpublished observations). For plasmid-mediated expression, neuronal cultures at 3 d were trans-



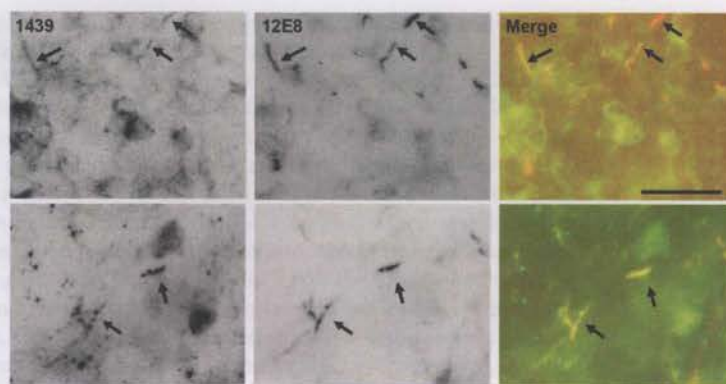


**Figure 3.** Colocalization of cofilin and pMAP occurs in ATP-depleted rat organotypic hippocampal slices. After ATP depletion, rod-like accumulations are evident in organotypic rat (postnatal day 8) hippocampal slices and are positive for both cofilin (labeled with 1439) and pMAP (labeled with 12E8) (arrows). Scale bar, 10  $\mu$ m.

ected using Lipofectamine 2000 (Invitrogen). Four days after transfection, neurons were treated with AM (1 or 2  $\mu$ M for 10 or 20 min).

**Microscopy.** Cells were fixed with 4% paraformaldehyde at 37°C for 30 min, permeabilized with 0.05% Triton X-100 or 100% ice-cold methanol, blocked in 5% goat serum, and stained for immunofluorescence. To optimize visualization of ADF/cofilin–actin rods, 0.1% EM-grade glutaraldehyde was added to the fixative. Epifluorescence images were obtained on a Zeiss Axioplan 2 microscope, captured with a CCD camera driven by AxioVision software. Single-labeled cells/sections were used to check for bleed-through in all double-label immunofluorescence studies. All captured images were converted to tagged image files for subsequent presentation. For fluorescence resonance energy transfer (FRET) analysis, cells (plated on glass-bottomed MatTek dishes) were imaged in PBS using a Zeiss LSM 510 and C-Apochromat 40 $\times$  water-immersion objective and the argon (488 nm) (for GFP donor) and HeNe1 (543) (for Alexa Fluor 555 acceptor) laser lines. For photobleaching of acceptor, regions of interest in the transfected cells were bleached using the 543 nm laser line at 100% power. FRET efficiency was calculated from the increase in the fluorescence intensity of the donor after the acceptor was selectively photobleached (Gervásio et al., 2008). The donor fluorescence was measured from at least five bleached and five unbleached rods per cell.

**Analysis and statistics.** For quantification of cells containing rod structures, cells with rods were counted for each treatment condition from randomly selected fields on each coverslip, and cells containing rod structures were then expressed as a percentage of the total cell population or mean number of rods per cell. Treatments and measurements were repeated in triplicate using independently prepared cell cultures. For determination of relative fluorescence intensities for phalloidin or ADF, immunofluorescent intensity was measured using ImageJ. Cells with abnormal nuclei, as indicated by 4',6'-diamidino-2-phenylindole (DAPI) staining, were excluded from the data. After adjustment to background, mean and SEM intensities were calculated for each condition. Significance was measured using Student's *t* test.

**Human tissue and rat hippocampal slices.** Free-floating sections (45  $\mu$ m) of formalin-fixed superior frontal cortex and basal forebrain from normal adult and confirmed Alzheimer's disease patients obtained from the New South Wales Brain Bank were immunostained as previously described (Cullen et al., 2005). Sections were incubated overnight at 4°C in primary 12E8 (see Fig. 1*a,b*) or AT8 antibody (see supplemental Fig. S1*a,b*, available at [www.jneurosci.org](http://www.jneurosci.org) as supplemental material). Bound antibody was visualized using Alexa Fluor-conjugated secondary antibody (Invitrogen) or using ABC-peroxidase (Vector Laboratories) and DAB (Sigma-Aldrich).

Organotypic rat hippocampal slices were grown for 14 d on membranes as described previously (Davis et al., 2009). Slices were treated with 2  $\mu$ M AM in PBS for 1 h, fixed in 4% formaldehyde for 1 h, permeabilized 90 s in 0.05% Triton X-100 in PBS, and immunostained overnight with 1439 (cofilin) (2  $\mu$ g/ml) and mouse 12E8 (4  $\mu$ g/ml) antibodies. Secondary antibody incubations were for 2 h.

## Results

### Neuritic pMAP accumulation in striated rods, resembling structures in postmortem Alzheimer brain, is induced in primary neurons by energy depletion

We used the monoclonal phosphorylation-dependent 12E8 antibody raised against the pMAP tau, an established early marker for neuropil threads in AD (Augustinack et al., 2002), to determine whether pMAP accumulates in primary neuronal models derived from human, rat, or chick after mitochondrial inhibition. Probing AD brain sections with the 12E8 antibody (Fig. 1*a,b*) or AT8 antibody (supplemental Fig. S1*a,b*, available at [www.jneurosci.org](http://www.jneurosci.org) as supplemental material) showed numerous striated rod-like inclusions within neuropil

threads and cytoplasmic accumulations of pMAP, indistinguishable from previous observations in human AD (Augustinack et al., 2002). Additionally, linear striations of rod accumulations labeled with cofilin antibodies were also observed in AD brains (supplemental Fig. S1*c*, available at [www.jneurosci.org](http://www.jneurosci.org) as supplemental material).

Treatment of primary human CNS neurons cultured for 7 d *in vitro*, with the mitochondrial complex III inhibitor AM elicited a rapid accumulation of 12E8-labeled protein into rod inclusions (Fig. 1*c*, arrows) comparable with those seen in the AD neurons (Fig. 1*b*, arrows). The rods sequestered the fraction of MAP serine-phosphorylated in the microtubule-binding domain KXGS motifs specific for the 12E8 antibody, rather than total MAP/tau because a polyclonal antibody against total tau yielded a more uniform labeling along neurites of both human and chick neurons (Fig. 1*c,d*). During AM treatment, primary chick CNS neurons derived from embryonic tectum also generated pMAP-positive rod-like structures (Fig. 1*d,e*) morphologically identical with those from human neurons. Thus, the readily accessible chick neurons are a useful model system for studying the mechanism by which pMAP accumulates into rods. The conserved 12E8 epitopes in the pMAP sequence reside within the microtubule binding domain in human tau (Ser262/Ser356 residues) and chicken tau (Ser253/Ser378) (supplemental Fig. S2*a,b*, available at [www.jneurosci.org](http://www.jneurosci.org) as supplemental material) (Yoshida and Goedert, 2002). Primary chick tectal neurons express five isoforms of tau that are highly homologous to human tau isoforms and exhibit conservation of phosphorylation-specific epitopes recognized by antibodies against human tau (supplemental Fig. S2*c*, available at [www.jneurosci.org](http://www.jneurosci.org) as supplemental material) (Yoshida and Goedert, 2002).

### pMAP-containing striations induced by ATP depletion colocalize with ADF/cofilin–actin rods

Actin dynamics are highly dependent on ATP availability (Bernstein and Bamburg, 2003), and ATP depletion is associated with an increase in cellular F-actin and an increase in ADF/cofilin activity (Minamide et al., 2000). It follows that acute inhibition of mitochondrial function used here to generate pMAP-immunostained rods, may result in changes to the actin cytoskeleton. Consistent with this, AM-treated chick neurons exhibited a 1.9-fold increase in overall phalloidin staining in cell bodies indicative of increased F-actin content (supplemental Fig. S3, available at [www.jneurosci.org](http://www.jneurosci.org) as supplemental material). The pMAP-positive rods, however, did not overlap



with phalloidin labeling (supplemental Fig. S3*b*, available at [www.jneurosci.org](http://www.jneurosci.org) as supplemental material).

In ATP-depleted rat hippocampal neurons, the rapid dephosphorylation of cofilin leads to the development of cofilin–actin rods in neurites (Minamide et al., 2000). These rods contain actin, as evidenced by both antibody immunostaining and ultrastructure, but do not stain with phalloidin, indicating they are probably saturated with ADF/cofilin, which stabilizes the “twisted” form of the filament and eliminates the phalloidin binding site (McGough et al., 1997). We therefore asked whether rods induced by ATP depletion contain both pMAP and ADF/cofilin. Double labeling revealed that ADF/cofilin–actin rods in part colocalize with pMAP in chick (Fig. 2*a–c*, asterisks), human (Fig. 2*d*, asterisk), and rat hippocampal neurons (Fig. 2*e*, asterisk). Colocalization of cofilin and pMAP in rod structures in ATP-depleted organotypic rat hippocampal slice cultures was also revealed (Fig. 3). Moreover, staining for  $\beta$ (III)-tubulin did not accumulate at rods, further suggesting the specificity of pMAP and ADF/cofilin in formation of neuritic rods (supplemental Fig. S4*b,c*, available at [www.jneurosci.org](http://www.jneurosci.org) as supplemental material). However, ADF/cofilin-stained rods that do not stain for pMAP (Fig. 2*c,e*, arrowheads) and pMAP-stained rods that do not stain for ADF (Fig. 2*b*, arrow) were both observed. Because optimal immunostaining for pMAP requires Triton X-100 permeabilization (avoiding methanol) and optimal immunostaining for ADF/cofilin requires methanol (avoiding Triton), structures that stain for one and not the other may be suboptimally permeabilized or immunostained. However, we cannot exclude that the detected inclusions may represent a heterogeneous population of rod structures. Surprisingly, in hippocampal neurons derived from rat, there was no change in the diffuse and uniform distribution of pMAP staining after ATP depletion, fixation in 4% paraformaldehyde and 0.1% glutaraldehyde, and brief (90 s) 0.05% Triton X-100 permeabilization, which looked identical with the staining of pMAP in untreated human, rat, and chick neurons (Fig. 1*f*). However, rat neurons subjected to AM-induced ATP depletion, followed by fixation in 4% formaldehyde and permeabilization as above, did exhibit rod-like 12E8 immunostaining (Fig. 2*e*), suggesting that glutaraldehyde fixation of pMAP when it is in a rod-like structure masks its epitope from 12E8 binding. Together, these results link ADF/cofilin–actin and pMAP inclusions within the same rod structures in neurites, which can be induced in cell culture by the common mechanism of acute ATP depletion through mitochondrial dysfunction.

To establish the activation state of ADF/cofilin during pMAP accumulation, we used an antibody specific for phosphorylated (inactive) ADF/cofilin (Minamide et al., 2000; Maloney et al., 2005). ADF/cofilin actin-binding activity is negatively regulated by phosphorylation of the N-terminal Ser3 (Huang et al., 2008; Kim et al., 2009). On ATP depletion with AM, ADF/cofilin was rapidly dephosphorylated (activated) in chick tectal neurons, as early as 2 min after treatment (Fig. 4*a,b*), consistent with studies in primary rat hippocampal neurons (Minamide et al., 2000). Peroxide ( $H_2O_2$ )-treated tectal neurons also showed nearly complete ADF/cofilin activation after 30 min (Fig. 4*a,b*). The time course for the redistribution of pMAP immunostaining into the rod-like inclusions (Fig. 4*c*) correlated with the rapid dephosphorylation of ADF/cofilin and the formation of ADF/cofilin–actin rods.

Based on the above results, we expected that the extent of pMAP incorporation into rods would be proportional to the level of intracellular ATP. To explore this relationship, we mea-

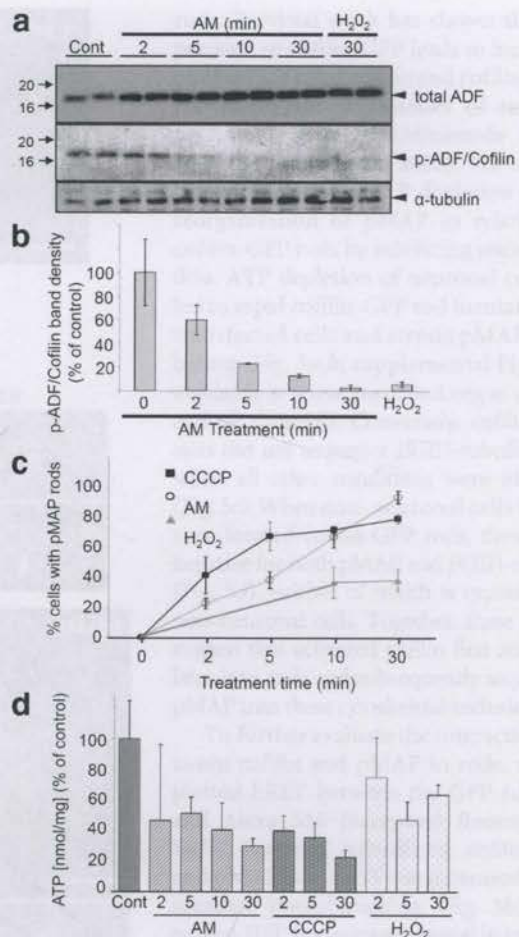


**Figure 4.** Mitochondrial inhibition induces activation of ADF/cofilin and is correlated to pMAP-positive rod formation. Dephosphorylation at the N-terminal (Ser3) leads to ADF/cofilin activation. *a*, Chick neurons were treated with AM or  $H_2O_2$  for the indicated times, lysed, and immunoblotted. Whereas total ADF levels (probed with 1439) remained the same (or slightly increased) compared with control cells, ATP depletion resulted in rapid dephosphorylation of ADF/cofilin as early as 2 min after AM treatment (p-ADF/cofilin antibody is Ser3-specific). Similarly,  $H_2O_2$  treatment induced almost complete dephosphorylation. *b*, Graph shows time course of ADF/cofilin dephosphorylation. Band intensities from duplicate samples were normalized to  $\alpha$ -tubulin loading controls and calculated as a percentage of control band intensities. *c*, Coverslips were treated with AM, CCCP, or  $H_2O_2$  and immunostained in parallel for quantification of the extent of rod generation. AM-treated cells ultimately contained the greatest abundance of pMAP-positive rods, although CCCP-treated cells initially developed rods more rapidly. Approximately 40% of  $H_2O_2$ -treated cells developed rods over 30 min. Data points and error bars represent mean and SEM values from three independent experiments. *d*, Luminescence measurements were performed to ascertain ATP levels after AM, CCCP, or  $H_2O_2$  treatment. Compared with control samples, cells treated with AM and CCCP showed a rapid decline in ATP levels, whereas those treated with  $H_2O_2$  showed a more modest decline. Error bars represent SEM of triplicate samples. Together, these data suggest an inverse correlation between number of pMAP rods formed and level of ATP.

sured ATP levels in tectal neurons before and after treatment with AM, CCCP (a mitochondrial uncoupling agent), or  $H_2O_2$  (Fig. 4*d*). Consistent with the notion that activation of ADF/cofilin induced by intracellular ATP depletion correlates with pMAP accumulation, there was an inverse relationship between the percentage of cells in the culture that contained pMAP-stained rods (Fig. 4*c*) and the level of ATP detected in the cell treatment groups (Fig. 4*d*). Cell viability tests revealed 95% cell survival in 10 min AM-treated chick neuronal cultures (compared with control cultures) and 77% survival in 30 min treated cultures (supplemental Fig. S4*d*, available at [www.jneurosci.org](http://www.jneurosci.org)



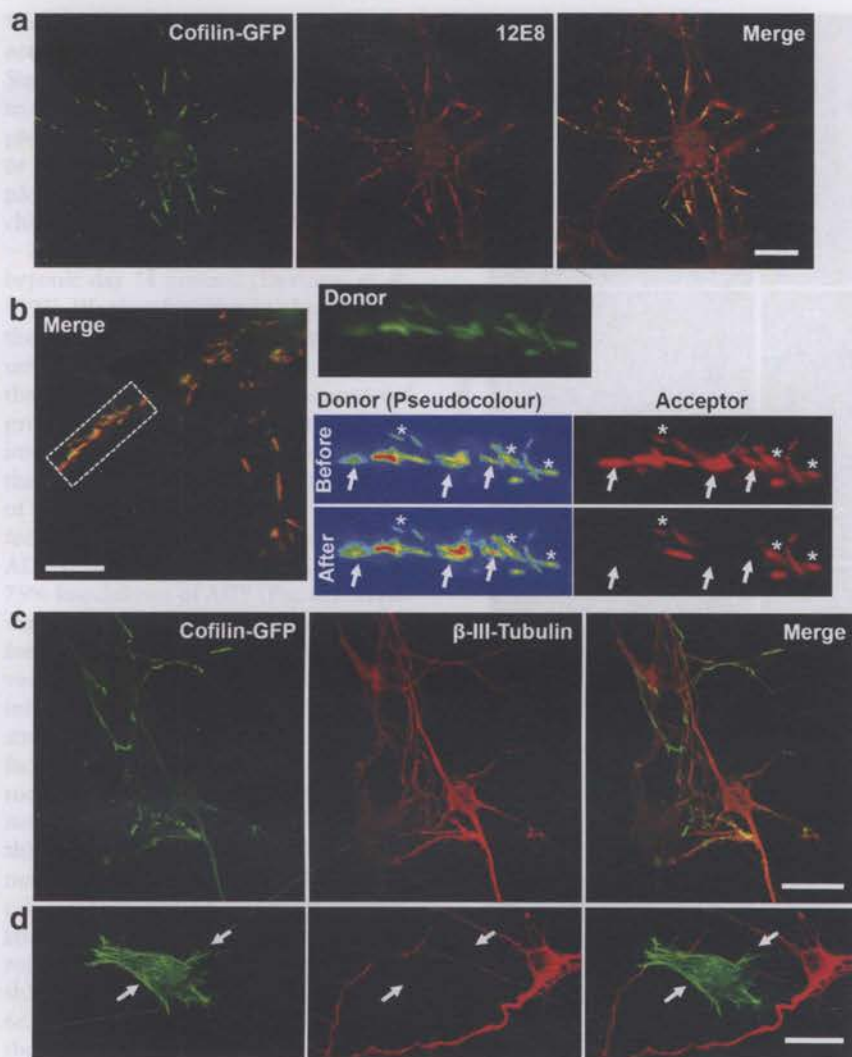


**Figure 5.** Cofilin-GFP forms rods that sequester pMAP during ATP depletion. Primary chick neurons were transfected with human cofilin-GFP (green) for 24 h, treated with AM to induce rod assembly, and pMAP immunolabeled with 12E8 and Alexa 555 secondary anti-mouse (red). **a**, Colocalization of cofilin-GFP rods (green) with 12E8 immunolabel (red) is evident in merged images (right panel, yellow). **b**, FRET measurements revealed a close proximity between pMAP immunolabel and cofilin-GFP rods. Images of donor (cofilin-GFP, green or pseudocolor) before and after photobleaching of acceptor (Alexa 555, red) are shown. Pseudocolor images of the donor signal demonstrate an increase in GFP fluorescence in acceptor-bleached rods (arrows) but not nonbleached rods (asterisks). A FRET efficiency of  $41 \pm 3\%$  (mean  $\pm$  SEM;  $n = 52$ ;  $p < 0.0001$ ) was quantified by measuring the percentage increase in donor fluorescence after acceptor bleaching. No significant FRET signal was seen in nonbleached rods (**b**, asterisks) in the same cells (donor fluorescence increase, mean  $\pm$  SEM,  $2.2 \pm 1.1\%$ ;  $n = 52$ ). **c**,  $\beta$ (III)-tubulin remains smooth and evenly distributed throughout cofilin-GFP transfected cells and is not enriched at cofilin-GFP rods. **d**, The specificity of pMAP sequestration is further illustrated in the occasional non-neuronal cell that was transfected with cofilin-GFP. These cells formed cofilin-GFP rods (arrows) but were negative for both  $\beta$ (III)-tubulin (red) and pMAP (data not shown). This also provides evidence that cofilin rods form in the absence of pMAP. Scale bars: **a**, **c**, **d**, 20  $\mu$ m; **b**, 10  $\mu$ m.

as supplemental material). Likewise, abundant pMAP-positive rod formation was recapitulated in primary human neurons, after 30 min AM treatment (mean  $\pm$  SD,  $24 \pm 2$  rods per field for AM-treated compared with  $8 \pm 1$  rods per field in controls;  $p < 0.001$ ). Together, these results suggest ATP depletion is an important correlate for redistribution of pMAP into rods.

#### Activated cofilin sequesters and is closely associated with pMAP in rods

Since ADF/cofilin–actin rods contained pMAP and rod formation depends on activation of ADF/cofilin, we asked whether transfected cofilin-GFP could sequester pMAP into

rods. Previous work has shown that expression of cofilin-GFP leads to increased pools of activated cofilin and cofilin–actin rod formation in neurites of rat hippocampal neurons (Minamide et al., 2000; Bernstein et al., 2006). We investigated the effects of ATP depletion on the reorganization of pMAP in relation to cofilin-GFP rods by inhibiting mitochondria. ATP depletion of neuronal cultures led to rapid cofilin-GFP rod formation in transfected cells and strong pMAP colabeling (Fig. 5*a,b*; supplemental Fig. S5*a*, available at [www.jneurosci.org](http://www.jneurosci.org) as supplemental material). Conversely, cofilin-GFP rods did not sequester  $\beta$ (III)-tubulin label when all other conditions were identical (Fig. 5*c*). When non-neuronal cells in culture formed cofilin-GFP rods, these were negative for both pMAP and  $\beta$ (III)-tubulin (Fig. 5*d*), neither of which is expressed in non-neuronal cells. Together, these results suggest that activated cofilin first accumulates into rods and subsequently sequesters pMAP into these cytoskeletal inclusions.

To further evaluate the interaction between cofilin and pMAP in rods, we exploited FRET between the GFP (donor) and Alexa 555 (acceptor) fluorophores. FRET between colocalized cofilin-GFP and pMAP/Alexa 555 was measured using acceptor photobleaching (Fig. 5*b*). The cofilin-GFP fluorescence signal in rods increased significantly after bleaching the Alexa 555 fluorophor (Fig. 5*b*, right, arrows), with a measured FRET efficiency of  $41 \pm 3\%$  (mean  $\pm$  SEM;  $n = 52$ ;  $p < 0.0001$ ) as measured by the percentage increase in donor fluorescence after acceptor bleaching. In contrast, cofilin-GFP fluorescence did not significantly increase in adjacent rods in the same cells in which the Alexa 555 fluorophor was not bleached (Fig. 5*b*, right, asterisks). Furthermore, a much reduced FRET signal was detected in neurons between cofilin-GFP and Alexa 555 immunostained pMAP in adjacent non-rod-forming regions of neurites and cell bodies (supplemental Fig. S5*b*, available at [www.jneurosci.org](http://www.jneurosci.org) as supplemental material).

Control experiments demonstrated no FRET between cofilin-GFP and control antibody-labeled epitopes— $\beta$ (III)-tubulin/Alexa 555 or Src/Alexa 555—even in regions in which the fluorescence appeared colocalized (supplemental Fig. S5*c,d*, available at [www.jneurosci.org](http://www.jneurosci.org) as supplemental material). Cells expressing free GFP and treated with AM to generate pMAP-positive rods labeled with 12E8/Alexa 555 also never produced FRET (supplemental Fig. S5*d*, available at [www.jneurosci.org](http://www.jneurosci.org) as supplemental material). These results demonstrate that cofilin-GFP and the secondary antibody labeling pMAP are colocalized  $<10$  nm apart within the cytoskeletal rod complex, indicating a close proximity of pMAP and cofilin in these inclusions.



### Silencing ADF prevents pMAP accumulation in rods

Since induction of ADF/cofilin rods leads to the reorganization and sequestering of pMAP, we asked whether silencing ADF or cofilin would prevent sequestering of pMAP under the same conditions. During chick brain development, ADF comprises ~75% of the total ADF/cofilin from embryonic day 14 onward (Devineni et al., 1999). We therefore chose to knock down the total cellular pool of ADF specifically, using a plasmid for expression of a shRNA that yields an siRNA when expressed and processed. The shRNA was transfected into chick neurons and coexpressed from the same plasmid as GFP for visualization of transfected cells. Four days posttransfection, cells were immunolabeled for ADF (Fig. 6*a*) and quantified, revealing 75% knockdown of ADF (Fig. 6*e*). Treating transfected cultures with AM (1  $\mu$ M for 10 min) and staining for pMAP revealed that significant silencing of ADF inhibited accumulation of pMAP into rod structures, whereas surrounding untransfected cells contained an abundance of rods (Fig. 6*d*, asterisks). In control chick neuronal cultures transfected for 4 d with shRNA specific for human PAK2, immunolabeling revealed no decrease in total cellular ADF (Fig. 6*b,e*). pMAP accumulated in rod-like inclusions both in surrounding nontransfected neurons and in shRNA PAK2 transfected neurons (Fig. 6*c*, asterisks and arrowhead). Together, these results suggest that the presence of ADF/cofilin is necessary for sequestration of pMAP into rod-like structures.

### Latrunculin B enhances and jasplakinolide represses pMAP staining in rods

Since activation of ADF/cofilin coincided with pMAP recruitment into ADF/cofilin–actin rods, we asked whether other manipulations of F-actin assembly could influence pMAP sequestration to rods. To address this, we used pharmacological manipulation (enhancing or suppressing) of F-actin pools and stained for pMAP. Latrunculins sequester monomeric G-actin to form a nonpolymerizable 1:1 complex, thereby inhibiting F-actin reassembly and thus promoting overall F-actin depolymerization (Coué et al., 1987). Latrunculins, however, compete weakly with ADF/cofilin for actin binding (Bernstein et al., 2006) and can actually induce ADF/cofilin–actin rod formation (Pendleton et al., 2003). The decline in the phalloidin-stainable F-actin pool after Lat B treatment is indeed evident (Fig. 7*a*), although

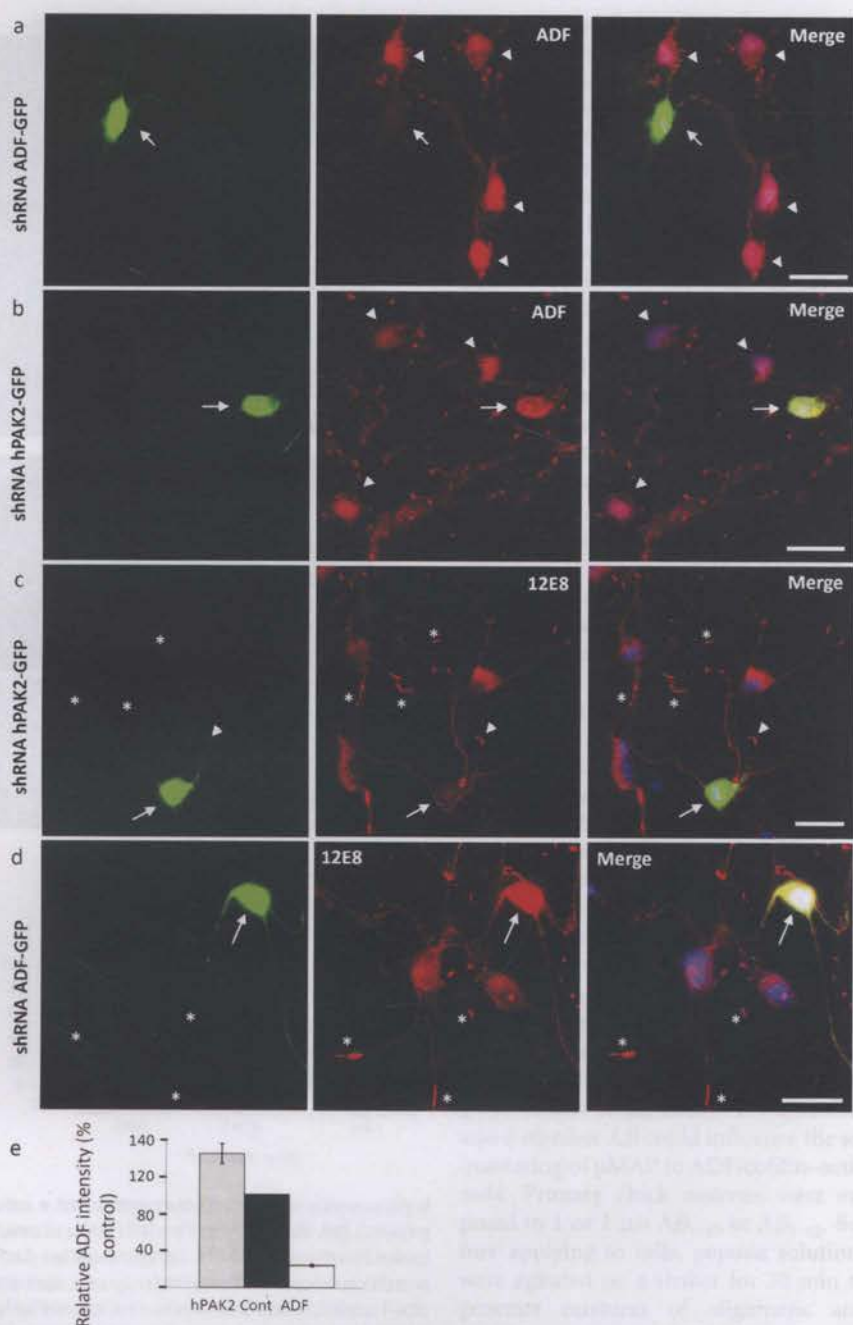


**Figure 6.** Reduction of the cellular ADF/cofilin pool inhibits the formation of rods and sequestration of pMAP. *a*, ADF was knocked down in primary chick tectal neurons by expression of shRNA from a plasmid also encoding GFP for visualization of transfected cells. In cultures transfected for 4 d, ADF immunolabeling using the 1439 antibody demonstrated significant ADF knockdown in transfected cells (arrow) compared with surrounding nontransfected cells (arrowheads). *b*, Cells transfected with an shRNA specific for human PAK2 as a control (arrow) showed no reduction of ADF compared with surrounding nontransfected cells (arrowheads). *c, d*, Transfected cultures were treated with 1  $\mu$ M AM and immunolabeled with 12E8 to determine whether pMAP accumulates into rod-like structures after significant reduction of ADF. Whereas hPAK2 shRNA-transfected cells (*c*, arrow) formed pMAP-positive rods (arrowhead) comparable with surrounding nontransfected cells (asterisks), ADF shRNA-transfected cells (*d*, arrow) never accumulated pMAP-positive rods, although surrounding cells frequently did (asterisks). Images represent single examples from >50 ADF shRNA transfected cells in three independent experiments. *e*, Quantification of ADF (1439) staining intensity revealed a 75% knockdown in ADF shRNA-transfected cells compared with nearby nontransfected (control) cells (transfected cell staining intensity, mean  $\pm$  SEM, 24.1  $\pm$  1.5, expressed as percentage of control cells;  $n = 25$ ). In contrast, ADF staining intensity of hPAK2 shRNA-transfected cells compared with surrounding nontransfected cells was not reduced (intensity, mean  $\pm$  SEM, 144.2  $\pm$  10.8%;  $n = 25$ ). Scale bars, 20  $\mu$ m.



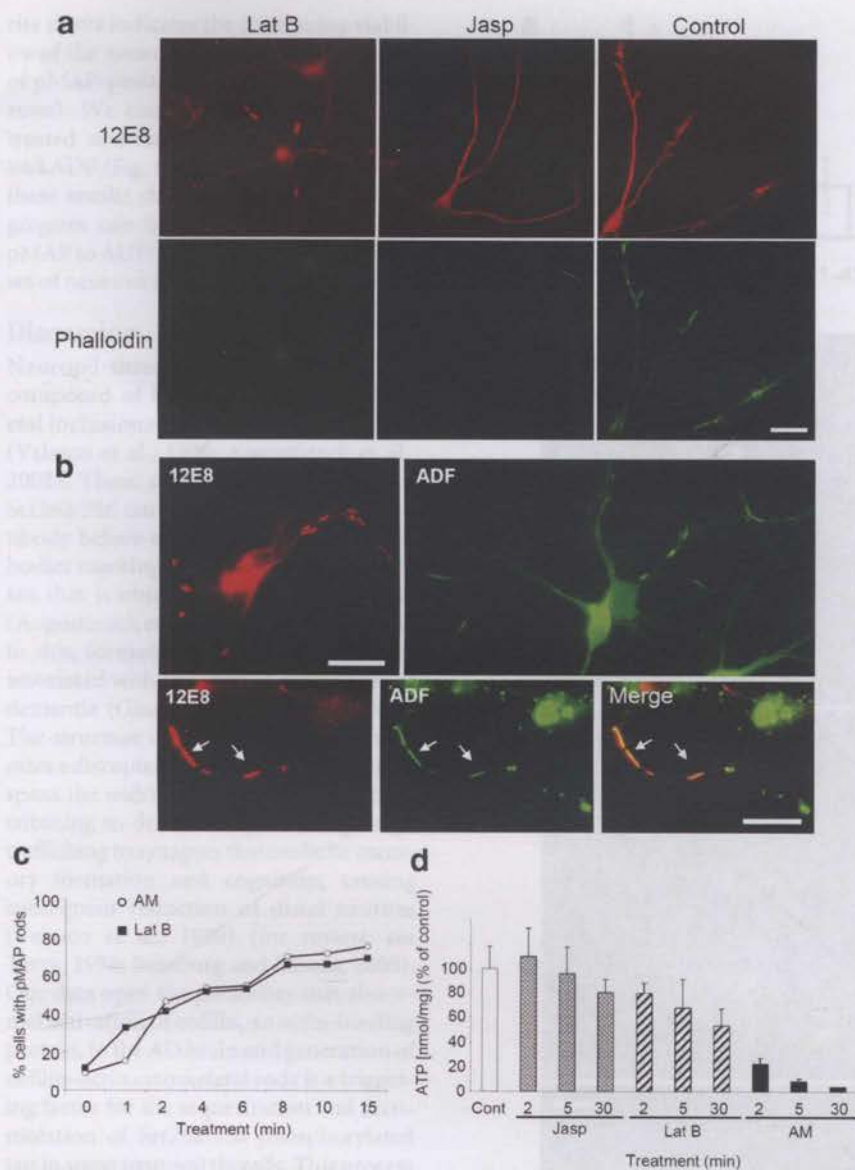


**Figure 7.** Dynamic F-actin enhances pMAP and actin rod formation. *a*, After treatment with Lat B but not Jasp, the assembly of pMAP into rod-like structures occurred. The chick neurons were stained for pMAP (12E8) and F-actin (phalloidin-488). Costaining with phalloidin showed only very weak labeling of F-actin in both Lat B- and Jasp-treated cells. *b*, Treating cells with Lat B induced formation of pMAP (red; 12E8) and ADF (green; 1439) rods, as seen in single stainings. Colabeling revealed frequent colocalization of both proteins (arrows). *c*, To compare the rate and abundance of rod formation under either mitochondrial inhibition or F-actin manipulation, rods were counted in cells treated with AM or Lat B for increasing times, as indicated. The pattern of rod formation in each condition was comparable. *d*, To ascertain the relationship between rod formation and ATP levels under these conditions, luminescence assays were conducted. Whereas Jasp-treated cells had levels of ATP comparable with controls and AM-treated cells had a dramatic decrease, only moderate decline in ATP levels in Lat B-treated cells was evident. Error bars represent the SEM from triplicate samples. Scale bars, 20  $\mu$ m.

it should be noted that phalloidin cannot stain ADF/cofilin saturated F-actin. In contrast, Jasp binds and stabilizes F-actin resulting in a net decrease in the G-actin pool (Bubb et al., 1994). Since Jasp competes for the phalloidin-binding site on F-actin, stabilized F-actin cannot be visualized with fluorescent phalloidin in the presence of Jasp (Fig. 7*a*). However, ADF/cofilin cannot bind to phalloidin-stabilized F-actin (Minamide et al., 2000) and thus also would not likely bind to the Jasp-stabilized actin filaments.

Antibody labeling of Lat B-treated neurons revealed formation of both pMAP- and ADF-positive rods, which frequently colocalized in double-labeling experiments (Fig. 7*b*). In contrast,

neurons treated with Jasp (or cotreated with Jasp and AM) exhibited a total absence of pMAP and ADF rods (Fig. 7*a*). We then compared the rate and abundance of pMAP-stained rods after Lat B compared with AM treatments and found the chronology of their formation indistinguishable between conditions (Fig. 7*c*). That Lat B treatment only moderately reduced ATP in neurons (Fig. 7*d*) yet still induced ADF/cofilin–actin and pMAP rod formation comparable with mitochondrial inhibitors suggests that ATP depletion is not a direct cause of rod formation, but an upstream event. These data collectively suggest that subunit release from F-actin is required for the generation of pMAP-positive rods and that in neurons this can be induced by ADF/cofilin activation. It also appears that ADF/cofilin binding to F-actin is essential for the formation of cytoskeletal rods. Dissociated actin subunits saturated with activated ADF/cofilin thereby form cytoskeletal rod inclusions that appear to sequester and accumulate pMAP.

#### $A\beta$ peptides enhance pMAP accumulation at ADF/cofilin rods

In AD, the relationships between pMAP/tau pathologies, cofilin–actin pathologies, and amyloid pathologies arising from  $A\beta$  peptide oligomerization and/or aggregation are poorly understood. Synthetic  $A\beta_{1-42}$  has been shown to induce cofilin–actin rod pathology in up to 20% of neurons in dissociated rodent hippocampal cultures (Maloney et al., 2005), with the majority of these neurons located in the dentate gyrus (Davis et al., 2009). We therefore asked whether  $A\beta$  could influence the sequestering of pMAP to ADF/cofilin–actin rods. Primary chick neurons were exposed to 1 or 2  $\mu$ M  $A\beta_{1-40}$  or  $A\beta_{1-42}$ . Before applying to cells, peptide solutions were agitated on a shaker for 30 min to generate mixtures of oligomeric and fibrillar structures (Goldsbury et al., 2000). The solutions were then diluted into cell culture medium and added to cells at a final concentration of 1 or 2  $\mu$ M. After exposure to the peptides for 20 h, the cells were fixed and immunostained for

pMAP. Less rods were generated in cultures treated with  $A\beta$  compared with those treated with the mitochondrial inhibitors, consistent with previous studies of ADF/cofilin–actin rod generation in hippocampal neurons treated with  $A\beta$  peptides (Maloney et al., 2005). However, when mean numbers of pMAP-positive rods per cell were quantified on vehicle control and  $A\beta$ -treated coverslips, a significant increase in the number of rods was revealed in  $A\beta$ -treated cells (Fig. 8*a*). No difference was observed between cells treated with 1 and 2  $\mu$ M peptide or between cells treated with  $A\beta_{1-40}$  and  $A\beta_{1-42}$ . The presence of F-actin-rich active growth cones in  $A\beta$ -treated neurons containing pMAP rods in the neu-



rite shafts indicates the continuing viability of the neurons, despite the formation of pMAP-positive rods (Fig. 8*b*, white arrows). We confirmed that rods in A $\beta$ -treated neurons contained both pMAP and ADF (Fig. 8*c*, arrows). In conclusion, these results show that synthetic A $\beta$  aggregates can induce the recruitment of pMAP to ADF/cofilin–actin rods in a subset of neurons in these primary cultures.

## Discussion

Neuropil threads of the AD brain are composed of linear arrays of cytoskeletal inclusions containing the pMAP tau (Velasco et al., 1998; Augustinack et al., 2002). These structures are positive for Ser262/356 tau labeled with the 12E8 antibody before extensive staining by antibodies marking hyperphosphorylation of tau that is observed in late-stage disease (Augustinack et al., 2002). Corresponding to this, formation of neuropil threads is associated with the early clinical stages of dementia (Giannakopoulos et al., 2007). The structure of neuropil threads implicates a disrupted cytoskeletal network that spans the width of the neurite likely contributing to dementia by blocking cargo trafficking to synapses that underlie memory formation and cognition, causing subsequent retraction of distal neurites (Velasco et al., 1998) (for review, see Terry, 1998; Bamberg and Bloom, 2009). Our data open the possibility that abnormal activation of cofilin, an actin-binding protein, in the AD brain and generation of cofilin–actin cytoskeletal rods is a triggering factor for the sequestration and accumulation of Ser262/356 phosphorylated tau in some neuropil threads. This process may well represent an early pathogenic event in AD neurodegeneration.

Neurodegenerative stimuli including oxidative stress, mitochondrial dysfunction, excitotoxic glutamate, ischemia, and soluble forms of A $\beta$  lead to activation of cofilin and the related protein ADF and the generation of ADF/cofilin–actin rods in primary neuronal cell culture (for review, see Bamberg and Bloom, 2009). These rods resemble the cofilin aggregates that are widely distributed in the AD brain (Minamide et al., 2000). At a low ratio to actin and in an active (dephosphorylated) state, ADF/cofilin maximally enhance subunit turnover of F-actin, dynamically remodeling the actin cytoskeleton and thus playing an integral role in regulating actin-dependent synaptic stabilization (for review, see Bamberg and Bloom, 2009). ADF/cofilin bind cooperatively to F-actin, and, at higher ratios to actin, they

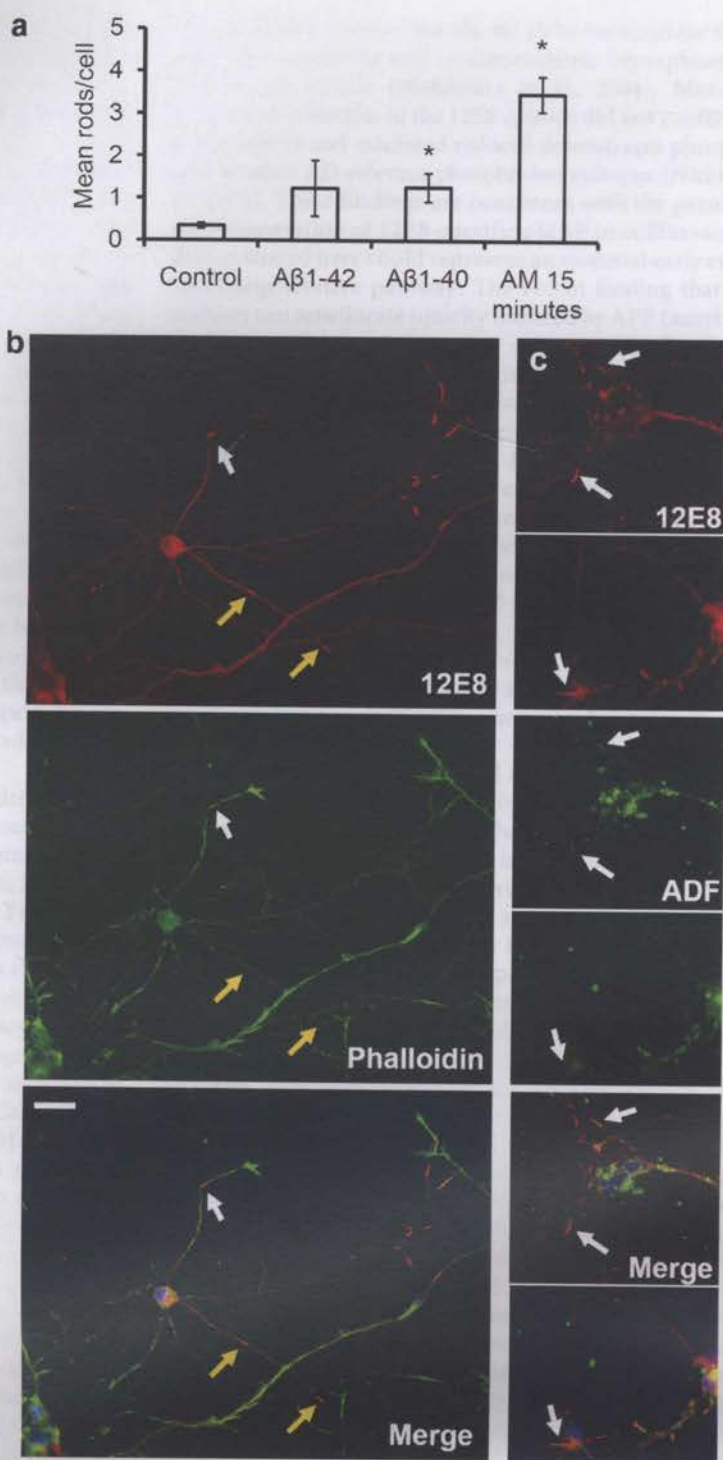


**Figure 8.** Amyloid peptides enhance pMAP sequestration to rods in primary chick neurons. Primary neurons were treated for 20 h with solutions of A $\beta$  peptides (1 or 2  $\mu$ M) and double-labeled with the 12E8 antibody (red) and either phalloidin-488 or ADF (both green) as indicated. **a**, The mean number of pMAP-positive rods per cell was quantified in >10 fields on control coverslips and coverslips treated with A $\beta$  peptides for 20 h or AM for 15 min. pMAP-positive rods per cell increased significantly after incubation with AM or A $\beta$  solutions compared with vehicle (DMSO) control (mean  $\pm$  SEM, 1.3  $\pm$  0.3 rods/nuclei for both aged A $\beta$ <sub>1-40</sub> and A $\beta$ <sub>1-42</sub> and 3.5  $\pm$  0.4 rods/nuclei for AM-treated compared with 0.4  $\pm$  0.1 rods/nuclei for control cells; \* $p$  < 0.02;  $n$  > 20; results are from duplicate experiments). Since no difference was seen between 1 versus 2  $\mu$ M peptide treatments, results have been pooled. **b**, pMAP-positive rods in A $\beta$ -treated neurons (shown here for A $\beta$ <sub>1-40</sub>) often formed at distal regions near the base of phalloidin-positive (F-actin-rich) active growth cones (white arrows). They also formed in neurite shafts associated with collapsed growth cones (**b**, yellow arrows). **c**, Rods assembling in A $\beta$ -treated neurons (shown here for A $\beta$ <sub>1-40</sub>) accumulated both pMAP (red) and ADF (green) (arrows). Merged images (plus DAPI in blue) are shown in bottom panels. Scale bar, 20  $\mu$ m.



can saturate regions of filaments and stabilize the pieces of filaments that remain after severing (Andrianantoandro and Pollard, 2006; Chan et al., 2009). Because ADF/cofilin bind to a minor, slightly twisted conformation of F-actin, they stabilize this “twisted” form, which prevents binding of the commonly used F-actin stain, phalloidin (McGough et al., 1997). In the brain, mitochondrial dysfunction and energy depletion associated with AD (Smith et al., 2005; Wang et al., 2009) could feasibly serve as a pathway for F-actin remodeling in neurons, since up to 50% of neuronal energy is dedicated to actin dynamics (Bernstein and Bamburgh, 2003). We propose mitochondrial dysfunction is one potential pathway upstream of the assembly of cytoskeletal rods because direct electron transport chain inhibitors elicit cofilin activation, concomitant with rod assembly in primary neurons and organotypic rat hippocampal brain slices. This pathway results in a precipitous drop in ATP, and the release of the cofilin phosphatase chronophin from an inhibitory complex with Hsp90, resulting in cofilin–actin rod formation (Huang et al., 2008). However, cofilin–actin rods can also be induced while maintaining higher levels of cellular ATP, such as with peroxide (Fig. 4), which activates the cofilin phosphatase slingshot by oxidizing and removing inhibition by 14-3-3 and leads to almost complete cofilin dephosphorylation and cofilin–actin rod formation (Kim et al., 2009). The common thread is an increased pool of active ADF/cofilin with respect to the amount of F-actin such that ADF/cofilin-saturated pieces of F-actin are available and coalesce into rods.

What is the role of pMAP at the cofilin–actin rods? Rods isolated from neurons and non-neuronal cell lines contain ADF/cofilin:actin in a 1:1 complex and indeed can be formed *in vitro* from these purified proteins (L. S. Minamide, S. Maiti, J. A. Boyle, R. C. Davis, J. A. Coppinger, Y. Bao, T. Y. Huang, J. Yates, G. M. Bokoch, and J. R. Bamburgh, unpublished results). Thus, as is also shown here, pMAP is not essential for cofilin–actin rod formation. Nevertheless, pMAP association with most cofilin–actin rods occurs very early in the rod formation process. Rods isolated from cortical neurons and those formed from endogenous proteins from a non-neuronal cell line both have similar stabilities to alterations in pH, ionic strength, reducing agents,  $\text{Ca}^{2+}$ /EGTA, ATP, and detergents. Therefore the presence of pMAP on the neuronal rods does not appear to confer in them any special property related to their stability. The question then arises—do the rods confer any special property on the associated pMAP? The tandem arrays of the rapidly formed cofilin–actin rods are similar in size and distribution to the neuritic striations of the neuropil threads in AD. The ultrastructure of most striated neuropil threads from AD brain clearly shows these to consist of the ~20-nm-diameter paired helical filaments (PHFs) (Velasco et al., 1998), not of the cofilin–actin bundles containing ~10-nm-diameter filaments that we observe in organotypic hippocampal slices treated with  $\text{A}\beta_{1-42}$  peptide oligomers (Davis et al., 2009). Thus, we suggest that the cofilin–actin rods serve as a template for recruitment and binding of pMAP, and that this association facilitates additional phosphorylation of pMAP and its self-assembly leading to the eventual replacement of the cofilin–actin rods with PHF bundles. Additional long-term studies are needed to test this hypothesis.

Supporting the concept that pMAP/tau accumulation and toxicity is linked to interactions with the actin cytoskeleton is work in *Drosophila* models that showed that toxicity of overexpressed hyperphosphorylated tau could be modified by genetic ablation or coexpression of actin-associated proteins (Fulga et al., 2007). Interestingly, tau phosphorylation at the

12E8 antibody epitope was shown to be essential for the initiation of tau toxicity and its downstream hyperphosphorylation in *Drosophila* (Nishimura et al., 2004). Mutated tau nonphosphorylatable at the 12E8 epitope did not confer toxicity in *Drosophila* and exhibited reduced downstream phosphorylation at other AD-relevant phospho-tau epitopes (Nishimura et al., 2004). These findings are consistent with the premise that the sequestration of 12E8-specific pMAP to cofilin–actin rods demonstrated here could represent an essential early event in a neurodegenerative pathway. The recent finding that tau reduction can ameliorate toxicity induced by APP (amyloid precursor protein) overexpression or exposure of cells to  $\text{A}\beta$  oligomers is also consistent with the key involvement of pMAP/tau in response to toxic events (King et al., 2006; Roberson et al., 2007). Potential deleterious effects of cytoskeletal rods on neurons are multifold. First, rods that assemble in axons and dendrites of cultured neurons form transport blockades inhibiting the free movement of vesicles and organelles leading to synaptic dysfunction (Jang et al., 2005; Maloney et al., 2005, 2008). Second, the accumulation of actin and cofilin in rod structures could directly impinge on the availability of cofilin for its function in modulating actin dynamics at the synapse (Hotulainen et al., 2009). Likewise, the sequestration of pMAP/tau to the rod matrix could adversely affect the role of tau in stabilizing and regulating the axonal MT network of tracks for fast axonal transport.

The generation of cytoskeletal rods in response to stressors may be an initial compensatory response to slow down energy-consuming actin dynamics and thereby protect neurons under conditions in which ATP supply is compromised (Bernstein et al., 2006). However, repeated or prolonged stress would likely be detrimental. Increasing evidence suggests declining mitochondrial function and reduced energy metabolism to be early events in the AD brain, preceding severe pathological changes (Smith et al., 2005; Wang et al., 2009). Aging is the major risk factor for sporadic AD, and on the one hand, electron transport chain activity declines with age, whereas on the other, oxidative stress increases, potentially impacting on the availability of ATP in cells (Lin and Beal, 2006). Moreover, the reduction of glucose uptake in AD brain cells and concomitant decline in glycolysis would also negatively impact ATP levels. Precedents of local mitochondrial dysfunction could be multifold and varied in the aging brain, for example, low brain perfusion attributable to vascular insufficiency, stroke, and  $\text{A}\beta$  peptide-mediated perturbation of mitochondria (Cullen et al., 2005; Du et al., 2008; Cho et al., 2009). Mechanisms linking this metabolic dysfunction with the formation of neuropathological lesions in the AD brain need to be established. Interestingly, it was demonstrated that environmental toxin inhibitors of mitochondrial respiratory chain complexes induce somatic inclusions of phosphorylated tau in neuronal cell culture and neurodegeneration in tau-related disease (Escobar-Khondiker et al., 2007).

Advanced neuropathology involving pMAP and cofilin accumulation and aggregation may be a result of increased vulnerability to normal environmental stress in brains expressing mutant tau (i.e., in hereditary frontotemporal dementias) or from elevated oxidative/mitochondrial stress in brains expressing wild-type endogenous tau (in sporadic AD). In a healthy brain, a fine balance between these stressors and compensatory defense mechanisms must normally occur, given that development of tau pathology and AD are not an inevitable part of aging. Recent evidence showing that neuronal cell bodies attached to dystrophic neurites in AD-related transgenic mice are still viable and



otherwise healthy (Adalbert et al., 2009) holds promise for future work to develop methods to disrupt the formation of the cofilin–actin rods and/or the interaction between cofilin and pMAP for establishing new therapeutic strategies to combat this disease early in its development.

## References

- Adalbert R, Nogradi A, Babetto E, Janeckova L, Walker SA, Kerschensteiner M, Misgeld T, Coleman MP (2009) Severely dystrophic axons at amyloid plaques remain continuous and connected to viable cell bodies. *Brain* 132:402–416.
- Andrianantoandro E, Pollard TD (2006) Mechanism of actin filament turnover by severing and nucleation at different concentrations of ADF/cofilin. *Mol Cell* 24:13–23.
- Augustinack JC, Schneider A, Mandelkow EM, Hyman BT (2002) Specific tau phosphorylation sites correlate with severity of neuronal cytopathology in Alzheimer's disease. *Acta Neuropathol* 103:26–35.
- Bamburg JR, Bloom GS (2009) Cytoskeletal pathologies of Alzheimer disease. *Cell Motil Cytoskel* 66:635–649.
- Bernstein BW, Bamburg JR (2003) Actin-ATP hydrolysis is a major energy drain for neurons. *J Neurosci* 23:1–6.
- Bernstein BW, Chen H, Boyle JA, Bamburg JR (2006) Formation of actin-ADF/cofilin rods transiently retards decline of mitochondrial potential and ATP in stressed neurons. *Am J Physiol Cell Physiol* 291:C828–C839.
- Braak H, Alafuzoff I, Arzberger T, Kretschmar H, Del Tredici K (2006) Staging of Alzheimer disease-associated neurofibrillary pathology using paraffin sections and immunocytochemistry. *Acta Neuropathol* 112:389–404.
- Brummelkamp TR, Bernards R, Agami R (2002) A system for stable expression of short interfering RNAs in mammalian cells. *Science* 296:550–553.
- Bubb MR, Senderowicz AM, Sausville EA, Duncan KL, Korn ED (1994) Jasplakinolide, a cytotoxic natural product, induces actin polymerization and competitively inhibits the binding of phalloidin to F-actin. *J Biol Chem* 269:14869–14871.
- Carlier M-F, Laurent V, Santolini J, Melki R, Didry D, Xia G-X, Hong Y, Chua N-H, Pantaloni D (1997) Actin depolymerizing factor (ADF/cofilin) enhances the rate of filament turnover: implication in actin-based motility. *J Cell Biol* 136:1307–1322.
- Chan C, Beltzner CC, Pollard TD (2009) Cofilin dissociates Arp2/3 complex and branches from actin filaments. *Curr Biol* 19:537–545.
- Cho DH, Nakamura T, Fang J, Cieplak P, Godzik A, Gu Z, Lipton SA (2009) S-nitrosylation of Drp1 mediates beta-amyloid-related mitochondrial fission and neuronal injury. *Science* 324:102–105.
- Coué M, Brenner SL, Spector I, Korn ED (1987) Inhibition of actin polymerization by latrunculin A. *FEBS Lett* 213:316–318.
- Cullen KM, Kócsi Z, Stone J (2005) Vascular relationships of haem-rich deposits in the aging cerebral cortex. *J Cereb Blood Flow Metab* 25:1656–1667.
- Davis RC, Maloney MT, Minamide LS, Flynn KC, Stonebraker MA, Bamburg JR (2009) Mapping cofilin-actin rods in stressed hippocampal slices and the role of cdc42 in amyloid  $\beta$ -induced rods. *J Alzheimers Dis* 18:35–50.
- Devineni N, Minamide LS, Niu M, Safer D, Verma R, Bamburg JR, Nachmias VT (1999) A quantitative analysis of G-actin binding proteins and the G-actin pool in developing chick brain. *Brain Res* 823:129–140.
- Du H, Guo L, Fang F, Chen D, Sosunov AA, McKhann GM, Yan Y, Wang C, Zhang H, Molkentin JD, Gunn-Moore FJ, Vonsattel JP, Arancio O, Chen JX, Yan SD (2008) Cyclophilin D deficiency attenuates mitochondrial and neuronal perturbation and ameliorates learning and memory in Alzheimer's disease. *Nat Med* 14:1097–1105.
- Escobar-Khondiker M, Höllerhage M, Muriel MP, Champy P, Bach A, Depienne C, Respondek G, Yamada ES, Lannuzel A, Yagi T, Hirsch EC, Oertel WH, Jacob R, Michel PP, Ruberg M, Höglinger GU (2007) Annonacin, a natural mitochondrial complex I inhibitor, causes tau pathology in cultured neurons. *J Neurosci* 27:7827–7837.
- Fulga TA, Elson-Schwab J, Khurana V, Steinhilb ML, Spire TL, Hyman BT, Feany MB (2007) Abnormal bundling and accumulation of F-actin mediates tau-induced neuronal degeneration in vivo. *Nat Cell Biol* 9:139–148.
- Garcia ML, Cleveland DW (2001) Going new places using an old MAP: tau, microtubules and human neurodegenerative disease. *Curr Opin Cell Biol* 13:41–48.
- Gervásio OL, Whitehead NP, Yeung EW, Phillips WD, Allen DG (2008) TRPC1 binds to caveolin-3 and is regulated by Src kinase—role in Duchenne muscular dystrophy. *J Cell Sci* 121:2246–2255.
- Giannakopoulos P, von Gunten A, Kovari E, Gold G, Herrman FR, Hof PR, Bouras C (2007) Stereological analysis of neuropil threads in the hippocampal formation: relationships with Alzheimer's disease neuronal pathology and cognition. *Neuropathol Appl Neurobiol* 33:334–343.
- Goedert M, Spillantini MG (2006) A century of Alzheimer's disease. *Science* 314:777–781.
- Goldsbury C, Whiteman IT, Jeong EV, Lim Y-A (2008) Oxidative stress increases levels of endogenous amyloid-beta peptides secreted from primary chick brain neurons. *Aging Cell* 7:771–775.
- Goldsbury CS, Wirtz S, Müller SA, Sunderji S, Wicki P, Aebi U, Frey P (2000) Studies on the in vitro assembly of a beta 1-40: implications for the search for a beta fibril formation inhibitors. *J Struct Biol* 130:217–231.
- Guillemin GJ, Cullen KM, Lim CK, Smythe GA, Garner B, Kapoor V, Takikawa O, Brew BJ (2007) Characterization of the kynurenine pathway in human neurons. *J Neurosci* 27:12884–12892.
- Haass C, Selkoe DJ (2007) Soluble protein oligomers in neurodegeneration: lessons from the Alzheimer's amyloid beta-peptide. *Nat Rev Mol Cell Biol* 8:101–112.
- He TC, Zhou S, da Costa LT, Yu J, Kinzler KW, Vogelstein B (1998) A simplified system for generating recombinant adenoviruses. *Proc Natl Acad Sci U S A* 95:2509–2514.
- Hotulainen P, Llano O, Smirnov S, Tanhuanpää K, Faix J, Rivera C, Lappalainen P (2009) Defining mechanisms of actin polymerization and depolymerization during dendritic spine morphogenesis. *J Cell Biol* 185:323–339.
- Huang TY, Minamide LS, Bamburg JR, Bokoch GM (2008) Chronophin mediates an ATP-sensing mechanism for cofilin dephosphorylation and neuronal cofilin-actin rod formation. *Dev Cell* 15:691–703.
- Jang DH, Han JH, Lee SH, Lee YS, Park H, Lee SH, Kim H, Kaang BK (2005) Cofilin expression induces cofilin-actin rod formation and disrupts synaptic structure and function in *Aplysia* synapses. *Proc Natl Acad Sci U S A* 102:16072–16077.
- Kim JS, Huang TY, Bokoch GM (2009) Reactive oxygen species regulate a slingshot-cofilin activation pathway. *Mol Biol Cell* 20:2650–2660.
- King ME, Kan HM, Baas PW, Erisir A, Glabe CG, Bloom GS (2006) Tau-dependent microtubule disassembly initiated by prefibrillar beta-amyloid. *J Cell Biol* 175:541–546.
- Lin MT, Beal MF (2006) Mitochondrial dysfunction and oxidative stress in neurodegenerative diseases. *Nature* 443:787–795.
- Maloney MT, Minamide LS, Kinley AW, Boyle JA, Bamburg JR (2005)  $\beta$ -secretase-cleaved amyloid precursor protein accumulates at actin inclusions induced in neurons by stress or amyloid- $\beta$ : a feedforward mechanism for Alzheimer's disease. *J Neurosci* 25:11313–11321.
- Maloney MT, Kinley A, Pak C, Bamburg JR (2008) ADF/cofilin, actin dynamics and disease. *Protein Rev* 8:83–187.
- McGough A, Pope B, Chiu W, Weeds A (1997) Cofilin changes the twist of F-actin: implications for actin filament dynamics and cellular function. *J Cell Biol* 138:771–781.
- Minamide LS, Striegel AM, Boyle JA, Meberg PJ, Bamburg JR (2000) Neurodegenerative stimuli induce persistent ADF/cofilin-actin rods that disrupt distal neurite function. *Nat Cell Biol* 2:628–636.
- Nishimura I, Yang Y, Lu B (2004) PAR-1 kinase plays an initiator role in a temporally ordered phosphorylation process that confers tau toxicity in *Drosophila*. *Cell* 116:671–682.
- Pendleton A, Pope B, Weeds A, Koffer A (2003) Latrunculin B or ATP depletion induces cofilin-dependent translocation of actin into nuclei of mast cells. *J Biol Chem* 278:14394–14400.
- Roberson ED, Searce-Levie K, Palop JJ, Yan F, Cheng IH, Wu T, Gerstein H, Yu GQ, Mucke L (2007) Reducing endogenous tau ameliorates amyloid  $\beta$ -induced deficits in an Alzheimer's disease mouse model. *Science* 316:750–754.
- Schaar BT, Kinoshita K, McConnell SK (2004) Doublecortin microtubule affinity is regulated by a balance of kinase and phosphatase activity at the leading edge of migrating neurons. *Neuron* 41:203–213.
- Seubert P, Mawal-Dewan M, Barbour R, Jakes R, Goedert M, Johnson GV, Litsky JM, Schenk D, Lieberburg I, Trojanowski JQ (1995) Detection





## SHORT TAKE

Oxidative stress increases levels of endogenous amyloid- $\beta$  peptides secreted from primary chick brain neurons

Claire Goldsbury,<sup>1</sup> Ineka T. Whiteman,<sup>1,2</sup>  
Erica V. Jeong<sup>1,2</sup> and Yun-An Lim<sup>1</sup>

<sup>1</sup>Brain and Mind Research Institute, University of Sydney,  
Camperdown, NSW 2050, Australia

<sup>2</sup>Discipline of Anatomy and Histology, Bosch Institute, School of  
Medical Sciences, University of Sydney, Sydney, NSW 2006,  
Australia

## Summary

**Oxidative damage is associated with Alzheimer's disease and mild cognitive impairment, but its relationship to the development of neuropathological lesions involving accumulation of amyloid- $\beta$  (A $\beta$ ) peptides and hyperphosphorylated tau protein remains poorly understood. We show that inducing oxidative stress in primary chick brain neurons by exposure to sublethal doses of H<sub>2</sub>O<sub>2</sub> increases levels of total secreted endogenous A $\beta$  by 2.4-fold after 20 h. This occurs in the absence of changes to intracellular amyloid precursor protein or tau protein levels, while heat-shock protein 90 is elevated 2.5-fold. These results are consistent with the hypothesis that aging-associated oxidative stress contributes to increasing A $\beta$  generation and up-regulation of molecular chaperones in Alzheimer's disease. Key words: Alzheimer's disease; amyloid- $\beta$  peptide; oxidative stress.**

Extracellular plaques containing aggregated amyloid- $\beta$  (A $\beta$ ) peptides and intracellular neurofibrillary tangles of hyperphosphorylated tau protein are the two salient pathological hallmarks of the Alzheimer's disease (AD) brain. A $\beta$  is generated by consecutive cleavages of amyloid precursor protein (APP) by  $\beta$ -secretase ( $\beta$ -site APP cleaving enzyme 1, BACE 1) and the  $\gamma$ -secretase protein complex of which presenilin is the catalytic subunit (Hardy, 2006). Familial mutations in APP or presenilin lead to increased generation and/or aggregation of A $\beta$  peptides and cause early-onset AD (Hardy, 2006). Aggregated A $\beta$  interferes with synaptic plasticity and causes neuronal cell death

(Lambert *et al.*, 1998; Townsend *et al.*, 2006; Kaye *et al.*, 2004; Wogulis *et al.*, 2005). This and other evidence supports the amyloid hypothesis which postulates that toxicity exerted by aggregated A $\beta$  initiates AD, with synaptic dysfunction, neurofibrillary pathology and oxidative injury constituting downstream events (Hardy, 2006).

A number of studies, however, suggest that oxidative damage occurs in mild cognitive impairment (MCI) and early stages of sporadic AD, before widespread plaque and tangle development (Sayre *et al.*, 1997; Butterfield *et al.*, 2006; Nunomura *et al.*, 2006; Williams *et al.*, 2006; Lovell & Markesbery, 2008). Stress-activated BACE 1 and  $\gamma$ -secretase have been proposed to contribute to the deposition of A $\beta$  peptides in sporadic AD (Tamagno *et al.*, 2008). Supporting this idea, expression and activity of BACE 1 is elevated in the brains of sporadic AD patients (Fukumoto *et al.*, 2002; Holsinger *et al.*, 2002). In addition, BACE 1 is a demonstrated stress-induced protease that is up-regulated in response to oxidative stress (Tamagno *et al.*, 2005; Tong *et al.*, 2005), energy depletion (Velliquette *et al.*, 2005), traumatic brain injury (Blasko *et al.*, 2004) or cerebral ischemia (Wen *et al.*, 2004; Tesco *et al.*, 2007), all of which are events associated with increased sporadic AD risk. These findings suggest that oxidative stress is upstream of A $\beta$  in AD and that A $\beta$  might be generated as a compensatory response in neurons attempting to attenuate oxidative stress (Smith *et al.*, 2002; Lee *et al.*, 2006). In addition, neurofibrillary degeneration may exacerbate the oxidative damage and elevation of A $\beta$  (Yan *et al.*, 1995). In this context, mutations in APP that cause familial AD or in tau that cause frontotemporal dementias could contribute to neurodegeneration in part by increasing neuronal vulnerability to oxidative stress (Marques *et al.*, 2003; Dias-Santagata *et al.*, 2007).

Intracellular A $\beta$  has been linked to secretory pathway dysfunction and apoptosis (LeBlanc, 1995; Gasparini *et al.*, 1997; Zhang *et al.*, 1997; Ohyagi *et al.*, 1999; Gouras *et al.*, 2005) and its elevation following oxidative stress has been demonstrated in neuroblastoma cells (Misonou *et al.*, 2000; Paola *et al.*, 2000; Tamagno *et al.*, 2005, 2008; Zheng *et al.*, 2006), rat cortical neurons (Hasegawa *et al.*, 2005), astrocytes (Busciglio *et al.*, 2002), mixed fetal guinea pig brain cells (Ohyagi *et al.*, 1999) and mammalian lenses (Frederikse *et al.*, 1996). Since A $\beta$  peptides largely accumulate in the extracellular spaces of the AD brain, we were interested in determining whether oxidative stress by exposure to H<sub>2</sub>O<sub>2</sub> influences secretion of A $\beta$  peptides from neurons derived from embryonic chick brain. The human and chicken A $\beta$  peptide sequences are identical and chick neurons ubiquitously secrete A $\beta$ , making this a relevant and readily accessible model

## Correspondence

Claire Goldsbury, Brain and Mind Research Institute, University of Sydney,  
100 Mallett St, Camperdown, NSW 2050, Australia. Tel.: +61 2 9351 0878;  
fax: +61 2 9351 0731; e-mail: cgoldsbury@usyd.edu.au

C.G. conceived and executed experiments and wrote the paper; I.T.W.,  
E.J. and Y.-A.L. executed experiments.

Accepted for publication 16 July 2008



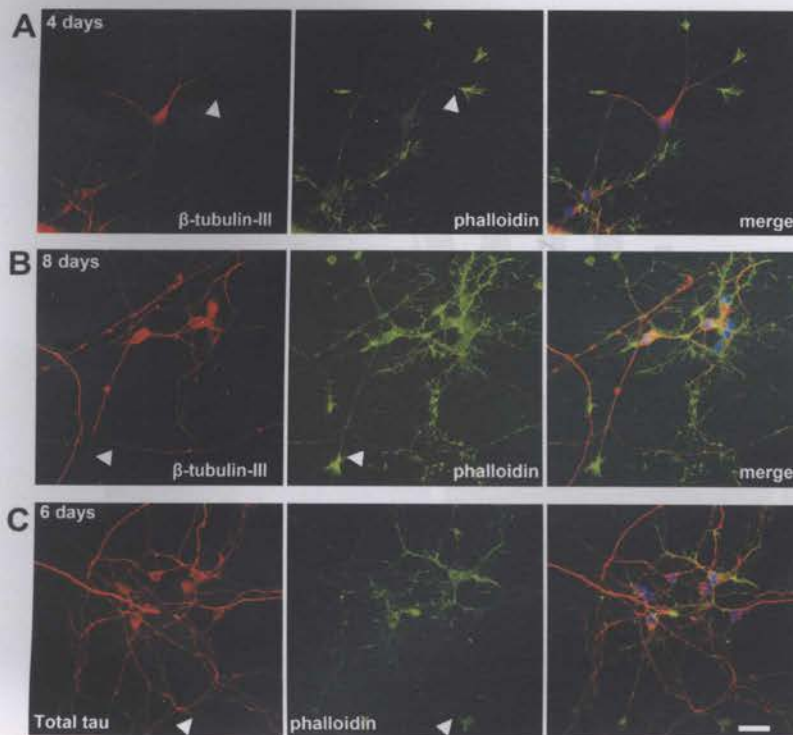


**Fig. 1** Characterization of primary embryonic chick tectal neurons. Labeling with neuron-specific markers (red) beta tubulin-III (mouse monoclonal, Abcam) (A, B) and tau (rabbit polyclonal, Dako) (C), demonstrated that at least 97% of cells in the cultures are neuronal after up to 8 days *in vitro*. Beta tubulin-III and tau labeling extends through the neuronal processes to the base of F-actin (green)-rich growth cones (arrows). Scale bar = 20  $\mu$ m.

for investigating the modulation of endogenous APP processing in neurons (Esselmann *et al.*, 2004; Carrodeguas *et al.*, 2005).

Cell cultures were prepared from 7-days-in-ovo embryonic chick tecta and were characterized as ~97% neuronal after 8 days *in vitro*, estimated by the proportion of cells positively labeled by the neuron-specific markers beta tubulin-III and tau protein (Fig. 1A–C) (detailed methods provided in Supporting information). At least  $92 \pm 13\%$  of cells were viable following treatment with up to  $50 \mu\text{M}$  H<sub>2</sub>O<sub>2</sub> for 20 h (mean  $\pm$  standard deviation,  $n \geq 150$  cells) (Fig. 2A,B). A sharp decline in viability was observed at H<sub>2</sub>O<sub>2</sub> concentrations  $> 50 \mu\text{M}$  ( $63 \pm 13\%$  and  $10 \pm 13\%$  at  $125 \mu\text{M}$  and  $250 \mu\text{M}$  H<sub>2</sub>O<sub>2</sub>, respectively; mean  $\pm$  standard deviation,  $n \geq 150$  cells) (Fig. 2A). A $\beta$  peptides were immunoprecipitated from culture medium after 20 h exposure to sublethal concentrations of 10–20  $\mu\text{M}$  H<sub>2</sub>O<sub>2</sub> (Fig. 2C,D). H<sub>2</sub>O<sub>2</sub> caused a  $2.4 \pm 0.6$ -fold increase in secreted A $\beta$  (mean fold increase  $\pm$  standard error of mean,  $n = 12$  H<sub>2</sub>O<sub>2</sub> treated and  $n = 10$  control, Student's *t*-test:  $p < 0.05$ ; Fig. 2E). No changes were observed in total endogenous APP (Fig. 2F) or tau protein levels in the corresponding cell lysates (Fig. 2D), but heat-shock protein 90 (Hsp90) levels were elevated  $2.5 \pm 0.3$ -fold (mean fold increase  $\pm$  standard error of mean,  $n = 9$  H<sub>2</sub>O<sub>2</sub> treated and  $n = 9$  control, Student's *t*-test:  $p < 0.01$ ; Fig. 2D,G). Notably, heat-shock proteins are up-regulated in AD brain (Hamos *et al.*, 1991; Dickey *et al.*, 2007).

In summary, we demonstrate that exposure to nonlethal doses of peroxidative stress for 20 h significantly increases the accumulation of extracellular A $\beta$  in primary chick neuronal cultures. This is accompanied by increased cellular Hsp90. These

results suggest that A $\beta$ , in addition to causing oxidative stress through generation of reactive oxygen species (Behl *et al.*, 1994), may be generated by neurons in response to increased oxidative stress during aging (Lee *et al.*, 2006; Nunomura *et al.*, 2006). Chick brain neurons secrete a highly conserved pattern of A $\beta$  peptides analogous to that normally found in human cerebrospinal fluid (A $\beta$ 1-37/38/39/40/42) (Esselmann *et al.*, 2004). Here, we observe an overall increase in total A $\beta$  levels induced by H<sub>2</sub>O<sub>2</sub>. Further studies are needed to determine whether any A $\beta$  isoforms in particular are specifically increased by oxidative insults, what mechanism this might involve and whether oxidative stress also influences the phosphorylation and/or distribution of tau protein in these neurons. The conserved properties of APP trafficking and processing (Goldsbury *et al.*, 2006), as well as the analogous sequence and phosphorylation patterns of tau protein in chick neurons (Yoshida & Goedert, 2002), make this primary culture system a promising model for delineating the cell biology and pathological modulation of AD-related proteins.

## Acknowledgments

C.G. is supported by a University of Sydney International Senior Research Fellowship and I.W. by an Australian Postgraduate Award. This work was supported by the University of Sydney Bosch Institute Advanced Microscopy Facility under the direction of Dr Louise Cole. We thank Professor Christian Haass for kindly providing the 3552 A $\beta$  antibody. We are grateful to Baiada Poultry, for the provision of fertilized chicken eggs. We thank Damien Holsinger for critical comments on the manuscript.

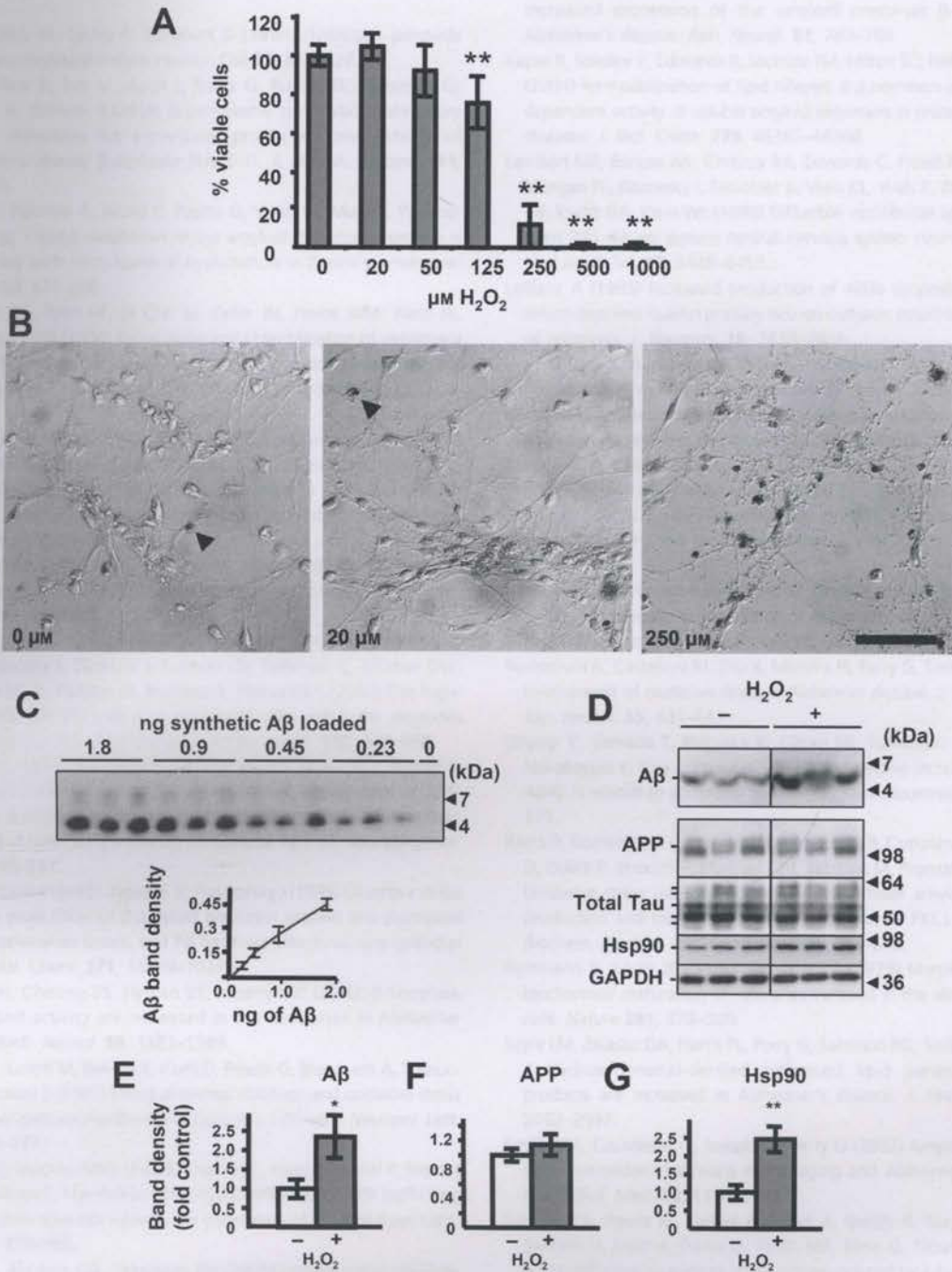


**Fig. 2** Elevated extracellular amyloid- $\beta$  (A $\beta$ ) peptides derived from primary chick tectal neurons after 20 h of H<sub>2</sub>O<sub>2</sub> exposure. Cell viability sharply decreases following exposure to H<sub>2</sub>O<sub>2</sub> at concentrations > 50  $\mu\text{M}$  (A). Only occasional Trypan Blue-positive cells are seen with H<sub>2</sub>O<sub>2</sub> concentrations < 50  $\mu\text{M}$  (B) (arrowheads). Scale bar = 100  $\mu\text{m}$ . Chemiluminescent detection of synthetic A $\beta$ 1-40 standards (Bachem) after immunoblotting demonstrates the linearity of the band density (C). Increased levels of extracellular A $\beta$  peptides are observed after H<sub>2</sub>O<sub>2</sub> treatment. APP (6E10), total tau (Dako) and Hsp90 (Abcam) are shown from corresponding cell lysates for three H<sub>2</sub>O<sub>2</sub>-treated cultures and three control cultures (D). A $\beta$  is elevated 2.4-fold by H<sub>2</sub>O<sub>2</sub> exposure (E). In the corresponding cell lysates, no change in total APP is observed (F) but there is a 2.5-fold increase in Hsp90 from H<sub>2</sub>O<sub>2</sub>-treated cultures (G). Membranes were probed with GAPDH antibody to confirm equal protein loading. Significance was determined by Student's *t*-test: \**p* < 0.05, \*\**p* < 0.01.



## References

- Behl C, Davis JB, Lesley R, Schubert D (1994) Hydrogen peroxide mediates amyloid  $\beta$  protein toxicity. *Cell* **77**, 817–827.
- Blasko I, Beer R, Bigl M, Apelt J, Franz G, Rudzki D, Ransmayr G, Kampfl A, Schliebs R (2004) Experimental traumatic brain injury in rats stimulates the expression, production and activity of Alzheimer's disease  $\beta$ -secretase (BACE-1). *J. Neural. Transm.* **111**, 523–536.
- Busciglio J, Pelsman A, Wong C, Pigino G, Yuan M, Mori H, Yankner BA (2002) Altered metabolism of the amyloid  $\beta$  precursor protein is associated with mitochondrial dysfunction in Down's syndrome. *Neuron* **33**, 677–688.
- Butterfield DA, Poon HF, St Clair D, Keller JN, Pierce WM, Klein JB, Markesbery WR (2006) Redox proteomics identification of oxidatively modified hippocampal proteins in mild cognitive impairment: insights into the development of Alzheimer's disease. *Neurobiol. Dis.* **22**, 223–232.
- Carrodeguas JA, Rodolosse A, Garza MV, Sanz-Clemente A, Pérez-Pé R, Lacosta AM, Domínguez L, Monleón I, Sánchez-Díaz R, Sorribas V, Sarasa M (2005) The chick embryo appears as a natural model for research in beta-amyloid precursor protein processing. *Neuroscience* **134**, 1285–1300.
- Dias-Santagata D, Fulga TA, Duttaray A, Feany MB (2007) Oxidative stress mediates tau-induced neurodegeneration in *Drosophila*. *J. Clin. Invest.* **117**, 236–245.
- Dickey CA, Kamal A, Lundgren K, Klosak N, Bailey RM, Dunmore J, Ash P, Shoraka S, Zlatkovic J, Eckman CB, Patterson C, Dickson DW, Nahman NS Jr, Hutton M, Burrows F, Petrucelli L (2007) The high-affinity HSP90-CHIP complex recognizes and selectively degrades phosphorylated tau client proteins. *J. Clin. Invest.* **117**, 648–658.
- Esselmann H, Maler JM, Kunz N, Otto M, Paul S, Lewczuk P, Rütger E, Kornhuber J, Wiltfang J (2004) Lithium decreases secretion of A $\beta$ 1-42 and C-truncated species A $\beta$ 1-37/38/39/40 in chicken telencephalic cultures but specifically increases intracellular A $\beta$ 1-38. *Neurodegener. Dis.* **1**, 236–241.
- Frederikse PH, Garland D, Zigler JS Jr, Piatigorsky J (1996) Oxidative stress increases production of  $\beta$ -amyloid precursor protein and  $\beta$ -amyloid (A $\beta$ ) in mammalian lenses, and A $\beta$  has toxic effects on lens epithelial cells. *J. Biol. Chem.* **271**, 10169–10174.
- Fukumoto H, Cheung BS, Hyman BT, Irizarry MC (2002)  $\beta$ -Secretase protein and activity are increased in the neocortex in Alzheimer disease. *Arch. Neurol.* **59**, 1381–1389.
- Gasparini L, Racchi M, Benussi L, Curti D, Binetti G, Blanchetti A, Trabucchi M, Govoni S (1997) Effect of energy shortage and oxidative stress on amyloid precursor protein metabolism in COS cells. *Neurosci. Lett.* **231**, 113–117.
- Goldsbury C, Mocanu MM, Thies E, Kaether C, Haass C, Keller P, Biernat J, Mandelkow E, Mandelkow EM (2006) Inhibition of APP trafficking by tau protein does not increase the generation of amyloid- $\beta$  peptides. *Traffic* **7**, 873–888.
- Gouras GK, Almeida CG, Takahashi RH (2005) Intraneuronal A $\beta$  accumulation and origin of plaques in Alzheimer's disease. *Neurobiol. Aging* **26**, 1235–1244.
- Hamos JE, Oblas B, Pulaski-Salo D, Welch WJ, Bole DG, Drachman DA (1991) Expression of heat shock proteins in Alzheimer's disease. *Neurology* **41**, 345–350.
- Hardy J (2006) Alzheimer's disease: the amyloid cascade hypothesis: an update and reappraisal. *J. Alzheimers Dis.* **9**(3 Suppl.), 151–153.
- Hasegawa T, Ukai W, Jo DG, Xu X, Mattson MP, Nakagawa M, Araki W, Saito T, Yamada T (2005) Homocysteic acid induces intraneuronal accumulation of neurotoxic A $\beta$ 42: implications for the pathogenesis of Alzheimer's disease. *J. Neurosci. Res.* **80**, 869–876.
- Holsinger RM, McLean CA, Beyreuther K, Masters CL, Evin G (2002) Increased expression of the amyloid precursor  $\beta$ -secretase in Alzheimer's disease. *Ann. Neurol.* **51**, 783–786.
- Kayed R, Sokolov Y, Edmonds B, McIntire TM, Milton SC, Hall JE, Glabe CG (2004) Permeabilization of lipid bilayers is a common conformation-dependent activity of soluble amyloid oligomers in protein misfolding diseases. *J. Biol. Chem.* **279**, 46363–46366.
- Lambert MP, Barlow AK, Chromy BA, Edwards C, Freed R, Liosatos M, Morgan TE, Rozovsky I, Trommer B, Viola KL, Wals P, Zhang C, Finch CE, Krafft GA, Klein WL (1998) Diffusible, nonfibrillar ligands derived from A $\beta$ 1-42 are potent central nervous system neurotoxins. *Proc. Natl Acad. Sci.* **95**, 6448–6453.
- LeBlanc A (1995) Increased production of 4kDa amyloid- $\beta$  peptide in serum deprived human primary neuron cultures: possible involvement of apoptosis. *J. Neurosci.* **15**, 7837–7846.
- Lee HG, Zhu X, Nunomura A, Perry G, Smith MA (2006) Amyloid beta: the alternate hypothesis. *Curr. Alzheimer Res.* **3**, 75–80.
- Lovell MA, Markesbery WR (2008) Oxidatively modified RNA in mild cognitive impairment. *Neurobiol. Dis.* **29**, 169–175.
- Marques CA, Keil U, Bonert A, Steiner B, Haass C, Müller WE, Eckert A (2003) Neurotoxic mechanisms caused by the Alzheimer's disease-linked Swedish amyloid precursor protein mutation: oxidative stress, caspases, and the JNK pathway. *J. Biol. Chem.* **278**, 28294–28302.
- Misonou H, Morishima-Kawashima M, Ihara Y (2000) Oxidative stress induces intracellular accumulation of amyloid  $\beta$ -protein (A $\beta$ ) in human neuroblastoma cells. *Biochemistry* **39**, 6951–6959.
- Nunomura A, Castellani RJ, Zhu X, Moreira PI, Perry G, Smith MA (2006) Involvement of oxidative stress in Alzheimer disease. *J. Neuropathol. Exp. Neurol.* **65**, 631–641.
- Ohyagi Y, Yamada T, Nishioka K, Clarke NJ, Tomlinson AJ, Naylor S, Nakabeppu Y, Kira J, Younkin SG (1999) Selective increase in cellular A $\beta$ 42 is related to apoptosis but not necrosis. *Neuroreport* **11**, 167–171.
- Paola D, Domenicotti C, Nitti M, Vitali A, Borghi R, Cottalasso D, Zaccheo D, Odetti P, Strocchi P, Marinari UM, Tabaton M, Pronzato MA (2000) Oxidative stress induces increase in intracellular amyloid  $\beta$ -protein production and selective activation of  $\beta$ I and  $\beta$ II PKCs in NT2 cells. *Biochem. Biophys. Res. Commun.* **268**, 642–646.
- Pettmann B, Louis JC, Sensenbrenner M (1979) Morphological and biochemical maturation of neurones cultured in the absence of glial cells. *Nature* **281**, 378–380.
- Sayre LM, Zelasko DA, Harris PL, Perry G, Salomon RG, Smith MA (1997) 4-Hydroxynonenal-derived advanced lipid peroxidation end products are increased in Alzheimer's disease. *J. Neurochem.* **68**, 2092–2097.
- Smith MA, Casadesus G, Joseph JA, Perry G (2002) Amyloid- $\beta$  and tau serve antioxidant functions in the aging and Alzheimer brain. *Free Radic. Biol. Med.* **33**, 1194–1199.
- Tamagno E, Parola M, Bardini P, Piccini A, Borghi R, Guglielmotto M, Santero G, Davit A, Danni O, Smith MA, Perry G, Tabaton M (2005)  $\beta$ -Site APP cleaving enzyme up-regulation induced by 4-hydroxynonenal is mediated by stress-activated protein kinases pathways. *J. Neurochem.* **92**, 628–636.
- Tamagno E, Guglielmotto M, Aragno M, Borghi R, Autelli R, Giliberto L, Muraca G, Danni O, Zhu X, Smith MA, Perry G, Jo DG, Mattson MP, Tabaton M (2008) Oxidative stress activates a positive feedback between the  $\gamma$ - and  $\beta$ -secretase cleavages of the  $\beta$ -amyloid precursor protein. *J. Neurochem.* **104**, 683–695.
- Tesco G, Koh YH, Kang EL, Cameron AN, Das S, Sena-Esteves M, Hiltunen M, Yang SH, Zhong Z, Shen Y, Simpkins JW, Tanzi RE (2007) Depletion of GGA3 stabilizes BACE and enhances  $\beta$ -secretase activity. *Neuron* **54**, 721–737.



- Tong Y, Zhou W, Fung V, Christensen MA, Qing H, Sun X, Song W (2005) Oxidative stress potentiates BACE1 gene expression and A $\beta$  generation. *J. Neural. Transm.* **112**, 455–469.
- Townsend M, Shankar GM, Mehta T, Walsh DM, Selkoe DJ (2006) Effects of secreted oligomers of amyloid  $\beta$ -protein on hippocampal synaptic plasticity: a potent role for trimers. *J. Physiol.* **572**, 477–492.
- Veliquette RA, O'Connor T, Vassar R (2005) Energy inhibition elevates  $\beta$ -secretase levels and activity and is potentially amyloidogenic in APP transgenic mice: possible early events in Alzheimer's disease pathogenesis. *J. Neurosci.* **25**, 10874–10883.
- Wen Y, Onyewuchi O, Yang S, Liu R, Simpkins JW (2004) Increased  $\beta$ -secretase activity and expression in rats following transient cerebral ischemia. *Brain Res.* **1009**, 1–8.
- Williams TI, Lynn BC, Markesbery WR, Lovell MA (2006) Increased levels of 4-hydroxynonenal and acrolein, neurotoxic markers of lipid peroxidation, in the brain in mild cognitive impairment and early Alzheimer's disease. *Neurobiol. Aging* **27**, 1094–1099.
- Wogulis M, Wright S, Cunningham D, Chilcote T, Powell K, Rydel RE (2005) Nucleation-dependent polymerization is an essential component of amyloid-mediated neuronal cell death. *J. Neurosci.* **25**, 1071–1080.
- Yan SD, Yan SF, Chen X, Fu J, Chen M, Kuppasamy P, Smith MA, Perry G, Godman GC, Nawroth P, Zweier JL, Stern D. (1995) Non-enzymatically glycosylated tau in Alzheimer's disease induces neuronal oxidant stress resulting in cytokine gene expression and release of amyloid  $\beta$ -peptide. *Nat. Med.* **1**, 693–699.
- Yoshida H, Goedert M (2002) Molecular cloning and functional characterization of chicken brain tau: isoforms with up to five tandem repeats. *Biochemistry* **41**, 15203–15211.
- Zhang L, Zhao B, Yew DT, Kusiak JW, Roth GS (1997) Processing of Alzheimer's amyloid precursor protein during H<sub>2</sub>O<sub>2</sub>-induced apoptosis in human neuronal cells. *Biochem. Biophys. Res. Commun.* **1997**, 845–848.
- Zheng L, Roberg K, Jerhammar F, Marcusson J, Terman A (2006) Oxidative stress induces intralysosomal accumulation of Alzheimer amyloid  $\beta$ -protein in cultured neuroblastoma cells. *Ann. N. Y. Acad. Sci.* **1067**, 248–251.

## Supporting Information

Additional supporting information may be found in the online version of this article.

### Appendix S1 Supplementary experimental procedures

Please note: Wiley-Blackwell are not responsible for the content or functionality of any supporting information supplied by the authors. Any queries (other than missing material) should be directed to the *Aging Cell* Central Office.